Universidad de Oviedo

Programa de Doctorado en Ingeniería de Procesos y Ambiental

# DESARROLLO DE REACTORES DE LECHO FLUIDIZADO PARA LA CAPTURA DE $CO_2$ CON CaO

María Elena Diego de Paz

Tesis Doctoral

2014

Universidad de Oviedo

Programa de Doctorado en Ingeniería de Procesos y Ambiental

# Desarrollo de reactores de lecho fluidizado para la captura de $CO_2$ con CaO

Tesis Doctoral

María Elena Diego de Paz

2014

# AUTORIZACIÓN PARA LA PRESENTACIÓN DE TESIS DOCTORAL

**Año Académico: 2014/2015**

| **1.- Datos personales del autor de la Tesis** | | |
|---|---|---|
| Apellidos:<br>**Diego de Paz** | Nombre:<br>**María Elena** | |
| DNI/Pasaporte/NIE: | Teléfono: | Correo electrónico: |

| **2.- Datos académicos** | |
|---|---|
| Programa de Doctorado cursado:<br>**Ingeniería de procesos y ambiental (Mención de calidad MCD2005-00213)** | |
| Órgano responsable:<br>**Universidad de Oviedo** | |
| Departamento/Instituto en el que presenta la Tesis Doctoral:<br>**Departamento de Ingeniería Química y Tecnología del Medio Ambiente** | |
| **Título definitivo de la Tesis** | |
| Español/Otro Idioma:<br>**Desarrollo de reactores de lecho fluidizado para la captura de $CO_2$ con CaO** | Inglés:<br>**Development of fluidized bed reactors to capture $CO_2$ with CaO** |
| Rama de conocimiento:<br>**Tecnologías de captura de $CO_2$** | |

| **3.- Autorización del Director/es y Tutor de la tesis** | |
|---|---|
| D/Dª: **(DIRECTOR)**<br>**Juan Carlos Abanades García** | DNI/Pasaporte/NIE: |
| Departamento/Instituto:<br>**Instituto Nacional del Carbón (INCAR-CSIC)** | |
| | |
| D/Dª: **(DIRECTOR)**<br>**Borja Arias Rozada** | DNI/Pasaporte/NIE: |
| Departamento/Instituto/Institución:<br>**Instituto Nacional del Carbón (INCAR-CSIC)** | |
| **Autorización del Tutor de la tesis** | |
| D/Dª:<br>**Aurelio B. Vega Granda** | DNI/Pasaporte/NIE: |
| Departamento/Instituto:<br>**Departamento de Ingeniería Química y Tecnología del Medio Ambiente (Universidad de Oviedo)** | |

Autoriza la presentación de la tesis doctoral en cumplimiento de lo establecido en el Art.30.1 del Reglamento de los Estudios de Doctorado, aprobado por el Consejo de Gobierno, en su sesión del día 17 de junio de 2013 (BOPA del 25 de junio de 2013)

Oviedo, 18 de Septiembre de 2014

Director/es de la Tesis — Tutor de la Tesis

Fdo.: Juan Carlos Abanades  Fdo.: Borja Arias Rozada  Fdo.: Aurelio B. Vega Granda

**SR. DIRECTOR DE DEPARTAMENTO DE INGENIERÍA QUÍMICA Y TECNOLOGÍA DEL MEDIO AMBIENTE/**
**SR. PRESIDENTE DE LA COMISIÓN ACADÉMICA DEL PROGRAMA DE DOCTORADO EN INGENIERÍA DE PROCESOS Y AMBIENTAL**

# RESOLUCIÓN DE PRESENTACIÓN DE TESIS DOCTORAL

**Año Académico: 2014/2015**

| **1.- Datos personales del autor de la Tesis** | | |
|---|---|---|
| Apellidos:<br>**Diego de Paz** | Nombre:<br>**María Elena** | |
| DNI/Pasaporte/NIE: | Teléfono: | Correo electrónico: |

| **2.- Datos académicos** | |
|---|---|
| Programa de Doctorado cursado:<br>**Ingeniería de Procesos y Ambiental** | |
| Órgano responsable:<br>**Universidad de Oviedo** | |
| Departamento/Instituto en el que presenta la Tesis Doctoral:<br>**Departamento de Ingeniería Química y Tecnología del Medio Ambiente** | |
| **Título definitivo de la Tesis** | |
| Español/Otro Idioma:<br>**Desarrollo de reactores de lecho fluidizado para la captura de $CO_2$ con CaO** | Inglés:<br>**Development of fluidized bed reactors to capture $CO_2$ with CaO** |
| Rama de conocimiento:<br>**Tecnologías de captura de $CO_2$** | |
| Señale si procede:<br>x Mención Internacional<br>x Idioma de presentación de la Tesis distinto al español<br>x Presentación como compendio de publicaciones | |

| **3.- Autorización del Presidente de la Comisión Académica / Director del Departamento** | |
|---|---|
| D/Dª:<br>**Salvador Ordóñez García** | DNI/Pasaporte/NIE: |
| Departamento/Instituto:<br>**Departamento de Ingeniería Química y Tecnología del Medio Ambiente** | |

**Resolución**

La Comisión Académica del Programa de Doctorado en Ingeniería de Procesos y Ambiental /El Departamento de Ingeniería Química y Tecnología del Medio Ambiente en su reunión de fecha 23 de Septiembre de 2014, acordó la presentación de la tesis doctoral a la Comisión de Doctorado, previa comprobación de que la tesis presentada y la documentación que la acompaña cumplen con la normativa vigente, según lo establecido en el Art.30.7 del Reglamento de los Estudios de Doctorado, aprobado por el Consejo de Gobierno, en su sesión del día 17 de junio de 2013 (BOPA del 25 de junio de 2013)

Además, informa:

| | Favorable | Desfavorable |
|---|---|---|
| Mención Internacional | x | ☐ |
| Idioma | ☐ | ☐ |
| Presentación como compendio de publicaciones | x | ☐ |

**Justificación**

La memoria depositada cumple con los requerimientos necesarios para ser defendida dentro del Programa de Doctorado de Ingeniería de Procesos y Ambiental

En Oviedo a 23 de Septiembre de 2014

Presidente de la Comisión Académica del Programa de Doctorado/Director de Departamento

Fdo.: Salvador Ordóñez García

Contra la presente resolución podrá interponer recurso de alzada ente el Excmo. Sr. Rector Magfco. de esta Universidad en el plazo de un mes a contar desde el siguiente a la recepción de la presente resolución, de acuerdo con lo previsto en el artículo 114 de la Ley 30/92, de 26 de noviembre, del Régimen Jurídico de las Administraciones Públicas y Procedimiento Administrativo Común (B.O.E. de 27 de noviembre), modificada por la Ley 4/1999, de 13 de enero (B.OE. de 14 de enero)

# Agradecimientos

En primer lugar me gustaría dar las gracias a todas las personas que de una forma u otra han contribuido a que esta Tesis sea posible.

A mis directores, Juan Carlos Abanades García y Borja Arias Rozada. Muchas gracias por todas las oportunidades que me habéis dado a lo largo de estos años, por confiar en mí e involucrarme en distintos proyectos, por estar disponibles en todo momento y por vuestra dedicación al trabajo. Gracias también por todo lo que he aprendido durante esta etapa, ya que sin vuestra ayuda y disposición no hubiera sido lo mismo.

A Mónica Alonso Carreño, con la que también he tenido la oportunidad de compartir mucho tiempo y trabajo durante esta Tesis, gracias por todo lo que me has aportado.

Al Consejo Superior de Investigaciones Científicas (CSIC) por la financiación recibida para la realización de esta Tesis y por facilitar el desarrollo de este trabajo en el Instituto Nacional del Carbón (INCAR).

A Aurelio Vega Granda, por aceptar ser el tutor de esta Tesis en la Universidad de Oviedo y facilitarme todos los trámites necesarios.

A todas las personas que forman o han formado parte del grupo de captura de $CO_2$: Jose Ramón, Chema, Yolanda, Juanamari, Montse, Belén, Nuria y en especial a Fer, especialista indiscutible del Leco.

A Gemma y a Isabel, por los trabajos que hemos realizado en común y porque siempre estáis dispuestas a ayudar en lo que se necesite.

A todas las empresas que han permitido que la planta piloto de La Pereda sea una realidad (Endesa, Hunosa y Foster Wheeler) y a todas las personas que han trabajado en el proyecto, en especial a Andrés, Luis, María, Javier, Jon y Diego. También ha sido muy importante el trabajo de Marta, Maite,

Berto, Benja, Luis, Canor, Jero y Héctor, ya que sin ellos los experimentos en la planta no hubieran sido posibles y además han hecho que el ambiente de trabajo sea inmejorable.

De igual modo me gustaría agradecer a Gas Natural Fenosa su implicación en el proyecto de la planta piloto de La Robla, en especial a John y Carlos. También a David, Eli, Alberto y Fran por su dedicación durante todas las horas (y son muchas) de experimentos.

A todas las personas que he conocido durante las estancias que he realizado. En especial, gracias al Prof. Scheffknecht por acogerme en su grupo de investigación de la Universidad de Stuttgart y a Glykeria por hacer que me sintiera como en casa y por tu implicación durante los experimentos que hemos hecho juntas. Muchas gracias también al Prof. John Dennis por darme la posibilidad de una estancia en la Universidad de Cambridge, y a Belén por tratarme tan bien durante el tiempo que estuve allí.

A Rubén, Ángela, Tomás, Juanamari y todos los que forman el grupo del *coffee break* por los buenos momentos que me habéis hecho pasar y las risas que vienen muy bien para cargar las pilas. También a todas las personas del Incar con las que he tenido el placer de cruzarme en este tiempo, entre ellas Bea, Nacho y todos mis compañeros de sala.

Muchas gracias también a Elena, por esos cafés después de trabajar, esas conversaciones entre doctorandas y ese positivismo que anima a cualquiera! A Laura, por las charlas, las visitas a la máquina expendedora y por sus historietas que parecen sacadas de una película de ciencia ficción. También a Sergio, David, Cris…, compañeros de cenas, comidas y demás actividades aventureras, por el apoyo y los ánimos en esta etapa final.

A Meldi y a Kike, gracias por ayudarme siempre en todo lo que estaba en vuestra mano.

Finalmente es muy especial para mí el agradecimiento a mi familia. Gracias de corazón a mis padres, por haber estado siempre ahí, apoyándome en los malos momentos y disfrutando de los buenos, y por todos los consejos (acertados sin duda) que me habéis dado. A Gema, mi hermana, gracias por todo tu apoyo y paciencia y por darme un punto de vista distinto de las cosas. A mis abuelos, que siempre han estado ahí pendientes de todo. Por último, a Kike, una persona muy especial en mi vida. Muchas gracias por comprenderme, por el apoyo constante e incondicional, por saber sacarme de mis bucles *do*, por tu confianza, porque siempre estás dispuesto a ayudarme y por todos los momentos que hemos compartido y que sí seguirán.

# Índice

# Resumen

Los niveles de emisión de $CO_2$ han experimentado un gran incremento en los últimos años debido principalmente al empleo de combustibles fósiles para satisfacer el crecimiento de la demanda energética global. Esto ha provocado cambios en las tendencias del sistema climático, contribuyendo de este modo a lo que hoy se conoce como cambio climático. Es por ello que necesitamos disponer de opciones que permitan reducir las emisiones de $CO_2$ hasta alcanzar niveles compatibles con cambios asumibles del sistema climático. Sin embargo, todas las previsiones apuntan indudablemente a un mayor consumo de combustibles fósiles en las próximas décadas, lo que supondría, en ausencia de otras medidas, un incremento sustancial en las concentraciones de $CO_2$ en la atmósfera. Una de las alternativas que se plantea a corto y medio plazo consiste en desacoplar las emisiones de $CO_2$ del empleo de combustibles fósiles por medio del desarrollo de los procesos de captura de $CO_2$. El objetivo de estos procesos es separar el $CO_2$ de las corrientes gaseosas generadas en grandes focos de emisión estacionarios para proceder a su confinamiento permanente. En este sentido, una de las tecnologías propuestas es la captura de $CO_2$ mediante ciclos de carbonatación-calcinación, que constituye el objeto de estudio de la presente Tesis Doctoral.

El trabajo realizado durante esta Tesis se ha centrado en el desarrollo de la tecnología de captura de $CO_2$ a alta temperatura empleando CaO como sorbente en algunas de sus principales rutas de proceso con el objetivo de avanzar hacia su implantación a escala industrial. Para ello se han llevado a cabo estudios experimentales a escala de planta piloto, así como trabajos de modelado de los reactores involucrados en el sistema e implementación de mejoras en el proceso. En concreto, esta memoria se ha estructurado en las dos secciones que se indican a continuación.

La primera sección comprende el trabajo experimental llevado a cabo en una planta piloto de captura de $CO_2$ post-combustión que trata gases reales de combustión procedentes de una central térmica, así como las campañas experimentales realizadas en una planta piloto de combustión de biomasa y captura de $CO_2$ *in situ*. En ambos casos se presentan los resultados obtenidos bajo diversas condiciones de operación, junto con el estudio de la influencia de variables de proceso clave y la validación de los modelos de reactor disponibles con los datos experimentales.

La segunda sección de esta Tesis consta de un conjunto de trabajos dirigidos a profundizar en distintos aspectos de los sistemas de captura de $CO_2$ mediante la tecnología de carbonatación-calcinación. En primer lugar se incluye un estudio hidrodinámico del sistema de reactores interconectados de lecho fluidizado circulante empleados en esta tecnología. También se ha realizado un análisis del efecto que tiene la presencia de inertes (azufre y cenizas) en el sistema en cuanto a su influencia en las características de la corriente de sólidos que circula entre reactores y la eficacia de captura de $CO_2$. Finalmente, la última parte de esta Tesis se centra en el estudio de una novedosa estrategia de reactivación del sorbente: la recarbonatación. Para ello se ha realizado un estudio cinético de la reacción de recarbonatación bajo distintas condiciones de operación y se ha empleado la información obtenida para la modelización y diseño preliminar de un reactor de recarbonatación.

# Abstract

$CO_2$ emission levels have experienced a sharp increase in recent years mainly due to the use of fossil fuels to meet the increasing global energy demand. This phenomenon has promoted changes in the behaviour of the climate system and has contributed to what is known as climate change. This is the main reason why we need options that allow $CO_2$ emissions to be reduced to levels that are assumable and compatible with the climate system. However, all predictions clearly indicate that fossil fuel consumption will increase over the next few decades, and this will entail a substantial increase in $CO_2$ atmospheric concentration unless other measures are adopted. One of the alternatives proposed for the short and medium term consists in decoupling $CO_2$ emissions from fossil fuels usage by developing $CO_2$ capture processes. The objective of these processes is to separate the $CO_2$ present in the gas streams produced in large stationary emission sources for its permanent storage. To this end, $CO_2$ capture by means of carbonation-calcination cycles is one of the proposed technologies and constitutes the subject of study of the present Doctoral Thesis.

The work conducted for this Thesis has been focused on the development of the $CO_2$ capture technology at high temperature using CaO as sorbent in some of its main process routes as a step towards its implementation at industrial scale. For this purpose, several pilot-scale experimental tests were carried out, as well as studies related to the modeling of the reactors involved in the system and the incorporation of improvements to the process. Specifically, this dissertation consists of the two sections outlined below.

The first section comprises the experimental tests performed at a post-combustion $CO_2$ capture pilot plant which uses real flue gases from an industrial power plant and also includes the experimental campaigns carried out in a pilot plant of simultaneous combustion and *in situ* $CO_2$ capture. The

results obtained under different operating conditions are presented for both cases. A study of the influence of the key process variables and the validation of available reactor models using the experimental data are also provided.

The second section of this Thesis comprises a series of in-depth studies into some of the aspects of $CO_2$ capture processes based on the carbonation-calcination technology. First, a hydrodynamic study of the interconnected circulating fluidized bed reactors used in this technology is presented. Moreover, the effects of the presence of inerts (sulfur and ashes) on the characteristics of the circulating solids and $CO_2$ capture efficiency are evaluated. The final part of this Thesis is focused on a novel sorbent reactivation strategy: recarbonation. For this purpose, a kinetic study of the recarbonation reaction has been carried out under different operating conditions and the information obtained has been used for the modeling and preliminary design of a recarbonation reactor.

# Lista de publicaciones

La Tesis Doctoral presentada en esta memoria está basada en el trabajo contenido en las publicaciones indicadas a continuación, y que serán referidas en el texto mediante números romanos:

I. Arias, B., Diego, M. E., Abanades, J. C., Lorenzo, M., Diaz, L., Martínez, D., Alvarez, J. y Sánchez-Biezma, A. (2013), 'Demonstration of steady state $CO_2$ capture in a 1.7$MW_{th}$ calcium looping pilot', *Int. J. Greenhouse Gas Control,* 18, 237-245.

II. Alonso, M., Diego, M. E., Pérez, C., Chamberlain, J. R. y Abanades, J. C. (2014), 'Biomass combustion with in situ $CO_2$ capture by CaO in a 300 $kW_{th}$ circulating fluidized bed test facility', *Int. J. Greenhouse Gas Control*, 29, 142-152.

III. Diego, M. E., Arias, B. y Abanades, J. C. (2012), 'Modeling the solids circulation rates and solids inventories of an interconnected circulating fluidized bed reactor system for $CO_2$ capture by calcium looping', *Chem. Eng. J.,* 198–199, 228-235.

IV. Diego, M. E., Arias, B., Alonso, M. y Abanades, J. C. (2013), 'The impact of calcium sulfate and inert solids accumulation in post-combustion calcium looping systems', *Fuel,* 109, 184-190.

V. Grasa, G., Martínez, I., Diego, M. E. y Abanades, J. C. (2014), 'Determination of CaO Carbonation Kinetics under Recarbonation Conditions', *Energy Fuels,* 28, 4033-4042.

VI. Diego, M. E., Arias, B., Grasa, G. y Abanades, J. C. (2014), 'Design of a Novel Fluidized Bed Reactor to Enhance Sorbent Performance in $CO_2$ Capture Systems Using CaO', *Ind. Eng. Chem. Res.,* 53, 10059-10071.

Durante el período de esta Tesis Doctoral se han escrito además las siguientes publicaciones, que no han sido incluidas en esta memoria puesto que su contenido está fuera de los objetivos de esta Tesis o bien se superponen parcialmente con el trabajo incluido en los anteriores:

- Arias, B., Cordero, J. M., Alonso, M., Diego, M. E. y Abanades, J. C. (2013), 'Investigation of $SO_2$ capture in a circulating fluidized bed carbonator of a Ca looping cycle', *Ind. Eng. Chem. Res.,* 52, 2700-2706.

- Sánchez-Biezma, A., Paniagua, J., Diaz, L., Lorenzo, M., Alvarez, J., Martínez, D., Arias, B., Diego, M. E. y Abanades, J. C. (2013), 'Testing postcombustion $CO_2$ capture with CaO in a 1.7 $MW_{th}$ pilot facility', *Energy Proc.*, 37, 1-8.

- Duelli (Varela), G., Charitos, A., Diego, M. E., Stavroulakis, E., Dieter, H., Scheffknecht, G., 'Investigations at a 10 $kW_{th}$ Calcium Looping Dual Fluidized Bed Facility: Limestone Calcination and $CO_2$ Capture under High $CO_2$ and Water Vapour Atmosphere', *Int. J. Greenhouse Gas Control*, enviado.

- Diego, M.E., Arias, B., Grasa, G., Abanades, J. C., Díaz, L., Lorenzo, M., Sánchez-Biezma, A., 'Calcium Looping with Enhanced Sorbent Performance: Experimental Testing in a Large Pilot', *Energy Proc.*, enviado.

# Lista de figuras

# 1. Introducción

## 1.1 Cambio climático y emisiones de $CO_2$

En el último siglo se ha producido un cambio sin precedentes en las tendencias del sistema climático (IPCC 2013). Fenómenos tales como el incremento de la temperatura en la atmósfera terrestre, el calentamiento y acidificación de los océanos, la fundición de los casquetes polares y el aumento del nivel de mar han experimentado un impulso significativo durante este tiempo (IPCC 2013). Estas alteraciones, pese a estar también influenciadas por causas naturales como las variaciones en la radiación solar y la actividad volcánica, encuentran su origen principalmente en el gran aumento de las concentraciones atmosféricas de gases de efecto invernadero (GEI) con respecto a la época preindustrial, dando lugar a lo que hoy entendemos por cambio climático. En concreto, el cambio climático se define como el cambio del clima atribuido directa o indirectamente a la actividad humana, que altera la composición de la atmósfera terrestre y que se suma a la variabilidad natural del clima observada durante períodos de tiempo comparables (definición adoptada en la Convención Marco de las Naciones Unidas sobre el Cambio Climático de 1992).

Los niveles totales de emisión de GEI – $CO_2$, $CH_4$, $N_2O$, HFCs, PFCs y $SF_6$ – asociados a causas antropogénicas se han incrementado a razón de 0.4 gigatoneladas de $CO_2$ equivalentes ($GtCO_2$-eq) anuales desde 1970 hasta el año 2000, mientras que en el período comprendido entre los años 2000 y 2010 este aumento ha sido de 1 $GtCO_2$-eq anual (IPCC 2014). En total, las emisiones de GEI de origen antropogénico han experimentado un crecimiento del 80% desde 1970, alcanzando las 49 $GtCO_2$-eq en 2010 (IPCC 2014). Esta tendencia es el resultado del progresivo aumento de la población mundial así como de los cambios surgidos en los hábitos de

consumo, que han dado lugar a una mayor demanda energética y a cambios en el uso de la tierra (deforestación).

Los GEI que se emiten en mayor medida a la atmósfera son $CH_4$, $N_2O$ y, principalmente, $CO_2$, siendo este último el GEI que más contribuye al cambio climático, pese a que su potencial de calentamiento global es menor. La curva Keeling mostrada en la Figura 1 presenta la evolución de la concentración de $CO_2$ en la atmósfera medida en el observatorio de Mauna Loa (Hawái). Los niveles atmosféricos de $CO_2$ han experimentado un incremento continuado desde un valor de 315 ppm registrado por primera vez en 1958 hasta alcanzar 397 ppm en agosto de 2014, llegando a superar las 400 ppm en varias ocasiones desde mayo de 2013. De igual modo, la temperatura media global se ha ido incrementando hasta alcanzar en la actualidad un aumento de 0.8ºC con respecto a los niveles preindustriales (IPCC 2013).

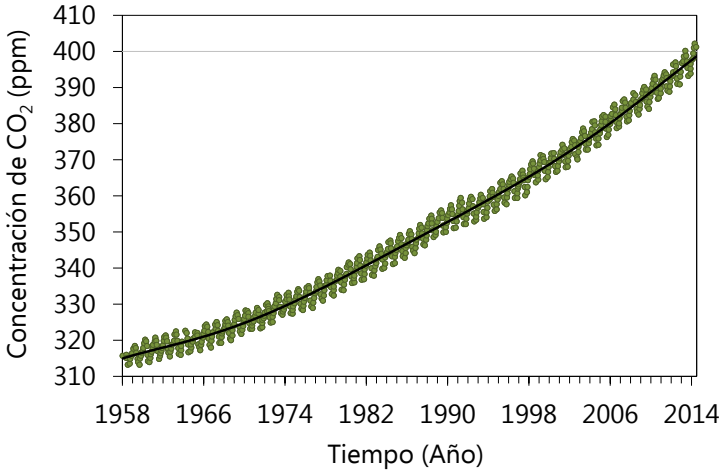


**Figura 1.** Evolución de la concentración de $CO_2$ en el observatorio de Mauna Loa (Hawái) desde 1958 (Fuente: Scripps Institution of Oceanography at UC San Diego (2014)).

El aumento de las emisiones de $CO_2$ está marcado fundamentalmente por el crecimiento en el uso de combustibles fósiles. Uno de los sectores más

dependientes de este tipo de combustibles es el energético, dentro del cual se incluyen tanto la generación de energía eléctrica y de calor como el consumo directo de combustibles para el transporte, la industria y edificios, entre otros. Se estima que más del 80% de la energía global consumida procede de combustibles fósiles, siendo el sector energético el responsable de más de dos tercios de las emisiones globales de GEI (IEA 2013a). Asimismo, las emisiones de $CO_2$ asociadas a la energía aumentaron un 1.4% en 2012 con respecto a los valores del año anterior y ascendieron hasta las 31.6 $GtCO_2$ (IEA 2013a). Esta tendencia al alza en las emisiones de $CO_2$ se ha venido repitiendo año tras año, especialmente en las últimas décadas, y las previsiones apuntan a que será así durante mucho tiempo si no se toman nuevas medidas. Es por ello que el sector energético es una pieza clave a tener en cuenta en la reducción de emisiones para la lucha contra el cambio climático.

Con el objetivo de evaluar los impactos de distintas políticas energéticas a nivel global y local, la Agencia Internacional de la Energía define tres escenarios posibles para el sector energético hasta el año 2035 (IEA 2013b): el escenario 450, que muestra las tendencias necesarias para estabilizar la concentración atmosférica de $CO_2$ en 450 ppm y, por tanto, limitar el aumento de la temperatura global a 2ºC con una probabilidad del 50%; el escenario de las políticas actuales, en el que los mercados energéticos se ven únicamente afectados por las medidas aprobadas hasta mitad del año 2013; y el escenario de nuevas políticas, considerado el escenario central del informe, que tiene en cuenta no sólo las acciones ya definidas, sino también aquellos compromisos que han sido anunciados pero cuya implementación aún no ha sido concretada. De este modo, se incluyen medidas relacionadas con energías renovables, eficiencia energética, combustibles y vehículos alternativos, precio del carbono, expansión de la energía nuclear y la reforma de las subvenciones a los combustibles fósiles (IEA 2013b). Las previsiones del escenario de nuevas políticas estiman que la demanda

global de energía se incrementará en un 33% en el período 2011-2035, debido fundamentalmente al despegue de las economías emergentes como China, India, países del sudeste asiático y de Oriente Medio, a las que se asocia más del 90% del crecimiento de dicha demanda (IEA 2013b). Los combustibles fósiles seguirán teniendo un gran protagonismo tal y como se muestra en la Figura 2 debido a su gran disponibilidad y su precio moderado en comparación con otros recursos, y a pesar de una ligera disminución de su participación en el *mix* energético satisfarán el 76% de la demanda de energía primaria en 2035 (IEA 2013b). Como consecuencia, las emisiones de GEI relacionadas con el sector energético se incrementarán en un 20% hasta alcanzar las 37.2 $GtCO_2$ en 2035, lo que supone un gran exceso en comparación con los niveles requeridos en el escenario 450 (21.6 $GtCO_2$ en 2035). De hecho se estima que de llegar a tales niveles de emisión de $CO_2$, el incremento medio de la temperatura global a largo plazo se situaría en torno a los 3.6ºC con respecto a los niveles preindustriales.

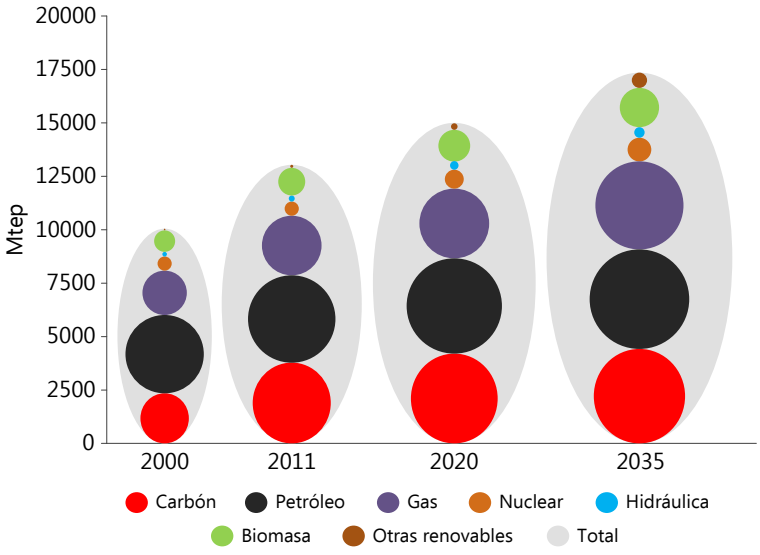


**Figura 2.** Demanda mundial de energía primaria por tipo de recurso energético: histórico y previsiones según el escenario de nuevas políticas para los años 2020 y 2035 (Datos tomados de IEA (2013b)).

Todos los escenarios estudiados coinciden en que la demanda de electricidad crecerá más que la demanda de cualquier otra forma final de energía. En el escenario de nuevas políticas su tasa de crecimiento será igual al 2.2% anual, con un total acumulado del 69% en el período 2011-2035 hasta alcanzar los 32150 TWh (37087 TWh generados, incluyendo las pérdidas de energía en las redes de transmisión y distribución y el consumo energético durante la producción eléctrica) (IEA 2013b). La contribución de todas las fuentes energéticas aumentará, y pese a que se prevé que las energías renovables contribuyan en un 31% a la generación eléctrica en 2035, los combustibles fósiles continuarán siendo la principal fuente de electricidad (IEA 2013b). Su contribución a la producción eléctrica disminuirá desde el 68% contabilizado en 2011 hasta el 57% en 2035, siendo responsables de la generación de 21181 TWh (escenario de nuevas políticas). Esta bajada será absorbida fundamentalmente por el incremento de la presencia de energías renovables, puesto que la energía nuclear continuará teniendo una participación del 12% (IEA 2013b).

Todas las previsiones apuntan indudablemente a un mayor consumo de combustibles fósiles para satisfacer la demanda energética global. En términos de disponibilidad de recursos esto no supone un problema, ya que en la actualidad las reservas de carbón, petróleo y gas natural superan ampliamente los niveles de consumo previstos en las próximas décadas. El problema reside en las emisiones de $CO_2$ asociadas. El IPCC (del inglés, *Intergovernmental Panel on Climate Change*) estima que para limitar el aumento de temperatura en 2ºC con un 50% de probabilidad el nivel máximo de emisión es de 1133 $GtCO_2$ a partir de 2012 (IEA 2013b; IPCC 2013), de las cuales 884 $GtCO_2$ corresponden al período 2012-2050 (IEA 2013c). Sin embargo, se calcula que si se quemaran todas las reservas probadas hasta el año 2012 se generarían unas emisiones totales de 2860 $GtCO_2$ (IEA 2013b). Esta discordancia pone en evidencia la imposibilidad de emplear una gran parte de los recursos fósiles disponibles

si se adoptan políticas restrictivas para la lucha contra el cambio climático (Carbon Tracker 2013; IEA 2013b). Sin embargo, se continúan realizando grandes inversiones para el descubrimiento y la explotación de nuevos yacimientos. Esto, además de una amenaza para el medio ambiente, supone un riesgo adicional, ya que muchas de las principales bolsas mundiales tienen una parte de sus activos ligada a los combustibles fósiles, pudiendo dar lugar a una burbuja de carbono similar a la reciente burbuja financiera (Carbon Tracker 2013).

En los últimos años se han establecido mecanismos para limitar las emisiones de $CO_2$. Uno de los más extendidos es el régimen de comercio de derechos de emisión de la Unión Europea (EU-ETS), iniciado en el año 2005, que afecta a los sectores de generación eléctrica, industria y aviación, y abarca aproximadamente el 45% de las emisiones de gases de efecto invernadero de la UE (IEA 2013a). Sin embargo, la acción de este mecanismo se ha visto limitada en los últimos tiempos puesto que el precio del carbono ha experimentado un descenso sustancial, desde casi 30 €/t de carbono a mediados de 2008 hasta menos de 3 €/t de carbono en abril de 2013, lo que hace poco atractivas las inversiones en tecnologías de bajas emisiones de $CO_2$ (IEA 2013b). Por otra parte, en Estados Unidos, la iniciativa regional de gases de efecto invernadero agrupa nueve estados y es también un exponente de este tipo de mecanismos. Cada vez más países y ciudades de todo el mundo se suman a este tipo de programas, tales como Nueva Zelanda, Australia, Japón, Kazajistán, California (EEUU) y Quebec y Alberta (Canadá), y se espera que próximamente Korea, algunas ciudades de China y Sudáfrica desarrollen planes similares (IEA 2013b).

En cualquier caso, es necesario contar con alternativas que permitan reducir las emisiones de $CO_2$ hasta niveles compatibles con cambios asumibles del sistema climático. Existen un conjunto de opciones que habitualmente se plantean para lograr este objetivo. Así, se propone el incremento de la eficiencia energética en la generación eléctrica, en la posterior distribución

de la electricidad y en el uso de combustibles, una mayor presencia de las energías renovables en el *mix* energético, la transición hacia combustibles con menores emisiones de $CO_2$, el aumento de la potencia instalada de generación de origen nuclear, y finalmente, el empleo de tecnologías de captura y almacenamiento de $CO_2$ (CAC), que permiten separar el $CO_2$ generado en procesos para la generación de electricidad, o en procesos industriales tales como la fabricación de cemento, hierro y acero entre otros (IEA 2013c). La Figura 3 representa la contribución individual de cada una de las anteriores alternativas a la reducción de emisiones requerida en el escenario de 2ºC (escenario 2DS) según la estimación de la Agencia Internacional de la Energía, que es consistente con el escenario 450 (IEA 2013b) anteriormente descrito. Es importante destacar que posponer la implementación de estas medidas, pese al ahorro económico inicial, conllevará un mayor coste a largo plazo debido a la necesidad de una posterior reducción drástica de las emisiones de $CO_2$.

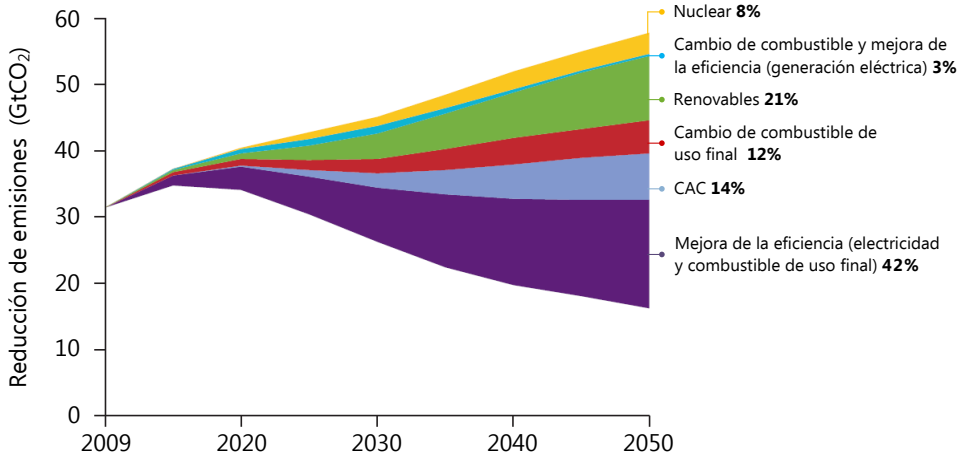


**Figura 3.** Comparación entre los niveles de emisión de los escenarios 2DS (comparable al escenario 450 (IEA 2013b)) y 6DS (comparable al escenario de políticas actuales (IEA 2013b)) y contribución de las distintas opciones a la reducción de emisiones hasta 2050 (Fuente: IEA (2013c)).

Como se muestra en la Figura 3, la contribución acumulada de la CAC al esfuerzo global de reducción de emisiones se prevé que sea de un 14% hasta 2050 (IEA 2013c). Su importancia estratégica reside en el hecho de que la captura y almacenamiento de $CO_2$ es la única tecnología disponible que permite resolver la tensión entre el rápido incremento de la demanda energética, la disponibilidad de combustibles fósiles y la reducción de las emisiones de $CO_2$. De hecho, se estima que en un escenario en el que no se implemente CAC el capital necesario para llevar las emisiones de $CO_2$ al mismo nivel sin CAC en el sector eléctrico aumentaría un 40% (IEA 2012a; IEA 2013c). Por tanto, la captura y almacenamiento de $CO_2$ se perfila como una herramienta clave en el futuro de los sectores de generación eléctrica e industrial en su camino para adaptarse a un sistema energético de bajas emisiones de $CO_2$.

## 1.2 Tecnologías de captura, transporte y almacenamiento de $CO_2$

Las tecnologías CAC buscan separar el $CO_2$ generado en los procesos industriales con el objetivo de obtener una corriente gaseosa concentrada en $CO_2$ susceptible de compresión, transporte y almacenamiento permanente. Estas tecnologías encuentran su principal aplicación en grandes fuentes estacionarias que emplean combustibles fósiles o biomasa en su operación y cuyas emisiones anuales superan las 0.1 $MtCO_2$ (IPCC 2005). Dentro este grupo se incluyen las centrales de generación de energía, las refinerías de petróleo, la industria cementera, del acero, del aluminio y la de fabricación de productos químicos, entre otros. Por su parte, las pequeñas fuentes emisoras procedentes de sectores tales como el residencial o el del transporte no se consideran dentro del intervalo de aplicación de las tecnologías CAC, pese a su contribución significativa a las emisiones globales de $CO_2$. Ello se debe a las características inherentes a estas fuentes, ya que además de su pequeño tamaño en muchos casos son

móviles, lo que provoca que la captura de $CO_2$ en estos casos sea más costosa y difícil desde un punto de vista técnico. No obstante, en un futuro se plantea que estos sectores empleen electricidad o hidrógeno generado en procesos que incorporen tecnologías CAC en su producción, lo que permitirá la captura indirecta de sus emisiones de $CO_2$.

### 1.2.1 Captura de $CO_2$

La captura de $CO_2$ es una etapa clave en las tecnologías CAC, ya que es la responsable de reducir el contenido de $CO_2$ de los gases emitidos en un proceso industrial concreto. Asimismo, tiene una gran influencia en términos económicos, ya que se estima que el coste de la etapa de captura (junto con el acondicionamiento y compresión de la corriente gaseosa de $CO_2$) representa aproximadamente el 75% de los costes totales de los procesos CAC (IPCC 2005; ZEP 2013a). Es por ello que los esfuerzos deben ir dirigidos principalmente hacia la reducción de costes en la etapa de captura, manteniendo a su vez los costes derivados del transporte y almacenamiento permanente de $CO_2$ en valores bajos (ZEP 2013a).

Todos los procesos de captura de $CO_2$ llevan implícito la separación de un componente de una corriente gaseosa. En función de dónde se localice la etapa de separación se distinguen tres tipos de sistemas de captura de $CO_2$, denominados post-combustión, pre-combustión y oxi-combustión, cuyo esquema se muestra en la Figura 4.

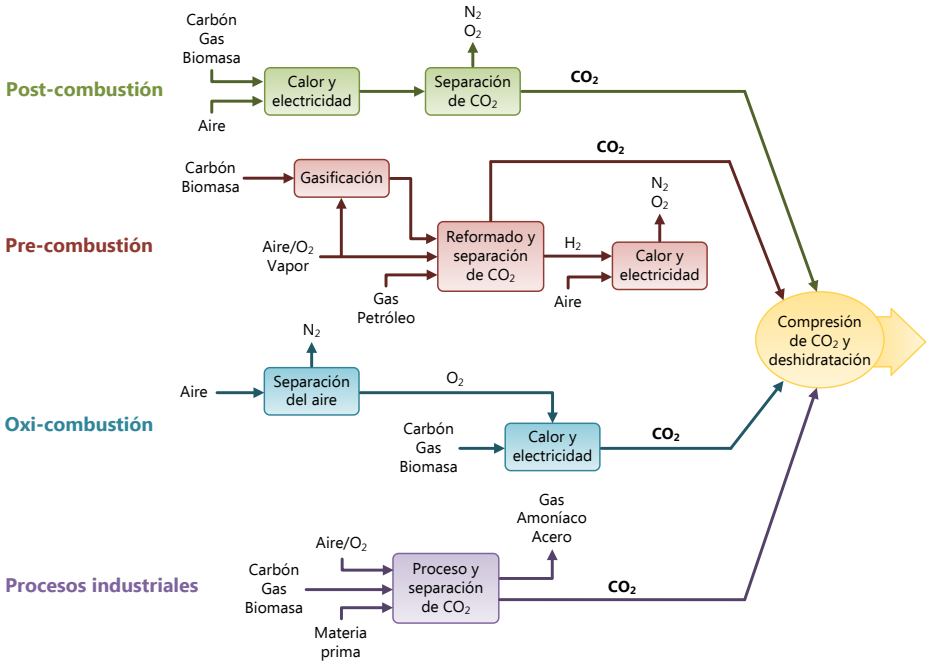


**Figura 4.** Representación esquemática de los tipos de sistemas de captura de $CO_2$ (Fuente: IPCC (2005)).

**Post-combustión**: esta familia de tecnologías se basa en la separación del $CO_2$ contenido en la corriente de gases generada como consecuencia del empleo de combustibles fósiles o biomasa en procesos de combustión en presencia de aire. De este modo, la etapa de separación da lugar a una corriente concentrada de $CO_2$, que también puede contener algunas impurezas y vapor de agua, fácilmente condensable. La gran ventaja de este tipo de sistemas es su relativa sencillez en lo que se refiere a su implementación en instalaciones ya existentes, puesto que no afectan al proceso de producción en sí, sino que se alimentan de las corrientes gaseosas generadas en el mismo. Por este motivo las tecnologías de post-combustión son ampliamente aceptadas para incorporar la CAC a centrales térmicas e instalaciones industriales de reciente construcción, ya que se podría aprovechar la inversión inicial. Se han propuesto varias tecnologías para la captura de $CO_2$ post-combustión y, entre ellas, la más desarrollada

es en la actualidad la absorción química mediante aminas. Este proceso emplea una torre de absorción para separar el $CO_2$ de la corriente gaseosa mediante su reacción con la amina y una torre de desorción en la que se regenera el solvente, dando lugar así a una corriente concentrada de $CO_2$. Las principales limitaciones del proceso son la degradación de las aminas, lo que requiere operaciones de acondicionamiento previo de la corriente gaseosa, y el elevado consumo energético de la etapa de desorción. Por otra parte, el empleo de amoniaco como solvente también ha sido propuesto y está actualmente en fase de estudio. Otra opción consiste en la captura del $CO_2$ del gas de combustión mediante su adsorción sobre un sorbente sólido, quedando así retenido por medio de interacciones superficiales. La desorción del $CO_2$ se realiza mediante variaciones de presión (PSA en inglés, *Pressure Swing Adsorption*) o temperatura (TSA en inglés, *Temperature Swing Adsorption*). En muchos casos es necesario un pretratamiento previo de los gases de combustión antes de someterlos a la etapa de captura de $CO_2$, con la consiguiente penalización energética asociada. También se ha propuesto la separación del $CO_2$ contenido en los gases de combustión empleando membranas que dan lugar a un transporte selectivo del $CO_2$ a través de las mismas. Su aplicación a procesos de post-combustión se ve limitada principalmente por la baja concentración de $CO_2$ en el gas a tratar (10-15%v $CO_2$). Finalmente, una línea de investigación que se ha desarrollado con fuerza en los últimos años consiste en la captura de $CO_2$ mediante el empleo de sorbentes sólidos que reaccionan con el $CO_2$ contenido en el gas de combustión y son, posteriormente, regenerados dando lugar a una corriente gaseosa concentrada en $CO_2$. Dentro de este grupo se encuentra la tecnología de captura de $CO_2$ mediante CaO, también conocida como *Calcium Looping*, que es la base de esta Tesis Doctoral.

**Pre-combustión**: en este sistema de captura la separación de gases tiene lugar antes de la generación de calor y/o electricidad. De este modo, ya sea mediante un proceso de gasificación (carbón o biomasa) o de reformado

(gas natural y derivados del petróleo) en presencia de aire u oxígeno y vapor de agua se genera una corriente de CO e $H_2$ (gas de síntesis). A continuación se produce la reacción de desplazamiento del gas de agua (WGS en inglés, *Water Gas Shift*), en la que el CO reacciona con vapor de agua generando $H_2$ y $CO_2$, que será posteriormente separado empleando alguno de los procesos mencionados para el caso de post-combustión o procesos comerciales de absorción física en los que el $CO_2$ de los gases de combustión se disuelve en un solvente a baja temperatura y alta presión, que es posteriormente regenerado invirtiendo estas condiciones (procesos Rectisol y Selexol). Mediante este proceso se logra una corriente gaseosa con una elevada concentración de hidrógeno que será empleada como fuente de energía. Este tipo de sistemas CAC son más convenientes para su aplicación en instalaciones de nueva construcción debido a su complejidad y requerimientos específicos.

**Oxi-combustión**: la principal característica de estas tecnologías es que la combustión no se lleva a cabo en presencia aire, sino de un comburente compuesto por una mezcla de oxígeno de alta pureza y $CO_2$ para facilitar el control de la temperatura. Esto evita la necesidad de un proceso de separación de $CO_2$ posterior a la reacción de combustión, puesto que la corriente gaseosa generada contiene básicamente $CO_2$ y vapor de agua, eliminándose este último por condensación. Sin embargo, los sistemas de oxi-combustión requieren una separación previa del $N_2$ del aire para la generación de una corriente de oxígeno de pureza adecuada. Esta etapa habitualmente se realiza por métodos criogénicos, y requiere un elevado aporte energético. En la actualidad se están llevando a cabo numerosas investigaciones con el objetivo de reducir esta demanda energética, puesto que se trata de un elemento clave para las tecnologías basadas en la oxi-combustión. Es por ello que en los últimos años ha evolucionado significativamente una nueva tecnología conocida como combustión con transportadores de oxígeno (CLC en inglés, *Chemical Looping Combustion*),

que presenta una separación del oxígeno del aire de modo distinto a la criogénica. El CLC se basa en el empleo de dos reactores (reactor de aire y reactor de combustible) entre los que circula una corriente sólida. Estas partículas son capaces de oxidarse en presencia de aire para, en un segundo reactor y en contacto con un combustible, liberar el oxígeno tomado en la etapa anterior aportando así una corriente pura de oxígeno a la combustión. Al igual que en el caso de la pre-combustión, las tecnologías de oxi-combustión son más adecuadas para instalaciones de nueva construcción.

Los sistemas industriales de captura descritos anteriormente están orientados principalmente a aplicaciones relacionadas con la generación eléctrica y de calor. Sin embargo, una opción de gran interés es la captura de $CO_2$ en las corrientes gaseosas generadas en diversos procesos industriales, tal y como se muestra en la Figura 4. En la actualidad esta separación se lleva a cabo para el acondicionamiento del gas natural, ya que es necesario limitar su contenido en $CO_2$ a aproximadamente 2% en volumen para evitar problemas de corrosión de tuberías, reducir un consumo energético adicional innecesario durante su transporte e incrementar su poder calorífico (IPCC 2005). También se incluye una etapa de captura de $CO_2$ en el proceso de fabricación de amoníaco con el objetivo de separar una corriente de $H_2$ a partir de la mezcla de $H_2$ y $CO_2$ generada mediante reformado o gasificación. El $CO_2$ obtenido mediante este procedimiento es generalmente empleado en la fabricación de urea (IPCC 2005). Aunque el objetivo último de estos procesos no es el almacenamiento de $CO_2$, su existencia sugiere que la captura de $CO_2$ es una realidad y se puede implementar en distintos procesos industriales, si bien es cierto que previamente se debe adaptar la tecnología a los requerimientos concretos de cada proceso, logrando además una penalización energética reducida. En concreto, se considera que los sectores de fabricación de acero y de cemento son candidatos especialmente

adecuados para una futura implementación de las tecnologías de captura de $CO_2$ (IPCC 2005).

### 1.2.2 Transporte de $CO_2$

Tras la obtención de una corriente concentrada de $CO_2$ el siguiente paso es su acondicionamiento y transporte hasta el emplazamiento del almacén final. Este transporte se puede realizar mediante gasoducto (terrestre o marítimo), barco, tren o carretera (IPCC 2005), aunque estos dos últimos medios sólo se prevé que participen en el transporte de $CO_2$ a pequeña escala para aplicaciones especiales (Boot-Handford *et al.* 2014).

Una de las opciones más factibles es el empleo de gasoductos, que son ya una realidad para el transporte de $CO_2$ destinado a la recuperación mejorada de petróleo (EOR en inglés, *Enhanced Oil Recovery*) en Estados Unidos y Canadá desde los años 70 (IPCC 2005; Boot-Handford *et al.* 2014). El transporte mediante gasoductos requiere una etapa de compresión previa del $CO_2$ hasta alcanzar condiciones supercríticas (31.1ºC y 74 bar) o un estado de fase densa (licuado) con el objetivo de reducir su volumen. El transporte de $CO_2$ supercrítico es más eficiente, ya que en estas condiciones el $CO_2$ tiene la viscosidad de un gas y la densidad de un líquido, con lo que resulta idóneo para su transporte a largas distancias. Sin embargo, en muchas ocasiones es difícil garantizar temperaturas superiores a la crítica a lo largo de todos los tramos del gasoducto, por lo que se opta por el transporte de $CO_2$ en fase densa. De este modo, se mantienen parte de las ventajas del estado supercrítico mientras que es posible operar con presiones entre 85 y 210 bar y una gran variedad de temperaturas (Boot-Handford *et al.* 2014). Se requieren además estaciones de recompresión en puntos intermedios que permiten mantener las altas presiones, especialmente cuando se trata de largas distancias. Cabe destacar que Estados Unidos cuenta con una red de gasoductos de 5800 km (IEA 2012b) que transportan entre 48 y 58 $MtCO_2$ anuales (Global CCS Institute 2013).

Pese a que el $CO_2$ transportado es en su mayoría de origen natural y tiene, por tanto, características distintas al antropogénico, esta experiencia es altamente beneficiosa para el rápido desarrollo de una gran red de transporte de $CO_2$ para las tecnologías CAC.

En lo que se refiere al transporte mediante barco, éste es más rentable económicamente en largas distancias (IPCC 2005; ZEP 2013b). Este modo de transporte requiere estaciones de almacenamiento intermedias y se adapta con mayor facilidad que los gasoductos a las fluctuaciones en la generación de $CO_2$ (Boot-Handford *et al.* 2014). Además, es posible emplear el conocimiento adquirido en el transporte marítimo de gas natural licuado y gases licuados derivados del petróleo y adaptarlo a las características específicas del $CO_2$, lo que favorece su rápido desarrollo como opción para el transporte en las tecnologías CAC.

Como ya se ha mencionado anteriormente, es necesario llevar a cabo un acondicionamiento previo de la corriente gaseosa para alcanzar las características requeridas para el transporte y posterior almacenamiento del $CO_2$. El $CO_2$ antropogénico generado durante los procesos de captura tiene generalmente menor pureza que el $CO_2$ de origen natural y, además de agua, la corriente gaseosa puede contener $N_2$, $CH_4$, CO, $O_2$, $H_2S$, $SO_x$, $NO_x$ e $H_2$, así como otros compuestos empleados durante el proceso de captura, deshidratación y control de la corrosión (Boot-Handford *et al.* 2014). La presencia de estas impurezas afecta a las propiedades físicas y de transporte del $CO_2$, y también puede generar problemas de operación relacionados con la seguridad ($H_2S$) y la corrosión ($H_2O$ y $O_2$) (Boot-Handford *et al.* 2014). Por tanto, el $CO_2$ a transportar debe cumplir unas especificaciones concretas que minimicen estos efectos. De hecho, se estima que para el transporte en tubería los compuestos no condensables deben reducirse por debajo del 4%, aunque se aceptan contenidos de hasta el 10% para distancias cortas (Boot-Handford *et al.* 2014). El agua, por su parte, debe condensarse previamente hasta alcanzar una concentración muy baja que evite

problemas de corrosión y de formación de hidratos y hielo (Boot-Handford *et al.* 2014). Además, en el transporte de $CO_2$ se deben tener en cuenta aspectos relacionados con la seguridad. Esto es especialmente importante en el transporte mediante gasoductos que atraviesan zonas altamente pobladas, en los que se debe prestar una especial atención a la posible existencia de fugas y sobrepresiones.

### 1.2.3 Almacenamiento de $CO_2$

El objetivo último de todo proceso de captura es el almacenamiento seguro y definitivo de la corriente de $CO_2$. El confinamiento permanente del $CO_2$ se puede conseguir a través del almacenamiento geológico, para lo que es necesario que el emplazamiento se sitúe por debajo de 800 m, ya que a partir de esta profundidad el $CO_2$ alcanza las condiciones del estado supercrítico por el efecto del gradiente geotérmico y la presión hidrostática, reduciendo significativamente su volumen. Es posible inyectar el $CO_2$ en tres tipos de formaciones geológicas: yacimientos de petróleo o gas agotados, acuíferos salinos marinos o terrestres y yacimientos de carbón no explotables.

Los yacimientos de carbón no explotables se pueden emplear para el almacenamiento de $CO_2$ si poseen una adecuada permeabilidad, lo que permitiría al mismo tiempo la recuperación mejorada del metano (ECBM, del inglés *Enhanced Coal Bed Methane*) que puede estar adsorbido en las fracturas presentes entre las capas del carbón. De este modo sería posible recuperar alrededor del 90% del metano disponible (IPCC 2005), que sería liberado por el desplazamiento inducido por el $CO_2$, quedando éste adsorbido en la superficie del carbón. Este proceso está aún en fase de desarrollo y la capacidad de almacenamiento de este tipo de yacimientos es limitada, puesto que no debe almacenarse $CO_2$ en aquellos emplazamientos con posibilidad de ser explotados posteriormente.

Las mejores formaciones para el almacenamiento de $CO_2$ son los yacimientos de hidrocarburos agotados y los acuíferos salinos. Ambos deben estar formados por una roca porosa, adecuada para albergar $CO_2$ entre sus granos, y una roca sello impermeable que se sitúa por encima e impide que el $CO_2$ migre hacia la superficie. De este modo se logra un almacenamiento efectivo de la corriente capturada de $CO_2$. Se estima que los acuíferos salinos son las formaciones que presentan la mayor capacidad de almacenamiento de $CO_2$, a pesar de que su geología y distribución es menos conocida que la de los yacimientos de hidrocarburos. Además están mucho más repartidos por todo el mundo, lo que favorece su accesibilidad (IPCC 2005). Por otra parte, los yacimientos agotados de petróleo y gas natural son opciones atractivas para el almacenamiento de $CO_2$, ya que son estructuras muy estudiadas y existe una gran infraestructura disponible (IPCC 2005). La ventaja de estos emplazamientos es que, especialmente en el caso de los yacimientos de petróleo, es posible recuperar una cantidad adicional de hidrocarburos al inyectar $CO_2$. Esta técnica, conocida como recuperación mejorada de petróleo o EOR, se basa en que el $CO_2$ inyectado desplaza y fuerza la salida de petróleo adicional. Esto ofrece un incentivo económico importante, ya que bajo una explotación normal hasta dos tercios del petróleo disponible pueden permanecer en el yacimiento porque su extracción no es rentable (Shell 2014). Es por ello que la EOR puede suponer una oportunidad para impulsar el desarrollo del almacenamiento de $CO_2$. Es importante también mencionar que la inyección de $CO_2$ en formaciones geológicas profundas se realiza mediante su compresión e inyección a través de pozos. Este proceso tiene la ventaja de que puede aprovechar una gran parte del conocimiento y la tecnología ya existente en la industria de exploración y producción de petróleo y gas natural.

El $CO_2$ almacenado queda retenido en la formación geológica en base a cuatro mecanismos de entrampamiento (IPCC 2005; IEA 2012b). Inicialmente, tras la inyección del $CO_2$ éste tiende a ascender de manera

natural hasta que es finalmente detenido por una roca sello impermeable que garantiza la estanqueidad del almacén. Este primer mecanismo es lo que se conoce como entrampamiento estructural. Por otra parte, una fracción del $CO_2$ queda retenida en los poros de la roca por fuerzas de capilaridad, dando lugar al entrampamiento residual. A medida que transcurre el tiempo desde la inyección el $CO_2$ se va disolviendo en el agua. Esta agua ácida es más densa y tiende a hundirse, lo que constituye el entrampamiento por disolución. Finalmente, el $CO_2$ disuelto puede reaccionar con los minerales presentes en la roca quedando el $CO_2$ permanentemente almacenado por lo que se conoce como entrampamiento mineral. A medida que va transcurriendo el tiempo se va avanzando en el mecanismo de entrampamiento, aumentando así la seguridad del almacenamiento (IPCC 2005).

En la actualidad varias instalaciones están llevando a cabo operaciones de almacenamiento de $CO_2$ a escala industrial. Una de los más conocidos es el proyecto Sleipner, que captura y almacena desde el año 1996 el $CO_2$ contenido en el gas natural (9% $CO_2$) que se extrae de un yacimiento situado en el mar del Norte. Desde entonces se inyectan aproximadamente 1 $MtCO_2$ al año en un acuífero salino marino a más de 800 metros de profundidad, y se llevan a cabo labores de investigación y monitorización para caracterizar su comportamiento (IPCC 2005; Statoil 2013a). Desde el inicio de este proyecto y hasta principios del año 2013 se han almacenado en la formación geológica más de 14 $MtCO_2$ (Statoil 2013a). Por otra parte, el proyecto In Salah (Argelia) ha operado también de un modo similar, almacenando más de 3 $MtCO_2$ que han sido separadas del gas natural (hasta 10% $CO_2$) en un acuífero salino. El ciclo de vida de este proyecto se extendió entre 2004 y 2011, año en el que finalizó la inyección como medida de seguridad principalmente debido a dudas relacionadas con la capacidad del almacén (Statoil 2013b). En 2008 comenzó la inyección de $CO_2$ procedente también del gas natural extraído (5-6% de $CO_2$) en Snøhvit (Mar

de Barents), en una formación salina marítima de roca arenisca porosa. En el año 2011 el almacenamiento de $CO_2$ se trasladó al yacimiento del que fue obtenido, a unos 2500 m por debajo del fondo marino, y a principios de 2013 ya se habían inyectado unas 2 $MtCO_2$ (Statoil 2013c). Por último, el proyecto Weyburn-Midale (Canadá) inyecta $CO_2$ para la recuperación mejorada de petróleo en yacimientos agotados desde el año 2000 a razón de 3 $MtCO_2$ anuales. Para ello emplea $CO_2$ procedente de una planta de gasificación situada en EEUU, que se captura, comprime y transporta hasta los yacimientos de Weyburn y Midale (PTRC 2013).

## 1.3 Tecnologías de carbonatación-calcinación para la captura de $CO_2$

Esta sección profundiza en las tecnologías que emplean la reacción de carbonatación-calcinación para la captura de $CO_2$, puesto que constituyen la base de esta Tesis Doctoral. Estas tecnologías hacen uso del CaO como sorbente sólido que reacciona reversiblemente con $CO_2$:

$$CaO_{(s)} + CO_{2\,(g)} \leftrightarrow CaCO_{3\,(s)} \qquad \Delta H_{R,\,298K} = -178.8\ kJ/mol$$

El empleo de CaO como sorbente de $CO_2$ fue ya sugerido por varios autores en el siglo XIX, aunque es en el siglo XX cuando se aplicó este concepto al proceso denominado *$CO_2$ acceptor gasification process* (Curran *et al.* 1967), que fue demostrado con éxito en una planta que procesaba 27 toneladas diarias de carbón (Fink *et al.* 1974). La novedad que incluía este proceso era la reacción del CaO (procedente de caliza o dolomita calcinada) con el $CO_2$ generado durante la gasificación del carbón con un doble objetivo: suministrar el calor necesario para la reacción de gasificación evitando así el alto coste derivado del empleo de oxígeno en el gasificador y, a la vez, obtener un gas rico en $H_2$ de alto valor energético. La finalidad de este proceso no era la captura de $CO_2$, puesto que en el regenerador o

calcinador se obtenía una corriente diluida de $CO_2$ como consecuencia de la quema del combustible adicional necesario en presencia de aire.

Sin embargo, posteriores estudios comenzaron a considerar la captura de $CO_2$ con CaO como un proceso en sí mismo, capaz de reducir las emisiones de $CO_2$ y que presenta unos requerimientos y características propias, tales como la necesidad de generar una corriente de $CO_2$ concentrada en el calcinador. Partiendo de esta base, Silaban y Harrison (1995) estudiaron la reacción de carbonatación-calcinación a distintas temperaturas, presiones y composiciones de gas con el objetivo de delimitar condiciones adecuadas de operación. Posteriormente, Shimizu *et al.* (1999) fueron los pioneros en proponer un proceso para la captura del $CO_2$ presente en los gases de combustión con CaO mediante un sistema de dos reactores de lecho fluidizado (carbonatador y calcinador) y quemando un combustible con oxígeno puro en el calcinador para generar una corriente altamente concentrada en $CO_2$.

La captura de $CO_2$ mediante ciclos de carbonatación-calcinación (CaL en inglés, *Calcium Looping*) se ha propuesto como alternativa en las configuraciones de pre- y post-combustión. En los procesos de pre-combustión, basados en la propuesta de Curran *et al.* (1967), la etapa de captura tiene lugar simultáneamente junto con la gasificación o reformado del combustible y la reacción conocida como *Water Gas Shift*. La regeneración del sorbente, por su parte, requiere un aporte de energía para la calcinación que se consigue mediante la quema de un combustible adicional con una mezcla $O_2/CO_2$ para evitar diluir la corriente de $CO_2$. Esto es muy problemático en sistemas a alta presión (necesarios para la mayor parte de los procesos de producción de hidrógeno a gran escala). No obstante, recientemente han aparecido configuraciones más avanzadas con ciclos Ca/Cu que emplean la energía liberada en la reducción exotérmica del óxido de cobre para la calcinación del $CaCO_3$ (Abanades *et al.* 2010), evitando así la necesidad de la unidad de separación del aire para la

obtención de oxígeno puro. Por otra parte, existe un grupo de procesos basados en la tecnología de carbonatación-calcinación cuyo objetivo es la captura del $CO_2$ generado durante la combustión, pudiendo distinguir entre aquellos en los que la etapa de carbonatación es simultánea a la combustión (*in situ*) y los que separan el $CO_2$ contenido en los gases de salida del combustor (post-combustión). Estos sistemas emplean dos reactores de lecho fluidizado, carbonatador y calcinador, en cuyo interior tiene lugar la captura de $CO_2$ y la regeneración del sorbente, respectivamente, obteniendo como resultado una corriente concentrada de $CO_2$ adecuada para su acondicionamiento, transporte y almacenamiento final. A continuación se exponen una serie de consideraciones que son comunes para la captura de $CO_2$ con CaO post-combustión e *in situ*. Sus características particulares se describen con más detalle en las secciones 1.3.1 y 1.3.2 respectivamente, ya que el desarrollo de estos nuevos procesos constituye el núcleo de la presente Tesis Doctoral.

Como se muestra en la Figura 5, la reacción de carbonatación-calcinación está sujeta a restricciones termodinámicas de equilibrio debido a su carácter reversible. Por tanto, la temperatura de las etapas de carbonatación y calcinación debe ser fijada en base a tales limitaciones. En este caso, y dado que la finalidad de este tipo de sistemas es maximizar la eficacia de captura de $CO_2$, la temperatura óptima de operación del carbonatador se encuentra en el intervalo entre 600 y 700ºC. Estas condiciones permiten alcanzar una baja concentración de $CO_2$ en el gas de salida del proceso a la vez que se mantiene una cinética de reacción rápida, lo que conlleva un diseño compacto del carbonatador. La etapa de calcinación, en cambio, se debe realizar a temperaturas alrededor de 900ºC con el objetivo de garantizar la calcinación del sorbente en una atmósfera altamente concentrada en $CO_2$.

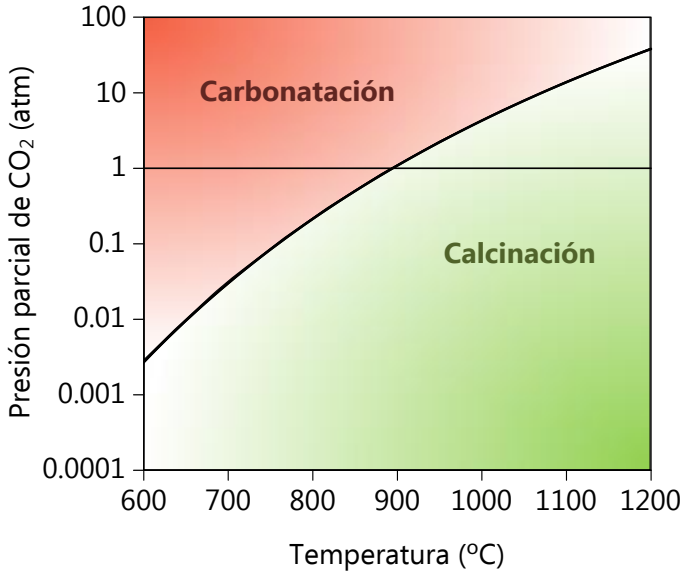


**Figura 5.** Curva de equilibrio entre CaO y $CaCO_3$ a presión atmosférica.

Es importante destacar que los procesos de captura de $CO_2$ basados en la tecnología de carbonatación-calcinación presentan una serie de ventajas competitivas que los hacen muy atractivos. En primer lugar, son procesos que operan a alta temperatura, de modo que es posible la recuperación efectiva de gran parte de la energía suministrada para la calcinación y su integración en un ciclo de vapor, lo que reduce significativamente la penalización energética del proceso (Shimizu *et al.* 1999; Abanades *et al.* 2005; Romeo *et al.* 2008; Hawthorne *et al.* 2009; Romano 2009; Lisbona *et al.* 2010; Yongping *et al.* 2010; Lasheras *et al.* 2011; Martínez *et al.* 2011a; Zhao *et al.* 2013). Otra característica importante es que las reacciones involucradas son ampliamente conocidas y además son rápidas, lo que permite el diseño de reactores compactos. Asimismo, el tratamiento de grandes flujos de gases de combustión o proceso requiere el empleo de reactores de lecho fluidizado circulante, que son reactores ya estudiados y desarrollados a escala industrial y, por tanto, es posible acelerar el escalado de la tecnología de carbonatación-calcinación aprovechando la información

disponible. Otro aspecto a tener en cuenta es que estos procesos emplean caliza como precursor de CaO, siendo éste un material abundante, bien distribuido a nivel mundial y barato. Finalmente, el CaO presente en el carbonatador y el calcinador permite la captura simultánea y efectiva de $SO_2$ (Li *et al.* 2005; Grasa *et al.* 2008; Manovic *et al.* 2009) y, además, existe la posibilidad de emplear el sorbente purgado del proceso como materia prima en los procesos de desulfuración (Sun *et al.* 2006; Grasa *et al.* 2008) o para la fabricación del cemento siempre que presente una composición compatible con las características requeridas para este material (Dean *et al.* 2011a; Dean *et al.* 2011b; Romeo *et al.* 2011; Telesca *et al.* 2014).

Sin embargo, un gran inconveniente asociado a esta tecnología es la desactivación que experimentan las partículas a medida que se someten a sucesivos ciclos de carbonatación-calcinación. Este fenómeno es el resultado del deterioro de la estructura porosa del sorbente durante la etapa de calcinación a consecuencia de la sinterización de las partículas (Borgwardt 1985; Fuertes *et al.* 1991; Abanades y Álvarez 2003), lo que reduce la superficie disponible para la absorción de $CO_2$ y, por tanto, la actividad del sorbente, que alcanza conversiones residuales del 7-8% (Grasa y Abanades 2006). Esta desactivación se ve especialmente favorecida cuando el calcinador opera a temperaturas superiores a 950ºC, lo que indica la necesidad de limitar la temperatura de calcinación (González *et al.* 2008). La disminución progresiva de la actividad de las partículas de CaO con los ciclos de carbonatación y calcinación obliga a alimentar continuamente caliza fresca al sistema al objeto de mantener la actividad del sorbente en valores adecuados para el proceso, a la vez que se extrae una purga equivalente. En la actualidad se están llevando a cabo numerosos estudios de reactivación del sorbente con la finalidad de incrementar la actividad de las partículas de CaO y reducir el aporte de caliza fresca. Es por ello que en los últimos años se han propuesto distintas técnicas de reactivación (incluidas en las revisiones de Blamey et al. (2010), Yu et al. (2011), Abanades

(2013) y Kierzkowska et al. (2013)) entre las que se encuentran la inclusión de una etapa de hidratación, el empleo de sorbentes dopados y sorbentes sintéticos, la auto-reactivación y la recarbonatación. Esta última alternativa forma parte del contenido de esta Tesis Doctoral y es analizada con mayor profundidad en la sección 4.3.

Por último cabe destacar que el sorbente también experimenta fenómenos de atrición durante el proceso, dando lugar a una fracción de partículas de tamaño reducido que puede no ser retenida en el sistema. Esta pérdida de estabilidad mecánica ocurre principalmente durante la primera calcinación (Coppola *et al.* 2012) y puede, por tanto, ser compensada mediante el suministro de una cantidad adicional de sorbente fresco.

### 1.3.1 Captura de $CO_2$ con CaO en sistemas post-combustión

La configuración más aceptada para los sistemas de CaL post-combustión, cuyo esquema se muestra en la Figura 6, consta de un carbonatador y calcinador de lecho fluidizado circulante. La preferencia por reactores circulantes frente a burbujeantes se debe en este caso a la necesidad de operar a altas velocidades de gas (3-6 m/s) para reducir el tamaño (sección transversal) de las instalaciones, ya que el flujo de gases de combustión a tratar es muy elevado (aproximadamente 300 $Nm^3/s$ para una central térmica de carbón de 1000 $MW_t$). En este proceso, los gases de combustión generados en la central térmica con un cierto contenido en $CO_2$, $F_{CO2\ in}$, se alimentan al carbonatador, donde el $CO_2$ reacciona a 650ºC con el lecho de partículas de CaO, $n_{Ca}$, quedando así retenido en forma de $CaCO_3$. Como resultado se generan una corriente gaseosa que presenta una baja concentración de $CO_2$ y se emite directamente a la atmósfera, $F_{CO2\ out}$, y una corriente sólida formada por $CaCO_3$ y CaO no reaccionado, $F_{Ca}$. Esta corriente parcialmente carbonatada se lleva al calcinador, en cuyo interior se quema un combustible con una mezcla de $O_2/CO_2$ para suministrar la energía requerida en la descomposición del $CaCO_3$, que tiene lugar a

temperaturas de 870-920ºC. El CaO generado se devuelve al carbonatador, $F_{Ca}$, y la corriente concentrada de $CO_2$ que abandona el calcinador, $F_{CO2\ calc}$, se somete a procesos de acondicionamiento y posterior compresión para su transporte y almacenamiento permanente. De este modo, los gases de salida del calcinador contienen el $CO_2$ capturado de los gases de combustión junto con el procedente de la combustión de carbón en el calcinador. Es importante mencionar que existe una alimentación de caliza fresca, $F_0$, que permite compensar el descenso en la actividad del sorbente debido a los sucesivos ciclos de carbonatación-calcinación. Además, del sistema se extrae una purga equivalente, $F_0$, que evita la concentración de inertes (cenizas y $CaSO_4$) en el sistema.

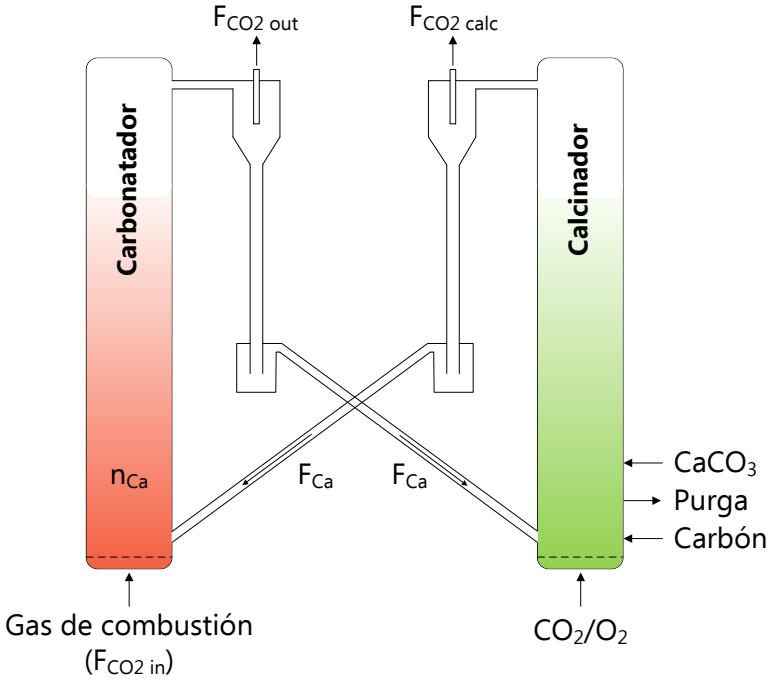


**Figura 6.** Esquema de la configuración de CaL post-combustión.

La tecnología de CaL post-combustión para el tratamiento del $CO_2$ presente en los gases de combustión ha experimentado una rápida evolución en los últimos años. Comenzó siendo un mero concepto, inicialmente propuesto

por Shimizu *et al.* (1999), y posteriormente estudiado por Abanades *et al.* (2005), quienes propusieron diversas alternativas al esquema clásico de la Figura 6 entre las que se encuentran la transferencia directa de calor al calcinador desde un combustor a través de paredes metálicas o indirecta mediante una corriente de sólidos a alta temperatura, y la captura de $CO_2$ *in situ* en el interior de un combustor-carbonatador de biomasa a baja temperatura (700ºC). La captura efectiva de $CO_2$ fue demostrada por primera vez en un carbonatador de lecho burbujeante discontinuo durante un corto número de ciclos de calcinación-carbonatación (11 ciclos) (Abanades *et al.* 2004), poniendo de manifiesto la necesidad de disponer de suficiente lecho activo de partículas de CaO. Estudios posteriores en plantas piloto de mayor tamaño obtuvieron también resultados satisfactorios, confirmando el potencial de esta tecnología. Lu *et al.* (2008) llevaron a cabo con éxito la captura de $CO_2$ con CaO en una instalación de 75 $kW_t$ ubicada en el CANMET (Ottawa-Canadá) que operaba en modo semi-continuo. Posteriormente, eficacias de captura de $CO_2$ de entre el 70 y 97% fueron obtenidas en experimentos realizados en una planta piloto de 30 $kW_t$ (INCAR-CSIC) en la que tanto el carbonatador como el calcinador son reactores de lecho fluidizado circulante interconectados (Abanades *et al.* 2009; Alonso *et al.* 2010). Subsiguientes campañas experimentales llevadas a cabo en esta instalación confirmaron estos resultados, que se interpretaron adecuadamente con un sencillo modelo de reactor en función de la actividad del sorbente y el inventario de sólidos del carbonatador (Rodríguez *et al.* 2011). Un estudio llevado a cabo por Charitos *et al.* (2010) en el IFK (Stuttgart-Alemania) reveló también la posibilidad de alcanzar en continuo eficacias de captura superiores al 90% en una instalación de 10 $kW_t$. Ensayos adicionales en esta planta, que emplea un carbonatador de lecho fluidizado circulante y un calcinador de lecho fluidizado burbujeante, permitieron capturar del orden de 8-10 $mol/m^2s$ de $CO_2$, que son valores análogos a los esperables a escala industrial (Charitos *et al.* 2011).

Como resultado del éxito obtenido en las plantas piloto mencionadas, la tecnología de CaL post-combustión ha alcanzado en los últimos años la escala de 1.7 $MW_t$ con una planta piloto con diseño básico realizado en el INCAR-CSIC y construida en La Pereda (Mieres-España) a través de un consorcio entre el CSIC, HUNOSA, ENDESA y la multinacional Foster Wheeler (Sánchez-Biezma *et al.* 2012; Sánchez-Biezma *et al.* 2013; *Publicación 1*). La descripción y los resultados experimentales obtenidos hasta el momento durante la operación de esta planta piloto se detallan en la sección 3.1, puesto que constituyen una parte esencial de esta Tesis. Otras instalaciones construidas y operadas recientemente también han dado lugar a resultados satisfactorios con eficacias de captura en el carbonatador del 85% en la planta piloto de 1 $MW_t$ Darmstadt (Galloy *et al.* 2011; Plötz *et al.* 2012; Kremer *et al.* 2013; Ströhle *et al.* 2014) y superiores al 90% en la planta piloto de 200 $kW_t$ en Stuttgart (Hawthorne *et al.* 2011; Dieter *et al.* 2012; Dieter *et al.* 2014), y actualmente se está construyendo en Heping (Taiwan) una planta de 1.9 $MW_t$ que consta de un carbonatador de lecho burbujeante y un calcinador rotatorio (Chang *et al.* 2013). Sin embargo, como se ha mencionado anteriormente, la configuración de carbonatador y calcinador como lechos fluidizados circulantes interconectados (elegida para la planta de La Pereda y más tarde para las de Darmstadt y Stuttgart) es la preferida para poner en contacto los altos flujos de gas (velocidades de gas en los reactores de 3-6 m/s) con los también elevados flujos de sólidos (del orden de 5-20 $kg/m^2s$). La existencia de muchos componentes y materiales característicos de centrales comerciales de combustión en lecho fluidizado circulante (como la propia central térmica de La Pereda) ha facilitado el rápido escalado que ha experimentado esta tecnología en tan sólo unos años. Las características similares de los sólidos que circulan en el sistema ($CaCO_3$, CaO, $CaSO_4$, cenizas) ha facilitado el diseño en detalle de dispositivos mecánicos (ciclones, líneas de retorno de sólidos, válvulas de sólidos o *loop-seals*, sistemas de control de flujo de sólidos, etc) partiendo de los conocimientos ya existentes.

En el diseño básico de los reactores de carbonatación y calcinación, existen dos variables clave: el flujo de CaO entre reactores y el inventario de partículas de CaO en el carbonatador, ya que determinan el tiempo de residencia de los sólidos en este reactor y el inventario de sólidos activos para la captura de $CO_2$. Para garantizar una eficacia de captura de $CO_2$ elevada, y teniendo en cuenta que normalmente se trabaja en condiciones de baja actividad del sorbente, es necesario disponer de inventarios de partículas en el carbonatador de hasta 1000 kg/m$^2$, y que la circulación de sólidos, medida como la relación $F_{Ca}/F_{CO2}$, esté entre 5 y 20. Valores de $F_{Ca}/F_{CO2}$ muy elevados no son deseables, ya que conllevan un elevado consumo energético en el calcinador para calentar la corriente de sólidos desde la temperatura de carbonatación a la de calcinación (Rodríguez *et al.* 2008) y reducen el tiempo de residencia en los reactores. Otra variable de proceso importante es el flujo de caliza fresca que se alimenta de modo continuo al sistema. Al igual que en el caso de la circulación de sólidos, se debe llegar a un valor óptimo de $F_0$ que represente un equilibrio entre una adecuada actividad de los sólidos y una mínima penalización energética para el sistema (Rodríguez *et al.* 2008; Romeo *et al.* 2009), lo que habitualmente se traduce en relaciones $F_0/F_{Ca}$ del orden de 0.1 en presencia de contenidos moderados de $CaSO_4$ y cenizas en el sistema. Estas condiciones permitirían capturar alrededor de 9-10 mol/m$^2$s de $CO_2$, que es el objetivo para sistemas de captura asociados a centrales térmicas de carbón convencionales.

La eficacia de captura de $CO_2$ se puede calcular en función de las principales variables de operación empleando los modelos del carbonatador propuestos hasta el momento (Hawthorne *et al.* 2008; Alonso *et al.* 2009; Charitos *et al.* 2011; Lasheras *et al.* 2011; Romano 2012; Ylätalo *et al.* 2012; Ylätalo *et al.* 2014). Uno de ellos es el modelo cero-dimensional sencillo planteado por Charitos *et al.* (2011), que está basado en el modelo de Alonso *et al.* (2009), y ha demostrado ser altamente efectivo en la

interpretación de datos experimentales obtenidos en planta piloto (Charitos *et al.* 2011; *Publicación I*). El parámetro clave de diseño de este modelo es el tiempo espacial activo, $\tau_a$, que establece el inventario activo de partículas de CaO con una actividad igual a la máxima capacidad de captura de $CO_2$ del sorbente, $X_{ave}$, necesario para tratar un determinado flujo de $CO_2$ y alcanzar un cierto valor de eficacia de captura. En los últimos años se han publicado también otros modelos que incluyen una descripción más sofisticada de los fenómenos que tienen lugar en el interior del carbonatador. Este es el caso de los modelos unidimensionales desarrollados por Hawthorne *et al.* (2008), Lasheras *et al.* (2011), Romano (2012), Ylätalo *et al.* (2012) e Ylätalo *et al.* (2014), que integran un submodelo hidrodinámico para tener en cuenta la distribución de las partículas dentro del reactor. De manera análoga se pueden encontrar en la literatura modelos que describen el funcionamiento del calcinador, como el propuesto por Martínez *et al.* (2013) u otros más avanzados como el modelo unidimensional de Ylätalo *et al.* (2012) o el modelo tridimensional desarrollado por Ylätalo *et al.* (2013).

Por otra parte, existen varios trabajos que realizan un estudio del consumo y la penalización energética asociada a los sistemas CaL post-combustión integrados en una central térmica convencional de carbón (Shimizu *et al.* 1999; Abanades *et al.* 2005; Romeo *et al.* 2008; Hawthorne *et al.* 2009; Romano 2009; Lisbona *et al.* 2010; Yongping *et al.* 2010; Lasheras *et al.* 2011; Martínez *et al.* 2011a; Zhao *et al.* 2013). Todos ellos coinciden en que es posible recuperar una gran parte de la energía suministrada al proceso en forma de energía eléctrica adicional generada mediante un nuevo ciclo de vapor, empleando para ello los principales focos de aprovechamiento de energía del proceso, que se indican a continuación: i) la energía liberada en el carbonatador debido a la reacción exotérmica que tiene lugar en su interior; ii) los gases de salida del carbonatador a 650ºC, que se enfrían hasta 100-130ºC previa expulsión por chimenea; iii) los gases de salida del calcinador a 870-920ºC, que se enfrían antes del proceso de purificación y

compresión; iv) el flujo de sólidos de purga a alta temperatura. Estos análisis incluyen además propuestas de integración de estas corrientes para minimizar así el impacto de la etapa de captura de $CO_2$ en el rendimiento neto del proceso. De manera general se obtiene que el empleo de la tecnología de carbonatación-calcinación para la captura de $CO_2$ en sistemas post-combustión (incluyendo la compresión de la corriente de $CO_2$) introduce una penalización energética de entre 6 y 8 puntos con respecto al rendimiento de la central térmica sin sistema de captura (Shimizu *et al.* 1999; Abanades *et al.* 2005; Romeo *et al.* 2008; Hawthorne *et al.* 2009; Romano 2009; Yongping *et al.* 2010; Lasheras *et al.* 2011; Martínez *et al.* 2011a), y el coste asociado se sitúa en torno a 20 €/t $CO_2$ evitado (Abanades 2013).

El calcinador es un elemento fundamental para la penalización energética de este tipo de sistemas, y es que este reactor requiere entre el 40 y 50% de la energía total suministrada, calculada como el conjunto de la energía asociada a la central térmica que genera los gases de combustión y al sistema de captura (Rodríguez *et al.* 2008). Esta energía se emplea para calentar los flujos de gases y sólidos que llegan al reactor y para la calcinación del flujo de caliza fresca alimentado y de la corriente de sólidos que llega del carbonatador (Rodríguez *et al.* 2008). Como ya se ha discutido previamente, el calcinador opera en condiciones de oxi-combustión, con la consiguiente penalización energética asociada ya que, pese a que el consumo de oxígeno en un sistema de CaL post-combustión es cercano a la mitad del necesario en una caldera de oxi-combustión de igual potencia total, la generación de oxígeno siempre supone un elevado consumo energético. El método de separación más desarrollado y capaz actualmente de suministrar grandes cantidades de oxígeno es la destilación criogénica del aire, cuyos requerimientos energéticos aumentan exponencialmente en función del grado de pureza deseado (Darde *et al.* 2009). Es por ello que

han surgido varias alternativas que buscan la reducción y/o eliminación del consumo de oxígeno puro en el calcinador, y se resumen a continuación.

Algunas de las opciones presentes en la literatura contemplan la transferencia de calor al calcinador a través de paredes metálicas (Abanades *et al.* 2005; Grasa y Abanades 2007; Strelow *et al.* 2012) o mediante tuberías a alta temperatura (Junk *et al.* 2013). Otra alternativa con gran potencial es la configuración de tres lechos (combustor, carbonatador y calcinador), que constituye en sí misma un nuevo diseño para una central térmica con captura de $CO_2$ integrada (Abanades *et al.* 2005; Martínez *et al.* 2011b). Este esquema se basa en el empleo de sólidos como transportadores de calor. El combustor, que opera a temperaturas cercanas a los 1000ºC, genera los gases de combustión que se alimentan al carbonatador y, al mismo tiempo, calienta la corriente de sólidos que procede del calcinador. Este flujo de partículas a alta temperatura circula continuamente entre el combustor y el calcinador, y contiene la energía necesaria para la calcinación. De este modo, se evita la necesidad de combustible y el consiguiente consumo de oxígeno en el interior de este reactor, reduciendo sustancialmente la penalización energética asociada a la captura de $CO_2$.

Otra posible configuración del sistema de carbonatación-calcinación destinada a minimizar o anular la necesidad de $O_2$ en el calcinador es la propuesta recientemente por Abanades *et al.* (2013), en la que se han aprovechado los resultados obtenidos en la Publicación IV de esta Tesis Doctoral. Este nuevo proceso hace uso de uno o varios combustores auxiliares adiabáticos que emplean aire como comburente y cuyos gases de salida se introducen, en último término, en el carbonatador del sistema. En este esquema, una fracción del gas de combustión generado en un combustor a alta temperatura se pone en contacto con los sólidos que salen del carbonatador en un precalentador ciclónico. De este modo, su temperatura se incrementa hasta valores próximos al equilibrio (nunca superiores para evitar su calcinación), reduciendo así la demanda de energía

del calcinador asociada a esta corriente. Además, otra fracción del gas de combustión calienta, en un segundo precalentador ciclónico, una corriente de sólidos recirculados del calcinador por encima de la temperatura de calcinación, proporcionando un aporte adicional de energía a este reactor (Abanades *et al.* 2013). Como consecuencia, se consigue reducir o incluso evitar la necesidad de combustible en el calcinador (Abanades *et al* 2013).

Las opciones presentadas en los párrafos anteriores, aunque prometedoras, están aún en fase de estudio y necesitan ser demostradas experimentalmente.

### 1.3.2 Captura de $CO_2$ *in situ* en sistemas de combustión de biomasa con CaO

La combustión de biomasa y captura del $CO_2$ generado presenta un gran interés como proceso generador de energía con emisiones negativas de $CO_2$ (IPCC 2014) para el que la tecnología de carbonatación-calcinación se erige como una alternativa con gran potencial. El concepto de captura de $CO_2$ *in situ* con CaO, desarrollado por Curran *et al.* (1967), se propuso inicialmente para sistemas de combustión de biomasa a presión (Wang *et al.* 2004; Abanades *et al.* 2005). Sin embargo, y debido a sus dificultades intrínsecas (altas temperaturas de calcinación y/o presurización y despresurización de corrientes), rápidamente fue adaptado a sistemas que operan a presión atmosférica.

El esquema del proceso se muestra en la Figura 7, y es análogo al representado en la Figura 6 para sistemas CaL post-combustión, con la diferencia de que en este caso las reacciones de combustión y captura de $CO_2$ tienen lugar simultáneamente en un único reactor denominado combustor-carbonatador. Esta particularidad del proceso hace que la biomasa sea un combustible idóneo para esta configuración, ya que su alta reactividad permite llevar a cabo la reacción de combustión a temperaturas

más bajas, lo que favorece la consecución de elevadas eficacias de captura de $CO_2$. De este modo, en el esquema de la Figura 7 el combustor-carbonatador opera a 700ºC y genera un flujo de $CO_2$ de combustión, $F_{CO2\ comb}$, que es capturado en forma de $CaCO_3$. La energía necesaria para descomposición endotérmica del $CaCO_3$ en el calcinador (870-920ºC) se aporta mediante la combustión de biomasa u otro combustible en presencia de una mezcla $O_2/CO_2$.

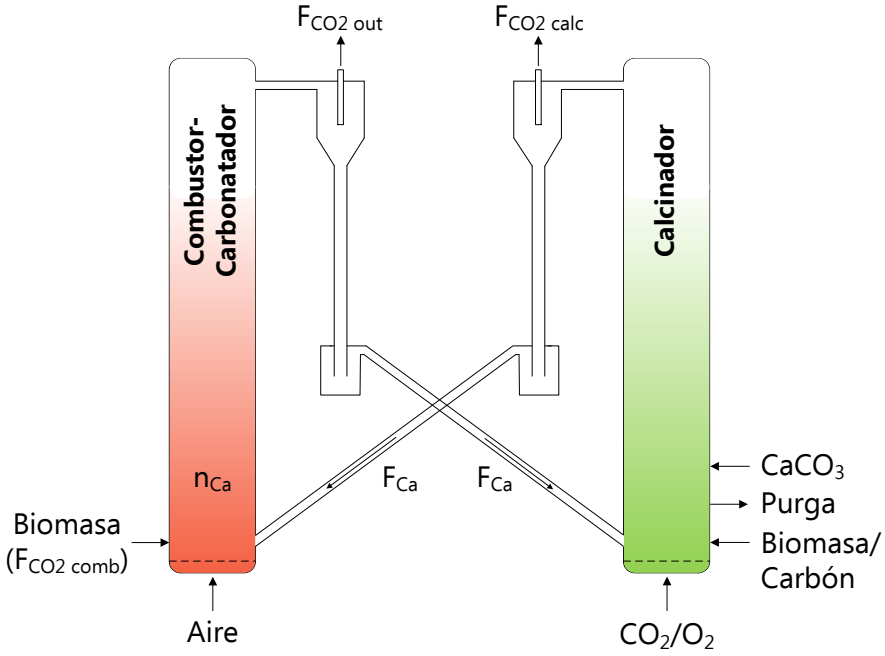


**Figura 7.** Esquema de la configuración de combustión de biomasa y captura de $CO_2$ *in situ* con CaO.

Este nuevo concepto presentado en la Figura 7 ha sido demostrado con éxito en una planta de 30 $kW_t$ ubicada en el INCAR-CSIC, en la que se obtuvieron eficacias de captura superiores al 80% en condiciones de suficiente inventario de partículas en el combustor-carbonatador y adecuada circulación de sólidos entre reactores (Abanades *et al.* 2011a; Alonso *et al.* 2011). Estos resultados experimentales fueron además

interpretados por medio de un modelo propuesto para el combustor-carbonatador que tiene en cuenta la generación y captura simultánea de $CO_2$ (Abanades *et al.* 2011a; Alonso *et al.* 2011). De igual modo se han obtenido resultados satisfactorios durante varias campañas experimentales llevadas a cabo en una planta piloto de 300 $kW_t$ situada en La Robla (León) (*Publicación II*). La descripción de la instalación, del procedimiento experimental empleado y de los principales resultados forma parte de la aportación de esta Tesis Doctoral en forma de la *Publicación II*, y se presenta en la sección 3.2.

De igual modo a como se ha descrito en la sección 1.3.1 para el caso de post-combustión, las variables que más influencian el comportamiento del combustor-carbonatador son el inventario de sólidos activos en el reactor y la circulación de sólidos entre reactores, que determina el tiempo de residencia de las partículas. Asimismo, una característica propia del proceso está relacionada con la composición que presentan ciertos tipos de biomasa, con un bajo contenido en cenizas y casi nulo en azufre, lo que contribuye a disminuir la cantidad de inertes en el sistema y a reducir la desactivación del sorbente como consecuencia de la formación de $CaSO_4$. Sin embargo, un aspecto negativo a considerar en este tipo de procesos es que la combustión a baja temperatura puede dar lugar a la generación de inquemados (CO, $C_xH_y$, etc) (Nussbaumer 2003). Durante los experimentos llevados a cabo en plantas piloto con la configuración de la Figura 7 se han detectado emisiones de CO e hidrocarburos (medidos como $CH_4$) en casos en los que la alimentación de biomasa, la mezcla entre el comburente y el combustible, la temperatura, el exceso de aire o el tiempo de residencia de la biomasa en el combustor no son adecuados (Alonso *et al.* 2011; *Publicación II*). Es por tanto importante evitar estas situaciones para reducir al mínimo la formación de este tipo de compuestos.

El sistema mostrado en la Figura 7 puede operar como una planta aislada o en combinación con otras configuraciones empleadas en la generación de

energía (Abanades *et al.* 2011b; Ozcan *et al.* 2014). Así, una opción para eliminar posibles inquemados en la corriente de gases del combustor-carbonatador es alimentar esta corriente a la caldera de combustión de una planta de generación convencional para asegurar así su combustión completa. En lo que se refiere a reducir el consumo asociado a la etapa de regeneración del sorbente, y dado que no se prevé que las plantas de combustión de biomasa alcancen tamaños tan elevados como las centrales de combustión de carbón, una alternativa consiste en hacer uso de la economía de escala. De este modo, el $O_2$ necesario para la calcinación del $CaCO_3$ se puede obtener en una unidad de separación del aire cercana de mayor tamaño que abastezca también a una caldera de oxi-combustión o al calcinador de una planta de captura de $CO_2$ post-combustión (Abanades *et al.* 2011b; Ozcan *et al.* 2014). También se puede aprovechar la sinergia entre un sistema CaL post-combustión y una planta de combustión de biomasa y captura *in situ*, de manera que exista un único calcinador capaz de aportar el flujo de CaO al carbonatador y al combustor-carbonatador, respectivamente (Abanades *et al.* 2011b; Ozcan *et al.* 2014).

Por último, los costes de este tipo de sistemas han sido analizados en una reciente publicación (Ozcan *et al.* 2014). De este estudio se desprende que los costes de la configuración de combustión de biomasa y captura de $CO_2$ *in situ* con CaO mostrada en la Figura 7 toman valores de 43 €/t $CO_2$ evitado, y se pueden reducir hasta -1.1 €/t $CO_2$ evitado si se consideran incentivos a la captura de $CO_2$ (precio de los derechos de emisión de 14 €/t $CO_2$) y al empleo de biomasa como combustible (certificado verde igual a 50 €/MWe) (Ozcan *et al.* 2014). Estos costes, ligeramente inferiores a los asociados a la configuración de oxi-combustión de biomasa, pueden alcanzar valores significativamente inferiores si se hace uso de la economía de escala con las configuraciones descritas en el anterior párrafo.

# 2. Objetivos y justificación de la Tesis

Como se ha discutido en el punto anterior, la captura de $CO_2$ mediante CaO en fuentes estacionarias de emisión es una tecnología que presenta un gran potencial para la reducción de los requerimientos energéticos y los costes de la etapa de captura de $CO_2$. Es por ello que la actividad de investigación desarrollada en esta Tesis Doctoral está dirigida a avanzar y consolidar el desarrollo de esta tecnología de captura de $CO_2$ en algunas de sus principales rutas de proceso, demostrando su viabilidad técnica a escalas crecientes en planta piloto y optimizando aquellos aspectos que se consideran más críticos en el desarrollo y escalado de dichos procesos.

Los estudios realizados hasta el momento en sistemas de combustión a escala de laboratorio en diversas plantas piloto indican que se trata de una opción viable y capaz de lograr altas eficacias de captura de $CO_2$ en condiciones de operación razonables. No obstante, es necesario obtener información de estos sistemas a escalas mayores de operación para poder predecir con mayor certeza su comportamiento a nivel industrial. De igual manera, es importante progresar en la optimización del proceso, así como en el desarrollo y validación de los modelos de los reactores del sistema, de modo que sean capaces de relacionar las principales variables de operación con las observaciones experimentales sobre el comportamiento de dichos reactores.

Por tanto, el principal objetivo del trabajo incluido en esta Tesis Doctoral consiste en el desarrollo y puesta a punto de los sistemas de generación de energía por combustión de carbón o biomasa que integran la separación de $CO_2$ a alta temperatura con CaO. De este modo, se pretende avanzar hacia la implantación a escala industrial de la tecnología de carbonatación-calcinación para la captura de $CO_2$.

Este objetivo general se ha satisfecho por medio de un conjunto de estudios concretos que se recogen en forma de publicaciones en esta memoria. Estos trabajos se agrupan en dos bloques atendiendo a su contenido.

El primer bloque se centra en la generación de una amplia base de datos experimentales a escala de planta piloto y la validación de los modelos de reactor con los datos obtenidos. Como resultado de este trabajo, se incluyen en esta Tesis dos publicaciones que contienen información de las campañas experimentales llevadas a cabo en dos instalaciones de captura de $CO_2$ que presentan configuraciones de post-combustión e *in situ*, respectivamente. En este capítulo se incluye una descripción de las plantas piloto y el procedimiento empleado, así como los resultados obtenidos y su interpretación mediante el cierre de los principales balances de materia en la instalación.

El segundo bloque está relacionado con el modelado de reactores y la implementación de mejoras en el proceso de captura. En este sentido, se presentan cuatro publicaciones en las que se investigan y optimizan distintos aspectos de este tipo de sistemas. En la primera de ellas se hace un estudio para caracterizar el comportamiento hidrodinámico de los sistemas de lechos fluidizados circulantes interconectados empleados en la captura de $CO_2$ con CaO, puesto que la hidrodinámica es un aspecto fundamental que determina el comportamiento de estos reactores. La segunda publicación realiza un análisis del impacto que tiene la presencia de azufre y cenizas en el sistema en términos de reducción de la actividad del sorbente y la disminución de la eficacia de captura de $CO_2$, y se examina el efecto derivado de un incremento en la capacidad de captura de $CO_2$ de las partículas de CaO. Finalmente, los últimos trabajos están basados en un nuevo proceso propuesto para la reactivación del sorbente denominado recarbonatación. En el primero se realiza un estudio cinético de la reacción de carbonatación en condiciones de alta temperatura y alta presión parcial de $CO_2$, características de la recarbonatación, y se obtienen los parámetros

cinéticos de esta reacción. Haciendo uso de esta información cinética, la última publicación propone un modelo de diseño para el reactor de recarbonatación (recarbonatador) capaz de anticipar la eficacia del reactor en función de las condiciones de operación, en base a la información cinética disponible y un conjunto de suposiciones sencillas sobre el contacto gas-sólido. Este modelo se emplea para la realización de un diseño preliminar de un reactor de recarbonatación para una planta industrial de captura de $CO_2$ con CaO.

# 3. Demostración experimental de tecnologías de carbonatación-calcinación a escala de planta piloto

Como parte del desarrollo de esta Tesis Doctoral se ha participado en el diseño, ejecución e interpretación de resultados de diversas campañas experimentales en dos instalaciones de lechos fluidizados circulantes interconectados de escala semi-industrial: la planta piloto de captura de $CO_2$ post-combustión de 1.7 $MW_t$ de La Pereda (Asturias) y la planta piloto de 300 $kW_t$ de La Robla (León) para la captura *in situ* de $CO_2$. Estos estudios se han centrado prioritariamente en el análisis del comportamiento del carbonatador o combustor-carbonatador respectivamente, ya que es el elemento que determina la eficacia de captura de $CO_2$ obtenida en los respectivos procesos. El calcinador se ha mantenido en condiciones adecuadas para la regeneración del sorbente y el suministro continuo de un flujo de CaO a los reactores donde se lleva a cabo la carbonatación de dicho sólido con $CO_2$. Estos experimentos han permitido ampliar la base de datos experimentales disponibles de captura de $CO_2$ con CaO a alta temperatura en una variedad de condiciones de operación más cercanas a las esperables a escala industrial. La mayor parte de estas campañas experimentales, diseñadas y dirigidas con personal del grupo de captura de $CO_2$ del INCAR, han abarcado una semana de duración.

Forman parte de este capítulo las *Publicaciones I y II*, mostradas en las secciones 3.1.3 y 3.2.3 respectivamente, en las que se detallan las condiciones de operación empleadas en cada caso y se discuten los resultados experimentales recogidos, mostrando la influencia de distintas variables. Estas publicaciones incluyen además un análisis de los datos obtenidos en base a modelos disponibles para el reactor de carbonatación que están ligados a su vez con los trabajos específicos de modelado de

reactores y optimización de proceso presentados con más detalle en el capítulo 4 de esta Tesis Doctoral.

## 3.1 Captura de $CO_2$ post-combustión en la planta piloto de 1.7 $MW_t$ de La Pereda

Esta planta piloto, ubicada en la central térmica de La Pereda (Asturias), fue diseñada tras el éxito alcanzado por la planta de lechos fluidizados circulantes interconectados de 30 $kW_t$ del INCAR-CSIC y la firma de un acuerdo por parte de ENDESA, HUNOSA y CSIC (Agrupación de Interés Económico AIE "La Pereda $CO_2$"). El acuerdo de la AIE se extendió durante la fase de diseño en detalle a la empresa Foster Wheeler como socio tecnológico para desarrollar la tecnología de CaL post-combustión al 50% con la AIE "La Pereda". La concesión de una subvención del séptimo Programa Marco (7PM) de la UE (proyecto "CaOling") al proyecto amplió su alcance a otros socios e instalaciones del Reino Unido (*Imperial College*), Alemania (IFK - Universidad de Stuttgart), Finlandia (Universidad de Lappeenranta) y Canadá (Universidad de Ottawa).

La construcción de la instalación se inició en el año 2010, y en octubre de 2011 comenzó su puesta en marcha. Los primeros experimentos que se llevaron a cabo en esta planta comenzaron en enero de 2012 y, hasta el momento, ha operado 2600 h con combustión de carbón, de las cuales 650 h han sido en modo captura de $CO_2$ y, en particular, 170 h con el calcinador operando en condiciones de oxi-combustión.

### 3.1.1 Descripción de la instalación experimental

El núcleo de la instalación, mostrada en la Figura 8, es un sistema de dos reactores, carbonatador y calcinador, que operan como lechos fluidizados circulantes interconectados. Estos reactores están fabricados con material refractario y presentan un diámetro interno de 0.65 y 0.75 m respectivamente, adecuado para alcanzar velocidades de gas de 2-5 m/s,

similares a las encontradas en calderas de lecho fluidizado. Su altura de 15 m permite además garantizar inventarios y tiempos de residencia adecuados de los sólidos.

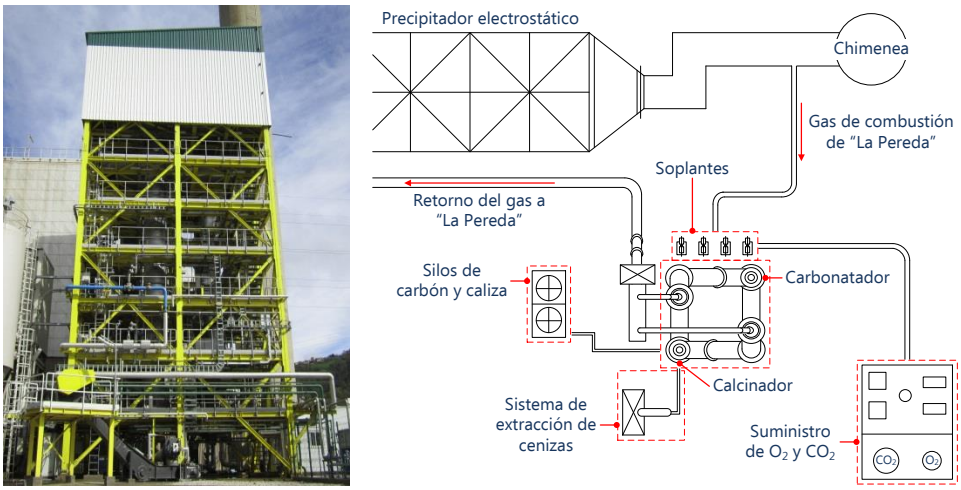


**Figura 8.** Izq.) Fotografía de la planta piloto de La Pereda. Dcha.) Integración de la planta piloto de captura de $CO_2$ de La Pereda con la central térmica.

Una característica muy importante de esta instalación es que se encuentra integrada con la central térmica de La Pereda (Asturias), de modo que el carbonatador se alimenta con una fracción del 1% aproximadamente de los gases de combustión de salida de la central, que es lo que corresponde a la generación de 1.7 $MW_t$. La central térmica, que es propiedad de HUNOSA, tiene una potencia de 50 $MW_e$ y emplea carbón bituminoso con un alto contenido en cenizas (alrededor del 36%) mezclado con estériles de escombrera, dando lugar a unos gases de combustión con una composición típica del 5.5%v $O_2$, 12.6%v $CO_2$, 7.0%v $H_2O$ y 250 ppm $SO_2$. Cuando estos gases se introducen en el carbonatador y tiene lugar la reacción entre el CaO y $CO_2$, se genera una gran cantidad energía que es necesario disipar para mantener la temperatura del reactor en torno a 650ºC. Para ello, el carbonatador dispone de un sistema de bayonetas retráctiles de 12 m refrigeradas por agua que permite variar la superficie de intercambio de

calor modificando el número de bayonetas utilizadas (hasta un máximo de cuatro) y moviendo las mismas verticalmente.

El calcinador de esta planta piloto cuenta con una alimentación continua de carbón, y puede operar en modo aire o en condiciones de oxi-combustión. En este último caso, el $O_2$ y $CO_2$ requeridos para la mezcla proceden de tanques de gases licuados, que se evaporan y se llevan posteriormente a un mezclador que suministra la composición y el caudal deseados. Antes de introducirse al calcinador, el gas de entrada (aire o una mezcla $O_2/CO_2$) se precalienta a 150-170ºC empleando un calentador eléctrico de carcasa y tubos.

A la salida de cada reactor existe un ciclón de alta eficacia diseñado con un tamaño de corte de 5 µm. Las partículas retenidas en el ciclón se dirigen hacia una válvula de sólidos o *loop-seal* fluidizada con aire que tiene una doble salida, de modo que la corriente sólida puede dirigirse hacia el otro reactor (circulación externa) o hacia el mismo (circulación interna). El flujo de sólidos que va hacia uno u otro reactor se controla por medio de unas válvulas de sólidos (*cone valves*). Por otra parte, tanto el carbonatador como el calcinador cuentan también con un quemador de propano, con una potencia instalada total de más de 1 $MW_t$, lo que permite elevar su temperatura durante el proceso de arranque hasta alcanzar la temperatura de ignición del carbón.

Otra característica de esta planta es la posibilidad de alimentar continuamente caliza fresca al sistema, lo que permite mantener un valor adecuado de la actividad del sorbente y compensar las pérdidas de sólidos a través de los ciclones por atrición. La caliza se introduce junto con el carbón al calcinador a través de un tornillo sin fin, previo paso por el sistema de dosificación. Existe también la opción de purgar sólidos del sistema de un modo continuo a través de una extracción ubicada en el lecho del calcinador, limitando así la acumulación de cenizas y $CaSO_4$.

La integración de esta planta piloto con la central térmica de La Pereda se muestra en la Figura 8 (dcha.). Como se puede observar en este esquema, existe una tubería que permite dirigir una pequeña fracción de los gases de salida de la central al carbonatador, tras su paso por el precipitador electrostático. Una vez finalizado el proceso de captura, las dos corrientes de gases que abandonan el sistema a través de los ciclones del carbonatador y calcinador se unen, y posteriormente se enfrían mediante su mezcla con una corriente de aire. Estos gases, ya a 350ºC, se devuelven a la corriente gaseosa principal de la central térmica en la zona del economizador (recuperación de calor) situada antes del precipitador electrostático, y finalmente se emiten a través de la chimenea.

La planta piloto de captura de $CO_2$ de La Pereda está ampliamente instrumentalizada para facilitar el seguimiento y control de los procesos que ocurren en el interior de los reactores. En la instalación se mide continuamente i) la temperatura en distintos puntos del interior de los reactores y de las corrientes gaseosas de entrada y salida del sistema mediante termopares tipo K; ii) la presión diferencial y relativa en distintos puntos de la instalación a través de sondas de presión; iii) los flujos de gas que se alimentan a los reactores y *loop-seals* empleando medidores tipo Venturi; iv) la composición del gas de entrada de la central térmica (contenido en $CO_2$, $O_2$, $SO_2$, $NO_x$) y la composición de las corrientes de salida del carbonatador y calcinador ($CO_2$, $O_2$, CO, $SO_2$, $NO_x$), utilizando analizadores de gases EMERSON NGA 2000 MLT; v) la humedad del gas procedente de la central térmica mediante la comparación entre el contenido en $O_2$ medido por el analizador y el registrado por una sonda de zirconio.

Además, existen varios puntos de extracción de muestras sólidas a distintas alturas en los reactores, lo que permite hacer un seguimiento a las partículas que participan en el proceso y obtener medidas de circulación mediante sondas isocinéticas. Estas muestras se someten a análisis para obtener su

distribución de tamaños y su composición química. Con este objetivo se emplea un analizador de carbono y azufre LECO CS230 que permite determinar el contenido en $CaCO_3$ y $CaSO_4$ de los sólidos, y un equipo de fluorescencia de rayos X SRS 3000 Bruker que mide su contenido en cenizas. Por último, se determina la reactividad de los sólidos con respecto al $CO_2$ y la máxima capacidad de captura de $CO_2$ por medio de una termobalanza descrita por González *et al.* (2008).

### 3.1.2 Procedimiento experimental

En esta sección se expone la secuencia de arranque de la planta piloto anteriormente descrita hasta alcanzar las condiciones adecuadas para llevar a cabo los experimentos de captura de $CO_2$.

Con la finalidad de facilitar el calentamiento inicial de la instalación, es importante partir de una carga de sólidos en el sistema que permita, además de un buen sellado de las *loop-seals*, una circulación adecuada entre reactores. Por tanto, el arranque se realiza con unos 1000 kg de sólidos en el interior del sistema, que pueden ser caliza fresca o bien sólidos procedentes de un experimento anterior. En este primer período tanto el carbonatador como el calcinador se fluidizan con aire y se calientan por medio de los quemadores que hay instalados a unos 4 m sobre la placa distribuidora. En este sentido es importante mantener un valor del caudal de aire a los reactores que facilite la circulación (de modo que los sólidos calentados por el quemador contribuyan a incrementar la temperatura del lecho del reactor contrario) sin consumir una gran cantidad de energía para su calentamiento. Además, durante esta primera etapa las bayonetas del carbonatador están retraídas lo máximo posible (la longitud insertada en el reactor es de 9 m) para facilitar el calentamiento del sistema.

Una vez que el lecho del calcinador alcanza una temperatura de 500ºC, se empieza a alimentar carbón lentamente, y cuando llega a 650ºC se apagan ambos quemadores y el flujo de carbón al calcinador se va incrementando

progresivamente hasta alcanzar condiciones de calcinación. A continuación se abre la válvula que hay entre el precipitador electrostático y la chimenea de la central térmica, lo que permite sustituir paulatinamente el caudal de aire de fluidización del carbonatador por el gas de combustión de la central térmica.

Durante la calcinación de la carga inicial la temperatura del calcinador aumenta gradualmente a medida que el grado de carbonato en el sistema disminuye. El carbonatador también se calienta, ya que recibe un flujo de CaO a alta temperatura que reacciona con $CO_2$ liberando energía en forma de calor. Para mantener la diferencia de temperaturas requerida entre los dos reactores se insertan las bayonetas a mayor profundidad en el carbonatador con el objetivo de disponer de mayor área de intercambio de calor y, si es necesario, se modifica la circulación entre reactores con cambios en la posición de la válvula que controla el flujo del carbonatador al calcinador. El método más fiable para estimar en línea el grado de calcinación del sorbente inicialmente presente en el sistema consiste en realizar el balance de carbono y calcular la diferencia entre el flujo de $CO_2$ de calcinación y el $CO_2$ capturado en el carbonatador, de modo que la coincidencia entre ambos valores es un indicativo del final de la calcinación de la carga inicial. También es posible anticipar el final de esta calcinación, aunque de un modo menos preciso, mediante un seguimiento de la temperatura del calcinador, puesto que ésta tiende a aumentar rápidamente cuando el contenido en $CaCO_3$ en el sistema es bajo. El proceso completo de calentamiento de la planta piloto hasta alcanzar temperaturas de calcinación tiene una duración aproximada de 20 horas, ya que esta planta contiene una gran masa de material refractario que consume mucha energía y tiempo para calentarse.

Una vez que la carga de caliza está suficientemente calcinada se disminuye la alimentación de carbón al calcinador, se ajusta la circulación entre reactores y se lleva el calcinador a condiciones de oxi-combustión. Para ello

se sustituye progresivamente la alimentación de aire al reactor por la mezcla $O_2/CO_2$ que contiene la composición de oxígeno deseada. Tras la estabilización del sistema se fijan las condiciones de operación y se añade, si es necesario, un flujo continuo de caliza fresca con la finalidad compensar las pérdidas de los sólidos más finos a través de los ciclones y sobre todo, estabilizar la actividad del sorbente en el valor deseado. También se realizan extracciones periódicas de sólidos desde el calcinador para evitar la acumulación excesiva de cenizas y $CaSO_4$. Además, se toman muestras sólidas del carbonatador y calcinador con el objetivo de caracterizar las partículas que participan en el proceso, y se determina experimentalmente el flujo de circulación de sólidos por medio de sondas isocinéticas.

A continuación se muestra la información experimental que es posible obtener durante la operación de esta planta piloto y que se emplea para analizar el comportamiento del sistema:

- Los analizadores miden continuamente la composición del gas de combustión de entrada al carbonatador y de las corrientes de salida de los dos reactores. Con esta información y los caudales de entrada a los reactores se puede calcular en todo momento la velocidad a la entrada y salida de los reactores, así como los flujos de $CO_2$ introducido, de combustión, capturado y de calcinación, lo que permite conocer la eficacia de captura de $CO_2$ del carbonatador.

- Los termopares distribuidos en distintos puntos de la planta piloto permiten conocer la temperatura de todas las corrientes gaseosas y sólidas de entrada a los reactores, y así, determinar el valor de la circulación de sólidos mediante un balance de energía. La medida de la temperatura a distintas alturas en el interior de los reactores es importante también para estimar cualitativamente en línea la circulación de sólidos, ya la presencia de valores homogéneos de

temperatura en el interior de los reactores constituye un indicativo de elevada circulación, y viceversa. Por otra parte, la temperatura media del carbonatador permite calcular la eficacia de captura de $CO_2$ de equilibrio, que marca el máximo teórico alcanzable en unas determinadas condiciones de operación.

- El inventario de sólidos y su distribución se puede determinar continuamente con las medidas de las sondas de presión ubicadas en el interior de cada reactor. Existen también transductores de presión relativos a distintas alturas en las tuberías de descarga de los ciclones hacia las *loop-seal*, lo que permite conocer el nivel de sólidos y anticipar posibles atascos.

- Las muestras sólidas obtenidas de la parte superior de los reactores aportan una información muy valiosa para el seguimiento del proceso. Su extracción mediante sondas isocinéticas hace posible conocer el flujo total de sólidos que sale de cada reactor, que es distinto al de circulación entre reactores cuando existe circulación interna. Además, el análisis posterior de las muestras permite determinar su actividad y su composición química. Estos valores son clave para el cierre de los balances de carbono del sistema y la validación de los modelos de reactor.

Toda esta información se recoge durante las campañas experimentales realizadas en la planta piloto. En ausencia de problemas en las pruebas, la duración de los experimentos depende de la información concreta que se desee obtener. No obstante, las campañas suelen prolongarse durante varios días puesto que la evolución hasta alcanzar estados estacionarios es más lenta en estas plantas de mayor tamaño. La *Publicación I* de esta Tesis Doctoral (sección 3.1.3) constituye un compendio de los principales resultados obtenidos durante los experimentos llevados a cabo en esta planta piloto en los que se ha participado, junto con su análisis e

interpretación por medio del cierre de balances de materia en el carbonatador.

### 3.1.3 Publicación I

**Demonstration of steady state $CO_2$ capture in a 1.7$MW_{th}$ calcium looping pilot**

Publicado en:

*International Journal of Greenhouse Gas Control*

*Volumen* 18

Páginas 237-245

Año 2013

International Journal of Greenhouse Gas Control 18 (2013) 237–245

Contents lists available at ScienceDirect

International Journal of Greenhouse Gas Control

journal homepage: www.elsevier.com/locate/ijggc

# Demonstration of steady state $CO_2$ capture in a 1.7 $MW_{th}$ calcium looping pilot

B. Arias [a,b,*], M.E. Diego [a,b], J.C. Abanades [a,b], M. Lorenzo [c], L. Diaz [c], D. Martínez [d], J. Alvarez [d], A. Sánchez-Biezma [a,b]

[a] Spanish Research Council, CSIC-INCAR, Spain
[b] Endesa Generación, Ribera del Loira 60, 28042 Madrid, Spain
[c] Hunosa, Avenida de Galicia 44, 33005 Oviedo, Spain
[d] Foster Wheeler Energía S.L.U., Gabriel García Márquez, 2, 28232 Madrid, Spain

ARTICLE INFO

*Article history:*
Received 7 June 2013
Received in revised form 22 July 2013
Accepted 25 July 2013

*Keywords:*
$CO_2$ capture
Calcium looping
Pilot testing

ABSTRACT

Calcium looping, CaL, is rapidly developing as a postcombustion $CO_2$ capture technology because its similarity to existing power plants using circulating fluidized bed combustors, CFBC. In this work we present experimental results from a pilot built to demonstrate the concept at the $MW_{th}$ scale. The pilot plant treats 1/150 of the flue gases of an existing CFBC power plant ("la Pereda") and it has been operated in steady state for hundreds of hours of accumulated experimental time. The pilot includes two 15 m height interconnected circulating fluidized bed reactors: a $CO_2$ absorber (or carbonator of CaO) and a continuous $CaCO_3$ calciner operated as an oxy-fuel CFBC. Operating conditions in the reactors are resembling those expected in large CaL $CO_2$ capture systems in terms of reactor temperatures, gas velocities, solid compositions and circulation rates and reaction atmospheres. The evolution of $CO_2$ capture efficiencies and solid properties ($CO_2$ carrying capacity and CaO conversion to $CaCO_3$ and $CaSO_4$) have been studied as a function of key operating conditions. It is demonstrated that $CO_2$ capture efficiencies over 90% are feasible with a supply of active CaO slightly over the molar flow of $CO_2$ entering the carbonator. Closure of carbon and sulphur balances has been satisfactory during steady state periods. A basic reactor model developed from smaller test facilities seems to provide a reasonable interpretation of the observed trends. This should facilitate the further scale up of this new technology.



## 1. Introduction

Postcombustion calcium looping technology has the theoretical potential to achieve a substantial reduction in energy penalties (Shimizu et al., 1999; Abanades et al., 2005; Romeo et al., 2008; Romano, 2009; Hawthorne et al., 2009; Yongping et al., 2010; Lasheras et al., 2011; Martínez et al., 2011a; Lisbona et al., 2010; Zhao et al., 2013) and cost (Abanades et al., 2007; Li et al., 2008; Romeo et al., 2009; Zhao et al., 2013) respect to more developed postcombustion and oxyfuel combustion systems. This is because CaL is the only $CO_2$ postcombustion technology able to generate additional power from the additional heat input required to drive the sorbent regeneration reaction (calcination of $CaCO_3$). Both carbonation and calcination reactions are carried out at very high temperatures (around 650 °C for carbonation and over 900 °C for calcination in a rich atmosphere of $CO_2$). The basic concept of postcombustion calcium looping, CaL, is represented in Fig. 1 and was first proposed by Shimizu et al. (1999). Other calcium looping processes concepts using combustion systems (Abanades et al., 2005, 2011; Ramkumar and Fan, 2010; Martínez et al., 2011b; Edwards and Materic, 2012; Junk et al., 2012) or precombustion systems (see review by Harrison, 2008) are being developed worldwide, but they are much less developed than the processes represented in Fig. 1. This is by far the concept that has experienced the fastest developing pace, because the strong similarities and synergies with existing combustion technology in circulating fluidized beds, including recent oxyfired CFB developments (Myöhänen et al., 2009).

As indicated in Fig. 1, the $CO_2$ is captured from the flue gas of an existing power plant using CaO particles as a sorbent (at 650 °C) and calcining the resulting $CaCO_3$ in a different unit to regenerate CaO while producing a rich stream of $CO_2$. In the most standard configuration, both the carbonator and calciner are large scale circulating fluidized bed reactors, CFBs, operating at velocities between 3 and 5 m/s to allow compact reactor designs. There is a need in this particular CaL concept of an Air Separation Unit to oxy-burn a substantial flow of coal in the calciner and supply the energy needed

* Corresponding author.
*E-mail address:* borja@incar.csic.es (B. Arias).

1750-5836/$ – see front matter © 2013 Elsevier Ltd. All rights reserved.
http://dx.doi.org/10.1016/j.ijggc.2013.07.014

**Nomenclature**

| | |
|---|---|
| $A_{carb}$ | carbonator cross-section ($m^2$) |
| $E_{carb}$ | $CO_2$ capture efficiency |
| $E_{carb\ eq}$ | maximum $CO_2$ capture efficiency allowed by the equilibrium |
| $E_{sulf}$ | $SO_2$ capture efficiency |
| $f_a$ | fraction of active particles in the carbonator bed |
| $F_{Ca}$ | Ca molar flow circulating between reactors (mol/$m^2$ s) |
| $F_{CO_2calc}$ | molar flow of $CO_2$ produced by calcination leaving the calciner (mol/s) |
| $F_{CO_2FO}$ | molar flow of $CO_2$ produced by calcination of fresh limestone (mol/s) |
| $F_{CO_2in}$ | molar flow of $CO_2$ entering the carbonator (mol/$m^2$ s) |
| $F_{CO_2out}$ | molar flow of $CO_2$ leaving the carbonator (mol/$m^2$ s) |
| $F_O$ | make-up flow of limestone (mol/s) |
| $G_s$ | solid flow circulation rate from carbonator to calciner (kg/$m^2$ s) |
| $k_s$ | reaction rate constant ($s^{-1}$) |
| $n_{ca}$ | total inventory of Ca in the carbonator bed (mol/$m^2$) |
| $n_{ca,total}$ | total inventory of Ca in the experimental facility (mol) |
| $n_{ca,active}$ | active inventory of Ca in the carbonator bed (mol/$m^2$) |
| $N_{th}$ | average number of carbonation calcination cycles of CaO particles in the system |
| $PM_s$ | average molar weight of the solids (kg/mol) |
| $t^*$ | time required to increase the carbonate content from $X_{calc}$ to $X_{ave}$ (s) |
| $T_{calc}$ | average calciner temperature (°C) |
| $T_{carb}$ | average carbonator temperature (°C) |
| $u_{gas}$ | gas velocity (m/s) |
| $W_s$ | total inventory of solids in the carbonator (kg/$m^2$) |
| $X_{ash}$ | mass ash content of the solids |
| $X_{ave}$ | average $CO_2$ carrying capacity |
| $X_{calc}$ | molar carbonate content of the solids in the calciner |
| $X_{carb}$ | molar carbonate content of the solids in the carbonator |
| $X_{ef}$ | total sorbent utilization |
| $X_{sulf}$ | molar sulphate conversion of the solids |
| $\Delta P$ | pressure drop in the riser (mbar) |
| $\varphi$ | gas–solid contacting effectivity factor |
| $\nu$ | volume fraction |

for $CaCO_3$ decomposition. It should be evident from Fig. 1 that the calciner resembles a full oxyfired new power plant system, where highly suitable heat sources for a new steam cycle are available. In particular, the energy used for the endothermic calcination reaction is fully recovered in the carbonator at a temperature around 650 °C. Furthermore, large make up flows of limestone to compensate for modest absorption capacity of highly cycled particles of CaO are economically feasible (Abanades et al., 2004), since fresh particles of CaO can be generated in the calciner by feeding a certain make up flow of crushed limestone (usually a very low cost material). This flow of limestone also purges inert materials (coal ashes and $CaSO_4$), and the integration of the rich purge of CaO with a cement plant or other large scale user of CaO (e.g. desulfurization sorbent in the existing power plant) allows for an even larger flow of sorbent make up (see review by Dean et al., 2011).

As recently noted by Sanchez-Biezma et al. (2012), great progress has been achieved in different projects around the world developing CaL. The most aggressive scale up of the technology has been pursued under the EU funded "CaOling" project (www.caoling.eu), that relied first in a demonstration of the concept in lab scale pilots with continuous solid circulation (Alonso et al., 2010; Charitos et al., 2010b, 2011; Rodríguez et al., 2011a,b). Also part of CaOling project was the design, commissioning and operation of a 1.7 $MW_{th}$ pilot in la Pereda (Spain) to test the postcombustion Ca-looping concept under a real industrial environment. This pilot entered operation in January 2012, establishing successfully the solid circulation system components and obtaining the first results operating in dynamic and continuous mode (Sanchez-Biezma et al., 2012). Other developing efforts in Germany have also achieved positive results in large pilots: the 1 $MW_{th}$ pilot in Darmstadt (Galloy et al., 2011; Plötz et al., 2012) and in 0.2 $MW_{th}$ in Stuttgart University (Hawthorne et al., 2011; Dieter et al., 2012). There is also a wider R&D community publishing valuable results at laboratory scale and small pilot level (see review by Blamey et al., 2010) and the IEAGHG created in 2009 a Network on High Temperature Solid Looping Cycles (www.ieaghg.org) where these actors meet regularly to discuss progress of the different variants of the CaL technology. Therefore, postcombustion CaL is now an established "promising technology" that faces similar credibility challenges than other emerging capture options. The main challenge is of course to progress in the experimental demonstration of the concept at increasing scale and realistic conditions, validating the benefits expected and overcoming the obstacles that may appear in the path towards large scale demonstration.

This paper is intended to contribute to the process of scaling up of this postcombustion CaL technology. We describe briefly the CaL test facility of La Pereda and the experimental method to reach steady state operation. We then present the experimental results from the pilot and how the closure of carbon and sulphur balances is achieved during continuous operation in air mode calcination as well as in oxy-combustion calcination mode. We then apply a modelling approach successfully used for the interpretation of experimental results from smaller pilots (Alonso et al., 2010, 2011; Rodríguez et al., 2011a; Charitos et al., 2011) that should be valuable for scaling up purposes.

## 2. Experimental

The pilot is only briefly summarized here as it has been described in detail elsewhere (Sánchez-Biezma et al., 2011). The calcium looping reactor system is made up of two interconnected CFB reactors of 15 m height with an internal diameter of 0.65 m in the carbonator and 0.75 m in the calciner. The reactors are connected to high efficiency cyclones: the cyclone of the carbonator separates the flue gas lean in $CO_2$ from the partially carbonated solids; the calciner cyclone separates the concentrated $CO_2$ stream leaving the oxyfired combustor from the solids rich in CaO. Solids fall by gravity from the cyclones to double loop seals, that are bubbling fluidized beds allowing for the control of the solid circulation between reactors. Part of the solids coming to each loop seal return to the reactor from which the solids are coming (internal solid circulation) and the rest circulates to the other reactor (from carbonator to calciner or from calciner to carbonator). The relevance of this internal solid circulation streams to maintain certain solids inventories in the reactors has been discussed elsewhere (Charitos et al., 2010a; Diego et al., 2012).

The calciner is able to operate under air combustion or under oxy-fuel combustion conditions, using $O_2$ and $CO_2$ coming from tanks of liquefied gases. The carbonator is equipped with removable cooling bayonet tubes which allow variable heat extraction from the reactor under different conditions of temperature, solid circulation flows and different intensity of the exothermic carbonation reaction of CaO. Flue gas from the power plant is blown to the

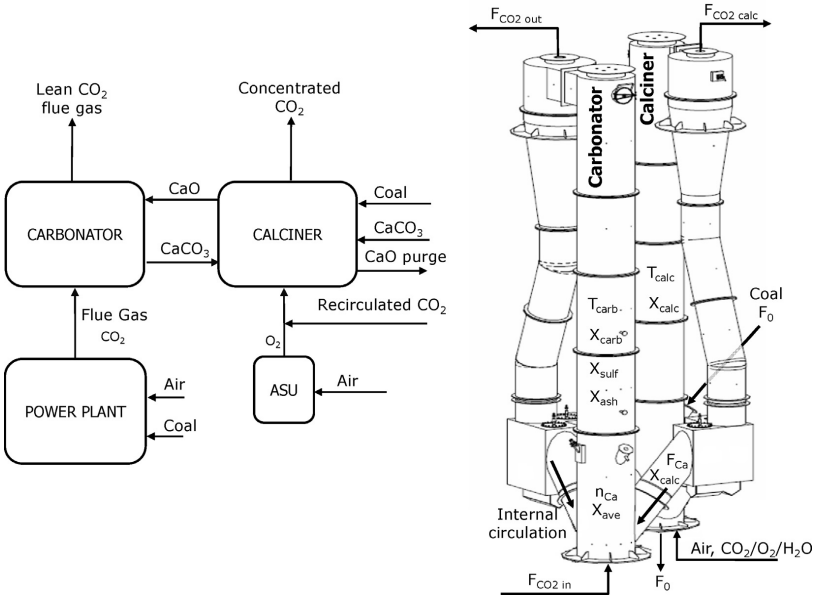


**Fig. 1.** General scheme of a power plant incorporating a Ca-looping system and schematics of the "la Pereda" pilot plant facility, with the main molar flows and operating variables involved in the test campaigns.

carbonator with a fan. There is a continuous limestone and coal feeding system connected to the calciner which allows working in a steady state combustion and sorbent feeding modes. There is also a continuous solid removal system in the calciner made up with a water cooled screw feeder. Instrumentation including temperature, pressure and continuous gas analysis from different points is available. Many other ports are available for solid sampling and local solid circulation rates measurement with isokinetic probes. Subsequent analysis of such solids samples (in terms of particle size distribution, chemical composition and reactivity towards $CO_2$ capture and $SO_2$ capture) are carried out in the lab, using thermogravimetric equipment described elsewhere (González et al., 2008).

The calciner has been run aiming at full conversion of $CaCO_3$ to CaO in all test discussed in this work. This has been possible by allowing a sufficiently high calcination temperatures (20–30 °C over the limit given by the equilibrium of $CO_2$ on CaO at the exit of the calciner) and a certain $O_2$ excess at the exit of the combustion-calciner reactor (over 5 vol%) to ensure high coal combustion efficiencies in the calciner. Optimization of combustion conditions of the calciner in order to reduce this level of $O_2$ is considered outside the scope of the present work. We focus in this work on investigation of the carbonator reactor operated with a steady state flow of CaO as indicated in Fig. 1.

Concerning the performance of the carbonator reactor, previous experience from small test facilities in continuous mode (Alonso et al., 2010; Rodríguez et al., 2011a; Charitos et al., 2011) has been used to define the experimental methodology to measure and characterize the main variables that affect the performance of the carbonator as a chemical reactor:

- The inventory of solids in the carbonator ($n_{Ca}$ in Fig. 1) is determined continuously through the measurement of the pressure difference between the plane above the distributor and the exit of the reactor. Occasional tests where the fluidization has been switched off and the solids have been extracted from the carbonator have confirmed the direct relationship between bed $\Delta P$ and the solid inventory (the contribution of the acceleration of the circulating solids to the $\Delta P$ in the carbonator is negligible).
- The average carbonator reactor temperature ($T_{carb}$ in Fig. 1). The carbonator reactor displays a certain axial temperature profile due to the effect of the bayonet tubes, the exothermic character of the carbonation reactor (more intense in the dense bottom part of the carbonator) and the arrival of high temperature solids from the calciner (at between 830 and 920 °C). Internal solid circulation (within the reactor through solid convective flows and through the recirculating solids from the cyclone-double loop seal system) can drastically reduce this difference of temperature to 20–30 °C, so that an average temperature in the reactor can be calculated.
- The molar flow of $CO_2$ entering the carbonator with the flue gas ($F_{CO_2 in}$ in Fig. 1). The inlet concentration of $CO_2$ changes little during the experiments (between 12 and 12.5 vol%) as this corresponds to the flue gas composition of the power plant. These concentrations are measured continuously, as well as the mass flow of flue gas entering the carbonator reactor.
- The average composition of the solids arriving to the carbonator and their activity towards $CO_2$ and $SO_2$ capture ($X_{carb}$ and $X_{sulf}$ in Fig. 1). This cannot be monitored continuously but frequent solid sampling from suitable entry and exit ports is feasible using isokinetic probes. Chemical analysis of the solids samples taken during each experiment is carried out in order to determine the CaO, $CaCO_3$ and $CaSO_4$ content. The solids samples are also tested in a TG equipment described elsewhere (Rodríguez et al., 2011a) to determine the $CO_2$ carrying capacity and the carbonation reaction rates.
- The molar circulation rate between carbonator and calciner reactors ($F_{Ca}$ in Fig. 1). As will be discussed later, when the system is operating in stationary state, this variable can be estimated by two methods in parallel: the closure of the carbon balance and

**Table 1**
Range of operating conditions and the main variables involved during $CO_2$ capture tests in "la Pereda" 1.7 $MW_{th}$ pilot plant.

| | | |
|---|---|---|
| Carbonator temperature (°C) | $T_{carb}$ | 600–715 |
| Carbonator superficial gas velocity inlet (m/s) | $u_{gas\ carb\ in}$ | 2.0–5.0 |
| Inlet $CO_2$ volume fraction to the carbonator | $v_{CO_2\ carb\ in}$ | 0.12–0.14 |
| Inlet $SO_2$ concentration to the carbonator ($ppm_v$) | $C_{SO_2}$ | 100–250 |
| Inventory of solids in the carbonator ($kg/m^2$) | $W_s$ | 100–1000 |
| Maximum $CO_2$ carrying capacity of the solids | $X_{ave}$ | 0.10–0.70 |
| Calciner temperature (°C) | $T_{calc}$ | 820–950 |
| Inlet $O_2$ volume fraction to the calciner | $v_{O_2\ calc\ in}$ | 0.21–0.35 |
| Inlet $CO_2$ volume fraction to the calciner | $v_{CO_2\ calc\ in}$ | 0–0.75 |
| $CO_2$ capture efficiency | $E_{carb}$ | 0.4–0.95 |
| $SO_2$ capture efficiency | $E_{sulf}$ | 0.95–1.00 |

the closure of the heat balance in the carbonator. The total solid circulation rate through the risers can also be measured using a suction probe in isokinetic conditions at the exit of the riser. The carbonator riser is 15 m height and solids are largely disengaged from the gas at this height. Therefore, upwards solid circulation at that point is close to total solid circulation.

The test campaigns carried out in the pilot plant add up to more than 1800 h of operation of the interconnected reactors in combustion mode in the calciner. A total of 380 h have been achieved in $CO_2$ capture mode (with capture efficiencies between 40% and 95%), out of which 170 h have been achieved in $CO_2$ capture mode with stable oxyfuel combustion of coal in the calciner. Table 1 summarizes the main range of operating conditions used during $CO_2$ capture tests in the pilot.

## 3. Results and discussion

As mentioned above the focus of this paper is on steady state results, but it may be of interest to discuss first the main transitions in the system from the start up to the steady state periods. A typical experimental run starts with the calcination of a batch of limestone in the facility, that is used initially as a heat carrier to transfer heat from the reactors (where the start up propane burners operate) to the rest of the installation. Once the initial batch of solids is calcined, the calciner is switched to oxy-fuel combustion mode. After that, fresh limestone is fed to the calciner only to adjust the activity of the sorbent and compensate for attrition losses, while solids are removed to keep constant the total inventory in the system and to avoid the accumulation of inert solids ($CaSO_4$ and ashes). Fig. 2 presents a typical experiment from the onset of the calcination of the initial total solid inventory in the system to the steady state period in oxyfuel combustion–calcination mode. The main events are highlighted in the figure and summarized in the auxiliary table included in the figure. During this particular test, the inlet gas velocity was kept between 3.6 and 3.9 m/s in the carbonator and between 3.8 and 4.2 m/s in the calciner.

The initial period corresponds to the calcination of the solids present in the system, and this process can be followed using several parallel approaches. The first one is by determining the composition of the solids extracted periodically from the system. Fig. 2c shows the carbonate and sulphate molar composition of the solids taken from the carbonator reactor at different times. During this period of the experiment, the carbonate content of the solids in the carbonator dropped from 54 to 5 wt.% between 8:00 and 11:00. It can be also observed that the sulfate accumulates in the system as there is no extraction of the solids from the reactors during this period.

Another approach to follow the calcination period is by comparing the $CO_2$ released by calcination in the calciner and the $CO_2$ captured in the carbonator. Fig. 2b shows the comparison of both terms along the experiment. During the initial 3 h, there is a net production of $CO_2$ in the calciner due to the calcination of the carbonate present in the initial inventory of solids (see in Fig. 2b). However, it can be seen in Fig. 2b that once the batch of solids is completely calcined, the $CO_2$ produced by calcination becomes equal to the $CO_2$ captured in the carbonator. During this initial period, the net amount of $CO_2$ released in the carbonator calculated from the difference between the $CO_2$ calcined and captured is about 7.2 kmol. This value matches the amount of $CO_2$ that should be produced by the calcination of the initial batch of solids present in the system (that has an initial carbonate content of 54 wt.%). The agreement between both values also indicates that the total inventory of solids in the system can be estimated sufficiently accurately using pressure measurements in the facility. The $CO_2$ produced in the calciner increased above the $CO_2$ captured in the carbonator from 13:30 due to continuous addition of fresh limestone into the system from that point.

Attending now to the $CO_2$ capture efficiency, $E_{carb}$, this is quite low (below 0.4) at the beginning of the calcination period (see Fig. 2c) due to the low amount of CaO present in the system. But, as the calcination progresses and the CaO content in the solids increases, $E_{carb}$ rises to a value close to that limited by the equilibrium. The equilibrium $CO_2$ capture efficiency ($E_{carb\ eq}$) shown in Fig. 2c has been calculated using the average temperature in the carbonator.

The temperature of the calciner and the efficiency of the calcination also changes with time in the first few hours of this experiment (Fig. 2a). As the initial batch of solids is being calcined, the temperature of the calciner increases progressively until it reaches a value above 900 °C. This trend in the calciner temperature tends to cause an increase in the temperature of the solids arriving to the carbonator, thus increasing the temperature of this reactor and reducing the equilibrium $CO_2$ capture efficiency. In these conditions it is necessary to adjust the heat transfer area provided by the bayonet tubes to stabilize the carbonator temperature at the target temperature in the experiment. At 12:00, the calciner was switched to oxy-combustion mode by supplying a mixture of $O_2/CO_2$.

At 13:30, the $X_{ave}$ of the sorbent had decreased to a residual value of 0.067 after more than 5 h without adding fresh limestone into the system. Thus, a continuous flow of limestone was set up at this point to increase the activity of the sorbent circulating in the system. This flow of fresh limestone increased progressively the $X_{ave}$ up to a value 0.18 at 23:00. The addition of the limestone also increases progressively the inventory of solids in the system, which reaches a maximum value of 900 $kg/m^2$ at 18:00 in the carbonator reactor. From this point, solids were removed using the ash extraction system in order to maintain the inventory of solids below this value in this particular experiment. During this period, the increase of $X_{ave}$ and the inventory of solids led to an increase of the $CO_2$ capture efficiencies, which almost reaches the maximum $CO_2$ capture efficiency limited by the equilibrium from 20:00. The addition of fresh limestone and the extraction of solids also reduced the $CaSO_4$ content to around 5 mol%.

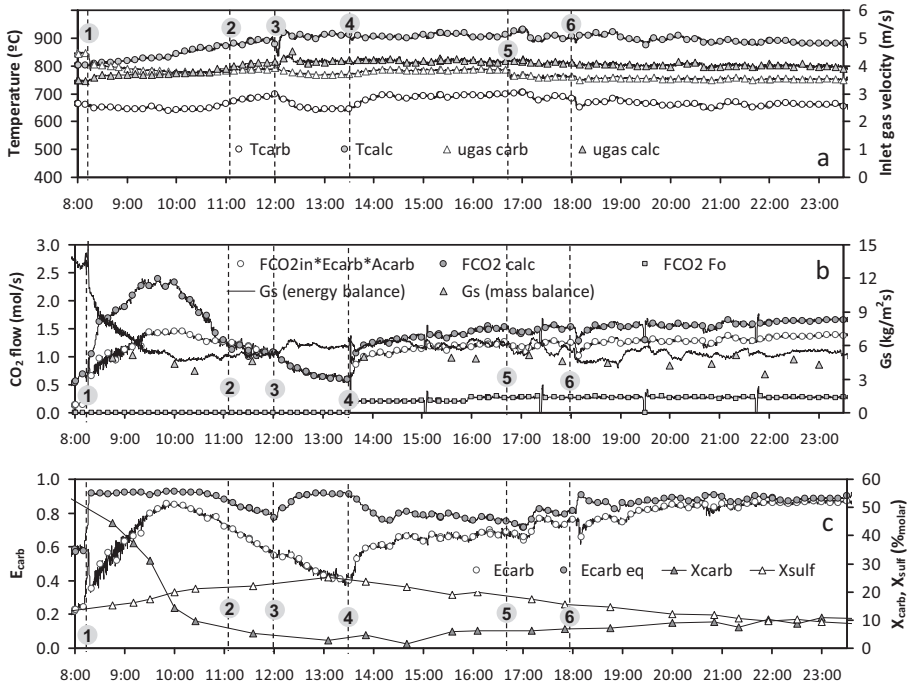


| Event | Time | Description |
|---|---|---|
| 1 | 8:05 | Start of calcination of the batch of solids and feeding of flue gas |
| 2 | 11:00 | End of calcination of the batch of solids |
| 3 | 12:00 | Switch to oxy-combustion mode |
| 4 | 13:30 | Continuous limestone feeding |
| 5 | 16:50 | Modification of carbonator inlet gas velocity |
| 6 | 18:00 | First solid extraction from the calciner |

**Fig. 2.** Example of a typical experimental run in la Pereda pilot plant.

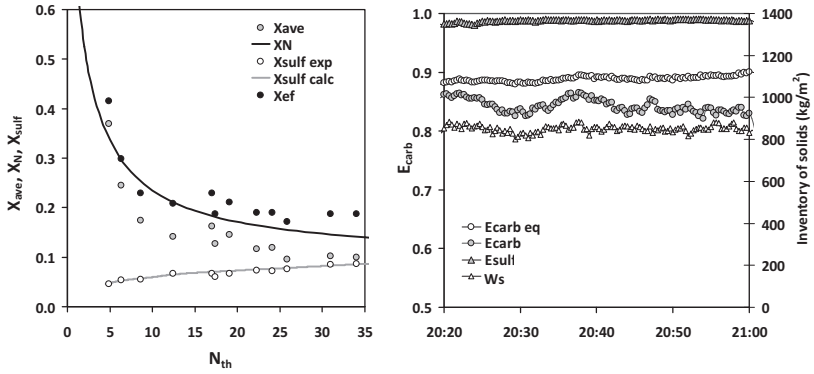


**Fig. 3.** (a) Evolution of sorbent utilization with the average number of carbonation–calcination cycles of particles in the system and (b) $CO_2$ capture and $SO_2$ capture efficiencies when operating with residual $CO_2$ carrying capacity.

As stated above, after several hours of stable operation, the activity of the material circulating between reactors decays towards a residual activity. This concept of residual activity was first detected in thermogravimetric studies (Grasa and Abanades, 2006; Lysikov et al., 2007; Chen et al., 2009) but has also been observed in continuous tests of sufficient duration in stationary state (Charitos et al., 2011). It is important to confirm this general deactivation trend of the sorbent in the "la Pereda" pilot. An example of the steady state experiments conducted with this purpose was carried out during 12 h without feeding limestone, allowing the sorbent activity to fall towards the residual value. Attrition losses were negligible during this test because the bed inventory was made up with what was left after calcination (in air combustion mode) of the large batch of fresh limestone. It is already known (Jia et al., 2007; González et al., 2010; Coppola et al., 2012) that attrition mainly takes place in the first calcination of the material. We confirmed that the attrition rate drastically reduces afterwards, as the particles "surviving" the first calcination are those with best mechanical properties and the internal sintering taking place during carbonation–calcination cycles further strengthen the particles. Attrition during calcination is highly dependent on limestone type and attrition conditions in CaL systems should be identical to those present in large scale CFBC systems. Fig. 3a shows the evolution with time of the $CO_2$ carrying capacity ($X_{ave}$) of the solid samples extracted from the system during this test against the effective number of cycles. In this continuous and well mixed reactor system, the effective number of carbonation-calcination cycles of the solids has been calculated using the following equation:

$$N_{th} = \frac{\int_0^t F_{CO_2 in} A_{carb} E_{carb}(t) dt}{n_{Ca,total} X_{ave}} \quad (1)$$

This number, $N_{th}$, is only an approximation that accounts for the number of times that the moles of $CO_2$ captured could carbonate the total inventory of Ca ($n_{Ca,total}$) up to its average $CO_2$ carrying capacity ($X_{ave}$) (see Charitos et al., 2011 for a more detailed methodology). In Eq. (1), $E_{carb}(t)$ represents the instantaneous $CO_2$ capture efficiency, while $n_{Ca,total}$ stands for the total inventory in the system. $X_{ave}$ is measured at different time points analyzing the samples taken from the system and its value is considered constant between these points. The product, $F_{CO_2 in} E_{carb}(t)$, is calculated continuously through gas analysis, while the total calcium moles, $n_{Ca,total}$, are known through measurements of bed inventories and the chemical analysis of the solid samples.

As can be seen in Fig. 3a, the drop in the $CO_2$ carrying capacity observed during this experiment is consistent with the deactivation curve (Grasa and Abanades, 2006) when it is tested in a TGA in absence of $SO_2$ (shown as a solid black line in Fig. 3a). Sulfation conversion of the solids increases with $N_{th}$, as the total inventory of material in the reactor system (including loop seals and standpipes) progressively reacts with $SO_2$. More than 95% of the $SO_2$ coming into the carbonator in the flue gas from the existing CFBC power plant (200–300 $ppm_v$ during this period) and more than 95% of the sulfur in the coal feed to the calciner, is captured by the solids circulating in the CaL system.

This is consistent with results recently reported by Arias et al. (2012) from experiments carried out in a 30 kWth pilot. Furthermore, by knowing the amount of Ca in the system and the $SO_2$ that is captured in the carbonator and calciner, the evolution of the sulphate conversion, $X_{sulf}$, can be calculated (shown as solid grey line in Fig. 3a). Excellent closure of the $SO_2$ mass balance was achieved, as can be seen from the good agreement between experimental and calculated values. Fig. 3a also shows the total sorbent utilization which is the sum of the $CO_2$ carrying capacity and $CaSO_4$ molar conversion. As can be seen in this Figure, the total sorbent utilization ($X_{ef} = X_{sulf} + X_{ave} = 0.19$) is higher than the expected and after 35 cycles the sorbent with a molar fraction of 0.086 in $CaSO_4$ is still able to achieve a molar carbonate conversion of 0.1. This qualitative trend (effective sorbent utilizations higher than expected) has been confirmed in other similar tests and has economic implications for the CaL systems as it will make more feasible to operate the system with low make up flows of fresh limestone.

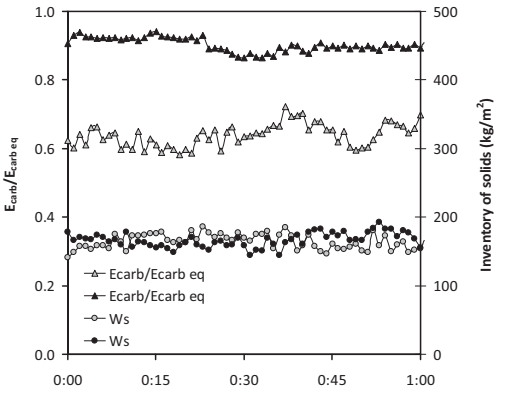


**Fig. 4.** Comparison of two steady states of 1 h ($u_{gas\ carb\ in}$ = 4.0–4.3 m/s, average carbonator temperature = 660–690 °C, $X_{ave}$ = 0.11 (grey), $X_{ave}$ = 0.21 (black)).

It is interesting to note that the "deactivated" material ($N_{th}$ > 35) circulating between calciner and carbonator in Fig. 3a is still able to capture $CO_2$ in the carbonator with an efficiency over 80%, as long as there is sufficient bed inventory in the reactor. This is shown in Fig. 3b, that corresponds to an experimental period of 50 min at the end of the experimental run of 12 h without addition of limestone when the $CO_2$ carrying capacity ($X_{ave}$) of the solids present in the system was around 0.10. Fig. 3b also represents the $SO_2$ capture efficiency in the carbonator at the same time period. In this figure we can see that the $SO_2$ capture efficiency in the carbonator was kept well above 0.95. The high $SO_2$ removal obtained during the $CO_2$ capture tests in the pilot plant confirms the trends observed at laboratory scale and in the 30 kWth facility which indicated that CFB carbonator are excellent desulfurization units (Arias et al., 2012).

As indicated in Table 1, many other stationary state periods where tested using a range of operating conditions and operating in steady state. Fig. 4 shows an example of one hour of operation in two such steady states, comparing the effect of the average activity of the solids, $X_{ave}$, on the normalized $CO_2$ capture efficiency ($E_{carb}/E_{carb\ eq}$) which is an indication of the carbonator reactor efficiency. In both experiments, the inventory of solids in the carbonator was kept at the same value and the inlet gas velocity to the carbonator was around 4.0–4.3 m/s. During the first steady state (shown in grey), the activity of the solids ($X_{ave}$) was around 0.11. Under these experimental conditions, the normalized $CO_2$ capture efficiency achieved was around 0.65, and increased to 0.90 during the second steady (shown in black) state when the activity of the sorbent is 0.21. This is consistent with previous works (Alonso et al., 2010; Charitos et al., 2010b; Rodríguez et al., 2011a) that have shown that two of the most relevant operating parameters in a carbonator reactor are the inventory of solids in the bed and the average activity of the solids in such reactor. Therefore the trends observed during all stationary state periods such as the example in Fig. 4 have been analyzed following the methodology reported in these references.

The $CO_2$ capture efficiency in the carbonator is defined as the amount of $CO_2$ captured respect to the $CO_2$ fed to the carbonator and can be calculated as follows:

$$E_{carb} = \frac{F_{CO_2 in} - F_{CO_2 out}}{F_{CO_2 in}} \quad (2)$$

where $F_{CO_2}$ is molar flow of $CO_2$ (mol/m$^2$ s). In a steady state, the overall $CO_2$ mass balance of the system can be written and calculated using three approaches.

($CO_2$ reacting with CaO in the bed)

= ($CaCO_3$ formed in the circulating stream of CaO)

= ($CO_2$ removed from the gas phase) (3)

Each term of this equation can be calculated independently using experimental measurements available in the pilot plant, and the values can be compared to analyze the closure of the carbon balances at steady state in the system. The $CO_2$ removed from the gas phase is the most reliable term in the mass balance of Eq. (3) as this can be calculated directly from the continuous measurements of flue gas fed into the carbonator and the gas composition entering and leaving the reactor. Additional sources of $CO_2$ in the carbonator from the combustion of unconverted fuel in the calciner are evaluated from small differences detected in the flow of oxygen after and before the carbonator.

It is also helpful to interpret the carbonator performance to compare the $CO_2$ carbonation efficiency ($E_{carb}$) with the maximum $CO_2$ removal efficiency achievable from the gas phase ($E_{carb\,eq}$). This is estimated from the minimum $CO_2$ molar fraction ($y_{CO_2\,eq}$) allowed by the equilibrium (Barker, 1962) which is a function of the average temperature in the carbonator.

Under steady state conditions, when there is no accumulation of $CaCO_3$ in the carbonator bed, the fraction of $CO_2$ captured from the gas phase has to be the same as the $CaCO_3$ formed in the circulating stream of CaO. Thus, the following mass balance should be fulfilled:

$$E_{carb} F_{CO_2\,in} = F_{Ca} \times (X_{carb} - X_{calc}) \quad (4)$$

where $F_{Ca}$ is the molar flow (mol/m$^2$ s) of CaO entering into the carbonator, $X_{carb}$ is the carbonate content of the solids leaving the carbonator and $X_{calc}$ is the carbonate content of the solids coming from the calciner and entering the carbonator. If the solid circulation rate between reactors ($G_s$) is known, the molar flow ($F_{Ca}$) can also be obtained from the analysis of the samples taken from the reactors.

$$F_{Ca} = \frac{G_s(1 - X_{ash})}{PM_s} \quad (5)$$

Considering the calciner and carbonator as perfect mixed reactors, it can be assumed that the composition of the solids in these beds is the same as the one measured at the exit of the reactors. Then, the molar flow of CaO ($F_{Ca}$) can be estimated from the Eq. (4) above and from the experimental determination of carbonate and ash content of the solids extracted from carbonator and calciner during the experiment. As was indicated above, another approach to calculate the mass flow of solids between reactors is to solve an energy balance to the carbonator. Since the pilot is refractory lined, heat losses are modest and can be calibrated. Therefore, it is possible to determine during steady state conditions the total solid circulation rate of solids arriving to the carbonator ($G_s$) from the calciner loop seal of Fig. 1. All the terms in the heat balance can be estimated continuously from instrumentation available in the pilot plant and the measurements from the heat balance calibrated to correct systematic deviations. As an example, Fig. 2b showed both the calculated solid circulation rate ($G_s$) through calciner during the experimental run from the heat balance and the same Gs calculated from Eqs. (4) and (5).

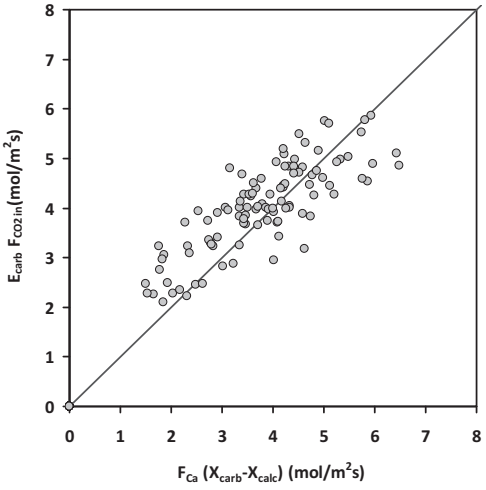


**Fig. 5.** Comparison between the $CO_2$ removed from the gas phase in the carbonator and the increment in $CaCO_3$ flow between reactors.

Fig. 5 compares the two terms in the carbon balance of Eq. (4) for all stationary states achieved in the operation of the plant in $CO_2$ capture mode. As can be seen from Fig. 5, the $CaCO_3$ formed by carbonation and circulating in the stream of solids between reactors reasonably agrees with the $CO_2$ removed from the gas phase. The main source of uncertainty in this mass balance closure concerns the representativity of the values of $X_{calc}$ and $X_{carb}$ used in Eq. (4).

The other relevant $CO_2$ mass balance closure expressed in Eq. (3) is particularly useful for reactor design: this concerns the comparison of the flow of $CO_2$ captured from the gas phase and the flow of $CO_2$ reacting with the CaO particles present in the carbonator bed inventory at any particular time. This second term can be estimated as the product of two parameters, the amount of solids present in the bed and the average reaction rate of the solids.

$$F_{CO_2\,in} E_{carb} = n_{Ca,active} \left(\frac{dX}{dt}\right)_{reactor} \quad (6)$$

To close this mass balance, we have applied the carbonator model proposed by Alonso et al. (2009) and the methodology used by Charitos et al. (2011) to interpret the experimental trend observed in the lab scale Ca-looping facilities. Parallel efforts to build more elaborate reactor models for the carbonator and calciner reactors are on going within the CaOling project (Ylätalo et al., 2012). The reactor model used in the present work considers the CFB carbonator as a perfect mixed reactor for the solid phase and a plug flow reactor for the gas phase. For the average reaction rate of the solids, we assume that the particles react at a constant rate until they reach their maximum carbonate conversion ($X_{ave}$) and after that point the reaction rate is zero. This simplification of the reaction rate is consistent with the experimental data available (see for example, Grasa et al., 2008) and it has been shown to be accurate enough for the interpretation of the experimental data in the small facilities (Charitos et al., 2011). According to this assumption, the reaction rate of the particles depends on the $CO_2$ carrying capacity of the sorbent ($X_{ave}$) and the average $CO_2$ concentration in the carbonator and can be expressed as follows:

$$\left(\frac{dX}{dt}\right)_{reactor} = k_s \varphi X_{ave} \left(\overline{y_{CO_2} - y_{CO_2\,eq}}\right) \quad (7)$$

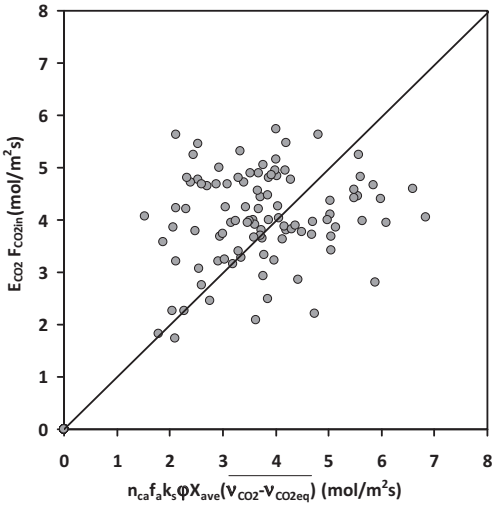


**Fig. 6.** Comparison between the $CO_2$ removed from the gas phase and the $CO_2$ reacting with CaO in the carbonator bed.

where $k_s$ is a constant reaction rate that depends on the limestone used and $\varphi$ is a gas–solid contacting factor defined by Rodríguez et al. (2011a). Once defined the reaction rate term, the active inventory of calcium can be defined taking into account the assumption of a perfect mixing reactor. According to this, the fraction of active solids in the carbonator ($f_a$) is that corresponding to the fraction of particles with a residence time lower than the time needed to increase the carbonate content from $X_{calc}$ to $X_{ave}(t^*)$.

$$n_{Ca,active} = n_{Ca}f_a = n_{Ca}(1 - e^{-t^*/(n_{Ca}/F_{Ca})}) \quad (8)$$

The characteristic carbonation reaction time ($t^*$) can be calculated by determining $X_{calc}$ and $X_{ave}$ from the solids taken and using the reaction rate defined in Eq. (7) (see references Alonso et al., 2009, 2010; Rodríguez et al., 2011a,b; Charitos et al., 2011). By combining Eqs. (7) and (8) into Eq. (6), a simple expression can be obtained that links all the operating parameters in the Ca-looping system with the $CO_2$ capture efficiency:

$$E_{carb}F_{CO_2\,in} = n_{Ca}k_s\varphi f_a X_{ave}\left(\overline{\nu_{CO_2} - \nu_{CO_2\,eq}}\right) \quad (9)$$

The apparent constant rate ($k_s\varphi$) in Eq. (9) can be calculated as a fitting parameter by comparing the $CO_2$ capture from the gas phase and the $CO_2$ reacting with the CaO in the carbonator bed using Eq. (6). The constant rate ($k_s$) can be measured in TGA for the limestone used for the tests (an average value of 0.45 $s^{-1}$ consistent with other similar limestones as reported in Grasa et al., 2008).

Fig. 6 shows the final comparison between the $CO_2$ removed from the gas phase and the $CO_2$ reacting with CaO in the carbonator bed. As can be seen, there is only a rough closure of this mass balance, which can still be considered reasonable when taking into account the inherent uncertainties in the determination of the parameters involved in Eq. (9). These are discussed in more detail in a previous work reporting data from a much smaller pilot (Rodríguez et al., 2011a,b). The qualitative similarities in the closure of the $CO_2$ mass balances represented in Figs. 5 and 6 with those reported from a smaller pilot provides confidence about the scalability of these results in what refers to $CO_2$ capture in the carbonator reactor.

## 4. Conclusions

The results obtained in a 1.7 $MW_{th}$ pilot confirm that postcombustion calcium looping is a promising technology for $CO_2$ capture that can strongly benefit for scaling up purposes from existing knowledge on mature Circulating Fluidized Bed Combustion Technologies. $CO_2$ capture efficiencies over 90% have been achieved in a wide range of experimental conditions in the CFB carbonator, including continuous operation using solids with modest $CO_2$ carrying capacities. Closure of carbon and sulphur balances has been satisfactory during steady state periods lasting for up to 380 h of accumulated experimental time with $CO_2$ capture, including 170 h with the calciner operating under oxy-fuel combustion mode.

A valuable data base of results has been acquired for model validation and scale up purposes, including tests conducted in full oxy-combustion mode in the calciner. A basic reactor model has been used to interpret the results obtained. The apparent reaction rates and $CO_2$ carrying capacities of the materials in the system are in agreement with those found from smaller facilities. The positive experience in the 1.7 $MW_{th}$ La Pereda pilot plant should facilitate the scale up of this new technology and provide the necessary confidence for the demonstration of Ca-looping technology making use of the available expertise in CFB combustion and parallel developments in related oxy-fuel combustion.

## Acknowledgment

The research presented in this work has received partial funding from the European Community's Seventh Framework Programme (FP7/2007-2013) under the GA 241302-CaOling Project and from the PCTI Asturias Regional Government. M.E. Diego acknowledges a fellowship grant under the CSIC JAE Programme, co-funded by the European Social Fund. M. Fernández, M. Pereiro and A. Méndez have been excellent operators of the rig during the experimental runs of the pilot.

## References

Abanades, J.C., Alonso, M., Rodríguez, N., 2011. Biomass combustion with in situ $CO_2$ capture with CaO. I. Process description and economics. Industrial and Engineering Chemistry Research 50, 6975–6981.
Abanades, J.C., Anthony, E.J., Wang, J., Oakey, J.E., 2005. Fluidized bed combustion systems integrating $CO_2$ capture with CaO. Environmental Science and Technology 39, 2861–2866.
Abanades, J.C., Grasa, G., Alonso, M., Rodríguez, N., Anthony, E.J., Romeo, L.M., 2007. Cost structure of a postcombustion $CO_2$ capture using CaO. Environmental Science and Technology 41, 5523–5527.
Abanades, J.C., Rubin, E.S., Anthony, E.J., 2004. Sorbent cost and performance in $CO_2$ capture systems. Industrial and Engineering Chemistry Research 43, 3462–3466.
Alonso, M., Rodríguez, N., Abanades, J.C., 2009. Modelling of a fluidized bed carbonator to capture $CO_2$ for a combustion flue gas. Chemical Engineering Science 64, 883–891.
Alonso, M., Rodríguez, N., González, B., Grasa, G., Murillo, R., Abanades, J.C., 2010. Carbon dioxide capture from combustion flue gases with a calcium oxide chemical loop. Experimental results and process development. International Journal of Greenhouse Gas Control 4, 167.
Alonso, M., Rodríguez, N., González, B., Arias, B., Abanades, J.C., 2011. Biomass combustion with in situ $CO_2$ capture by CaO. II. Experimental results. Industrial and Engineering Chemistry Research 50, 6982–6989.
Arias, B., Cordero, J.M., Alonso, M., Diego, M.E., Abanades, J.C., 2012. Investigation of $SO_2$ capture in a circulating fluidized bed carbonator of a Ca looping cycle. Industrial and Engineering Chemistry Research 52, 2700–2706.
Barker, E.H., 1962. The calcium oxide–calcium dioxide system in the pressure range 1–300 atmospheres. Journal of the Chemical Society 70, 464–470.
Blamey, J., Anthony, E.J., Wang, J., Fennell, P.S., 2010. The calcium looping cycle for large-scale $CO_2$ capture. Progress in Energy and Combustion Science 36, 260–279.
Charitos, A., Hawthorne, C., Bidwe, A.R., Korovesis, L., Schuster, A., Scheffknecht, G., 2010a. Hydrodynamic analysis of a 10 kWth calcium looping dual fluidized bed for post-combustion $CO_2$ capture. Powder Technology 200, 117–127.
Charitos, A., Hawthorne, C., Bidwe, A.R., Sivalingam, S., Schuster, A., Spliethoff, H., Scheffknecht, G., 2010b. Parametric investigation of the calcium looping process for $CO_2$ capture in a 10 kWth dual fluidized bed. International Journal of Greenhouse Gas Control 4, 776–784.

Charitos, A., Rodrí'guez, N., Hawthorne, C., Alonso, M., Zieba, M., Arias, B., Kopanakis, G., Scheffknecht, G., Abanades, J.C., 2011. Experimental validation of the calcium looping $CO_2$ capture process with two circulating fluidized bed carbonator reactors. Industrial and Engineering Chemistry Research 50, 9685–9695.

Chen, Z., Song, H.S., Portillo, M., Lim, C.J., Grace, J.R., Anthony, E.J., 2009. Long-term calcination/carbonation cycling and thermal pre-treatment for $CO_2$ capture by limestone and dolomite. Energy and Fuels 23, 1437–1444.

Coppola, A., Montagnaro, F., Salatino, P., Scala, F., 2012. Fluidized bed calcium looping: the effect of $SO_2$ on sorbent attrition and $CO_2$ capture capacity. Chemical Engineering Journal 445, 207–208.

Dean, C.C., Blamey, J., Florin, N.H., Al-Jeboori, M.J., Fennell, P.S., 2011. The calcium looping cycle for $CO_2$ capture from power generation, cement manufacture and hydrogen production. Chemical Engineering Research and Design 89, 836–855.

Diego, M.E., Arias, B., Abanades, J.C., 2012. Modeling the solids circulation rates and solids inventories of an interconnected circulating fluidized bed reactor system for $CO_2$ capture by calcium looping. Chemical Engineering Journal 198-199, 228–235.

Dieter, H., Hawthorne, C., Bidwe, A.R., Zieba, M., Scheffknecht, G., 2012. The 200 kWth dual fluidized bed calcium looping pilot plant for efficient $CO_2$ capture: plant operating experiences and results. In: Proceeding of the 21st International Conference on Fluidized Bed Combustion, Naples (Italy), pp. 397–404.

Edwards, S.E.B., Materic, V., 2012. Calcium looping in solar power generation plants. Solar Energy 86, 2494–2503.

Galloy, A., Ströhle, J., Epple, B., 2011. Design and operation of a 1 $MW_{th}$ carbonate and chemical looping CCS test rig. VGB Power Tech 91, 64–98.

González, B., Alonso, M., Abanades, J.C., 2010. Sorbent attrition in a carbonation/calcination pilot plant for capturing $CO_2$ from flue gases. Fuel 89, 2918–2924.

González, B., Grasa, G.S., Alonso, M., Abanades, J.C., 2008. Modeling of the Deactivation of CaO in a Carbonate Loop at High Temperatures of Calcination. Industrial and Engineering Chemistry Research 47, 9256–9262.

Grasa, G.S., Abanades, J.C., 2006. $CO_2$ capture capacity of CaO in long series of carbonation/calcination cycles. Industrial and Engineering Chemistry Research 45, 8846–8851.

Grasa, G., Abanades, J.C., Alonso, M., González, B., 2008. Reactivity of highly cycled particles of CaO in a carbonator/calcination loop. Chemical Engineering Journal 137, 561–567.

Harrison, D.P., 2008. Sorption-enhanced hydrogen production: a review. Industrial and Engineering Chemistry Research 47, 6486–6501.

Hawthorne, C., Dieter, H., Bidwe, A., Schuster, A., Scheffknecht, G., Unterberger, S., Käb, M., 2011. CO2 capture with CaO in a 200 kWth dual fluidized bed pilot plant. Energy Procedia 4, 441–448, 2011.

Hawthorne, C., Trossmann, M., Galindo, C.P., Schuster, A., Scheffknecht, G., 2009. Simulation of the carbonate looping power cycle. Energy Procedia 1, 1387–1394.

Jia, L., Hughes, R., Lu, D.Y., Anthony, E.J., 2007. Attrition of calcining limestone in circulating fluidized-bed systems. Industrial and Engineering Chemistry Research 46, 5199–5209.

Junk, M., Reitz, M., Ströhle, J., Epple, B., 2012. Thermodynamic evaluation and cold flow model testing of an indirectly heated carbonate looping process. In: 2nd International Conference on Chemical Looping, 26–28 September 2012, Darmstadt, Germany.

Lasheras, A., Ströhle, J., Galloy, A., Epple, B., 2011. Carbonate looping process simulation using a 1D fluidized bed model for the carbonator. International Journal of Greenhouse Gas Control 5, 686–693.

Li, Z.-S., Cai, N.-S., Croiset, E., 2008. Process analysis of $CO_2$ capture from flue gas using carbonation/calcination cycles. AIChE Journal 54, 1912–1925.

Lisbona, P., Martinez, A., Lara, Y., Romeo, L.M., 2010. Integration of carbonate $CO_2$ capture cycle and coal-fired power plants. A comparative study for different sorbents. Energy and Fuels 24, 728–736.

Lysikov, A.I., Salanov, A.N., Okunev, A.G., 2007. Change of $CO_2$ carrying capacity of CaO in isothermal recarbonation–decomposition cycles. Industrial and Engineering Chemistry Research 46, 4633–4638.

Martínez, I., Murillo, R., Grasa, G., Abanades, J.C., 2011a. Integration of a Ca looping system for $CO_2$ capture in existing power plants. AIChE Journal 57, 2599–2607.

Martínez, I., Murillo, R., Grasa, G., Rodríguez, N., Abanades, J.C., 2011b. Conceptual design of a three fluidised beds combustion system capturing $CO_2$ with CaO. International Journal of Greenhouse Gas Control 5, 498–504.

Myöhänen, K., Hyppänen, T., Pikkarainen, T., Eriksson, T., Hotta, A., 2009. Near Zero $CO_2$ emissions in coal firing with oxyfuel CFB boiler. Chemical Engineering and Technology 3, 355–363.

Plötz, S., Bayrak, A., Galloy, A., Kremer, J., Orth, M., Wieczorek, M., Ströhle, J., Epple, B., 2012. First carbonate looping experiments with a 1 $MW_{th}$ test facility consisting of two interconnected CFBs. In: Proceedings of the 21st International Conference on Fluidized Bed Combustion, Naples (Italy), pp. 421–428.

Ramkumar, S., Fan, L.-S., 2010. Calcium looping process (CLP) for enhanced noncatalitic hydrogen production with integrated carbon dioxide capture. Energy and Fuels 24, 4408–4418.

Rodríguez, N., Alonso, M., Abanades, J.C., 2011a. Experimental investigation of a circulating fluidized-bed reactor to capture $CO_2$ with CaO. AIChE Journal 57, 1356–1366.

Rodríguez, N., Alonso, M., Abanades, J.C., Charitos, A., Hawthorne, C., Scheffknecht, G., Lu, D.Y., Anthony, E.J., 2011b. Comparison of experimental results from three dual fluidized bed test facilities capturing $CO_2$ with CaO. Energy Procedia 4, 393–401.

Romano, M., 2009. Coal-fired power plant with calcium oxide carbonation for post-combustion $CO_2$ capture. Energy Procedia 1, 1099–1106.

Romeo, L.M., Abanades, J.C., Escosa, J.M., Paño, J., Giménez, A., Sánchez-Biezma, A., Ballesteros, J.C., 2008. Oxyfuel carbonation/calcination cycle for low cost $CO_2$ capture in existing power plants. Energy Conversion and Management 49, 2809–2814.

Romeo, L.M., Lara, Y., Lisbona, P., Escosa, J.M., 2009. Optimizing make-up flow in a $CO_2$ capture system using CaO. Chemical Engineering Journal 147, 252–258.

Sánchez-Biezma, A., Ballesteros, J.C., Diaz, L., de Zárraga, E., Álvarez, F.J., López, J., Arias, B., Grasa, G., Abanades, J.C., 2011. Postcombustion $CO_2$ capture with CaO. Status of the technology and next steps towards large scale demonstration. Energy Procedia 4, 852–859.

Sanchez-Biezma, A., Paninagua, J., Díaz, L., Lorenzo, M., Alvarez, J., Martínez, D., Arias, B., Diego, M.E., Abanades, J.C., 2013. Testing postcombustion $CO_2$ capture with CaO in a 1.7 MWt pilot facility. Energy Procedia 37, 1–8.

Shimizu, T., Hirama, T., Hosoda, H., Kitano, K., Inagaki, M., Tejima, K., 1999. A twin fluid-bed reactor for removal of $CO_2$ from combustion processes. Chemical Engineering Research and Design 77, 62–68.

Ylätalo, J., Ritvanen, J., Arias, B., Tynjälä, T., Hyppänen, T., 2012. 1-Dimensional modelling and simulation of the calcium looping process. International Journal of Greenhouse Gas Control 9, 130–135.

Yongping, Y., Rongrong, Z., Liqiang, D., Kavosh, M., Patchigolla, K., Oakey, J., 2010. Integration and evaluation of a power plant with a CaO-based $CO_2$ capture system. International Journal of Greenhouse Gas Control 4, 603–612.

Zhao, M., Andrew, I.M., Harris, T., 2013. Review of techno-economic models for the retrofitting of conventional pulverised-coal power plants for post-combustion capture (PCC) of $CO_2$. Energy and Environmental Science 6, 25–40.

## 3.2 Captura de $CO_2$ *in situ* en la planta piloto de 300 $kW_t$ de La Robla

Esta planta experimental de combustión de biomasa y captura simultánea de $CO_2$ surgió en el marco del proyecto nacional CENITCO2, posteriormente MENOSCO2, y comenzó a construirse en el año 2009 en el recinto de la central térmica de La Robla (León), propiedad de Gas Natural Fenosa. El diseño básico se basó en los trabajos realizados por el INCAR-CSIC en su planta de 30 $kW_t$ y el diseño en detalle se llevó a cabo entre las empresas Aries y Socoin. Tras su puesta en marcha y la realización de algunas pruebas aisladas sin éxito, el INCAR-CSIC rediseñó varios componentes clave, entre los que destaca un nuevo sistema de intercambio de calor con camisas de agua en la línea de retorno de sólidos hacia el combustor-carbonatador, varias modificaciones sobre las *loop-seals* y la instrumentación de la planta. La primera campaña experimental con combustión y captura simultánea de $CO_2$ tuvo lugar en noviembre de 2012. Desde entonces esta instalación ha acumulado 750 h con combustión de biomasa, de las cuales 550 h corresponden a captura de $CO_2$ *in situ*.

### 3.2.1 Descripción de la instalación experimental

El bucle principal del sistema actual mostrado en la Figura 9 está formado por un reactor combustor-carbonatador y un calcinador de lecho fluidizado circulante. Los sólidos que salen de cada reactor se dirigen, tras pasar por un ciclón primario, hacia una válvula de sólidos o *loop-seal* que se fluidiza con aire y permite la circulación de sólidos entre reactores (en esta instalación no hay posibilidad de circulación interna). Existen también unos ciclones secundarios que ayudan a retener los sólidos que salen junto con el gas por los ciclones primarios antes de su expulsión a través de la chimenea, lo que permite cerrar con buena precisión el balance de sólidos en el sistema y detectar disfunciones en las *loop-seals*.

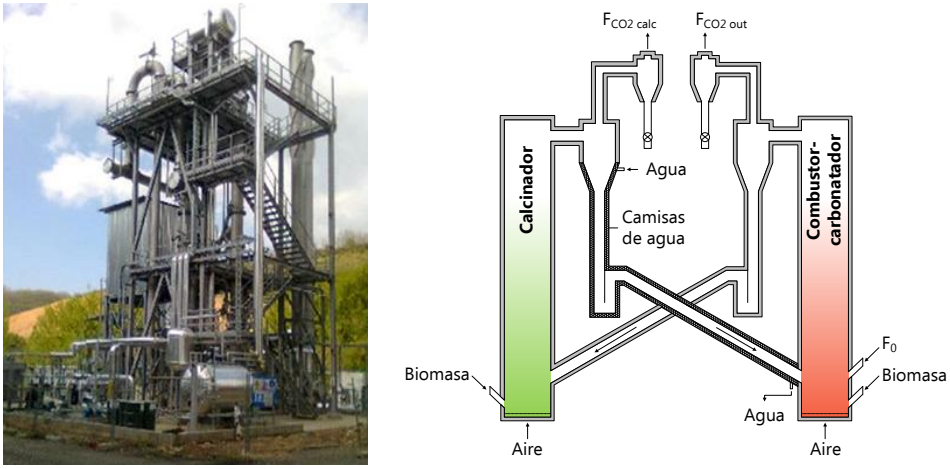


**Figura 9.** Izq.) Fotografía de la planta piloto de La Robla. Dcha.) Esquema de la instalación experimental de captura de $CO_2$ de La Robla.

La estructura de ambos reactores está hecha de material refractario con un diámetro interno de 0.4 m, de modo que la velocidad del gas (2-4 m/s) es del orden de la encontrada en calderas de biomasa de lecho fluidizado circulante. En el diseño de la planta también se tuvo en cuenta la necesidad de altos inventarios y tiempos de residencia de los sólidos en los reactores, por lo que tanto el combustor-carbonatador como el calcinador tienen una altura de 12 m. Es importante destacar que aunque el concepto de captura de $CO_2$ *in situ* con CaO implica condiciones de oxi-combustión en el calcinador, en este caso y por sencillez, este reactor opera únicamente en condiciones de combustión con aire.

Esta instalación emplea pellets de madera de pino como combustible con una composición del 50.72% C, 6.11% H, 0.20% N, 0.01% S y 42.96% O (base seca), que se alimentan a los dos reactores a través de tornillos sin fin refrigerados. Durante el arranque, y hasta que se alcanzan temperaturas de 550ºC aproximadamente, el sistema calienta el aire de entrada a los reactores mediante dos quemadores de propano que tienen una potencia de 100 $kW_t$ cada uno. También existe la posibilidad de introducir caliza

continuamente al combustor-carbonatador para compensar las pérdidas de las partículas más finas que abandonan el sistema con el gas de salida y mantener suficiente inventario de CaO activo. De igual modo, se pueden extraer sólidos del sistema a través del calcinador y del combustor-carbonatador, en este último de manera continua.

Un aspecto importante durante la operación de la planta es la extracción del calor generado tanto en la reacción de combustión como en la reacción de carbonatación para mantener una temperatura adecuada en el combustor-carbonatador. Con este objetivo, se ha optado por enfriar la corriente de partículas que llega a este reactor, y para ello se han dispuesto una serie de camisas de agua independientes en el circuito de los sólidos que salen del calcinador, desde la parte tronco-cónica del ciclón primario hasta la entrada al combustor-carbonatador, como se muestra en la Figura 9 (dcha.).

Durante la realización de los experimentos se miden en continuo numerosas variables. Al igual que se ha descrito en la sección 3.1.1 para la planta piloto de La Pereda, en esta planta también hay instalados i) termopares tipo K que permiten conocer la temperatura en distintos puntos de la instalación en todo momento; ii) transductores de presión diferenciales y relativos; iii) medidores másicos para conocer el aire que entra a los reactores y *loop-seals*; iv) un analizador de gases que determina el porcentaje de $CO_2$, $O_2$ y CO, y otro que mide además $C_xH_y$ como contenido en $CH_4$, y que pueden intercambiarse para medir la corriente gaseosa de salida de cualquiera de los dos reactores; v) tres sondas de zirconio (en las zonas central y alta del combustor-carbonatador, y en la parte alta del calcinador) que miden el porcentaje de oxígeno y permiten detectar si una fracción del aire que se introduce a las *loop-seals* sale directamente a través del ciclón (*split*), ya que cuando esto ocurre el contenido en $O_2$ medido por el analizador es superior al detectado por la sonda de zirconio. Por otra parte, las muestras sólidas se extraen de la zona superior de los reactores por medio de sondas isocinéticas que permiten determinar además la circulación de sólidos entre

reactores. Las muestras generadas durante los experimentos se caracterizan como se ha descrito en la sección 3.1.1 para conocer su distribución de tamaño, composición química y reactividad con $CO_2$, con la salvedad de que en este caso no se determina su contenido en cenizas dada su escasa presencia en la biomasa empleada como combustible.

### 3.2.2 Procedimiento experimental

A continuación se detalla el protocolo experimental que se sigue para iniciar un experimento de captura de $CO_2$ con CaO en la planta piloto de La Robla.

En primer lugar se cargan aproximadamente 300 kg de caliza en el sistema y, una vez distribuida en los reactores y *loop-seals*, se arrancan los quemadores de propano para iniciar el calentamiento. Durante este período inicial tanto el combustor-carbonatador como el calcinador se mantienen con un caudal bajo de aire con objeto de mantener velocidades de gas por debajo de 1 m/s y limitar la circulación de sólidos "fríos", lo que favorece que el lecho de los reactores se caliente lo más rápidamente posible. Una vez que el lecho tiene una temperatura de 400ºC se comienza a alimentar un pequeño flujo de biomasa, no sin antes comprobar que los gases de salida de los ciclones secundarios están por encima de 100ºC. Esto se debe a que esta zona es la más fría de la instalación, y de este modo se asegura la evaporación del agua generada por la combustión del propano en todo el circuito, ya que podría ocasionar, en contacto con los sólidos circulantes, problemas de atascos en la instalación. Cuando el lecho alcanza los 550ºC se apagan los quemadores de propano y se aumenta la velocidad de alimentación de biomasa a ambos reactores para compensar la pérdida de potencia de calentamiento. A temperaturas cercanas a 650ºC se activa la circulación en el sistema incrementando el flujo de aire de los reactores y *loop-seals*, así como el de biomasa para continuar aumentando la temperatura. Es en este momento cuando la temperatura de las líneas de interconexión y *loop-seals* comienza a aumentar a gran velocidad en

contacto con una corriente de sólidos calientes, y es importante activar el flujo de agua a través de las camisas de refrigeración situadas en la línea de sólidos desde el calcinador al combustor-carbonatador antes de que se alcancen los 300ºC para prevenir el estrés térmico de los materiales. Finalmente, cuando la temperatura de los reactores ronda los 700ºC, se limita la biomasa en el combustor-carbonatador para mantener esta temperatura y se aumenta la potencia de combustión en el calcinador hasta conseguir condiciones de calcinación. Finalmente, se adaptan las condiciones de operación a las deseadas en cada caso para la realización del experimento. La duración aproximada del proceso completo descrito anteriormente es de 10 horas.

La calcinación de la carga tiene lugar en estas condiciones de flujo interconectado, de modo que el CaO activo que se va generando reacciona en el combustor-carbonatador con el $CO_2$ resultante de la combustión de biomasa, dando lugar a un flujo continuo de $CaCO_3$. Es importante destacar que durante esta etapa de calcinación y también en la operación posterior se descargan y pesan los sólidos retenidos en los ciclones secundarios cada cierto intervalo de tiempo para cerrar el balance de sólidos. Además, esta operación permite detectar y corregir casos de disfunción de las *loop-seals*, ya que si esto ocurre la cantidad de partículas que se recoge en los ciclones secundarios es inusualmente alta. A medida que el inventario de sólidos del sistema va aumentando su grado de calcinación se aprecia un incremento progresivo de la eficacia de captura de $CO_2$ en el combustor-carbonatador y, además, la temperatura del calcinador se va incrementando para la misma cantidad de biomasa alimentada y similar circulación de sólidos.

Durante los experimentos llevados a cabo en esta instalación se registra una gran cantidad de señales que permiten el control y seguimiento del proceso de un modo análogo a como se ha expuesto en la sección 3.1.2 para la planta piloto de La Pereda. No obstante, además de la medición de las variables mencionadas en dicha sección, la planta piloto de La Robla cuenta

con sondas de zirconio que miden el contenido de oxígeno en el interior del combustor-carbonatador y el calcinador. De este modo, cuando se comparan las concentraciones de oxígeno a la salida de los reactores con la de los analizadores es posible detectar la existencia de *split* en el aire de fluidización de las *loop-seals* hacia los ciclones primarios.

La duración de los experimentos que se desarrollan en esta planta es variable, aunque al igual que en el caso de La Pereda, el objetivo es operar la instalación durante tiempos largos (días) para probar varias condiciones de proceso y dar tiempo a que se alcancen estados estacionarios de operación. Los resultados obtenidos en esta planta piloto durante diversas campañas experimentales se presentan en la *Publicación II* contenida en la sección 3.2.3, que incluye además una discusión de los resultados y la aplicación de un modelo del combustor-carbonatador que considera combustión y captura de $CO_2$ simultáneas.

### 3.2.3 Publicación II

**Biomass combustion with in situ $CO_2$ capture by CaO in a 300 $kW_{th}$ circulating fluidized bed test facility**

Publicado en:

*International Journal of Greenhouse Gas Control*

*Volumen* 29

Páginas 142-152

Año 2014

International Journal of Greenhouse Gas Control 29 (2014) 142–152

Contents lists available at ScienceDirect

International Journal of Greenhouse Gas Control

journal homepage: www.elsevier.com/locate/ijggc

# Biomass combustion with in situ $CO_2$ capture by CaO in a 300 $kW_{th}$ circulating fluidized bed facility

M. Alonso [a,*], M.E. Diego [a], C. Pérez [b], J.R. Chamberlain [b], J.C. Abanades [a]

[a] Spanish Research Council, INCAR-CSIC, C/ Francisco Pintado Fe, 26, 33011 Oviedo, Spain
[b] Gas Natural Fenosa, GNF, Avenida de San Luis 77, Madrid, Spain

ARTICLE INFO

*Article history:*
Received 9 July 2014
Received in revised form 5 August 2014
Accepted 6 August 2014

*Keywords:*
Biomass combustion
$CO_2$ capture
Negative emissions
Calcium looping
BECCS

ABSTRACT

This paper reports experimental results from a new 300 $kW_{th}$ calcium looping pilot plant designed to capture $CO_2$ "in situ" during the combustion of biomass in a fluidized bed. This novel concept relies on the high reactivity of biomass as a fuel, which allows for effective combustion around 700 °C in air at atmospheric pressure. In these conditions, CaO particles fed into the fluidized bed combustor react with the $CO_2$ generated during biomass combustion, allowing for an effective $CO_2$ capture. A subsequent step of regeneration of $CaCO_3$ in an oxy-fired calciner is also needed to release a concentrated stream of $CO_2$. This regeneration step is assumed to be integrated in a large scale oxyfired power plant and/or a larger scale post-combustion calcium looping system.

The combustor-carbonator is the key reactor in this novel concept, and this work presents experimental results from a 300 $kW_{th}$ pilot to test such a reactor. The pilot involves two 12 m height interconnected circulating fluidized bed reactors. Several series of experiments to investigate the combustor-carbonator reactor have been carried out achieving combustion efficiencies close to 100% and $CO_2$ capture efficiencies between 70 and 95% in dynamic and stationary state conditions, using wood pellets as a fuel. Different superficial gas velocities, excess air ratios above stoichiometric requirements, and solid circulating rates between combustor-carbonator and combustor-calciner have been tested during the experiments. Closure of the carbon and oxygen balances during the combustion and carbonation trials has been successful. A simple reactor model for combustion and $CO_2$ capture in the combustor-carbonator has been applied to aid in the interpretation of results, which should facilitate the future scaling up of this process concept.



## 1. Introduction

Calcium looping, CaL, or "carbonate looping" embraces a range of $CO_2$ capture technologies where CaO is used as a regenerable sorbent of $CO_2$. During the $CO_2$ absorption step at atmospheric pressure, the carbonation reaction of CaO with $CO_2$ at temperatures between 600 and 750 °C takes place. During the regeneration step, calcination of $CaCO_3$ at temperatures above 870 °C in a rich atmosphere of $CO_2$ is achieved by oxyfuel combustion of an additional fuel in the calciner. Several recent reviews (Blamey et al., 2010; Anthony, 2011; Abanades, 2013; Boot-Handford et al., 2014) have highlighted the theoretical benefits of this technology that arise from the possibility to efficiently recover the energy used for sorbent regeneration.

The CaL technology is being rapidly scaled up as a post-combustion $CO_2$ capture system because of the similarity of the key reactors (carbonator and calciner) with those in existing power plants using circulating fluidized bed combustors, CFBCs. The post-combustion process scheme was early proposed by Shimizu et al. (1999) and further developed in the early 2000s at laboratory and bench scales in our group (Abanades, 2002; Abanades and Alvarez, 2003; Abanades et al., 2004). This was followed by the publication of results from several lab scale fluidized bed pilots (10 s $kW_{th}$) involving continuous solid circulation (Alonso et al., 2010; Charitos et al., 2010, 2011; Rodriguez et al., 2011a). More recently, steady state results have been reported from 0.2 $MW_{th}$ pilot located in Stuttgart University (Hawthorne et al., 2010; Dieter et al., 2014) and a 1 $MW_{th}$ pilot in Darmstadt (Galloy et al., 2011; Ströhle et al., 2014; Plötz et al., 2012). Other large scale pilots are being built in Taiwan (Chang et al., 2013). The largest calcium looping pilot (1.7 $MW_{th}$) successfully operated in post-combustion mode is located in La Pereda CFBC power plant (Spain) and has recently reported

* Corresponding author. Tel.: +34 985119090; fax: +34 985297662.
*E-mail address:* mac@incar.csic.es (M. Alonso).

http://dx.doi.org/10.1016/j.ijggc.2014.08.002
1750-5836/

**Nomenclature**

*Notation*

| | |
|---|---|
| $E$ | $CO_2$ capture efficiency |
| $F$ | molar flow rate, mol/m$^2$ s |
| $F_0$ | molar fresh limestone make-up, mol/m$^2$ s |
| $F_{Ca}$ | calcium molar flow rate between reactors, mol/m$^2$ s |
| $f_a$ | active fraction of solids |
| $G_s$ | solids circulation flow rate, kg/m$^2$ s |
| $h$ | reaction height, m |
| $k$ | volumetric reaction constant, s$^{-1}$ |
| $k_{s,ap}$ | apparent superficial carbonation reaction constant, s$^{-1}$ |
| $n_{Ca}$ | calcium mol in the combustor-carbonator, mol/m$^2$ |
| $Q$ | mass flow rate, kg/h |
| $T$ | temperature, °C |
| $u$ | gas velocity, m/s |
| $W$ | solids inventory in the combustor-carbonator, kg/m$^2$ |
| $X$ | carbonate molar fraction |
| $X_{ave}$ | maximum carrying capacity |

*Subscripts*

| | |
|---|---|
| bio | biomass |
| carb | at combustor-carbonator |
| calc | at calciner |
| comb | combustion |
| out | at the exit of combustor-carbonator |
| eq | at equilibrium conditions |
| $O_{2,0}$ | $O_2$ at the inlet of combustor-carbonator |
| $O_{2,e}$ | $O_2$ at the excess |

*Greek letters*

| | |
|---|---|
| $\nu$ | volumetric fraction (vol%) |
| $\alpha$ | stoichiometric coefficient |

several hundreds of hours of steady state results treating 1/150th of the flue gases of the existing coal power plant and achieving continuous calcination of $CaCO_3$ by oxy-combustion of coal in a CFBC (Sánchez-Biezma et al., 2012; Arias et al., 2013).

In this work we deal with a particular process variant of a Calcium looping system that intends to exploit the high temperature CaO/$CaCO_3$ chemical loop to achieve the effective capture of $CO_2$ "in situ" during the combustion of biomass in a fluidized bed boiler (Abanades et al., 2011a). The use of biomass as a fuel in CCS systems (Bio-CCS or BECCS) leads to processes with negative emissions of $CO_2$ (Ishitani and Johansson, 1996; Obersteiner et al., 2001; Rhodes and Keith, 2008). BECCS technologies may need to be deployed to meet the lowest targets of atmospheric $CO_2$ concentration (Koornneef et al., 2012; IPCC, 2014) as these technologies are the only option to reverse historical emissions of $CO_2$.

The schematic concept of the particular Calcium Looping process considered in this work is represented in Fig. 1. It includes two interconnected circulating fluidized bed combustors ($CFBC_S$). One of the $CFBC_s$ is operating at modest combustion temperatures (700 °C) to allow for simultaneous $CO_2$ capture by carbonation of CaO (the equilibrium partial pressure of $CO_2$ on CaO at atmospheric pressure is just 3.0 vol% at 700 °C). The $CaCO_3$ formed in this CFB combustor-carbonator reactor circulates to the second CFBC operated in oxyfuel combustion mode at a typical biomass combustion temperature range (840–900 °C) (Saidur et al., 2011), where the $CO_2$ is released and the CaO regenerated to circulate back to the CFB combustor-carbonator. The concept has been already demonstrated by our group in a 30 $kW_{th}$ test facility over a range of

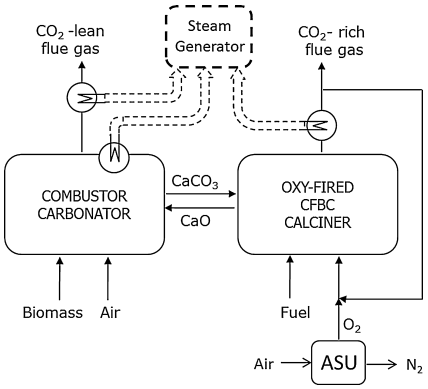


**Fig. 1.** General scheme for the biomass combustion with in situ $CO_2$ capture by CaO process.

operating conditions (Alonso et al., 2011). Overall $CO_2$ capture efficiencies higher than 80% were achieved with sufficiently high solids circulation rates of CaO and solids inventories in the combustor-carbonator.

The fundamental advantage of the system of Fig. 1 respect to stand alone oxy-fired scheme is that the $O_2$ consumption is about 1/3 of the equivalent oxy-fired system burning the same total flow of biomass and fuel. A recent economic and process analysis of the concept of Fig. 1 (Ozcan et al., 2014) has revealed the technical and economic boundary conditions for this niche application of calcium looping and biomass firing in power plants to be economically viable. The close similarity of each of the main reactors in the system with commercial CFBC power plants enables an evaluation of electricity and $CO_2$ avoided cost (Ozcan et al., 2014) that indicates that this process achieves around 43 €/tonne $CO_2$ avoided, only slightly lower than the cost of a stand-alone oxy-fired system burning biomass operating under comparable conditions. However, a further advantage of this system is that it can be adapted to a wider range of regulatory conditions and avoided cost can even take negative values when there are economic incentives for the both the storage of $CO_2$ from biomass firing and green certificate for biomass use in air fired power plants. The in situ calcium looping option becomes more economical and more flexible to adapt to different market conditions than air-fired biomass plants and oxy-fired plants alone. This is particularly the case when the biomass plant is co-located with an oxy-fired coal power plant or a much larger post-combustion calcium looping plant supplying the CaO to the combustor carbonator (Ozcan et al., 2014).

The purpose of this work is to report experimental results from a 300 $kW_{th}$ pilot designed, built and operated to demonstrate the viability of the process in an industrial environment and with sufficiently long duration tests (up to a week-long). The pilot is located at a 655 $MW_e$ coal power plant of "GNF-La Robla" (León, Spain). Several series of experiments, specially focused in the demonstration of the simultaneous combustion-carbonation reactor concept, have been successfully achieved so far. The interpretation of experimental results with a simple reactor model for combustion and $CO_2$ capture by CaO in the combustor-carbonator are also discussed in this work to aid in future scaling up of this novel $CO_2$ capture concept with negative emissions.

## 2. Experimental

Two interconnected circulating fluidized bed reactors (combustor-carbonator and calciner) are at the core of the pilot plant used to carry out the experimental campaigns in this work. The height of both reactors is 12 m and the internal diameter is about 0.4 m. Although the process concept of Fig. 1 involves $O_2/CO_2$ combustion in one of the reactors, the design of this pilot has been simplified to operate in air-combustion mode in both reactors. This allows to test under more controlled conditions the novel reactor in the system (the combustor-carbonator). Air is blown to both $CFBC_s$ using two fans and is introduced as primary air to the bottom of the reactors by nozzles. Only a small fraction of secondary air (about 10 vol%) comes as secondary air with the biomass feed. The solids that exit the reactors are separated by means of primary cyclones and sent through standpipes to the bubbling bed loop-seals, which are equipped with two chambers fluidized with air. The particles that abandon the loop-seals go into a dipleg where they flow by gravity towards the opposite reactor. There are also two secondary cyclones that recover very few solids under normal operating conditions but that act as a security solid separation devices when a malfunction in the operation in the primary cyclones occurs (for example by a rupture of the gas seal in the loop-seals).

Both reactors are refractory lined (grey shaded area in Fig. 2) to reduce heat losses and maintain the high temperatures required by the process. The same happens to the cyclone, the standpipe, the loop-seal and the dipleg that carry solids from the combustor-carbonator to the calciner, where the presence of refractory avoids excessive cooling of the particles and reduces the amount of fuel required to heat this stream up to calcination temperature. The thermal insulation of the upper part of the primary cyclone and the secondary cyclone of the calciner has been reinforced to minimize drops in temperature in such region leading to deposit formation due to carbonation of CaO particles under the richer $CO_2$ atmospheres abandoning the calciner.

A critical aspect in the pilot design has been the temperature control system in the combustor-carbonator. In order to balance the strong exothermic character of the combustion-carbonation reactions taking place at the bottom of the reactor, it was decided to cool down the solids entering the bottom of the combustor-carbonator and coming from the calciner. For this purpose, water jackets (black shaded area in Fig. 2) were placed over the truncated-cone region of the cyclone, along the standpipe, the loop-seal and the dipleg associated to the calciner to extract heat from the solids flowing from the calciner to the combustor-carbonator. As will be shown later, this heat transfer strategy proved to be successful in sustaining the required temperatures for simultaneous combustion and carbonation in the reactor.

Biomass pellets are continuously fed into the combustor-carbonator and the calciner reactors by water-cooled screw feeders. There is also the possibility to introduce a continuous make-up flow of fresh limestone into the combustor-carbonator by means of a screw feeder. This flow contributes to maintain a stable inventory of solids, since a fraction of fine particles leave the facility either through the secondary cyclones or suspended on the gas that exits the facility through the stack. Solids can be extracted continuously during operation from the combustor-carbonator and in batches from the calciner by opening the valves located in the bottom of the reactors. There are also sampling ports at the exit of the reactors that allow the extraction of solids samples and measure solids circulation rate with isokinetic probes. These solid samples are further analysed by a C/S analyser and a thermogravimetric analyser and the results obtained are used to close the carbon balance and to provide reactivity information for model validation purposes. There are also temperature and pressure taps distributed in different locations in the facility. Zirconia oxygen probes are installed at the middle and the upper part of the combustor-carbonator and at the upper part of the calciner to acquire instant $O_2$ concentrations in those locations. The dry gas composition at the exit of the reactors is registered by using two gas analysers after the secondary cyclones. Both gas analysers measure continuously the $CO_2$, $O_2$ and CO content of the gas and one of them also measures the $C_xH_y$ as a $CH_4$ concentration. They can be switched between reactors, so that they can both be used to characterize the gas stream generated either in the combustor-carbonator or the calciner. The $CO_2$ capture efficiency can be estimated from these gas concentration measurements by

$$E_{carb} = \frac{F_{CO_2,comb} - F_{CO_2,out}}{F_{CO_2,comb}} \quad (1)$$

where $F_{CO_2,comb}$ is the $CO_2$ flowrate generated by combustion and estimated from an oxygen balance, using the continuous $O_2$ measurement at the exit of the combustor-carbonator by the oxygen probe and the analyser in order to take into account a certain split of air across the loop-seal, the flow rate of air through the reactor and the loop-seal and the elemental analysis of the fuel fed to the reactor. The detailed procedure is described elsewhere (Abanades et al., 2011b).

In addition, it is useful to compare continuously the experimental capture efficiency, $E_{carb}$, with the maximum $CO_2$ capture allowed by the equilibrium, $E_{eq}$ that can be estimated by:

$$E_{eq} = \frac{F_{CO_2,comb} - F_{CO_2,eq}}{F_{CO_2,comb}} \quad (2)$$

and the $F_{CO_2,eq}$ is calculated from (Barker, 1973):

$$\nu_{CO_2,eq} = 4.137 \times 10^7 e^{-20474/T} \quad (3)$$

All the experimental campaigns were carried out feeding wood pellets, whose composition and heating values are listed in Table 1. Additionally, two Spanish limestones and another one coming from Germany, which had initial mean particle diameter of 93 μm, 348 μm and 87 μm respectively, were used.

The standard experimental procedure starts with heating the reactors and the solid beds with two propane burners until the bed temperatures are around 300 °C and the gas lines are above 100 °C in order to avoid effects related to water condensation. Then, biomass is fed to both reactors but the gas velocity is kept low in order to increase the temperature at the bottom of the reactors as soon as possible by limiting the solids circulation between reactors. Once the temperature at the bottom of the reactors is higher than 550 °C, the propane burners are switched off and the biomass feed rate to the reactors is increased. When the temperature is over 650 °C, the inlet gas velocity as well as the biomass feed rate are increased in order to increase the solids circulation rate between the reactors and to heat up the primary loop (i.e. the

**Table 1**
Analysis of the biomass pellets used during the experiments (mass basis).

| | | |
|---|---|---|
| Proximate analysis | Moisture (%) | 6.9 |
| | Ash (%) | 0.4 |
| | Volatile (%) | 84.4 |
| | Fixed carbon[b] (%) | 8.3 |
| Ultimate analysis[a] | C (%) | 50.7 |
| | H (%) | 6.11 |
| | N (%) | 0.20 |
| | S (%) | 0.01 |
| | O[b] (%) | 42.3 |
| | LHV (MJ/kg) | 19.2 |
| | HHV (MJ/kg) | 20.4 |

[a] Dry basis.
[b] By difference.

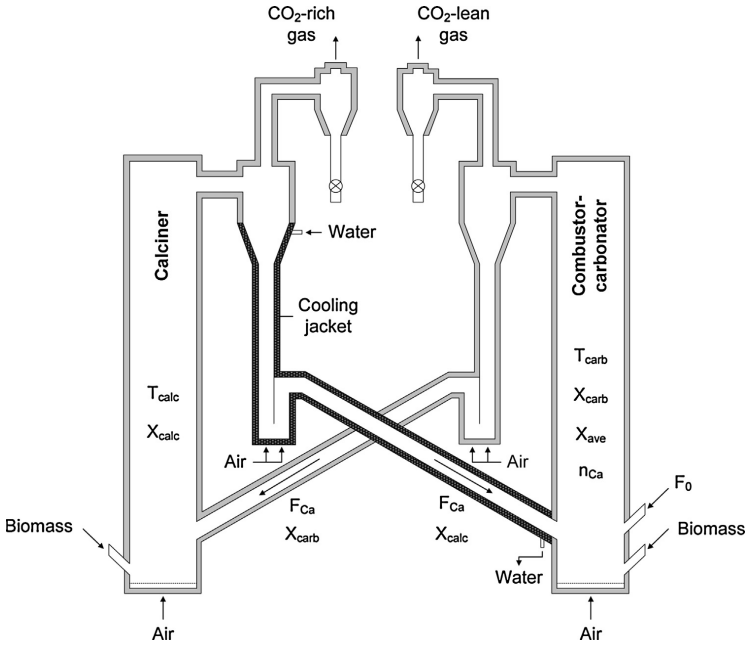


**Fig. 2.** Scheme of "La Robla" calcium looping pilot plant with the main inputs and operating variables. The grey shaded area is refractory lined, the black shaded area is cooled areas through water jackets.

**Table 2**
Experimental range of the main operating conditions in the tests of La Robla pilot plant.

| | | |
|---|---|---|
| Combustor-carbonator temperature (°C) | $T_{carb}$ | 630–720 |
| Combustor-carbonator average gas velocity (m/s) | $u_{carb}$ | 0.9–2.8 |
| Combustor-carbonator solids inventory (kg/m$^2$) | $W$ | 60–380 |
| Excess $O_2$ concentration (vol%) | $v_{O_2,e}$ | 3–12 |
| $CO_2$ concentration from combustion (vol%) | $v_{CO_2,comb}$ | 6–15.4 |
| Maximum average $CO_2$ carrying capacity of solids | $X_{ave}$ | 0.12–0.73 |
| Solids circulation flow rate (kg/m$^2$ s) | $G_s$ | 1–5 |
| Calciner temperature (°C) | $T_{calc}$ | 800–950 |

primary cyclones, standpipes, loop-seals and diplegs). When the temperature at the exit of the calciner primary cyclone is around 300 °C, the water jackets are switched on in order to prevent material stresses. At a temperature around of 700 °C inside the reactors, the inlet gas velocity of the calciner and the biomass feed rate are adjusted in order to increase the average temperature in the calciner. Whereas the biomass feed rate and the inlet gas velocity of the combustor-carbonator are adjusted to maintain the average temperature in the reactor.

## 3. Results and discussion

The test campaigns carried out in the pilot plant involve 750 h in combustion mode of which 550 h were in combustion and in situ $CO_2$ capture mode. The experimental range of the main operating conditions is summarized in Table 2.

An example of a typical experiment in La Robla is shown in Fig. 3, following the experimental procedure described above. The figure is divided in 4 intervals that are briefly summarized in the auxiliary table included in the figure. The first interval is highly dynamic and corresponds to the end of the start-up period, with an arbitrary starting point ($t$ = 0:00 h) that marks the switching off of the propane burners and the increasing of the feeding of biomass to both reactors. During this first interval the main inlet gas velocity of the combustor-carbonator was increased in order to increase the solids circulation flow rate and heat up the full primary solid circulation loop represented in Fig. 1. The limestone make-up feed was switched on and off several times during this interval in order to maintain certain solids inventory in the combustor-carbonator during this non-steady state period (Fig. 3b). The $CO_2$ capture efficiency as well as the maximum $CO_2$ capture efficiency fluctuated accordingly between 22–80% and 48–88% respectively (Fig. 3c). The excess air ratio during this experiment varied to be able to maintain a certain gas velocity while varying the biomass feed rate to sustain reactor temperatures. However, this change in $O_2$ concentration at the exit of the combustor-carbonator (between 7 vol% and 12 vol% in this experiment) had little effect on $CO_2$ capture efficiencies of Fig. 3c. The capture $CO_2$ molar flowrate varied between 0.2 and 1.8 mol/m$^2$ s during this period (Fig. 3b).

The second period in Fig. 3 registers the evolution of the system after setting a certain fuel and air flows to the reactors ($Q_{bio\text{-}carb}$ = 40 kg/h, $Q_{bio\text{-}calc}$ = 76 kg/h, $u_{calc}$ = 2.8 m/s, $u_{carb}$ = 2.3 m/s). As a result the average calciner temperature increased from 800 to 860 °C and the average combustor-carbonator varied between 650 and 740 °C. During this period, there is substantial oscillation in the solids inventory as a consequence of the discontinuously fresh make-up feed (see changes in void dots in Fig. 3b). The $CO_2$ capture molar flow rate increased from 0.9 mol/m$^2$ s to 2.3 mol/m$^2$ s during this period (Fig. 3b) and the $CO_2$ capture efficiency (defined as in Eq. (1)) increased from 22% to a maximum of 87% at 7:20 h whereas the maximum capture efficiency (given by Eq. (2)) was very close to the experimental capture efficiency as the inventory of solids in the reactor increased (period 2 of Fig. 3b).

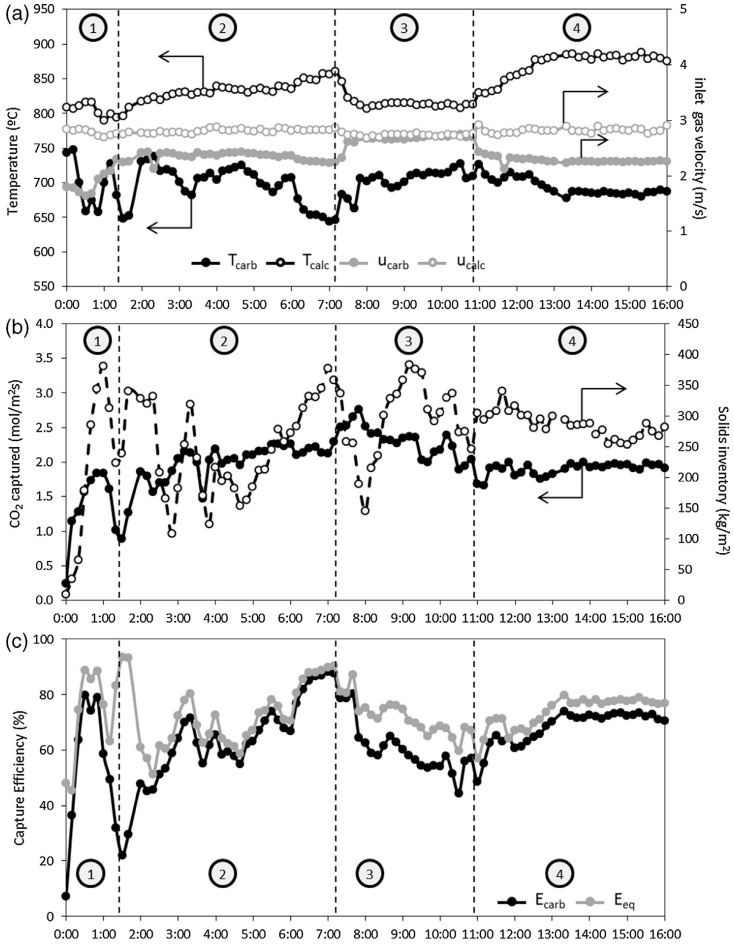


| Interval | Time | Description |
|---|---|---|
| 1 | 0:00 -1:40 | End of the start-up period |
| 2 | 1:40 - 7:20 | Stable flows of biomass and air |
| 3 | 7:20 - 10:50 | Increase the gas velocity to combustor-carbonator |
| 4 | 10:50 - 16:00 | Decrease the gas velocity to combustor-carbonator with stable make-up flow of limestone |

**Fig. 3.** Example of an experimental run in La Robla pilot plant burning biomass pellets of Table 1 and feeding Omyacarb limestone of average dp of 93 μm and $CaCO_3$ content >98%.

The third period in Fig. 3, between 7:20 h and 10:50 h, registers the effect of an increase of the inlet gas velocity to the combustor-carbonator from 2.3 to 2.7 m/s. As can be seen, the average calciner temperature and the difference between calciner temperature and combustor-carbonator temperature decreased due to the increase of solid circulation rate between reactors. The $CO_2$ capture molar flow rate increased to 2.7 mol/m$^2$ s at the beginning of this period as a consequence of the rapid increased in the CaO circulation flowrate. Nonetheless, it tended to decreased to 1.6 mol/m$^2$ s because the calcination intensity was reduced (Fig. 3b) in the calciner, since the temperature droped from 860 to 815 °C at the end of the period, and also as a consequence of the higher temperatures found within the combustor-carbonator (Fig. 3a). The experimental capture efficiency, $E_{carb}$, and the equilibrium efficiency, $E_{eq}$, decreased due to the decrease in the calcination rate linked to lower temperatures in the calciner and due to the increase in the average temperature in the combustor-carbonator.

The fourth experimental period, between 10:50 and 16:00 h, corresponds to a situation as in period 2, but with a continuous flow of limestone around 60 kg/h to sustain stable solid inventories in the combustor-carbonator at around 300 kg/m$^2$. As can be seen, the experimental $CO_2$ capture is very close to the theoretical

maximum during this period for these values of solid inventory in the combustor-carbonator and a stationary state regime is achieved in these conditions that can be extended for much longer periods of time. The longest experiment in steady state conditions has lasted 100 h in this particular pilot. The interruptions in operation or the forced changes in the steady state operating conditions have arisen from malfunction and problems associated to the auxiliary equipment necessary in these small scale pilots (biomass feeding system interruptions, problems with the discharge of solids from the secondary cyclone, deposits of $Ca(OH)_2$ and $CaCO_3$ in the cooled parts downstream of the first cyclone, etc.).

Using the information from steady states periods (2 h duration with stable conditions as in period 4 of Fig. 3), the influence of some operating variables discussed in the following paragraphs.

The effect of the solids inventory on the normalized $CO_2$ capture efficiency ($E_{carb}/E_{eq}$) is shown in the example of Fig. 4a. Two parts of steady states periods with nearly identical set of operating conditions but different bed inventories are represented. The normalized carbonation efficiency is very close to 1 for the higher solids inventory (black line), which indicates that the bed is an extremely efficient reactor capturing the $CO_2$ generated during combustion. In contrast, despite the high value of the average $CO_2$ carrying capacity of the particles used in these particular experiments ($X_{ave}$ = 0.4), when solids inventory is around 100 kg/m$^2$ the average normalized carbonation efficiency drops down to around 0.7. In order to highlight the effect of the average $CO_2$ carrying capacity, Fig. 4b shows the normalized $CO_2$ capture efficiency for other two periods at similar operating conditions. As in the previous case, due to the low solids inventory (80 kg/m$^2$) even at an average $CO_2$ carrying capacity as high as 0.4, the normalized $CO_2$ capture efficiency is around 0.8. When the $CO_2$ carrying capacity of solids decreased to 0.15, the normalized $CO_2$ capture efficiency decreased to around 0.65. These results emphasize the need of sufficient active solids inventory in the combustor-carbonator in order to maximize the $CO_2$ capture efficiency, compensating the modest average activity of the solids with increased total bed inventories.

Fig. 5 includes two examples to illustrate some effects of the average combustor-carbonator temperature on the reactor performance. Fig. 5a corresponds to a rapid decrease of reactor temperature (continuous line of $T_{carb}$) when there is sufficient inventory of active material in the bed. In these conditions, the normalized $CO_2$ capture efficiency (white dots) remains almost constant and close to 1. However, as it indicated from equations (1–3), the net $CO_2$ capture efficiency increases when the carbonation temperature decreases as it is shown by the $E_{carb}$ (black dots) curve. Therefore, in the absence of other limitations, the temperatures needed to achieve high $CO_2$ capture efficiencies in the combustor-carbonator temperature should be as close as possible to around 650° (as in other CaL systems). However, there are indications that the combustion efficiencies sharply decrease at these low temperatures. As shown in Fig. 5b, the emissions of unburned gases (CO, $CH_4$ and other hydrocarbons) are highly sensitive temperatures below 700 °C.

During the tests carried out in this work, the CO and $CH_4$ concentrations were monitored continuously by the on-line gas analysers. Fig. 5b illustrates the strong dependency of combustor-carbonator temperatures with CO. As indicated in Fig. 5b the bed inventory also plays a role in the emission of CO even at temperatures around 700 °C. When the solid inventory is low ($W$ = 80 kg/m$^2$) the average CO concentration increased from 0.3 vol% to almost 0.6 vol% (grey symbols and line). However if the solids inventory is higher (285 kg/m$^2$), at identical combustion conditions, the average CO goes up from 0.1 vol% to just over 0.25 vol% (black symbols and line). As discussed by Werther et al. (2000) emissions of CO are a complex function of one or more of the following factors: a low combustion temperature, a low quality of the mixture between the air and the biomass and a low residence time of the combustible gases in the combustion zone. Other possible factor affecting CO emissions is related to different temperatures and solid loading in the primary cyclone (Leckner and Karlsson, 1993). These factors are highly dependent of the experimental set up and we do not have sufficient information in the pilot to elucidate between these effects. $CH_4$ emissions were below the detection limit (0.01 vol%) at normal operating conditions with temperatures over 700 °C, $O_2$ content over 7 vol% and bed inventories over 60 kg/m$^2$. The equivalent patterns of trace $CH_4$ emissions were much more complex and uncertain in this particular experimental set up and are omitted in this discussion. We leave as beyond the scope of this first work a detailed discussion of trace emissions. It is however obvious from the experimental results obtained so far that a narrow temperature window (around 700 °C) has to be maintained in the combustor-carbonator to operate the concept of Fig. 1 with acceptable $CO_2$ capture efficiencies and minimum emissions of unburned gases.

In order to facilitate a more quantitative interpretation of experimental results the closure of basic mass balances is a first. The methodology to analyse the results is only briefly explained here because it does not differ from previous studies conducted in a 30 kW$_{th}$ test rig published elsewhere (Alonso et al., 2009, 2011; Abanades et al., 2011b; Charitos et al., 2011) and applied also for post-combustion CaL experiments in other test rigs (Alonso et al., 2010; Charitos et al., 2010, 2011; Rodriguez et al., 2011a,b; Arias et al., 2013). The general $CO_2$ mass balance in the combustor carbonator at steady state conditions can be written as:

$$(CO_2 \text{ from combustion} - CO_2 \text{ in flue gas}) = (\text{net gain in } CaCO_3 \text{ in the circulating solid stream}) = (CO_2 \text{ reacting in the bed of CaO}) \quad (4)$$

All these terms can be estimated independently from the experimental data. The first term of Eq. (4) is the $CO_2$ captured from the combustion flue gas generated in the combustor-carbonator. This can be estimated continuously from oxygen mass balance in the combustor-carbonator and the $CO_2$ content in the gas stream leaving this reactor, which allow the calculation of $F_{CO_2,comb}$ and $F_{CO_2,out}$, respectively (see Eq. (1) to estimate $E_{carb}$). The second term can be experimentally estimated from the measurements of circulation flow rates and the difference in carbonate contents between the samples extracted at the exit of the combustor-carbonator and at the exit of the combustor-calciner. To measure solid circulation rates we used isokinetic probes at the exit of both reactors. Moreover, using the heat balance between the water flow through the jackets to cool the circulating solids stream from calciner to combustor-carbonator (see Fig. 1) it is also possible to establish a correlation for the continuous monitoring of solids circulation rates. The difference in the carbonate content of the solids samples ($X_{carb}$ and $X_{calc}$) extracted from the upper part of the reactors was determined by calcination in nitrogen and/or air (to distinguish small contributions from unburned char particles). So, the first $CO_2$ mass balance that can be experimentally checked in the pilot unit is:

$$F_{CO_2,comb}E_{carb} = F_{Ca}(X_{carb} - X_{calc}) \quad (5)$$

Since the make-up flow of fresh limestone is added to the combustor-carbonator, the value of $X_{carb}$ was slightly corrected in steady state experiments to discount the contribution to $X_{carb}$ of the fraction of fresh limestone in the circulating solids abandoning the combustor-carbonator. The application of this mass balance revealed a large difference between experiments conducted with fine limestone ($dp_0 < 100$ μm) and coarser limestones (average

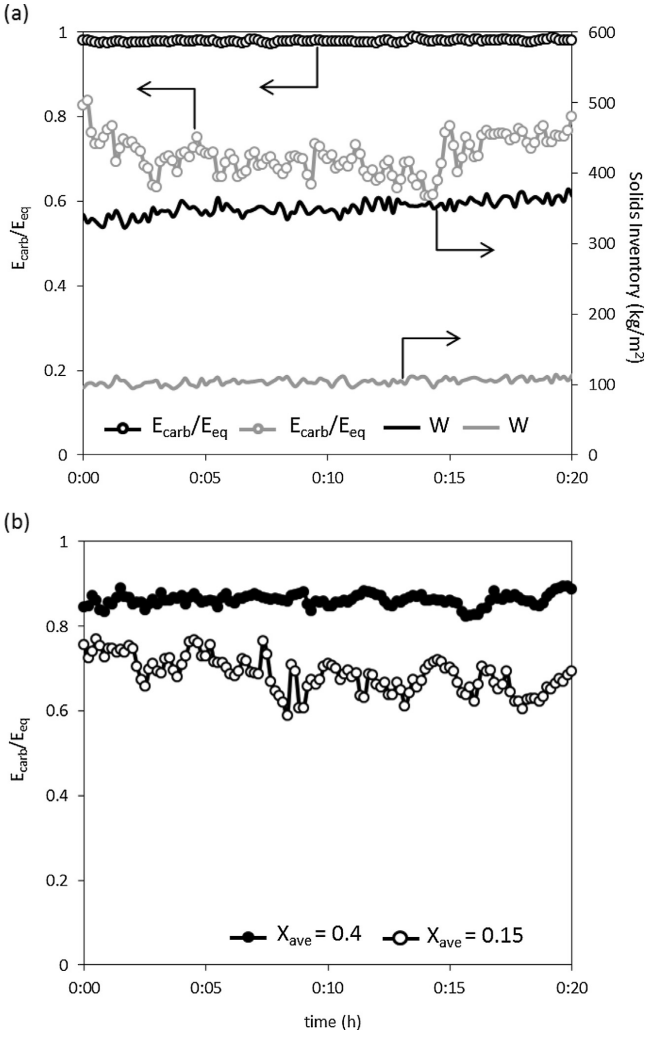


**Fig. 4.** Effect of operating variables on the normalized $CO_2$ capture efficiency. (a) Effect of the solids inventory at $T_{carb}$ = 650 °C and inlet gas velocity of 2.4 m/s and $X_{ave}$ = 0.4. (b) Effect of the $CO_2$ carrying capacity of solids at an inlet gas velocity of 1.8 m/s, $T_{carb}$ = 700 °C and a solids inventory of 80 kg/m$^2$.

$dp_0$ = 348 μm). As can be seen in Fig. 6, the mass balance is relatively well closed for experiments carried out with fine particles (black dots) but it is not fulfilled during the experiments with coarse limestone feed (white dots in Fig. 6). We detected that the carbonate content in the combustor carbonator was much higher than usual in these experiments. It can be speculated that a certain segregation phenomena of dense and coarser limestone particles in this reactor is allowing a substantial step change in carbonate content between the average particles in the bed inventory in this reactor respect to the finer solids actually leaving the reactor and arriving to the calciner. This segregation mechanism was confirmed by measurements of particle size distributions in samples from the bottom of the reactor and samples extracted by the isokinetic probe at the top of reactor. The average particle diameter in the bottom of bed was 200 μm, between 2 and 2.5 times higher than the average particle diameter at the exit of the combustor carbonator and calciner. Since most experiments reported in this work have been conducted with fine limestones ($dp_0$ < 100 μm) no more effort has been placed in analysing the complex segregation phenomena behind the (white dot) results of Fig. 6.

$$F_{CO_2,comb}E_{carb} = n_{Ca,active}\left(\frac{dX}{dt}\right)_{reactor} \quad (6)$$

This equation expresses the fact that a certain inventory of active CaO particles in the combustor-carbonator is responsible of the capture of $CO_2$ from the flue gas by means of a certain average reaction rate of carbonation in the reactor ($dX/dt$). In order to attempt the closure of this mass balance, a simple carbonator model discussed

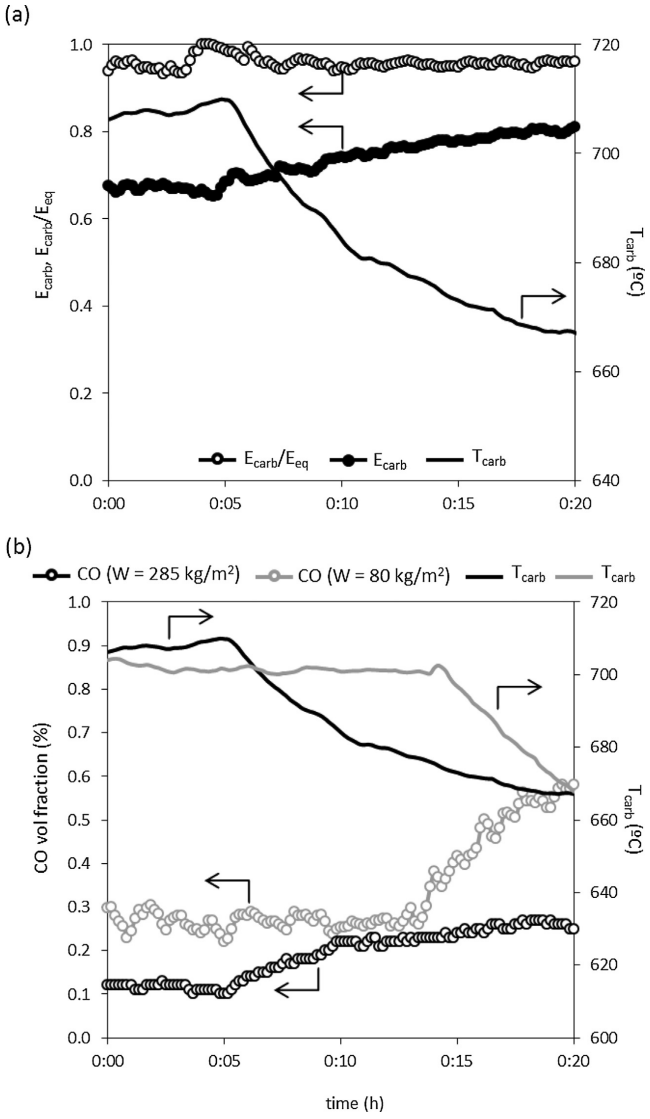


**Fig. 5.** Effect of the average combustor-carbonator. (a) Capture efficiencies at solids inventory of 285 kg/m$^2$ and $X_{ave}$ 0.3 (b) CO emissions as a function of combustor-carbonator temperature and solids inventory. (Grey symbols at solids inventory of 80 kg/m$^2$. Black symbols at solids inventory 285 kg/m$^2$.) Inlet gas velocity 2.3 m/s.

in a previous work (Alonso et al., 2009) is adopted here, which assumes perfect mixing of solids and plug flow for the gas phase. Experimental data obtained in dynamic mode or in transient conditions (like those in experimental periods in 1–3 in Fig. 1) or data obtained with coarse materials (segregation effects noted in Fig. 6) where not considered in the fitting exercise of the model to the experiments. Only those experimental periods with fine particles (well mixed in the combustor-carbonator) and sufficient stability, represented by average values of temperature, solid inventory, average activity of the solids in the reactors, gas velocities and stable values of experimental efficiencies ($E_{carb}$) and $CO_2$ generation by combustion, were considered. In these conditions, it can be assumed that particles react at a constant rate until the maximum carrying capacity ($X_{ave}$) is reached and after that point the reaction rate becomes zero:

$$\left(\frac{dX}{dt}\right)_{reactor} = k_{S,ap} X_{ave} (\overline{v_{CO_2}} - v_{CO_2,eq})$$
$$\left(\frac{dX}{dt}\right)_{reactor} = 0 \quad \text{if} X \geq X_{ave} \tag{7}$$

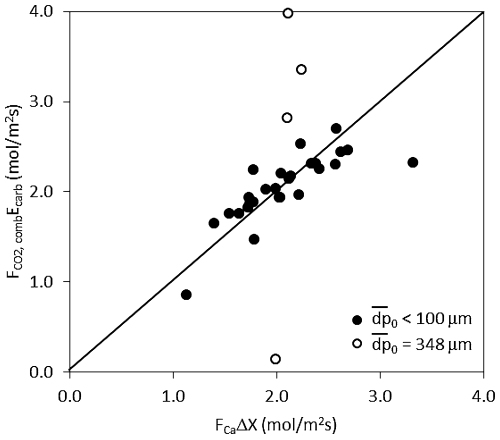


**Fig. 6.** Comparison between the molar $CO_2$ removed from the combustion flue gas generated in the combustor-carbonator and the net increase of the carbonate molar flow between reactors. The second $CO_2$ mass balance incorporates the kinetics of the $CO_2$ carbonation reaction taking place in the combustor-carbonator reactor.

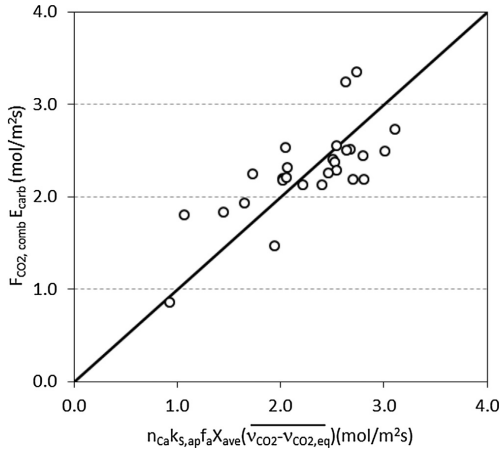


**Fig. 7.** Closure of the mass balance between the $CO_2$ removed from the gas phase and $CO_2$ reacted in the reactor bed.

where $k_{S,ap}$ is the apparent reaction constant ($s^{-1}$).

In order to calculate the average $CO_2$ concentration during "in situ" combustion of biomass in the combustor-carbonator, it is further assumed that the $O_2$ concentration decays exponentially in the bed from the inlet $O_2$ concentration ($v_{O_2,0}$) to the measured exit concentration (experimental $v_{O_2,exit}$). In these conditions, the final expression for the average $CO_2$ concentration over the bed is as follows (Abanades et al., 2011b):

$$(\overline{v_{CO_2}-v_{CO_2,eq}}) = \frac{u}{h}\frac{\alpha(v_{O_2,0}-v_{O_2,e})}{k_{carb}-k_{comb}}\left[(1-e^{-k_{comb}(h/u)})-\frac{k_{comb}}{k_{carb}}(1-e^{-k_{carb}(h/u)})\right] \quad (8)$$

where $k_{carb}$ and $k_{comb}$ are the volumetric kinetic constants associated with the carbonation and the combustion reactions, respectively.

Finally, taking into account the assumption of perfect mixing the active fraction of the solids can be defined as the fraction of particles with a residence time lower than the time needed to increase the carbonate content from $X_{calc}$ to $X_{ave}$, $t^*$.

$$n_{Ca,active} = n_{Ca}f_a = n_{Ca}(1-e^{-t^*/(n_{Ca}/F_{Ca})}) \quad (9)$$

The characteristic carbonation time, $t^*$, can be calculated from the measurements of $X_{calc}$ and $X_{ave}$ from the solids taken and using the reaction rate defined by Eq. (7) (Alonso et al., 2009; Charitos et al., 2011; Arias et al., 2013). By combining Eqs. (7)–(9) into equation (6), the model is fully defined and a simple expression can be obtained:

$$F_{CO_2,comb}E_{carb} = n_{Ca}f_ak_{S,ap}X_{ave}(\overline{v_{CO_2}-v_{CO_2,eq}}) \quad (10)$$

where the average $CO_2$ concentration is calculated from Eq. (8) and $k_{comb}$ from the exit $O_2$ concentration measurements (see details in Abanades et al., 2011b).

The apparent reaction constant ($k_{S,ap}$) can be calculated from the experimental data as it is the only fitting parameter in Eq. (10), and it leads to a value of 0.095 $s^{-1}$, The final comparison between the $CO_2$ removed from the gas phase and the $CO_2$ reacted with the bed using this value for $k_{S,ap}$ is shown in Fig. 7. The closure of the balance is reasonable as the slope of the data is close to 1. This is consistent with results reported from smaller pilot plant and from other post-combustion systems (Abanades et al., 2011b; Alonso et al., 2011; Charitos et al., 2011; Rodriguez et al., 2011a,b; Arias et al., 2013),

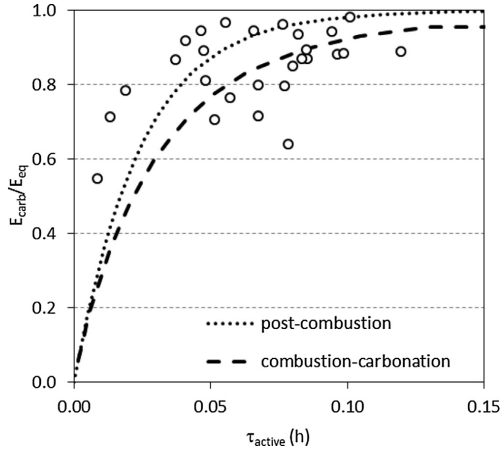


**Fig. 8.** Normalized capture efficiency as a function of the active space time and model predictions for post-combustion and combustion–carbonation assumptions.

which provides confidence for the future scalability of the model and the data.

Finally, a different way of comparison between experimental data and model predictions is shown in Fig. 8 using the normalized $CO_2$ capture efficiency is represented as a function of the active space time ($\tau_{active}$) defined by (Charitos et al., 2011) as:

$$\tau_{active} = \frac{n_{Ca}}{F_{CO_2,comb}}f_aX_{ave} \quad (11)$$

where the solids inventory, the solids activity and the reaction rate are linked through the active fraction $f_a$. From Eq. (11), it can be deduced that a low $X_{ave}$ can be compensated with high solids inventory independently of the combustion sub-model adopted to estimate the $CO_2$ average concentration in the bed. So, in theory, it is possible to achieve similar $\tau_{active}$ values for very different values of solids inventory and $X_{ave}$.

In the case of Fig. 8, the model predictions were estimated for two different model cases: assuming that the combustion constant reaction was infinite (equivalent to a post-combustion where the flue gas resulting from the biomass combustion is all generated at the entrance of the combustor-carbonator) and assuming that the $CO_2$ molar flow from combustion was generating along the bed (combustion-carbonation case referred above). For this purpose, the value of the input parameters in the model were chosen on the basis of the average parameters and operating conditions found in the experimental data. As Fig. 8 shows, the experimental data are mostly around both extreme model lines. In order to ensure a normalized $CO_2$ carbonation efficiency close to 0.9 it is necessary an active space time higher than 0.1 h. These results are an important validation of the simple model described in this work as an important tool for future design and scale-up exercises.

## 4. Conclusions

A novel biomass combustion process involving the "in situ" $CO_2$ capture by CaO in a circulating fluidized bed has been validated in a 300 $kW_{th}$ pilot operated in continuous mode. The operation of the combustor-carbonator reactor supplied by a continuous flow of CaO generated in a continuous fluidized bed calciner achieved 550 h in capture mode. The experimental results confirm the need to operate in a narrow temperature window around 700 °C in the combustor-carbonator, to maximize both combustion and $CO_2$ capture efficiencies. CO and $CH_4$ emissions are an important concern at lower temperatures and the $CO_2$ capture efficiency rapidly drops at higher temperatures limited by the equilibrium of $CO_2$ on CaO. In general, the importance of a sufficient inventory of active CaO in the combustor carbonator (by increasing the $CO_2$ carrying capacity of the circulating solids and/or by increasing the total solids inventory) is confirmed as a critical variable to interpret result from the twin reactor system. The closure of the carbon balance in the system ($CO_2$ capture in the flue gas vs net carbonate circulating from combustor carbonator to calciner) has been successful when fine solid materials are used in the experiments. However, large discrepancies have been detected in experiments conducted with large particles, probably due to segregation effects of denser and coarser particles in the reactor bed inventory.

The application of a simple model for the carbonator-combustor reactor, that assumes perfect and instant mixing of solids and plug flow for the gas phase is sufficient to approximate the experimental results with a reasonable apparent reaction constant. Active space times over 0.1 h are needed to ensure $CO_2$ capture efficiencies close or over 90%. The experimental results and the fitting parameters obtained in this work should be a valuable tool for scaling up of this technology.

## Acknowledgments

This work was partially funded under the MENOS $CO_2$ project (CDTI, Spanish Ministry of Economy and Competitivity). M.E. Diego acknowledges the award of a fellowship Grant under the CSIC JAE Programme, co-funded by the European Social Fund.

## References

Abanades, J.C., 2002. The maximum capture efficiency of $CO_2$ using a carbonation/calcination cycle of CaO/$CaCO_3$. Chem. Eng. J. 90, 303–306.
Abanades, J.C., 2013. Calcium looping for $CO_2$ capture in combustion systems. In: Scala, F. (Ed.), Fluidized bed technologies for near-zero emission combustion and gasification. Woodhead Publishing Limited, Cambridge, pp. 931–971.
Abanades, J.C., Alonso, M., Rodriguez, N., 2011a. Biomass combustion with in situ $CO_2$ capture with CaO, I. Process description and economics. Ind. Eng. Chem. Res. 50, 6972–6981.
Abanades, J.C., Alonso, M., Rodriguez, N., 2011b. Experimental validation of in situ $CO_2$ capture with CaO during the low temperature combustion of biomass in a fluidized bed reactor. Int. J. Greenh. Gas Control 5, 512–520.
Abanades, J.C., Alvarez, D., 2003. Conversion limits in the reaction of $CO_2$ with lime. Energy Fuels 17, 308–315.
Abanades, J.C., Anthony, E.J., Lu, D.Y., Salvador, C., Alvarez, D., 2004. Capture of $CO_2$ from combustion gases in a fluidized bed of CaO. AIChE J. 50, 1614–1622.
Alonso, M., Rodriguez, N., Gonzalez, B., Arias, B., Abanades, J.C., 2011. Biomass combustion with in situ $CO_2$ capture by CaO. II. Experimental results. Ind. Eng. Chem. Res. 50, 6982–6989.
Alonso, M., Rodriguez, N., Gonzalez, B., Grasa, G., Murillo, R., Abanades, J.C., 2010. Carbon dioxide capture from combustion flue gases with a calcium oxide chemical loop. Experimental results and process development. Int. J. Greenh. Gas Control 4, 167–173.
Alonso, M., Rodriguez, N., Grasa, G., Abanades, J.C., 2009. Modelling of a fluidized bed carbonator reactor to capture $CO_2$ from a combustion flue gas. Chem. Eng. Sci. 64, 883–891.
Anthony, E.J., 2011. Ca looping technology: current status, developments and future directions. Greenh. Gas Sci. Technol. 1, 36–47.
Arias, B., Diego, M.E., Abanades, J.C., Lorenzo, M., Diaz, L., Martínez, D., Alvarez, J., Sánchez-Biezma, A., 2013. Demonstration of steady state $CO_2$ capture in a 1.7 $MW_{th}$ calcium looping pilot. Int. J. Greenh. Gas Control 18, 237–245.
Barker, R., 1973. Reversibility of the reaction $CaCO_3 \leftrightarrow CaO + CO_2$. J. Appl. Chem. Biotechnol. 23, 733–742.
Blamey, J., Anthony, E.J., Wang, J., Fennell, P.S., 2010. The calcium looping cycle for large-scale $CO_2$ capture. Prog. Energy Combust. Sci. 36, 260–279.
Boot-Handford, M.E., Abanades, J.C., Anthony, E.J., Blunt, M.J., Brandani, S., Mac Dowell, N., Fernández, J.R., Ferrari, M.C., Gross, R., Hallett, J.P., Haszeldine, R.S., Heptonstall, P., Lyngfelt, A., Makuch, Z., Mangano, E., Porter, R.T.J., Pourkashanian, M., Rochelle, G.T., Shah, N., Yao, J.G., Fennell, P.S., 2014. Carbon capture and storage update. Energy Environ. Sci. 7, 130–189.
Chang, M.H., Huang, C.M., Liu, W.H., Chen, W.C., Cheng, J.Y., Chen, W., Wen, T.W., Ouyang, S., Shen, C.H., Hsu, H.W., 2013. Design and experimental investigation of calcium looping process for 3-$kW_{th}$ and 1.9-$MW_{th}$ facilities. Chem. Eng. Technol. 36, 1525–1532.
Charitos, A., Hawthorne, C., Bidwe, A.R., Sivalingam, S., Schuster, A., Spliethoff, H., Scheffknecht, G., 2010. Parametric investigation of the calcium looping process for CO2 capture in a 10 kW(th) dual fluidized bed. Int. J. Greenh. Gas Control 4, 776–784.
Charitos, A., Rodriguez, N., Hawthorne, C., Alonso, M., Zieba, M., Arias, B., Kopanakis, G., Scheffknecht, G., Abanades, J.C., 2011. Experimental validation of the calcium looping $CO_2$ capture process with two circulating fluidized bed carbonator reactors. Ind. Eng. Chem. Res. 50, 9685–9695.
Dieter, H., Bidwe, A.R., Varela-Duelli, G., Charitos, A., Hawthorne, C., Scheffknecht, G., 2014. Development of the Calcium Looping $CO_2$ Capture Technology from Lab to Pilot Scale at IFK. University of Stuttgart. Fuel.
Galloy, A., Ströhle, J., Epple, B., 2011. Design and operation of a 1 $MW_{th}$ carbonate and chemical looping CCS test rig. VGB PowerTech 91, 64–68.
Hawthorne, C., Dieter, H., Bidwe, A.R., Schuster, A., Scheffknecht, G., Unterberger, S., Käb, M., 2010. $CO_2$ capture with CaO in a 200 $kW_{th}$ dual fluidized bed pilot plant. In: 10th International Conference on Greenhouse Gas Control Technologies. Energy Procedia, Amsterdam, Netherlands.
IPCC, 2014. Mitigation of climate change. Working group III. In: Edenhofer, O., Pichs-Madruga, R., Sokona, Y., Kadner, S., Minx, J., Brunner, S. (Eds.), Contribution to the IPCC 5th Assessment Report. Summary for Policymakers. http://www.ipcc.ch/report/ar5/wg3/
Ishitani, H., Johansson, T.B., 1996. Energy supply mitigation options. In: Watson, R.T., Zinoyowera, M.C., Moss, R.H. (Eds.), Climate Change 1995: Impacts, Adaptations, and Mitigation of Climate Change: Scientific-Technical Analyses. Cambridge University Press, Cambridge, UK.
Koornneef, J., van Breevoort, P., Hamelinck, C., Hendriks, C., Hoogwijk, M., Koop, K., Koper, M., Dixon, T., Camps, A., 2012. Global potential for biomass and carbon dioxide capture, transport and storage up to 2050. Int. J. Greenh. Gas Control 11, 117–132.
Leckner, B., Karlsson, M., 1993. Gaseous emissions from circulating fluidized-bed combustion of wood. Biomass Bioenergy 4, 379–389.
Obersteiner, M., Azar, C., Kauppi, P., Mollersten, K., Moreira, J., Nilsson, S., Read, P., Riahi, K., Schlamadinger, B., Yamagata, Y., Yan, J., van Ypersele, J.P., 2001. Managing climate risk. Science 294, 786–787.
Ozcan, D.S., Alonso, M., Hyungwoong, A., Abanades, J.C., Brandani, S., 2014. Process and cost analysis of a biomass power plant with in-situ calcium looping $CO_2$ capture process. Ind. Eng. Chem. Res., http://dx.doi.org/10.1021/ie500606v.
Plötz, S., Bayrak, A., Galloy, A., Kremer, J., Orth, M., Wieczorek, M., Ströhle, J., Epple, B., 2012. Carbonate looping experiments with a 1 $MW_{th}$ test facility consisting of two interconnected CFBs. In: 21st Conference on Fluidized Bed Combustion, Naples, Italy.
Rhodes, J.S., Keith, D.W., 2008. Biomass with capture: negative emissions within social and environmental constraints: an editorial comment. Clim. Change 87, 321–328.
Rodriguez, N., Alonso, M., Abanades, J.C., 2011a. Experimental investigation of a circulating fluidized-bed reactor to capture $CO_2$ with CaO. AIChE J. 57, 1356–1366.
Rodriguez, N., Alonso, M., Abanades, J.C., Charitos, A., Hawthorne, C., Scheffknecht, G., Lu, D.Y., Anthony, E.J., 2011b. Comparison of experimental results from three dual fluidized bed test facilities capturing $CO_2$ with CaO. Energy Proc. 4, 393–401.

Saidur, R., Abdelaziz, E.A., Demirbas, A., Hossain, M.S., Mekhilef, S., 2011. A review on biomass as a fuel for boilers. Renew. Sustain. Energy Rev. 15, 2262–2289.

Sánchez-Biezma, A., Diaz, L., López, J., Arias, B., Paniagua, J., De Zarraga, E., Alvarez, J., Abanades, J.C., 2012. La Pereda $CO_2$: a 1.7 MW pilot to test post-combustion $CO_2$ capture with CaO. In: 21st International Conference on Fluidized Bed Combustion, Enzo albano Editore, Naples, pp. 365–372.

Shimizu, T., Hirama, T., Hosoda, H., Kitano, K., Inagaki, M., Tejima, K., 1999. A twin fluid-bed reactor for removal of $CO_2$ from combustion processes. Chem. Eng. Res. Des. 77, 62–68.

Ströhle, J., Junk, M., Kremer, J., Galloy, A., Epple, B., 2014. Carbonate looping experiments in a 1 $MW_{th}$ pilot plant and model validation. Fuel 127, 13–22.

Werther, J., Saenger, M., Hartge, E.U., Ogada, T., Siagi, Z., 2000. Combustion of agricultural residues. Prog. Energy Combust. Sci. 26, 1–27.

# 4. Modelado de reactores y optimización de proceso

Como ya se ha indicado en los objetivos incluidos en el capítulo 2, una parte importante de esta Tesis Doctoral se ha dedicado a la modelización y la búsqueda de condiciones de operación óptimas en los sistemas de captura de $CO_2$ descritos en la sección 1.3 que emplean la tecnología de carbonatación-calcinación. En primer lugar, se ha resuelto un modelo hidrodinámico aplicado a un sistema de dos lechos fluidizados circulantes interconectados con el objetivo de determinar los valores de circulación de sólidos entre reactores en función de condiciones de operación tales como el inventario de sólidos en los reactores o la velocidad del gas. Estos valores se han comparado con el flujo de sólidos necesario para alcanzar una determinada eficacia de captura de $CO_2$ en cada escenario, el cual viene dado por el modelo del carbonatador. Todo el procedimiento y los resultados obtenidos, que sirvieron para apoyar la elección de condiciones experimentales de operación en las campañas experimentales descritas en el capítulo 3, se muestran en detalle en la *Publicación III*, ubicada en la sección 4.1.1.

También se ha realizado un estudio sobre el contenido en cenizas y $CaSO_4$ del material circulante en función de diversas configuraciones de proceso, y se ha analizado su implicación en la eficacia de captura de $CO_2$ del sistema con la ayuda de un modelo actualizado del carbonatador. Al mismo tiempo, se ha estudiado el efecto de la adición de caliza fresca al sistema en términos de incremento de la actividad media del sorbente, disminución de la concentración de inertes (cenizas y $CaSO_4$) y aumento de la eficacia de captura de $CO_2$. Esta información se presenta en la sección 4.2.1 en forma de la *Publicación IV,* cuyos resultados y metodología son los habituales en la interpretación de los resultados experimentales referidos a composición de sólidos en los ensayos descritos en el capítulo 3.

Finalmente, otro aspecto que se ha considerado durante la realización de esta Tesis Doctoral es el análisis de un novedoso proceso de reactivación del sorbente (recarbonatación) que había sido planteado conceptualmente por el grupo de captura de $CO_2$ del INCAR-CSIC (Abanades *et al.* 2012; Arias *et al.* 2012). Para avanzar en la implantación de este sistema en los esquemas de carbonatación-calcinación descritos en las secciones 1.3.1 y 1.3.2 anteriores se hace necesario un análisis del proceso que incorpora un nuevo reactor denominado recarbonatador, donde los sólidos parcialmente carbonatados procedentes del carbonatador se ponen en contacto con $CO_2$, elevando así su contenido en $CaCO_3$ por recarbonatación y manteniendo la actividad del material resultante de la calcinación posterior en un nivel más alto. Para abordar el problema de diseño de este nuevo reactor se ha realizado un estudio cinético de la reacción de recarbonatación, considerando distintas condiciones de operación. Como resultado de esta investigación, se han obtenido los parámetros cinéticos de dicha reacción y se ha establecido el valor de la constante aparente de reacción en una expresión simplificada de la velocidad de recarbonatación. Con esta información y un modelo de contacto gas-sólido, se ha desarrollado un modelo para el reactor de recarbonatación que permite predecir la conversión que alcanzan los sólidos en su interior en función de las condiciones de operación, permitiendo así la realización de un diseño preliminar de un recarbonatador asociado a una instalación de CaL. Estos trabajos han sido recientemente publicados y se adjuntan como *Publicación V y Publicación VI* en las secciones 4.3.3 y 4.3.4 respectivamente.

## 4.1 Modelización del flujo de circulación de sólidos entre reactores

La circulación de sólidos entre reactores es una de las variables clave del proceso de captura, ya que determina el flujo de CaO disponible para su reacción con $CO_2$ y el tiempo de residencia de las partículas activas de CaO

en cada uno de los reactores. El flujo de sólidos circulantes necesario para lograr una determinada eficacia de captura se puede calcular mediante el modelo del carbonatador propuesto por Alonso *et al.* (2009) y mencionado en la sección 1.3.1 en función del flujo de $CO_2$ a tratar, la cinética de reacción, el inventario de sólidos en el carbonatador y la actividad del sorbente. Sin embargo, estos valores de circulación requeridos para la reacción no suelen coincidir con los que se establecen entre los reactores como resultado de las condiciones hidrodinámicas en las que trabaja el sistema. El análisis de estas diferencias es el objetivo de la *Publicación III*, que busca identificar una ventana de condiciones de operación que permita obtener flujos de circulación de sólidos adecuados para alcanzar altas eficacias de captura de $CO_2$.

La determinación del flujo de circulación de sólidos entre reactores requiere conocer la densidad de sólidos a la altura de salida del reactor, ya que son magnitudes proporcionales. Para ello se ha empleado el modelo hidrodinámico propuesto por Johnsson y Leckner (1995) para calderas de lecho fluidizado circulante, que establece el perfil de densidad de sólidos en función de la altura en el reactor. Este modelo considera que en el reactor existe una zona densa, con densidad de sólidos constante y propiedades de lecho burbujeante, sobre la que se localiza una zona en la que la densidad de sólidos disminuye de un modo exponencial. Este perfil exponencial es, a su vez, resultado de dos regiones relacionadas con la presencia de una zona intermedia con fuerte retromezcla de sólidos y otra de transporte con estructura núcleo-anillo (Johnsson y Leckner 1995).

Con estas suposiciones, y una vez fijados el inventario de sólidos, la altura de salida y la velocidad de gas en el carbonatador, así como la altura de la transición entre la zona intermedia y la de transporte (ambos términos del perfil de densidad de sólidos coinciden en este punto) y unas consideraciones adicionales sobre la zona densa, es posible calcular la

densidad de sólidos a la salida y, por tanto, el valor de la circulación de sólidos entre reactores.

Siguiendo este procedimiento se han estudiado diversos escenarios de operación para el carbonatador y se ha establecido una comparación entre los valores de circulación hidrodinámicos y los calculados en las mismas condiciones por medio del modelo del carbonatador. También se ha calculado el inventario mínimo de sólidos en el calcinador predicho por el modelo hidrodinámico para que el flujo de salida de sólidos de este reactor coincida con el determinado por el modelo del carbonatador. De igual modo, se ha estudiado el efecto de variables clave en el sistema tales como el inventario de partículas y la velocidad de gas en el carbonatador, y la actividad de los sólidos de CaO.

Asimismo, se ha realizado un balance de presión a un sistema de reactores de lecho fluidizado circulante interconectados bajo la suposición de que ambos ciclones descargan a un punto de igual presión. Este balance constata la gran importancia de la columna de sólidos que se forma en la tubería de descarga del ciclón hacia la *loop-seal* para mantener la estabilidad hidrodinámica de la instalación, ya que es la responsable de compensar las caídas de presión del reactor, conducto de salida y ciclón asociadas al sistema fluidizado circulante opuesto.

En la sección 4.1.1 se muestra la *Publicación III*, donde se define el procedimiento completo de cálculo, se discuten los resultados obtenidos y se proponen estrategias para la operación de este tipo de sistemas haciendo uso de líneas de retorno de sólidos que permiten recircular al propio reactor (sea el carbonatador o el calcinador) parte de los sólidos que abandonan dicho reactor, lo que está relacionado con el modo de operación de la planta piloto de La Pereda tal y como se indica en la sección 3.1.1.

### 4.1.1 Publicación III

**Modeling the solids circulation rates and solids inventories of an interconnected circulating fluidized bed reactor system for $CO_2$ capture by calcium looping**

Publicado en:

*Chemical Engineering Journal*

*Volumen* 198–199

Páginas 228-235

Año 2012

Chemical Engineering Journal 198-199 (2012) 228–235

Contents lists available at SciVerse ScienceDirect

Chemical Engineering Journal

journal homepage: www.elsevier.com/locate/cej

# Modeling the solids circulation rates and solids inventories of an interconnected circulating fluidized bed reactor system for $CO_2$ capture by calcium looping

M.E. Diego*, B. Arias, J.C. Abanades

*Spanish Research Council, Instituto Nacional del Carbón, CSIC, C/Francisco Pintado Fe, No. 26, 33011 Oviedo, Spain*

## HIGHLIGHTS

- We used CFBCs models to predict the hydrodynamics of a postcombustion CaL system.
- We compared the predicted solids circulation rates to those required for $CO_2$ capture.
- We found that these solids circulation rates usually mismatch.
- The evolution of the mismatch with the key variables was studied.
- Some operating strategies to match both circulation rates are shown.

## ARTICLE INFO

*Article history:*
Received 10 April 2012
Received in revised form 22 May 2012
Accepted 24 May 2012
Available online 5 June 2012

*Keywords:*
$CO_2$ capture
Calcium looping
Carbonation
CFB
Hydrodynamics

## ABSTRACT

Postcombustion $CO_2$ capture systems that use CaO as a regenerable $CO_2$ sorbent in two interconnected circulating fluidized beds (CFBs) are rapidly developing at increasing scale. The properties of the circulating materials, the reactor geometries and operating conditions (gas velocities and temperature ranges) are remarkably similar to those present in existing large scale circulating fluidized bed combustors, CFBCs. In this work a fluid-dynamic model published for CFBCs is adopted and applied to the study of the interconnected twin reactor calcium looping (CaL) system. The model was used to find operating windows that will allow the CaL system to be applied on a large scale. It was found that when operating at high gas velocities (4–5 m/s) in the carbonator, unacceptably high solids circulation rates might be present when high bed inventories are in place to achieve large $CO_2$ capture efficiencies. An additional loop to allow the internal circulation of the excess solids can be quantified with the help of the model used in this work.



## 1. Introduction

$CO_2$ capture and permanent geological storage can contribute significantly to reducing $CO_2$ emissions from large stationary sources [1]. There are several mature $CO_2$ capture technologies that can be deployed in the near term if a sufficient economic incentive is provided (basically a carbon price of around 30–50 €/t $CO_2$ avoided). A number of emerging technologies are also trying to reduce this cost. Among these emerging technologies, postcombustion calcium looping [2] has progressed to a high stage of development, from a theoretical concept and fundamental studies at particle level [3] to the point of small pilot scale validation in full continuous mode [4–6]. Preliminary results in pilots at the 1 $MW_{th}$ scale have been reported [7], and a 1.7 $MW_{th}$ interconnected circulating fluidized bed (CFB) facility designed to test the concept has also entered into operation [8].

CaL makes use of lime as a regenerable sorbent to capture $CO_2$ from the flue gases generated in a power plant. This process is based on carbonation–calcination cycles such as that depicted in Fig. 1.

The flue gas from the power plant and the solids stream from the calciner enter the carbonator, which operates at temperatures of around 650 °C. In this reactor, particles of CaO absorb $CO_2$ by means of the exothermic carbonation reaction, converting them into $CaCO_3$, and leading to an exit gas stream with a low $CO_2$ content. The solids stream leaving the carbonator is transported back to the calciner, where the $CaCO_3$ is calcined at temperatures of around 900 °C. As a result, it decomposes back into CaO, and is then returned to the carbonator. In order to attain such high temperatures coal is continuously fed into the calciner, since calcination

* Corresponding author. Tel.: +34 985 11 90 90; fax: +34 985 29 76 62.
*E-mail addresses:* marlen@incar.csic.es (M.E. Diego), borja@incar.csic.es (B. Arias), abanades@incar.csic.es (J.C. Abanades).

1385-8947/$ - see front matter © 2012 Elsevier B.V. All rights reserved.
http://dx.doi.org/10.1016/j.cej.2012.05.099

**Nomenclature**

| | |
|---|---|
| $a$ | decay constant of the splash zone ($m^{-1}$) |
| $E_{carb}$ | $CO_2$ capture efficiency |
| $F_{Ca}$ | calcium looping rate between reactors (mol/s) |
| $F_{CO2}$ | molar flow of $CO_2$ per unit area entering the carbonator (mol/($m^2$ s)) |
| $g$ | gravitational acceleration (m/$s^2$) |
| $G_s$ | solids circulation rate (kg/($m^2$ s)) |
| $G_{s\ CaL}$ | solids circulation rate calculated from the $CO_2$ capture reactor mass balance (kg/($m^2$ s)) |
| $G_{s\ HM}$ | solids circulation rate calculated from the hydrodynamic model (kg/($m^2$ s)) |
| $h$ | height (m) |
| $H_{exit}$ | exit height (m) |
| $H_{return}$ | height of the return of the solids to the reactor (m) |
| $H_x$ | bottom bed height (m) |
| $H_y$ | splash zone height (m) |
| $k_{sB}\ \varphi$ | apparent carbonation reaction rate constant ($s^{-1}$) |
| $K$ | decay constant of the transport zone ($m^{-1}$) |
| $n$ | factor related to the split of solids in the exit zone |
| $n_{Ca}$ | total inventory of Ca moles inside the carbonator (mol) |
| $T$ | temperature (°C) |
| $t^*$ | time required for a particle to attain a carbonation conversion equal to $X_{ave}$ (s) |
| $u$ | gas velocity (m/s) |
| $u_t$ | terminal velocity of the particles (m/s) |
| $X_{ave}$ | average $CO_2$ carrying capacity of the particles |
| $X_{carb}$ | carbonation conversion |
| $X_{inert}$ | mass fraction of inert solids in the solids carbonator stream |

*Greek symbols*

| | |
|---|---|
| $\eta$ | factor related to the split of solids in the exit zone |
| $\Delta P_{CB}$ | carbonator pressure drop between the entrance of solids from the loop-seal and the riser exit (Pa) |
| $\Delta P_{CC}$ | calciner pressure drop between the entrance of solids from the loop-seal and the riser exit (Pa) |
| $\Delta P_{cycl}$ | cyclone pressure drop (Pa) |
| $\Delta P_{dc}$ | pressure drop of the downcomer solids column (Pa) |
| $\Delta P_{duct}$ | pressure drop of the exit duct (Pa) |
| $\Delta P_{total\ R}$ | total reactor pressure drop (Pa) |
| $v_{CO2}$ | molar fraction of $CO_2$ |
| $v_{eq}$ | molar fraction of $CO_2$ at equilibrium conditions |
| $\rho$ | solids concentration (kg/$m^3$) |
| $\rho_x$ | solids concentration in the bottom bed (kg/$m^3$) |
| $\rho_{exit}$ | solids concentration at the reactor exit (kg/$m^3$) |

*Subscripts*

| | |
|---|---|
| $CB$ | carbonator |
| $CC$ | calciner |

is an endothermic reaction. The calciner reactor operates in oxyfired mode. Consequently, the coal burns using a mixture of $O_2$/$CO_2$ and produces a concentrated stream of $CO_2$ which can then be purified, compressed and stored [2]. A make-up flow of fresh limestone is fed into the calciner to compensate for the decay in the $CO_2$ capture capacity of the particles with the number of carbonation–calcination cycles. At the same time a purge is carried out to prevent the accumulation of ashes and $CaSO_4$ in the system. The heat requirements in the calciner can be considerable [2,9], leading to a large consumption of $O_2$ and coal in this reactor. However, one of the main advantages of the CaL process is that the energy input into the calciner can be recovered as high-quality heat from the high temperature solids streams and the exothermic carbonation reaction. As a result, the overall energy penalty is very low [2,10–17].

The experimental validation of the CaL concept has progressed rapidly. The effective capture of $CO_2$ from flue gases in a batch fluidized bed was first demonstrated in bubbling mode for a limited number of cycles [18]. Lu et al. [19] reported experimental results from a calcination–carbonation test carried out in a dual fluidized bed facility operating in semi-continuous mode. Charitos et al. [20] used a combination of a circulating fluidized bed system (where the carbonator is the riser) and a bubbling fluidized bed system (where the calciner is the reactor) operating in continuous mode in their 10 $kW_{th}$ test facility. However, it is clear from the mass and heat balances performed in a process similar to that of Fig. 1 that a twin CFB system where both the carbonator and the calciner behave as risers would be the most suitable choice for large-scale commercial facilities [2,21,22], as such systems will need to cope with a huge flow of flue gases at atmospheric pressure and a considerable flow of recirculated $CO_2$ in the oxyfired calciner. Alonso et al. [23] chose a configuration with two CFB interconnected by two loop-seals (see Fig. 2) and Rodríguez et al. [4] first reported long duration experimental results from a 30 $kW_{th}$ test facility at INCAR-CSIC, with $CO_2$ capture efficiencies of between 70% and 97%. Charitos et al. [5] reported optimum performance for a carbonator reactor built at IFK-Stuttgart operating in fast fluidization regime at velocities of up to 6 m/s and with capture rates fully comparable to those expected of large scale systems (8–10 mol $CO_2$/($m^2$s)). Larger pilots based on the configuration of Fig. 2, but using different solutions for controlling the solids circulation rates and inventories, are starting to report results [6,7] or are on the point of doing so [8]. Moreover, the reactor configuration of Fig. 2 has been proposed for biomass combustion with in situ

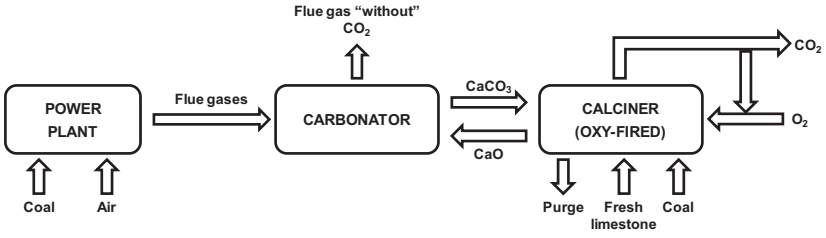


**Fig. 1.** Ca-looping scheme.

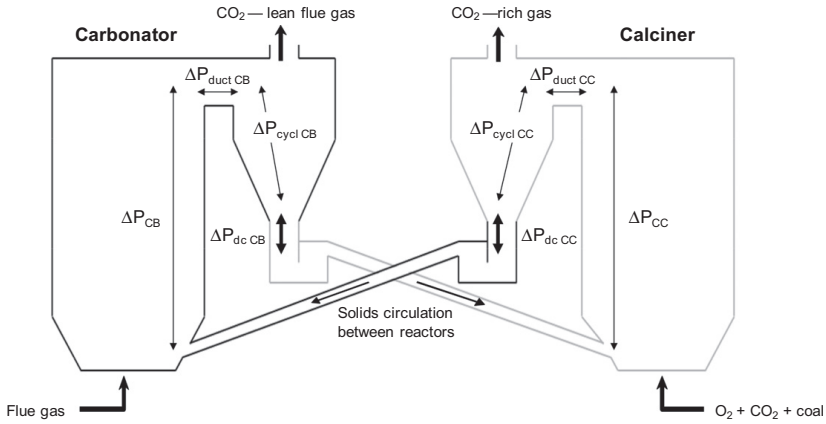


**Fig. 2.** Dual interconnected circulating fluidized bed reactors for CaL. The bold outline indicates the pressure loop associated to the carbonator reactor.

$CO_2$ capture by means of CaO [24]. A similar twin bed configuration has also been considered for biomass gasification and chemical looping (see review [25]). There is however very little information available on how these interconnected circulating fluidized beds will behave at large scale. In particular, taking into account the boundary conditions of CaL, it is only recently that some theoretical works have began to consider independent modeling of the hydrodynamics of CaL systems [26], including a preliminary test based on a cold model of the interconnected CFB configuration represented in Fig. 2 [27]. An increasing number of improved reactor models also incorporate basic hydrodynamic descriptions of the flow structure inside the carbonator reactor [16,22,28,29].

As in other CFB based facilities, it is well known that hydrodynamics plays a crucial role in the performance of the carbonator reactor in a CaL system, since the total amount of $CO_2$ captured in the system is closely related to the bed inventory in the carbonator and the solids circulation rate of active material between the reactors [4,5,21,23]. The objective of the present study is to solve a basic fluid-dynamic model for the reactor system of Fig. 2 with a view to its application in a large-scale CaL system, incorporating certain constraints that are known to be present in CaL reactor systems. The model is then used to identify operating windows that could yield suitable solids circulation rates and inventories for effective $CO_2$ capture.

## 2. Modeling approach

A pressure balance was formulated for an interconnected CFB system as represented in Fig. 2, based on the assumption that both cyclones in the loop discharge gas at a point where the pressure is the same. This leads to the following expressions:

$$\Delta P_{dc\,CC} = \Delta P_{CB} + \Delta P_{duct\,CB} + \Delta P_{cycl\,CB} \quad (1)$$

$$\Delta P_{dc\,CB} = \Delta P_{CC} + \Delta P_{duct\,CC} + \Delta P_{cycl\,CC} \quad (2)$$

Two pressure loops can be identified: the carbonator (bold outline in Fig. 2) and the calciner loop. The carbonator loop includes the carbonator itself ($\Delta P_{CB}$), its exit duct ($\Delta P_{duct\,CB}$), its cyclone ($\Delta P_{cycl\,CB}$), and the solids column in the calciner downcomer ($\Delta P_{dc\,CC}$). The calciner loop is formed by the calciner ($\Delta P_{CC}$), its exit duct ($\Delta P_{duct\,CC}$) and cyclone ($\Delta P_{cycl\,CC}$), together with the solids column in the carbonator downcomer ($\Delta P_{dc\,CB}$). Both loops are conceptually similar, although the fluidizing conditions in each reactor will determine the quantitative differences. Each loop is considered to begin with the reactor pressure drop, which is characterized by an exponential decay trend, related to the complex hydrodynamics at work in the interior of CFBs. This is followed by the exit duct and the cyclone pressure drops. After the cyclone, the downcomer can be divided into two parts: a zone where no solids are present, so there is no pressure drop, and another region containing a dense solids column where there is a strong pressure drop that compensates for all the previous pressure drops. Finally, there is a wide duct through which solids from the loop-seal return to the reactor by gravity, so that there is no pressure drop.

It should be pointed out that the dense columns of solids in the downcomers are decisive parts in any CFB unit because they are responsible for the closure of the pressure balances. According to Eqs. (1) and (2), when operating with two interconnected circulating fluidized beds as in the CaL system of Fig. 2, a rise in the pressure drop in the carbonator exit duct or cyclone, or the carbonator itself, must result in an increase in the pressure drop of the solids column in the calciner (more solids are accumulated in the calciner downcomer), and vice versa. This means that the solids column in the calciner downcomer compensates for changes in pressure drops in the carbonator loop, as its height increases or decreases in order to fulfill the pressure balance. On the contrary, the height of the solids column in the carbonator downcomer depends on the pressure drop of the elements included in the calciner loop (the calciner and its exit duct and cyclone).

A quantitative solution of Eqs. (1) and (2) requires a definition of the elements that contribute to the pressure balance, which are related to hydrodynamic factors. According to Pallarès et al. [30] models for predicting the hydrodynamics of a CFB unit can be classified into two groups: macroscopic semi-empirical models and models from first principles using CFD mathematical tools. The latter are highly complex and require long simulation times, as they describe the system's behavior from fundamental conservation equations held at boundary conditions defined on small control volumes. For the purpose of this work we have used simple models that allow us to make preliminary estimates of the general hydrodynamic behavior of the system from a macroscopic point of view. In order to choose the hydrodynamic model, it is important to bear in mind that the CaL process in Fig. 2 makes use of reactors operating in conditions similar to those of commercial CFB combustors in terms of type of particles, gas velocities and solids

circulation rates between reactors. This similarity is another benefit offered by CaL technology, since it allows us to take advantage of the knowledge acquired about the hydrodynamics of coal CFBCs and adapt it to CaL systems.

Pallarès et al. [30,31] distinguished six zones in a CFB unit that need to be modeled separately, in so far as their hydrodynamic behavior is concerned: a bottom bed, a freeboard, an exit zone (these three located in the reactor), an exit duct, a cyclone and a downcomer and particle seal. The dense bottom bed, with a constant concentration of solids, is similar to a bubbling bed [32], and is located in the lower part of the reactor. Above the bottom zone is the freeboard, which consists of a splash and a transport zone [32]. These two zones are of great importance as they determine the profiles of the solids concentration in the reactor. The splash zone shows a strong back-mixing, which is associated with the behavior of clustered solids, whereas the transport zone is characterized by a core/annulus flow, which also causes back-mixing [30,32]. Taking into account all of these considerations, Johnsson and Leckner [32] developed a model for predicting the vertical solids distribution profiles along the reactor:

$$\rho = (\rho_x - \rho_{exit}\exp(K(H_{exit} - H_x)))\exp(-a(h - H_x)) + \rho_{exit}\exp(K(H_{exit} - h)) \quad (3)$$

where $\rho$ is the solids concentration at a height equal to $h$, $\rho_x$ is the solids concentration in the bottom bed, $\rho_{exit}$ is the solids concentration at the gas outlet, $H_x$ is the bottom bed height, $H_{exit}$ is the exit height, and the parameters $a$ and $K$ are the decay constants for the splash and the transport zones respectively, which can be obtained by means of the following expressions [32]:

$$a \approx \frac{4u_t}{u} \quad (4)$$

$$K \approx \frac{0.23}{u - u_t} \quad (5)$$

where $u$ and $u_t$ are the gas velocity and the terminal velocity of the particles respectively. The terminal velocity can be calculated for individual particles using the equations of Haider and Levenspiel [33].

The Johnsson and Leckner [32] hydrodynamic model has been recently used to interpret the cold model experimental results obtained from a CaL configuration with two interconnected circulating fluidized beds [27]. It was also chosen in this work as the basis for modeling the hydrodynamics of the large scale CaL system in Fig. 2.

The first term in Eq. (3) refers to the splash zone and the second to the transport zone. Johnsson and Leckner [32] also defined the splash zone height above the air distributor, $H_y$, where the two terms of the model are equal:

$$(\rho_x - \rho_{exit}\exp(K(H_{exit} - H_x)))\exp(-a(H_y - H_x)) = \rho_{exit}\exp(K(H_{exit} - H_y)) \quad (6)$$

Considering that the pressure drop along the reactor ($\Delta P_{total\,R}$) is only due to the presence of solids, it can be obtained by integrating Eq. (3):

$$\Delta P_{total\,R} = \rho_x g H_x + \int_{H_x}^{H_{exit}} \rho g dh \quad (7)$$

When the particles reach the exit zone located in the upper part of the reactor, the solids stream splits into two: some particles go down, returning to the reactor, whereas the other solids follow the gas stream to the cyclone. This second fraction determines the amount of solids which are externally recirculated, which is referred to as the solids circulation. Some expressions have been developed for the calculation of the solids circulation rate, such as the correlation proposed by Pallarès et al. [30]. In our work, the output solids flow is obtained by means of the expression proposed by Ylätalo et al. [29]:

$$G_s = \eta u \rho_{exit}^n \quad (8)$$

where $\eta$ and $n$ are factors related to the split of solids in the exit zone.

As will be seen below, the pressure drops in the reactors are usually higher than the pressure drops in the cyclones and in the exit ducts. These two smaller terms in the pressure balance can be estimated from several correlations in the literature. For the exit duct, where gas and particles accelerate due to an increase in the gas velocity caused by a reduction in the cross-sectional area of the duct, Muschelknautz and Muschelknautz [34] proposed an expression and procedure for calculating the $\Delta P_{duct}$. The pressure drop in the cyclone can be estimated with the equation used by Pallarès et al. [30].

The final zone in a CFB system is formed by the downcomer and the loop-seal, both of which are assumed to behave like dense bubbling beds. A solids column forms in the downcomer, allowing the solids to flow from a lower to a higher pressure zone. The pressure drop caused by this column is calculated by closing the pressure balance of the system.

In order to illustrate the interdependence of the solids circulation rates and solids inventories in the CaL reactors on certain key design variables, operating conditions and particle properties, we will apply the model to a particular case study and analyze its degree of sensitivity.

## 3. Case study

This study is based on a reference CaL facility which treats flue gases from an average-sized 1000 $MW_{th}$ coal-fired power plant. A 90% $CO_2$ capture efficiency was set as the target for the carbonator. Full calcination conversion is assumed for the calciner. Calculations were made assuming a mean particle diameter of 200 μm and a solid density equal to 2000 kg/m$^3$, which are close to the values typical of CFBCs and reasonable for CaL systems, taking into account the presence of ashes in the system. The CaL facility employed has a configuration similar to that of Fig. 2, with identical carbonator and calciner reactors that have an exit height of 35 m and a cross-sectional area of 200 m$^2$. The latter value was chosen in order to achieve gas velocities in the reactors of approximately 5 m/s (common in CFBC technology), taking into account the amount of flue gases generated in a 1000 $MW_{th}$ coal-fired power plant. On the basis of these assumptions, it was calculated that the carbonator will treat a flue gas with an input of 10 mol/(m$^2$ s) $CO_2$, of which 9 mol/(m$^2$ s) will be captured by the circulating solids. For the sake of simplicity, the same gas velocity is assumed in both the

**Table 1**
Input parameters for the reference case.

| | | |
|---|---|---|
| Power plant capacity | $MW_{th}$ | 1000 |
| $H_{exit}$ | m | 35 |
| Reactor cross-sectional area | m$^2$ | 200 |
| $H_{return}$ | m | 2 |
| Carbonator inventory | kg/m$^2$ | 1000 |
| $F_{CO_2}$ | mol/(m$^2$ s) | 10 |
| $E_{carb}$ | % | 90 |
| $T_{CB}$ | °C | 650 |
| $T_{CC}$ | °C | 920 |
| $u_{CB}$, $u_{CC}$ | m/s | 5 |
| Solid density | kg/m$^3$ | 2000 |
| Mean particle diameter | μm | 200 |
| $X_{ave}$ | – | 0.2 |
| $X_{inert}$ | – | 0.3 |

carbonator and the calciner reactors. In order to calculate the gas properties, the gas inside the reactors is assumed to be air and $CO_2$ in the carbonator and the calciner, respectively. The solids used to estimate the Ca/C ratio arriving at the carbonator have an average $CO_2$ carrying capacity ($X_{ave}$) of 0.2. All of the input parameters and assumptions used in the reference case are summarized in Table 1.

The capture of $CO_2$ takes place in the carbonator, where a specific solids circulation rate is required in order to attain the targeted $CO_2$ capture efficiency. This solids circulation rate was determined by combining the carbon mass balance and the basic reactor model incorporating the average reaction rate of particles experimentally measured in lab scale carbonator reactors operating as risers [5]. The carbon mass balance between the $CO_2$ captured from the flue gas and the $CO_2$ circulating as $CaCO_3$ in the solids leaving the carbonator reactor leads to the following expression:

$$E_{carb}F_{CO_2} = F_{Ca}X_{carb} \tag{9}$$

where $E_{carb}$ is the $CO_2$ capture efficiency, $F_{CO_2}$ is the molar flow of $CO_2$ entering the carbonator, $F_{Ca}$ symbolizes the calcium looping rate between reactors and $X_{carb}$ is the carbonation conversion.

The carbon mass balance has to be closed with respect to the flow of $CO_2$ reacting with the active solids present in the reactor at any given time [21]:

$$E_{carb}F_{CO_2} = k_{sB}\varphi\left(1 - \exp\left(\frac{-t^*}{n_{Ca}/F_{Ca}}\right)\right)n_{Ca}X_{ave}(\overline{y_{CO_2} - y_{eq}}) \tag{10}$$

where $k_{sB}\ \varphi$ is the apparent reaction rate constant, $n_{Ca}$ is the total inventory of Ca moles inside the carbonator reactor and $t^*$ is the time required for a particle to attain a carbonation conversion equal to $X_{ave}$ [5,21]:

$$t^* = \frac{X_{ave}}{(dX/dt)_{reactor}} = \frac{X_{ave}}{k_{sB}\varphi X_{ave}(\overline{y_{CO_2} - y_{eq}})} \tag{11}$$

Taking into account the operating conditions of the CaL facility, $F_{Ca}$ and $X_{carb}$ values can be obtained by means of Eqs. (9)–(11) if $k_{sB}\ \varphi$ and the carbonator inventory are known. The apparent reaction rate constant was assumed to be 0.43 $s^{-1}$, as this was the value obtained in previous studies with INCAR-CSIC limestone [5]. A carbonator inventory of 1000 kg/$m^2$ was chosen as a value characteristic of CaL systems. On the basis of these assumptions, and assuming a mass fraction of inert solids ($X_{inert}$) equal to 0.3 in the solids carbonator stream, the solids circulation rate required from the carbonator to the calciner ($G_{s\ CaL\ CB}$) to achieve the targeted 90% $CO_2$ capture efficiency, is 4.6 kg/($m^2$s), corresponding to 50.8 mol Ca/($m^2$s).

Once the target for the solids circulation rates has been defined from the point of view of the operation of the carbonator reactor, the next design problem is to attain the correct solids inventory and solids circulation rates, taking into account the constraints and interrelationships between these two variables in the hydrodynamic model. As a first step, the solids circulation rate from the carbonator predicted using the hydrodynamic model ($G_{s\ HM\ CB}$) was calculated by means of the system of equations formed by (6) and (7). These equations contain the unknown parameters $\rho_{exit}$, $\rho_x$, $H_x$, $H_y$ and $\Delta P_{total\ R}$. In the absence of specific experimental data, a typical porosity of 0.8 was initially assumed for the bottom bed of the carbonator, making it possible to calculate $\rho_x$. The splash zone height ($H_y$) was set to be 2 m. This value was chosen in the light of the experimental data obtained by Johnsson and Leckner [32], who found that the value hardly changed despite working in different operating conditions (particle diameter and gas velocity) that are characteristic of CFBCs. As the targeted carbonator inventory was previously established at 1000 kg/$m^2$, $\Delta P_{total\ R}$ can be obtained, and the bottom bed height ($H_x$) and $\rho_{exit}$ are calculated with Eqs. (6) and (7). Following this procedure, we found that in most cases the $H_x$ yield was lower than 0, which means that there would be no bottom bed zone for particles of this type and these operating conditions. Consequently, the system of equations had to be solved again for $H_x = 0$, and $\rho_{exit}$ and $\rho_x$ as the solutions. For the reference case considered in this work, $G_{s\ HM\ CB}$ was found to be 7.4 kg/($m^2$s), which is clearly higher than $G_{s\ CaL\ CB}$. This is in principle a positive result, because it signifies that in a carbonator reactor operating with a solids circulation rate of $G_{s\ HM\ CB}$, the carbonate conversion of the solids will be lower and the availability of active CaO in the reactor will be higher, allowing even higher $CO_2$ capture efficiencies [4,5]. However, this high $CO_2$ capture efficiency is always limited by the equilibrium and it comes at the expense of an increase in calciner heat requirement, which is proportional to the flow of solids circulating from the carbonator to the calciner [9,35]. Therefore, it is important to maintain calciner heat requirements as low as possible because they contribute significantly to the total energy consumption and energy penalty (the need for $O_2$ in the calciner). Indeed, in an ideal design, the carbonator solids circulation should not be more than $G_{s\ CaL\ CB}$. In order to achieve this design target, a fraction of the solids flow leaving the carbonator needs to be returned to the carbonator (internal circulation) instead of being directed to the other CFB reactor (external circulation).

The division between internal and external solids circulation can be achieved by a range of possible solutions: by diverting pipes from the downlegs of the cyclones or by designing loop-seals that have two exits with adjustable openings. The second solution was demonstrated to be successful by Charitos et al. [26], who used a cone valve that was able to modify the opening in the two return legs of the solids. In large scale units, with several cyclones for each riser, as in the case of commercial CFBCs [36], it is reasonable to expect that only one or two cyclones will carry particles from the carbonator to the calciner, while the others would return the solids again to the carbonator. This configuration offers the additional benefit of keeping the pressure balance intact in each part of the cycle. Another option is the configuration recently proposed by Martínez el al. [37]. It is based on a mixing seal valve (which may also be used as an option to control the solids circulation between reactors) and has the additional advantage of a more compact design of the CaL system.

Any of these operational strategies will result in a solids external circulation rate between reactors close to the values of $G_{s\ CaL}$. However, it is essential to maintain a value of $G_{s\ HM} \geqslant G_{s\ CaL}$. The hydrodynamic model described in the previous paragraphs can be used to define the operating windows that will allow this inequality to be satisfied. It can be also used to estimate the variations that $G_{s\ CaL}$ and $G_{s\ HM}$ undergo when the design characteristics of the reactors and the key operating conditions are changed. This is discussed in more detail in the following sections, but first it is necessary to solve the central reference case for the conditions defined in Table 1.

Once $G_{s\ CaL\ CB}$ has been defined (which is equivalent to a molar stream of calcium leaving the carbonator of 50.8 mol Ca/($m^2$s)), it is possible to estimate $G_{s\ CaL\ CC} = 4.2$ kg/($m^2$s) taking into account the mass fraction of inerts (0.3 in the carbonator) and assuming complete calcination of the solids in the calciner. The next step is to calculate the minimum calciner inventory in order to obtain this solids circulation rate, taking into account the operating conditions (Table 1). For this purpose, the system of equations formed by (6) and (7) is used in a slightly different way to that of the carbonator. A bottom bed porosity of 0.8 is assumed and $H_y$ is taken to be equal to 2 m. As $G_{s\ CaL\ CC}$ is known, $\rho_{exit}$ is obtained from Eq. (8). In this way the system is solved and $H_x$ and $\Delta P_{total\ R}$ can be calculated. If $H_x$ is lower than zero (as was usually the case), the bottom bed

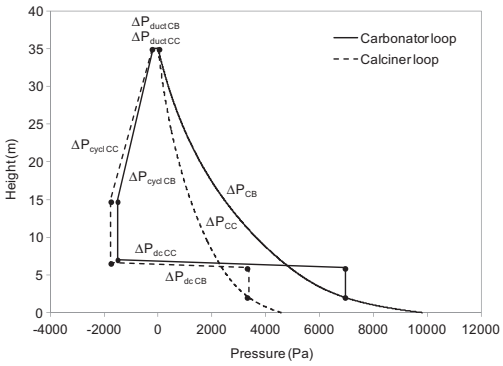


**Fig. 3.** Estimated pressure profiles in the system of Fig. 2 in the reference case conditions of Table 1.

does not exist, so the system of equations is solved again with $H_x = 0$, which will give the values of the $\Delta P_{total\ R}$ and $\rho_x$. The minimum calciner inventory obtained with this calculation procedure was found to be 470 kg/m$^2$ for the reference case. This inventory yields an average particle residence time of 112 s, that should be sufficient to attain a total calcination conversion in these conditions using a calciner temperature of approximately 900 °C [38]. However, it should be noted that, if a higher calciner inventory is required, the internal circulation will also allow longer residence times in the calciner reactor in order for full calcination conversions to be achieved.

The pressure profiles of the CaL facility for these operating conditions are depicted in Fig. 3, which shows that the main contributors to the pressure drop are the reactors and the solids columns in the downcomers. The carbonator pressure drop is greater than that of the calciner, because the inventory is higher in the carbonator. The solids column pressure drop is lower in the carbonator downcomer than in the calciner downcomer, as it must compensate for the lower pressure drops of the other elements in the loop (see Eqs. (1) and (2)).

### 3.1. Effect of the carbonator inventory

The solids circulation rates and pressure distributions in the system of Fig. 2 were studied for different carbonator inventories. The results of the study are summarized in Table 2. In general, minimum solids inventories are preferred during the design stage, in order to minimize the energy losses associated with blowing a large volume of gas through the bed of solids.

$G_{s\ HM\ CB}$ was found to be greater than $G_{s\ CaL\ CB}$ for carbonator inventories of 1000 and 1500 kg/m$^2$, and internal circulation rates of 2.8 and 5.7 kg/(m$^2$s) respectively are needed. However, the opposite trend occurs for a carbonator inventory of 500 kg/m$^2$, making it impossible to attain a $CO_2$ capture efficiency of 90% in these conditions. In such situations, there are two strategies that can be adopted in order to enhance the $CO_2$ capture efficiency: an increase in the bed inventory in the carbonator, which will lead to higher solids circulation rates and fewer solids circulation requirements, or as a second option (which can be implemented alone or in combination with the previous one), an increase in the carrying capacity of the particles, by replacing these solids with others of a higher activity (a higher make-up flow of limestone [39,40]), which will allow a lower solids circulation rate between the reactors. If the first strategy is adopted (where the carrying capacity of the particles is maintained at 0.20), the inventory of solids required in the carbonator for $G_{s\ HM\ CB}$ to equal $G_{s\ CaL\ CB}$ will be 620 kg/m$^2$. In this case, the solids will leave the carbonator with a $X_{carb} = 0.16$ at a rate of 5.0 kg/(m$^2$s). If the second approach is used, the carrying capacity of the solids will have to be increased up to a value of 0.25 in order for the system to operate with an inventory of solids in the carbonator of 500 kg/m$^2$ and a capture efficiency of 90%.

The minimum calciner inventories are quite close to each other (see Table 2). However, these inventories decrease slightly as the carbonator inventories rise, since the solids residence times are higher and the carbonation conversions increase slightly, reducing the $G_{s\ CaL\ CB}$ and $G_{s\ CaL\ CC}$ required by the system (i.e. a smaller minimum calciner inventory is needed in order to attain the necessary $G_{s\ CaL\ CC}$ values).

Up to now we have considered the carbonator inventory as the total reactor inventory. But the carbonator inventory that participates in the pressure balance ($\Delta P_{CB}$) only corresponds to the solids located above the height of the return of the solids to the reactor ($H_{return}$). This inventory may therefore change if variations in $H_{return}$ are taken into account when designing the riser. As in the case of the carbonator loop in Fig. 4, $H_{return}$ should not affect the $G_{s\ HM\ CB}$ because the shape of the pressure profile is assumed to be identical by the model used in this work.

However, a change in $H_{return}$ will influence the height of the column of solids in the calciner loop-seal, and vice versa (see pressure balance of Eqs. (1) and (2)). As one might expect, the higher the $H_{return}$, the lower the $\Delta P_{CB}$ ($\Delta P_{CB}$ is the pressure drop between the entrance and the exit of the solids in the carbonator), so that fewer solids are required in the calciner downcomer (and as a result, a less effective seal is formed by the loop-seal).

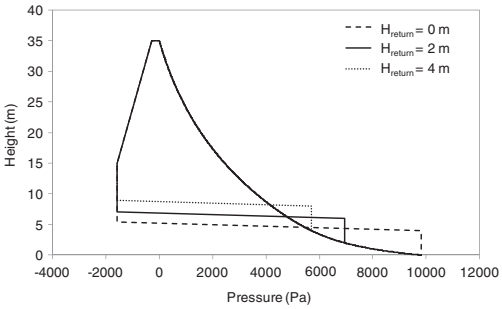


**Fig. 4.** Example of the pressure profiles of the carbonator loop with different return duct heights (0, 2 and 4 m) in the reference case (Table 1).

**Table 2**
Results for the carbonator operating with different bed inventories.

| Carbonator inventory (kg/m$^2$) | Calcium molar flow (mol/(m$^2$·s)) | $X_{carb}$ | $G_{s\ CaL\ CB}$ (kg/(m$^2$ s)) | $G_{s\ HM\ CB}$ (kg/(m$^2$ s)) | $G_{s\ CaL\ CC}$ (kg/(m$^2$ s)) | Minimum calciner inventory (kg/m$^2$) |
|---|---|---|---|---|---|---|
| 500 | 58.8 | 0.15 | 5.3 | 4.2 | 4.9 | 560 |
| 1000 | 50.8 | 0.18 | 4.6 | 7.4 | 4.2 | 470 |
| 1500 | 48.7 | 0.19 | 4.5 | 10.2 | 4.1 | 450 |

**Table 3**
Results for the reactors operating at different gas velocities.

| $u$ (m/s) | Calcium molar flow (mol/(m$^2$ s)) | $X_{carb}$ | $G_{s\ CaL\ CB}$ (kg/(m$^2$ s)) | $G_{s\ HM\ CB}$ (kg/(m$^2$ s)) | $G_{s\ CaL\ CC}$ (kg/(m$^2$ s)) | Minimum calciner inventory (kg/m$^2$) |
|---|---|---|---|---|---|---|
| 3 | 29.0 | 0.19 | 2.7 | 1.2 | 2.4 | 1630 |
| 4 | 39.6 | 0.18 | 3.6 | 3.9 | 3.3 | 710 |
| 5 | 50.8 | 0.18 | 4.6 | 7.4 | 4.2 | 470 |

**Table 4**
Results for different sorbent carrying capacities.

| $X_{ave}$ | Calcium molar flow (mol/(m$^2$ s)) | $X_{carb}$ | $G_{s\ CaL\ CB}$ (kg/(m$^2$ s)) | $G_{s\ HM\ CB}$ (kg/(m$^2$ s)) | $G_{s\ CaL\ CC}$ (kg/(m$^2$ s)) | Minimum calciner inventory (kg/m$^2$) |
|---|---|---|---|---|---|---|
| 0.10 | 115.5 | 0.08 | 9.8 | 7.4 | 9.4 | 1270 |
| 0.15 | 70.4 | 0.13 | 6.2 | 7.4 | 5.8 | 700 |
| 0.20 | 50.8 | 0.18 | 4.6 | 7.4 | 4.2 | 470 |

### 3.2. Effect of the gas velocity

Reductions in the load of a power plant fitted with a CaL system will lead to a decrease in the gas velocity in the carbonator reactor, thereby promoting changes in the hydrodynamic behavior of the facility. To address this issue, two additional gas velocities ($u$ = 3 and 4 m/s in both the carbonator and the calciner reactors) were used to solve the model. As can be seen from Table 3, at lower velocities less $G_{s\ CaL\ CB}$ is required to capture 90% of the $CO_2$. For the highest velocities of 4 and 5 m/s, $G_{s\ HM\ CB}$ is greater than $G_{s\ CaL\ CB}$, making it possible to operate the system via internal circulation in order to attain the targeted $CO_2$ capture efficiency. It should be noted that the higher the gas velocity, the higher the internal circulation because, although higher $G_{s\ CaL\ CB}$ are needed, higher $G_{s\ HM\ CB}$ are obtained. When the gas velocity acquires a value of 4 m/s, the $G_{s\ CaL\ CB}$ and $G_{s\ HM\ CB}$ values are quite close, so only a small variation in any of the parameters may lead to a situation where $G_{s\ HM\ CB}$ is lower than $G_{s\ CaL\ CB}$, as when $u$ = 3 m/s. In this case, the required $G_{s\ CaL\ CB}$ is not achievable in the carbonator under the operating conditions of Table 1. It would be impossible to attain such a high $CO_2$ capture efficiency, because this low gas velocity would not be sufficient to achieve the necessary solids circulation rate. In order to reach the targeted capture efficiency it would be necessary to increase the carbonator inventory up to a value higher than 2040 kg/m$^2$. As a final step, the minimum calciner inventories required to achieve $G_{s\ CaL\ CC}$ were established, a decreasing trend being observed as gas velocity increased. This is due to the fact that, although higher solids circulation rates are required to capture more $CO_2$ as the gas velocity increases in the carbonator, the high gas velocity also favors more rapid circulation rates even with lower solids riser inventories.

All the previous studies were carried out with the carbonator and the calciner operating at the same gas velocity, but these velocities may differ. In that case, the calciner usually operates with higher gas velocities than the carbonator, since coal combustion takes place inside the calciner, $CO_2$ is released in the calcination reaction and the calciner operating temperature is always higher than that in the carbonator. When taking this into account, the carbonator calculations remain the same for a given carbonator gas velocity (i.e. a given power plant capacity), and the only difference with regard to the case where both reactors have the same gas velocity is the minimum calciner inventory, which is lower because a smaller inventory is required in order to attain the same solids circulation rate for this reactor.

### 3.3. Effect of the sorbent carrying capacity

The $CO_2$ carrying capacity of lime particles ($X_{ave}$) is an important parameter for CaL systems. In this section, the solids circulation requirements are analyzed by varying the $X_{ave}$, while maintaining the other variables equal to those of the reference case (Table 1).

The solutions obtained from the carbon mass balance with the carbonator model and the hydrodynamic model for the different $X_{ave}$ are shown in Table 4. As expected, the higher the $X_{ave}$, the smaller the $G_{s\ CaL\ CB}$ and the $G_{s\ CaL\ CC}$, since a smaller solids circulation rate is needed to capture the same quantity of $CO_2$. This is because the particles are more active in the carbonator. As a result, the minimum calciner inventories decrease. On the other hand, the solids circulation rates obtained from the hydrodynamic model are independent of $X_{ave}$. When this average $CO_2$ carrying capacity acquires a value of 0.10, $G_{s\ HM\ CB}$ is lower than $G_{s\ CaL\ CB}$, which means that a 90% $CO_2$ capture efficiency cannot be achieved in these operating conditions. In this case, the minimum inventory of solids needed in the carbonator to achieve $G_{s\ HM\ CB} \geqslant G_{s\ CaL\ CB}$ will be 1320 kg/m$^2$.

## 4. Conclusions

The $CO_2$ capture efficiency of CaL facilities is closely related to the hydrodynamics of the interconnected carbonator and calciner reactors. The similarity between CaL systems and large scale CFBCs allows us to study the hydrodynamics of the CaL reactor system using hydrodynamic models developed for similar reactor geometries, solids properties and operating conditions. In principle, for a given set of operating conditions and bed inventories, the solids circulation rates between the reactors calculated from a hydrodynamic model ($G_{s\ HM}$) will not be the same as those estimated from the $CO_2$ capture reactor mass balance ($G_{s\ CaL}$). When $G_{s\ HM} > G_{s\ CaL}$ this mismatch can be redressed by allowing an internal circulation of solids in the risers. When $G_{s\ HM} < G_{s\ CaL}$ this mismatch has to be solved mainly by increasing the bed inventories and/or the activity of the solids (through higher make-up flows of limestone). The gas velocity also has a strong impact on the solids circulation rates, reducing $G_{s\ HM\ CB}$ by 84% when the gas velocities in the carbonator vary from 5 to 3 m/s for the reference conditions. For low gas velocities the solids circulation rate may be insufficient to sustain the $CO_2$ capture loop ($G_{s\ HM} < G_{s\ CaL}$). In these conditions it will be necessary to increase the sorbent carrying capacity of the material (at the expense of higher make-up flows) and/or the solids inventories. For a wide range of operating conditions, it is usually possible to adopt an operating strategy to suit both the solids circulation rates required for $CO_2$ capture and those imposed by the hydrodynamics of the system.

## Acknowledgements

M.E. Diego acknowledges a fellowship Grant under the CSIC JAE Programme, co-funded by the European Social Fund.

## References


[1] B. Metz, O. Davidson, H. Coninck, M. Loos, L. Meyer, Special Report on Carbon Dioxide Capture and Storage, first ed., Intergovernmental Panel on Climate Change, New York, 2005.

[2] T. Shimizu, T. Hirama, H. Hosoda, K. Kitano, M. Inagaki, K. Tejima, A twin fluid-bed reactor for removal of $CO_2$ from combustion processes, Chem. Eng. Res. Des. 77 (1999) 62–68.

[3] J.C. Abanades, D. Alvarez, Conversion limits in the reaction of $CO_2$ with lime, Energy Fuels 17 (2003) 308–315.

[4] N. Rodríguez, M. Alonso, J.C. Abanades, Experimental investigation of a circulating fluidized-bed reactor to capture $CO_2$ with CaO, AlChE J. 57 (2011) 1356–1366.

[5] A. Charitos, N. Rodríguez, C. Hawthorne, M. Alonso, M. Zieba, B. Arias, G. Kopanakis, G. Scheffknecht, J.C. Abanades, Experimental validation of the calcium looping $CO_2$ capture process with two circulating fluidized bed carbonator reactors, Ind. Eng. Chem. Res. 50 (2011) 9685–9695.

[6] C. Hawthorne, H. Dieter, A. Bidwe, A. Schuster, G. Scheffknecht, S. Unterberger, M. Käß, $CO_2$ capture with CaO in a 200 $kW_{th}$ dual fluidized bed pilot plant, Energy Proc. 4 (2011) 441–448.

[7] A. Galloy, J. Ströhle, B. Epple, Design and operation of a 1 $MW_{th}$ carbonate and chemical looping CCS test rig, VGB PowerTechnol 91 (2011) 64–68.

[8] A. Sánchez-Biezma, J.C. Ballesteros, L. Diaz, E. de Zárraga, F.J. Álvarez, J. López, B. Arias, G. Grasa, J.C. Abanades, Postcombustion $CO_2$ capture with CaO. Status of the technology and next steps towards large scale demonstration, Energy Proc. 4 (2011) 852–859.

[9] N. Rodríguez, M. Alonso, G. Grasa, J.C. Abanades, Heat requirements in a calciner of $CaCO_3$ integrated in a $CO_2$ capture system using CaO, Chem. Eng. J. 138 (2008) 148–154.

[10] J.C. Abanades, E.J. Anthony, J. Wang, J.E. Oakey, Fluidized bed combustion systems integrating $CO_2$ capture with CaO, Environ. Sci. Technol. 39 (2005) 2861–2866.

[11] L.M. Romeo, J.C. Abanades, J.M. Escosa, J. Paño, A. Giménez, A. Sánchez-Biezma, J.C. Ballesteros, Oxyfuel carbonation/calcination cycle for low cost $CO_2$ capture in existing power plants, Energy Convers. Manage. 49 (2008) 2809–2814.

[12] M. Romano, Coal-fired power plant with calcium oxide carbonation for postcombustion $CO_2$ capture, Energy Proc. 1 (2009) 1099–1106.

[13] C. Hawthorne, M. Trossmann, P. Galindo Cifre, A. Schuster, G. Scheffknecht, Simulation of the carbonate looping power cycle, Energy Proc. 1 (2009) 1387–1394.

[14] P. Lisbona, A. Martínez, Y. Lara, L.M. Romeo, Capture cycle and coal-fired power plants. A comparative study for different sorbents, Energy Fuels 24 (2010) 728–736.

[15] Y. Yongping, Z. Rongrong, D. Liqiang, M. Kavosh, K. Patchigolla, J. Oakey, Integration and evaluation of a power plant with a CaO-based $CO_2$ capture system, Int. J. Greenhouse Gas Contr. 4 (2010) 603–612.

[16] A. Lasheras, J. Ströhle, A. Galloy, B. Epple, Carbonate looping process simulation using a 1D fluidized bed model for the carbonator, Int. J. Greenhouse Gas Contr. 5 (2011) 686–693.

[17] I. Martínez, R. Murillo, G. Grasa, J.C. Abanades, Integration of a Ca looping system for $CO_2$ capture in existing power plants, AlChE J. 57 (2011) 2599–2607.

[18] J.C. Abanades, E.J. Anthony, D.Y. Lu, C. Salvador, D. Alvarez, Capture of $CO_2$ from combustion gases in a fluidized bed of CaO, AlChE J. 50 (2004) 1614–1622.

[19] D.Y. Lu, R.W. Hughes, E.J. Anthony, Ca-based sorbent looping combustion for $CO_2$ capture in pilot-scale dual fluidized beds, Fuel Process. Technol. 89 (2008) 1386–1395.

[20] A. Charitos, C. Hawthorne, A.R. Bidwe, S. Sivalingam, A. Schuster, H. Spliethoff, G. Scheffknecht, Parametric investigation of the calcium looping process for $CO_2$ capture in a 10 $kW_{th}$ dual fluidized bed, Int. J. Greenhouse Gas Contr. 4 (2010) 776–784.

[21] M. Alonso, N. Rodríguez, G. Grasa, J.C. Abanades, Modelling of a fluidized bed carbonator reactor to capture $CO_2$ from a combustion flue gas, Chem. Eng. Sci. 64 (2009) 883–891.

[22] M.C. Romano, Modeling the carbonator of a Ca-looping process for $CO_2$ capture from power plant flue gas, Chem. Eng. Sci. 69 (2012) 257–269.

[23] M. Alonso, N. Rodríguez, B. González, G. Grasa, R. Murillo, J.C. Abanades, Carbon dioxide capture from combustion flue gases with a calcium oxide chemical loop. Experimental results and process development, Int. J. Greenhouse Gas Contr. 4 (2010) 167–173.

[24] M. Alonso, N. Rodríguez, B. González, B. Arias, J.C. Abanades, Biomass combustion with in Situ $CO_2$ capture by CaO. II. Experimental results, Ind. Eng. Chem. Res. 50 (2011) 6982–6989.

[25] T. Pröll, P. Kolbitsch, J. Bolhàr-Nordenkampf, H. Hofbauer, A novel dual circulating fluidized bed system for chemical looping processes, AlChE J. 55 (2009) 3255–3266.

[26] A. Charitos, C. Hawthorne, A.R. Bidwe, L. Korovesis, A. Schuster, G. Scheffknecht, Hydrodynamic analysis of a 10 $kW_{th}$ calcium looping dual fluidized bed for post-combustion $CO_2$ capture, Powder Technol. 200 (2010) 117–127.

[27] P. Lisbona, A. Martínez, L.M. Romeo, Hydrodynamical model and experimental results of a calcium looping cycle for $CO_2$ capture, Appl. Energy (2011).

[28] J. Ströhle, A. Lasheras, A. Galloy, B. Epple, Simulation of the carbonate looping process for post-combustion $CO_2$ capture from a coal-fired power plant, Chem. Eng. Technol. 32 (2009) 435–442.

[29] J. Ylätalo, J. Ritvanen, B. Arias, T. Tynjälä, T. Hyppänen, 1-Dimensional modelling and simulation of the carbonate looping process, Int. J. Greenhouse Gas Contr. 9 (2012) 130–135.

[30] D. Pallarès, F. Johnsson, Macroscopic modelling of fluid dynamics in large-scale circulating fluidized beds, Prog. Energy Combust. Sci. 32 (2006) 539–569.

[31] D. Pallarès, F. Johnsson, Fluid dynamic modeling of large CFB units, in: J.R. Grace, J.-X. Zhu, H.I. de Lasa (Eds.), Proceedings of the 7th International Conference on Circulating Fluidized Beds, Niagara Falls, Canada, 2002, pp. 387–394.

[32] F. Johnsson, B. Leckner, Vertical distribution of solids in a CFB-Furnace, in: K.J. Heinschel (Ed.), 13th International Conference on Fluidized Bed Combustion, Orlando, Florida, USA, 1995, pp. 671–679.

[33] A. Haider, O. Levenspiel, Drag coefficient and terminal velocity of spherical and nonspherical particles, Powder Technol. 58 (1989) 63–70.

[34] E. Muschelknautz, U. Muschelknautz, Special design of short entrance ducts to recirculating cyclones, in: M. Kwauk, J. Li (Eds.), Proceedings of the 5th International Conference on Circulating Fluidized Beds, Beijing, 1996, pp. 597–602.

[35] L. Zhen-shan, C. Ning-sheng, E. Croiset, Process analysis of $CO_2$ capture from flue gas using carbonation/calcination cycles, AlChE J. 54 (2008) 1912–1925.

[36] J.R. Grace, A.A. Avidan, T.M. Knowlton, Circulating Fluidized Beds, Blackie Academic and Professional, 1997.

[37] A. Martínez, Y. Lara, P. Lisbona, L.M. Romeo, Energy penalty reduction in the calcium looping cycle, Int. J. Greenhouse Gas Contr. 7 (2012) 74–81.

[38] I. Martínez, G. Grasa, R. Murillo, B. Arias, J.C. Abanades, Kinetics of calcination of partially carbonated particles in a ca-looping system for $CO_2$ capture, Energy Fuels (2012).

[39] N. Rodríguez, M. Alonso, J.C. Abanades, Average activity of CaO particles in a calcium looping system, Chem. Eng. J. 156 (2010) 388–394.

[40] J.C. Abanades, The maximum capture efficiency of $CO_2$ using a carbonation/calcination cycle of $CaO/CaCO_3$, Chem. Eng. J. 90 (2002) 303–306.

## 4.2 Estimación del efecto de la acumulación de inertes

Como ya se ha mencionado anteriormente, es importante que el inventario de sólidos del sistema conste de una cierta fracción de CaO activo para garantizar el buen funcionamiento del proceso de captura de $CO_2$. Para que la capacidad de captura de $CO_2$ de la corriente de sólidos que llega al carbonatador sea adecuada ésta debe presentar un bajo contenido en inertes ($CaSO_4$ y cenizas) y una cierta actividad de las partículas de CaO. Limitar el contenido de inertes en el material circulante es beneficioso porque conlleva flujos de circulación de sólidos entre reactores más bajos y por tanto, una demanda energética en el calcinador reducida (Rodríguez *et al.* 2008).

Sin embargo, la presencia de $CaSO_4$ y cenizas es inevitable en los procesos de CaL post-combustión, debido al azufre que se introduce al sistema junto con el gas de combustión de la central térmica y al flujo de carbón que se alimenta continuamente al calcinador, que contiene además cenizas. Puesto que los sólidos están perfectamente mezclados en el sistema, la reducción de la fracción de inertes se consigue únicamente a costa de un aumento de la alimentación de caliza fresca (con el consiguiente aumento de costes) y la extracción de una purga equivalente. Esto puede no ser necesario, sin embargo, en los sistemas de captura de $CO_2$ con CaO *in situ* (ver sección 1.3.2) en función del tipo de biomasa elegido, ya que en muchos casos este combustible presenta muy bajo contenido en azufre y cenizas.

Con el objetivo de cuantificar en detalle el efecto de la presencia de inertes en un sistema de carbonatación-calcinación se han seleccionado tres configuraciones de proceso representativas que se resumen a continuación:

- Una instalación CaL que trata los gases de combustión procedentes de una central térmica de carbón pulverizado que no cuenta con unidad de desulfuración (Configuración 1). Esta configuración es de

alto contenido en azufre, lo que tiende a elevar la fracción de $CaSO_4$ en los sólidos circulantes y a desactivar el CaO con respecto a la captura de $CO_2$.

- Una planta CaL que se alimenta con los gases de combustión de una caldera de lecho fluidizado circulante (Configuración 2). El CaO presente en este tipo de calderas contribuye a la desulfuración de los gases y, por tanto, el carbonatador recibe un aporte reducido de $SO_2$ a través de la corriente gaseosa. Este esquema es equivalente a la configuración anterior si se hiciera pasar los gases de salida de la central térmica por una planta desulfuradora.

- Un sistema CaL como el del punto anterior que presenta además una etapa de reactivación del sorbente (Configuración 3) para minimizar el consumo de caliza fresca, $F_0$, y la extracción de purgas del sistema. Esto se traduce en un aumento de la fracción de cenizas y $CaSO_4$ en los sólidos circulantes del sistema que, en situaciones de muy bajo $F_0$, acaba compensando el aumento de reactividad respecto a la carbonatación que experimenta el CaO libre gracias al proceso de reactivación.

La estimación cuantitativa de la acumulación de $CaSO_4$ y cenizas en el sistema se realiza mediante la resolución simultánea de los balances de materia y energía en las unidades del proceso. Para determinar el impacto de estos compuestos sobre la actividad del sorbente y la eficacia de captura de $CO_2$, el balance de materia integra una versión actualizada del modelo del carbonatador desarrollado por Alonso *et al.* (2009). En esta versión se incluye el cálculo de la actividad media máxima del sorbente mediante la expresión desarrollada por Rodríguez *et al.* (2010), que tiene en cuenta la posibilidad de que las partículas no alcancen su conversión máxima en el carbonatador y/o el calcinador, aunque en este caso se asume que el calcinador trabaja en condiciones de calcinación total. Esta expresión incluye

también unas constantes de ajuste que permiten considerar la reactivación del sorbente para el caso de la Configuración 3. En lo que respecta al deterioro en la actividad del CaO por la presencia de azufre, se hace la suposición conservadora de que el azufre reacciona únicamente con el CaO activo, reduciendo así la actividad media de las partículas. De este modo, para el cálculo de la capacidad de captura de $CO_2$ efectiva del sorbente se descuenta la fracción de caliza fresca que reacciona con el azufre contenido en el gas de combustión y el carbón introducido al sistema, $X_{sulf}$.

La resolución conjunta de los balances de materia y energía en el sistema, junto con el modelo del carbonatador, permiten calcular la fracción de partículas activas, su actividad media máxima y su conversión de carbonatación, el flujo molar de calcio entre reactores, la cantidad de carbón y de oxígeno que se requiere en el calcinador y la eficacia de captura en el carbonatador.

Con el objetivo de simular el efecto de la adición de caliza fresca al sistema se resuelven los balances anteriores para distintas relaciones $F_0/F_{CO2}$, y se calcula su impacto sobre la eficacia de captura de $CO_2$, la capacidad media máxima de captura efectiva del sorbente, y la acumulación de cenizas y $CaSO_4$ en las corrientes sólidas. De este modo es posible determinar los valores de $F_0$ adecuados desde el punto de vista del comportamiento del sistema. También se analiza el efecto de la introducción de una etapa de reactivación de las partículas de CaO en base a la conversión residual alcanzada en cada caso.

El modelo empleado, las principales suposiciones y la secuencia de cálculo completo se incluyen en la sección 4.2.1 en forma de la *Publicación IV*, que muestra además un análisis de los resultados obtenidos.

### 4.2.1 Publicación IV

**The impact of calcium sulfate and inert solids accumulation in post-combustion calcium looping systems**

Publicado en:

*Fuel*

*Volumen* 109

Páginas 184-190

Año 2013

Fuel 109 (2013) 184–190

Contents lists available at SciVerse ScienceDirect

Fuel

journal homepage: www.elsevier.com/locate/fuel

# The impact of calcium sulfate and inert solids accumulation in post-combustion calcium looping systems

M. Elena Diego *, Borja Arias, Mónica Alonso, J. Carlos Abanades

*Spanish Research Council, INCAR-CSIC, C/Francisco Pintado Fe, 26, 33011 Oviedo, Spain*

## HIGHLIGHTS

- The effects of sulfur and the accumulation of inerts are quantitatively discussed.
- Mass and energy balances were solved together with an updated carbonator model.
- It was found that the main impact on CaL performance is due to the sulfur inlet.
- A minimum purge is required even when an effective reactivating step is carried out.

## ARTICLE INFO

*Article history:*
Received 15 October 2012
Received in revised form 15 November 2012
Accepted 19 November 2012
Available online 5 December 2012

*Keywords:*
$CO_2$ capture
Calcium looping
Coal combustion
Sulfation
Carbonation

## ABSTRACT

Postcombustion $CO_2$ capture by calcium looping (CaL) is being rapidly developed for coal combustion applications. This work discusses the impact of the accumulation of $CaSO_4$ and other inert solids on $CO_2$ capture efficiency and the overall CaL process performance. Several process configurations are considered, and the mass and energy balances and an updated carbonator reactor model are solved for each configuration. The minimum fresh sorbent requirements for sustaining a certain level of $CO_2$ capture efficiency are quantified as well as the effects of an increase in the make-up flow. It was found that the main effect on the CaL process is produced by the sulfur present in the coal fed to the calciner and in the flue gas entering the carbonator. For a typical set of operating conditions it was calculated that the deactivating effect caused by an increase of 0.5% in the sulfur content with respect to a reference coal (low ash content) fed to the calciner is similar to the effect caused by the accumulation of inerts when using a coal with 15% more ash.



## 1. Introduction

$CO_2$ capture and storage (CCS) has emerged as a suitable option for reducing $CO_2$ emissions from large stationary sources such as coal power plants [1]. Nowadays there are mature $CO_2$ capture technologies that could be commercially deployed if there are reasonable incentives due to carbon prices [1]. In order to reduce the costs associated with $CO_2$ capture, a number of new technologies are also emerging. One of the most promising processes is postcombustion Ca-looping (CaL), which has experienced a rapid scale up in the last few years. It has already been tested in small facilities (10s $kW_{th}$) operating in full continuous mode [2,3] and has currently reached the experimental testing phase in a 1.7 $MW_{th}$ pilot plant in La Pereda – Spain [4,5], a 200 $kW_{th}$ facility at IFK – Stuttgart [6,7] and a 1 $MW_{th}$ pilot plant at ETS in Darmstadt [8,9].

Postcombustion CaL was first proposed by Shimizu et al. [10], and is based on the use of lime as a sorbent to capture $CO_2$ by means of carbonation/calcination cycles. The most suitable configuration for the application of CaL on a large scale involves the use of two interconnected circulating fluidized bed (CFB) reactors (carbonator and calciner as shown in Fig. 1). In this process, the flue gas generated in the power plant is directed to a carbonator, where $CO_2$ reacts at temperatures between 600 and 700 °C with a stream of CaO particles. As a result, $CaCO_3$ is formed and a $CO_2$ depleted gas leaves the carbonator. The partially carbonated solid stream enters the calciner together with a continuous make-up flow of limestone fed to this reactor to compensate for the decay of the $CO_2$ capture capacity of the sorbent with the number of carbonation/calcination cycles. In the calciner coal burns under oxy-fired conditions [10] to attain the temperatures required to convert both the $CaCO_3$ from the carbonator and the fresh sorbent back to CaO (around 900 °C). Although the heat demand in this reactor (coal and $O_2$) is high [10,11], the overall energy penalty of the CaL process is low [10,12–19], since energy can be recovered from

* Corresponding author. Tel.: +34 985119090; fax: +34 985 297662.
*E-mail address:* marlen@incar.csic.es (M.E. Diego).

0016-2361/$ - see front matter © 2012 Elsevier Ltd. All rights reserved.
http://dx.doi.org/10.1016/j.fuel.2012.11.062

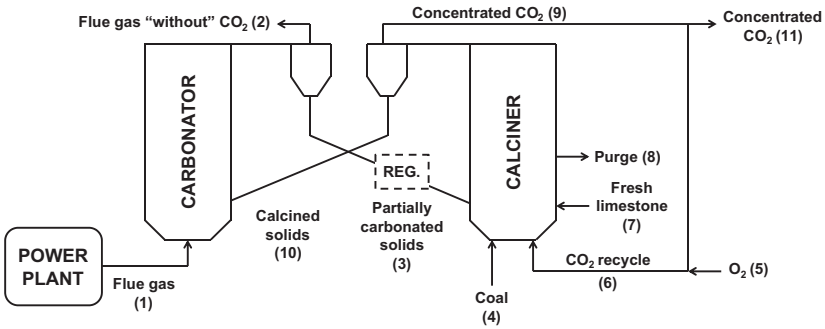


**Fig. 1.** General scheme of the CaL process for the three studied configurations. Dotted line indicates a possible location for the sorbent regenerator (REG.) in Configuration 3.

high-quality heat sources (the solids streams between reactors, the carbonator and the high temperature gases abandoning the reactors).

As a consequence of the nature of the CaL process, these systems have a continuous input of inert solids, mainly due to the coal fed into the circulating fluidized bed calciner but also because of the $SO_2$ in the flue gas entering the circulating fluidized bed carbonator. The $SO_2$ tends to react with the CaO present in both reactors of the system and forms $CaSO_4$. In order to prevent the accumulation of inerts in the system, solids should be purged from the calciner, which will contain mainly CaO, $CaSO_4$ and ashes. The flow rate of the solids purge is defined from a mass balance of the inerts fed to the process and the fresh limestone added to the calciner. The ratio between these two variables also determines the composition of the total inventory of solids in the system, which is known to affect the performance of the calcium looping process in terms of $CO_2$ capture efficiency and heat requirements in the calciner [11,20,21]. Some previous works give an overall view of the CaL process by formulating the mass and energy balances of the whole system, and they analyze the performance of CaL under certain operating conditions, such as different make-up flows of limestone or different solids circulating rates between reactors [11,21], even in the presence of sulfur [12,20]. However, these studies do not analyze the influence of ashes and the formation of $CaSO_4$ on $CO_2$ capture efficiency from a carbonator reactor point of view. This is a critical relationship to be quantified in the system. For a certain set of operating conditions, the solids inventory in the circulating fluidized bed carbonator will be fixed, and an increase in the concentration of inert solids in the system will translate into a low inventory of active Ca inside the reactor, thereby reducing the $CO_2$ capture efficiency. The aim of this work therefore is to quantitatively discuss these effects by analyzing several scenarios in relation to different power plant and $CO_2$ capture configurations. For this purpose, mass and energy balances were solved together with an updated carbonator reactor model, allowing us to calculate the $CO_2$ capture efficiency for each scenario. This simulation exercise provided useful information to determine the minimum make-up flow of limestone required to sustain a certain level of $CO_2$ capture efficiency as a function of the quality of the coal fed to the calciner and the $SO_2$ content in the flue gas entering the carbonator reactor from the power plant.

## 2. Methodology for process simulation

The process configurations analyzed in this work follow the general scheme depicted in Fig. 1, in which the flue gas coming from the power plant is fed into the carbonator of the CaL facility.

**Table 1**
Outline of the process configurations used in this work.

| Process configuration | Power plant | Sorbent reactivation |
|---|---|---|
| 1 | PC | No |
| 2 | CFBC | No |
| 3 | CFBC | Yes |

Table 1 summarizes the different configurations of the process, depending on the type of power plant emitting flue gases, the availability of $SO_2$ capture from the flue gas (with a flue gas desulfurization (FGD) unit in the pulverized coal (PC) power plant or an in situ $SO_2$ capture in the circulating fluidized bed combustion (CFBC) power plant) or the presence of a reactivation process.

Configuration 1 consists of a PC power plant that uses low sulfur fuel with no flue gas desulfurization unit. Some previous works study the effect of $SO_2$ on the sorbent activity in postcombustion CaL [22–26]. They have shown that $SO_2$ accelerates the decrease in $CO_2$ carrying capacity during cycling. Therefore, some authors [23] have highlighted the need for desulfurization of the flue gas entering the carbonator. However, the possibility of using the CaL process as a $CO_2$–$SO_2$ co-capture system translates into capital cost savings that may compensate for the additional limestone make-up requirements.

Configuration 2 is a CFBC power plant fitted with a CaL facility. High-efficient $SO_2$ capture (typically 90%) is assumed at the interior of the combustion chamber of the CFBC. For the purpose of this work, a similar PC + FGD + CaL configuration would give almost identical results to those obtained for this CFBC case. The only difference in favor of a CFBC power plant is that the purged material from the calciner can be used inside the CFBC as a sorbent to capture $SO_2$ from the flue gases.

Configuration 3 shows a similar scheme to that of Configuration 2, different only in that it incorporates a regenerator in the process. This reactivation step could be one of hydration [26–34], recarbonation [35] or any other means to increase the average activity of the circulating material or a fraction of such a solid stream. In order for the simulation to embrace any sorbent reactivation strategy no specific procedure to regenerate the solids is specified. The impact of the reactivation step is only considered through the increase in the average carrying capacity of the circulating material.

Mass and energy balances were solved for each configuration using an updated version of the carbonator model proposed by Alonso et al. [36]. This model assumes that the carbonator behaves as a continuous stirred tank reactor (CSTR) for the solids, so that the conversion of the particles is based on their residence time

distribution, whereas the carbonator performs as a plug flow reactor (PFR) for the gas phase. In this work the average reaction rate ($r_{ave}$) is expressed as [3]

$$r_{ave} = k_{sB}\varphi f_a N_{Ca} X_{ave}(\overline{v_{CO_2} - v_e}) \quad (1)$$

where $k_{sB}\varphi$ is the apparent reaction rate constant, $f_a$ is the active fraction of particles, $N_{Ca}$ is the total inventory of Ca moles inside the carbonator, $X_{ave}$ is the maximum average conversion of the solids, $v_{CO_2}$ is the volume fraction of $CO_2$ and $v_e$ is that in equilibrium conditions.

The fraction of particles that are active and able to react with $CO_2$ are those which have been in the carbonator for a shorter time than that required to achieve their maximum carbonate conversion, $t^*$ [36]. Therefore, $f_a$ is formulated in accordance with the CSTR residence time distribution [36]

$$f_a = \left(1 - \exp\left(\frac{-t^*}{N_{Ca}/F_R}\right)\right) \quad (2)$$

where $F_R$ is the calcium looping rate between the reactors and $t^*$ can be calculated from Eq. (3) [3,36]

$$t^* = \frac{X_{ave}}{(dX/dt)_{reactor}} = \frac{X_{ave}}{k_{sB}\varphi X_{ave}(\overline{v_{CO_2} - v_e})} \quad (3)$$

The maximum average carbonation conversion of lime particles can be obtained from the expression proposed by Rodríguez et al. [37], assuming total calcination conversion. This equation takes into account the fact that the carbonation reaction may not be completed each time that a particle leaves the carbonator,

$$X_{ave} = \frac{a_1 f_1^2 F_0}{F_0 + F_R f_{carb}(1 - f_1)} + \frac{a_2 f_2^2 F_0}{F_0 + F_R f_{carb}(1 - f_2)} + b \quad (4)$$

In Eq. (4) $F_0$ represents the make-up flow of fresh limestone and $a_1$, $f_1$, $a_2$, $f_2$ and $b$ are sorbent fitting constants of the $X_N$ vs. $N$ equation proposed by Li et al. [21]. $f_{carb}$ stands for the extent of carbonation of the particles and can be obtained from the following expression [36]

$$f_{carb} = \frac{X_{carb}}{X_{ave}} = \frac{f_a}{\ln(1/(1 - f_a))} \quad (5)$$

The previous $X_{ave}$ expression only considers the decay in the $CO_2$ capture capacity of lime resulting from the number of carbonation and calcination cycles. As was mentioned above, the impact of the $SO_2$ on the activity of the sorbent is difficult to quantify in a large scale system. A conservative assumption [12] can be made by assuming that sulfur reacts only with the active fraction of the sorbent, so that the effective maximum average conversion of the solids, $X_{ave,e}$, is obtained through the following expression,

$$X_{ave,e} = X_{ave} - X_{sulf} \quad (6)$$

In this equation $X_{sulf}$ is the fraction of the fresh limestone that reacts with the sulfur that enters into the system with the flue gas and the coal burnt in the calciner, $F_S$ [12]

$$X_{sulf} = \frac{F_S}{F_0} \quad (7)$$

Eqs. (4) and (6) do not directly reflect the positive impact of a potential sorbent reactivation stage (dotted box in Fig. 1). As discussed below, this will be taken into account when selecting the sorbent performance parameters ($a_1$, $a_2$, $f_1$, $f_2$ and $b$ implicit in the equation proposed by Li et al. [21] and used to obtain Eq. (6)) in Configuration 3 reported in Table 1.

Finally, the last term of the reaction rate expression (Eq. (1)) is the average of the difference between the $CO_2$ volume fraction in the carbonator and that in equilibrium conditions, which is obtained through Eq. (8) [36]

$$\overline{v_{CO_2} - v_e} = \frac{E_{carb}}{\left[-\frac{v_0}{(v_0 v_e - v_0)}E_{carb} + \left(\frac{(v_0 v_e - v_0) + (v_0 - v_e)v_0}{(v_0 v_e - v_0)^2}\right)\ln\left(\frac{(v_0 - v_e) + (v_0 v_e - v_0)E_{carb}}{(v_0 - v_e)}\right)\right]} \quad (8)$$

In this expression $E_{carb}$ symbolizes the $CO_2$ capture efficiency and $v_0$ is the $CO_2$ volume fraction at the carbonator inlet.

Taking into account all previous considerations, the carbon mass balance in the solids phase can be expressed as [36]

$$E_{carb} = \frac{F_R}{F_{CO_2}} X_{ave} \frac{f_a}{\ln(1/(1 - f_a))} \quad (9)$$

where $F_{CO_2}$ is the $CO_2$ molar flow that enters the carbonator.

Moreover, the carbon mass balance formulated for the gas phase at the carbonator exit is given by the following equation,

$$\frac{F_{CO_2} PM_{Ca}}{W_{Ca} f_a k_{SB} \varphi X_{ave}}\left[-\frac{v_0}{(v_0 v_e - v_0)}E_{carb} + \frac{v_0(v_0 - 1)}{(v_0 v_e - v_0)^2}\ln\left(\frac{(v_0 - v_e) + (v_0 v_e - v_0)E_{carb}}{(v_0 - v_e)}\right)\right] = 1 \quad (10)$$

where $PM_{Ca}$ and $W_{Ca}$ are the average molecular weight and the inventory of Ca compounds, respectively.

To solve the previous equations, we have defined the following input variables: the power plant capacity, the composition of the coals used in the boiler and the calciner, the inlet gas velocity in the carbonator and its total inventory, the kinetic and sorbent decay constants, the total solids circulation between reactors, the make-up flow of limestone and the oxygen content and temperature of the recycled gas stream that enters into the calciner. After the simultaneous formulation of the energy and mass balances, together with the Eqs. (5), (9), and (10) of the carbonator model, we can calculate the fraction of active particles, their maximum $CO_2$ carrying capacity and carbonation conversion, the calcium looping rate between reactors, the coal and $O_2$ required in the calciner, and $CO_2$ capture efficiency in the carbonator.

## 3. Results and discussion

In order to analyze the relationship between $CO_2$ capture efficiency and the input of ashes and $SO_2$ to the CaL system for the three configurations of Table 1, a common set of boundary conditions was defined. A power plant capacity of 1000 $MW_{th}$ was fixed for all the configurations, so that the $CO_2$ molar flow and the volume fraction entering the carbonator could be calculated. The chosen operating temperatures were 650 °C and 920 °C for the carbonator and calciner respectively. All reactors are assumed to operate under similar hydrodynamic conditions. For this purpose, the carbonator cross sectional area was calculated for all scenarios to maintain an inlet gas velocity in this reactor of 5 m/s. In addition, the total inventory of solids in the carbonator was set at 1000 kg/$m^2$ (including ashes and calcium sulfate). This inventory is assumed to be independent of the gas velocity in the carbonator and the solid circulation rate or the calcium ratio to the carbonator. This assumption only makes sense if modest changes are accepted in these variables and the possibility of an additional internal recycle of solids is considered in the scheme of Fig. 1 to decouple the solids inventory in the carbonator from the solids circulation between the reactors [38,39]. The $F_0/F_{CO_2}$ ratio was fixed at 0.1 for all configurations and no losses of lime due to attrition were considered for the mass balances, as the attrition effects are known to be closely related to the first calcination step [40] (so that the material subjected to attrition is mainly the make-up flow fed to the system), and they can be compensated for by introducing a higher make-up flow of limestone. For this comparison exercise, we have assumed a total external solids circulation rate to the calciner of 5 kg/$m^2$s which should be high enough to give high active

space times [3] to ensure high $CO_2$ capture efficiencies and reasonable heat requirements in the calciner of a CaL system [11]. The apparent reaction rate constant of active particles in the carbonator was taken as 0.43 $s^{-1}$ [3]. The $SO_2$ capture efficiency for both the carbonator and the calciner is assumed as 90% for each step. However, as a fraction of the gases leaving the calciner is recycled to this reactor, the overall calciner $SO_2$ capture efficiency increases.

The composition of the coal fed to the PC and CFB combustors is 68.0% C, 4.0% H, 1.0% S, 8.0% O, 8.0% $H_2O$, 1.0% N, 10.0% Ash (LHV: 28.0 MJ/kg). However, the CFB calciner requires a high quality coal in order to reduce the energy demand in the CaL facility [11] (74.0% C, 4.0% H, 0.5% S, 8.0% O, 8.0% $H_2O$, 0.5% N, 5.0% Ash (LHV: 30.0 MJ/kg)).

The amount of coal fed to the calciner is calculated by means of the energy balance. Coal is assumed to be burnt in the calciner with an oxidizing mixture containing 30%v $O_2$. The sulfur contained in the coal is mainly converted to calcium sulfate, as the CFB calciner is assumed to operate with a $SO_2$ capture efficiency of 90% for each step. The split between fly and bottom ashes from the coal (the latter are the only fraction that accumulates in the CaL system) was considered to be 50%. In addition, the flue gas coming from the power plant is assumed to be free of ashes.

Values of $a_1 = 0.1045$, $f_1 = 0.9822$, $a_2 = 0.7786$, $f_2 = 0.7905$ and $b = 0.07709$ were used as the fitting parameters of Eq. (4) to calculate $X_{ave}$ [37]. These parameters are fully consistent with the data reported by Grasa et al. [41], which can be expressed through Eq. (4) to make easier to estimate $X_{ave}$ under different conditions. Eq. (4) was also used to calculate $X_{ave}$ for the reactivation step, but in this case the parameters were adjusted to achieve a different residual conversion of the sorbent. For Configuration 3, the fitting constants in Eq. (4) are: $a_1 = 0.1288$, $f_1 = 0.9744$, $a_2 = 0.7248$, $f_2 = 0.7730$ and $b = 0.1666$. This corresponds to a residual sorbent conversion ($X_r$) of around 0.16, which is equal to that obtained experimentally through recarbonation [35] (see Fig. 2). Nevertheless, similar or even higher levels of sorbent reactivation can be attained by using other strategies, such as hydration [26–34] or other options which are also being studied to improve the $CO_2$ capture capacity of lime [42,43]. It should be also mentioned that the previous fitting parameters derive from thermogravimetric studies done in the absence of steam, which may enhance the activity of the sorbent [44,45]. Fig. 2 shows the adjustment of Eq. (4) (with the new fitting constants) to the experimental values obtained through recarbonation [35]. The curve for the case where there was no reactivation is also depicted.

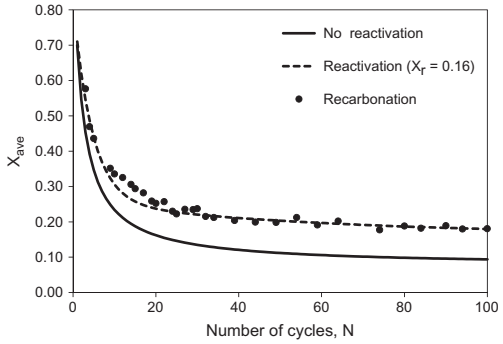


**Fig. 2.** $X_{ave}$ curves for no reactivation and reactivation up to $X_r = 0.16$, and experimental results obtained by recarbonation [35].

**Table 2**
Results from the mass and energy balances for the configurations of Table 1.

| Process configuration | $E_{carb}$ | $X_{ave,e}$ | $X_{carb}$ | $X_{sulf}$ |
|---|---|---|---|---|
| 1 | 0.50 | 0.080 | 0.075 | 0.079 |
| 2 | 0.80 | 0.124 | 0.114 | 0.034 |
| 3 | 0.93 | 0.235 | 0.135 | 0.036 |

The mass and energy balances were solved for the central set of operating conditions for each configuration of Table 1, and the results are shown in detail in Tables 2–4.

As expected, $CO_2$ capture efficiency is significantly lower in Configuration 1 (see Table 2). In this case, the high $SO_2$ input increases the inventory of inert solids and drastically reduces the average activity of the sorbent. In fact, the actual effective maximum average conversion of the particles takes on a value similar to that of the residual conversion of lime, even in the presence of the make-up flow. The sharp decrease in sorbent activity assumed for this scenario is the result of the direct effect of $X_{sulf}$ subtracting net points of $X_{ave}$ (Eq. (6)). This can be considered as a too conservative assumption, because $CaSO_4$ has been shown to be able to react not only with the active CaO for $CO_2$ capture but also with the non-active lime fraction [25]. However, in Configuration 2, when the flue gas is desulfurized in the CFB reactor prior to entering the $CO_2$ capture system, the $E_{carb}$ increases up to 80% for the same operating conditions due mainly to the higher $X_{ave,e}$. If the sorbent is subjected to a process to increase its average activity (Configuration 3), a $CO_2$ capture efficiency of 93% can be attained under the favorable conditions of this configuration.

In the case of the solids streams, it can be seen from Configurations 2 and 3 that the ash and $CaSO_4$ contents in the partially carbonated and calcined solids streams are similar (see Table 4), although they are slightly higher in the latter case because more coal is fed to the calciner in order to calcine the higher flow of $CaCO_3$ formed in the carbonator. On the other hand, the amount of $CaSO_4$ formed when using Configuration 1 is significantly higher (around 15%).

It is already clear from solving solutions of the reference configurations that the $CO_2$ capture process can achieve a low performance due to the reduction of sorbent activity and the accumulation of inerts in the system. In order to improve its performance (increase the activity of the sorbent and purge the inerts), the main process variable that needs to be adjusted is the make-up flow of fresh limestone. This section analyzes how the $F_0/F_{CO_2}$ ratio affects the $CO_2$ capture efficiency and the concentration of inerts, and the differences between each configuration. The procedure and the input variables used are the same as in the reference scenarios. The calculated $CO_2$ capture efficiencies are depicted in Fig. 3, whereas Figs. 5a and 5b show the weight percentage of ashes and $CaSO_4$ respectively in the stream of the partially carbonated solids that is transported from the carbonator to the calciner.

As can be seen in Fig. 3, for low values of $F_0/F_{CO_2}$, the higher the make-up flow, the higher the $CO_2$ capture efficiency due to the improvement of the effective maximum average conversion of the sorbent (depicted in Fig. 4) and the rise of the circulation rates of calcium between reactors as the inert solids concentration decreases. The rate at which the $E_{carb}$ increases as a function of the $F_0/F_{CO_2}$ ratio is different for each configuration. As mentioned in the previous section, these differences can be explained on the basis of the composition of the inventory of solids in the system and the effective maximum average conversion of the particles (see Fig. 4), which is reduced due to the presence of a larger amount of $SO_2$ in Configuration 1, and increased in Configuration 3 by the reactivation stage. It is also clear from Fig. 3 that after a certain value of $F_0/F_{CO_2}$ is reached (0.19, 0.14 and 0.07 for Configurations 1, 2

**Table 3**
Molar flows and compositions of the gas streams of Fig. 1.

| Configuration | Composition | Gas streams | | | | |
|---|---|---|---|---|---|---|
| | | Flue gas (1) | Flue gas "without" $CO_2$ (2) | $CO_2$ recycle (6) | Concentrated $CO_2$ (9) | Concentrated $CO_2$ (11) |
| 1 | Molar flow (kmol/s) | 13.3 | 12.3 | 8.3 | 10.1 | 4.1 |
| | $CO_2$ (%v) | 15.3 | 8.3 | 56.1 | 77.6 | 77.6 |
| | $SO_2$ (ppm) | 844 | 91 | 37 | 52 | 52 |
| 2 | Molar flow (kmol/s) | 13.3 | 11.6 | 9.7 | 12.2 | 5.1 |
| | $CO_2$ (%v) | 15.3 | 3.5 | 57.3 | 79.2 | 79.2 |
| | $SO_2$ (ppm) | 84 | 10 | 36 | 49 | 49 |
| 3 | Molar flow (kmol/s) | 13.3 | 11.4 | 10.5 | 13.2 | 5.7 |
| | $CO_2$ (%v) | 15.3 | 1.2 | 57.6 | 79.6 | 79.6 |
| | $SO_2$ (ppm) | 84 | 10 | 35 | 49 | 49 |

**Table 4**
Mass flows and compositions of the solids streams of Fig. 1.

| Configuration | Composition | Solids streams | | | | |
|---|---|---|---|---|---|---|
| | | Partially carbonated solids (3) | Coal (4) | Fresh limestone (7) | Purge (8) | Calcined solids (10) |
| 1 | Mass flow (kg/s) | 1005.6 | 31.3 | 20.3 | 13.3 | 959.9 |
| | $CaCO_3$ (%w) | 10.2 | – | 100 | – | – |
| | CaO (%w) | 69.7 | – | – | 79.1 | 79.1 |
| | Ash (%w) | 5.6 | – | – | 5.9 | 5.9 |
| | $CaSO_4$ (%w) | 14.5 | – | – | 15.0 | 15.0 |
| 2 | Mass flow (kg/s) | 1004.5 | 36.4 | 20.3 | 12.8 | 932.7 |
| | $CaCO_3$ (%w) | 16.2 | – | 100 | – | – |
| | CaO (%w) | 70.8 | – | – | 86.1 | 86.1 |
| | Ash (%w) | 6.6 | – | – | 7.1 | 7.1 |
| | $CaSO_4$ (%w) | 6.4 | – | – | 6.8 | 6.8 |
| 3 | Mass flow (kg/s) | 1004.5 | 39.0 | 20.3 | 12.9 | 920.9 |
| | $CaCO_3$ (%w) | 18.8 | – | 100 | – | – |
| | CaO (%w) | 67.6 | – | – | 85.2 | 85.2 |
| | Ash (%w) | 7.0 | – | – | 7.6 | 7.6 |
| | $CaSO_4$ (%w) | 6.6 | – | – | 7.2 | 7.2 |

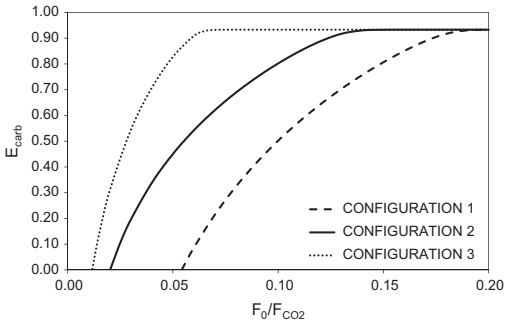


**Fig. 3.** Evolution of the $CO_2$ capture efficiency with the $F_0/F_{CO_2}$ ratio.

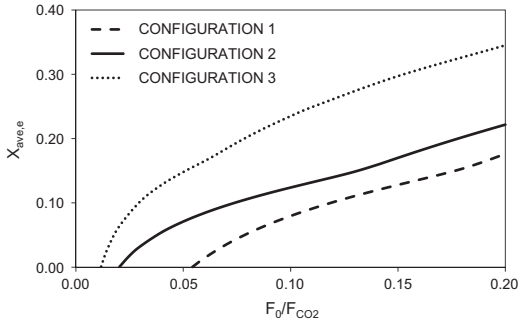


**Fig. 4.** Evolution of $X_{ave,e}$ with the $F_0/F_{CO_2}$ ratio for the different configurations.

and 3 respectively) the activity of the sorbent is no longer a limiting factor and $CO_2$ capture efficiencies are close to the maximum allowed by the equilibrium.

As it can be seen in Fig. 5a, the ash content in the system ($X_{ash}$) rises sharply as the $F_0/F_{CO_2}$ ratio approaches to zero. As shown above, for low $F_0/F_{CO_2}$ ratios the differences observed in the ash content are mainly due to changes in the coal requirements in the calciner, since different amounts of $CO_2$ are captured in each configuration, thus modifying the heat demand in the calciner. When the make-up flow increases the $CO_2$ capture efficiencies reach values close to equilibrium, and there are almost no differences in the ash content. The mass fraction of $CaSO_4$ in the carbonator (Fig. 5b), $X_{CaSO_4}$, follows the same trend as the ashes when comparing Configurations 2 and 3, because the input of $SO_2$ into the system is mainly due to the sulfur in the coal fed into the calciner. However, Configuration 1 shows significantly higher $X_{CaSO_4}$ values, since there is an additional input of sulfur to the CaL system from the flue gas.

It can be inferred from the previous results that the main impact on CaL performance is the input of sulfur into the system. In order to compare the deactivating effect of sulfur to that caused by the accumulation of inerts, a series of calculations were carried out. It was found that when the sulfur content of the coal burnt in the calciner was increased from 0.5% (reference case) to 1% (73.5%

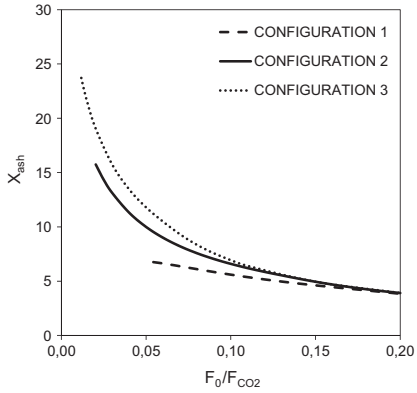


**Fig. 5a.** Mass fraction of ashes in stream (3).

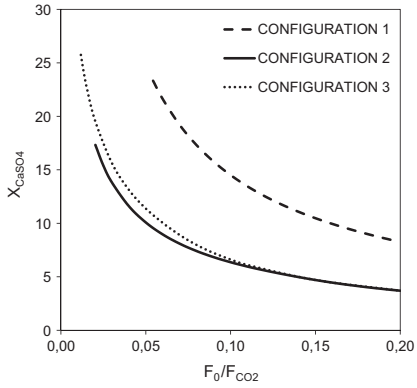


**Fig. 5b.** Mass fraction of $CaSO_4$ in stream (3).

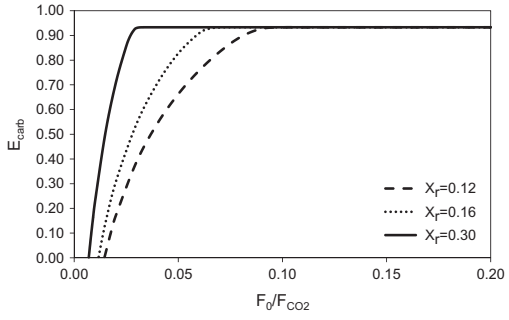


**Fig. 6.** Evolution of the $CO_2$ capture efficiency with the $F_0/F_{CO_2}$ ratio for different extents of reactivation in Configuration 3.

C, 4.0% H, 1.0% S, 8.0% O, 8.0% $H_2O$, 0.5% N, 5.0% Ash (LHV: 30.0 MJ/kg)) the $F_0/F_{CO_2}$ ratios required to maintain a $CO_2$ capture efficiency equal to 90% were 0.20, 0.15 and 0.08 for Configurations 1, 2 and 3 respectively. These values are similar to those required when using a coal with a sulfur content equal to that of the reference case with 20% ashes (58.0% C, 4.0% H, 0.5% S, 8.0% O, 8.0% $H_2O$, 1.5% N, 20.0% Ash (LHV: 24.5 MJ/kg)). Therefore, in these specific conditions, an increase in the coal sulfur content of 0.5% with respect to the reference coal has a similar effect to a rise of 15% in the ash percentage. However, it should be noted that the specific values can change as a function of the definition of the coal composition.

Finally, Fig. 6 summarizes the impact of different sorbent qualities on the $E_{carb}$ for different make up flows of sorbent. In general CaL technology pursues high $CO_2$ capture efficiencies while minimizing the make-up flow of sorbent. Unless there is a strong synergy with a cement producer (which would also impose limits on the composition of the purge material used), low limestone consumption is always an economic advantage [46,47]. $F_0$ can be reduced when using high-quality coals and/or when the sorbent is reactivated. The effect of the reactivation was analyzed for a system which follows the scheme of Configuration 3, where lime has residual conversions of 0.12, 0.16 (reference case of Configuration 3) and 0.30. In these cases, a 90% $CO_2$ capture efficiency is attained when the $F_0/F_{CO_2}$ ratio is 0.08, 0.06 and 0.03 respectively. Furthermore, the $CO_2$ capture efficiency was analyzed as a function of the $F_0/F_{CO_2}$ ratio, as depicted in Fig. 6. It can be seen that the $CO_2$ capture efficiency approaches zero for low $F_0/F_{CO_2}$ ratios, and these limiting ratios are lower when the extent of reactivation increases. However, it will always be necessary to feed a certain make-up flow of fresh limestone to attain reasonable $CO_2$ capture efficiencies, although the make-up flow can be reduced as a function of the reactivation level achieved by the sorbent.

## 4. Conclusion

CaL facilities for postcombustion $CO_2$ capture have a continuous input of ashes and $SO_2$ that depends on the flue gas desulfurization level in the reference plant and on the coal fed into the calciner. The increase in the feed of ashes and $SO_2$ to the system leads to a lower $CO_2$ capture efficiency due to the sulfation of the active CaO and a reduction in the inventory of active CaO in the carbonator. The results obtained in this work indicate that the main impact on CaL performance is caused principally by the input of sulfur into the system. With low sulfur coals (1% S in the boiler and 0.5% in the calciner) the introduction of a modest reactivation step ($X_r = 0.16$) reduces the make-up flow required to attain an $E_{carb} = 0.9$ of around 50%. However, even with an effective reactivating step leading to a lime residual conversion equal to 0.30, there is a need for a minimum make-up flow of limestone of about 0.03 ($F_0/F_{CO_2}$) to avoid the effects of the inerts.

The analysis carried out in this work confirms that when operating with low make-up flows, the carbonator efficiency shows high sensitivity to the composition of the coal of the calciner and the $SO_2$ content in the flue gas. The methodology proposed in this study seems to be a valuable tool for quantitatively selecting make-up flows for different configurations and different coal qualities.

## Acknowledgments

M.E. Diego acknowledges a fellowship Grant under the CSIC JAE Programme, co-funded by the European Social Fund. The financial support given by the RECaL project (RFCR-2012-RECaL) is also acknowledged.

## References

[1] Metz B, Davidson O, Coninck H, Loos M, Meyer L. Special report on carbon dioxide capture and storage. Intergovernmental panel on climate change. Cambridge, UK: Cambridge University Press; 2005.

[2] Rodríguez N, Alonso M, Abanades JC. Experimental investigation of a circulating fluidized-bed reactor to capture $CO_2$ with CaO. AIChE J 2011;57:1356–66.

[3] Charitos A, Rodriguez N, Hawthorne C, Alonso M, Zieba M, Arias B, et al. Experimental validation of the calcium looping $CO_2$ capture process with two circulating fluidized bed carbonator reactors. Ind Eng Chem Res 2011;50:9685–95.

[4] Sánchez-Biezma A, Ballesteros JC, Diaz L, de Zárraga E, Álvarez FJ, López J, et al. Postcombustion $CO_2$ capture with CaO. Status of the technology and next steps towards large scale demonstration. Energy Procedia 2011;4:852–9.

[5] Sánchez-Biezma A, Diaz L, López J, Arias B, Paniagua J, de Zárraga E, Álvarez J, Abanades JC. La Pereda $CO_2$: a 1.7 MW Pilot to test post-combustion $CO_2$ capture with CaO. In: 21st International conference on fluidized bed combustion, Naples (Italy); 2012, p. 365–72.

[6] Hawthorne C, Dieter H, Bidwe A, Schuster A, Scheffknecht G, Unterberger S, et al. $CO_2$ capture with CaO in a 200 $kW_{th}$ dual fluidized bed pilot plant. Energy Procedia 2011;4:441–8.

[7] Dieter H, Hawthorne C, Bidwe AR, Zieba M, Scheffknecht G. The 200 kWth dual fluidized bed calcium looping pilot plant for efficient $CO_2$ capture: plant operating experiences and results. In: 21st International conference on fluidized bed combustion, Naples (Italy); 2012, p. 397–404.

[8] Galloy A, Ströhle J, Epple B. Design and operation of a 1 $MW_{th}$ carbonate and chemical looping CCS test rig. VGB Power Tech 2011;91:64–8.

[9] Plötz S, Bayrak A, Galloy A, Kremer J, Orth M, Wieczorek M, Ströhle J, Epple B. First carbonate looping experiments with a 1 MWth test facility consisting of two interconnected CFBs. In: 21st International conference on fluidized bed combustion, Naples (Italy); 2012, p. 421–8.

[10] Shimizu T, Hirama T, Hosoda H, Kitano K, Inagaki M, Tejima K. A twin fluid-bed reactor for removal of $CO_2$ from combustion processes. Chem Eng Res Des 1999;77:62–8.

[11] Rodriguez N, Alonso M, Grasa G, Abanades JC. Heat requirements in a calciner of $CaCO_3$ integrated in a $CO_2$ capture system using CaO. Chem Eng J 2008;138:148–54.

[12] Abanades JC, Anthony EJ, Wang J, Oakey JE. Fluidized bed combustion systems integrating $CO_2$ capture with CaO. Environ Sci Technol 2005;39:2861–6.

[13] Romeo LM, Abanades JC, Escosa JM, Paño J, Giménez A, Sánchez-Biezma A, et al. Oxyfuel carbonation/calcination cycle for low cost $CO_2$ capture in existing power plants. Energy Convers Manage 2008;49:2809–14.

[14] Romano M. Coal-fired power plant with calcium oxide carbonation for postcombustion $CO_2$ capture. Energy Procedia 2009;1:1099–106.

[15] Hawthorne C, Trossmann M, Galindo Cifre P, Schuster A, Scheffknecht G. Simulation of the carbonate looping power cycle. Energy Procedia 2009;1:1387–94.

[16] Yongping Y, Rongrong Z, Liqiang D, Kavosh M, Patchigolla K, Oakey J. Integration and evaluation of a power plant with a CaO-based $CO_2$ capture system. Int J Greenhouse Gas Control 2010;4:603–12.

[17] Lasheras A, Ströhle J, Galloy A, Epple B. Carbonate looping process simulation using a 1D fluidized bed model for the carbonator. Int J Greenhouse Gas Control 2011;5:686–93.

[18] Martínez I, Murillo R, Grasa G, Abanades JC. Integration of a Ca looping system for $CO_2$ capture in existing power plants. AIChE J 2011;57:2599–607.

[19] Lisbona P, Martinez A, Lara Y, Romeo LM. Integration of carbonate $CO_2$ capture cycle and coal-fired power plants. A comparative study for different sorbents. Energy Fuels 2010;24:728–36.

[20] Romeo LM, Lara Y, Lisbona P, Escosa JM. Optimizing make-up flow in a $CO_2$ capture system using CaO. Chem Eng J 2009;147:252–8.

[21] Li. Z-s, Cai N-s, Croiset E. Process analysis of $CO_2$ capture from flue gas using carbonation/calcination cycles. AIChE J 2008;54:1912–25.

[22] Li Y, Buchi S, Grace JR, Lim CJ. $SO_2$ removal and $CO_2$ capture by limestone resulting from calcination/sulfation/carbonation cycles. Energy Fuels 2005;19:1927–34.

[23] Sun P, Grace JR, Lim CJ, Anthony EJ. Removal of $CO_2$ by calcium-based sorbents in the presence of $SO_2$. Energy Fuels 2006;21:163–70.

[24] Ryu H-J, Grace JR, Lim CJ. Simultaneous $CO_2/SO_2$ capture characteristics of three limestones in a fluidized-bed reactor. Energy Fuels 2006;20:1621–8.

[25] Grasa GS, Alonso M, Abanades JC. Sulfation of CaO particles in a carbonation/calcination loop to capture $CO_2$. Ind Eng Chem Res 2008;47:1630–5.

[26] Manovic V, Anthony EJ. Sequential $SO_2/CO_2$ capture enhanced by steam reactivation of a CaO-based sorbent. Fuel 2008;87:1564–73.

[27] Hughes RW, Lu D, Anthony EJ, Wu Y. Improved long-term conversion of limestone-derived sorbents for in situ capture of $CO_2$ in a fluidized bed combustor. Ind Eng Chem Res 2004;43:5529–39.

[28] Manovic V, Anthony EJ. Steam reactivation of spent CaO-based sorbent for multiple $CO_2$ capture cycles. Environ Sci Technol 2007;41:1420–5.

[29] Fennell PS, Davidson JF, Dennis JS, Hayhurst AN. Regeneration of sintered limestones sorbents for the sequestration of $CO_2$ from combustion and other systems. J Energy Inst 2007;80:116–9.

[30] Manovic V, Lu D, Anthony EJ. Steam hydration of sorbents from a dual fluidized bed $CO_2$ looping cycle reactor. Fuel 2008;87:3344–52.

[31] Grasa G, Murillo R, Alonso M, González B, Rodríguez N, Abanades JC. Steam reactivation of CaO-based natural sorbents applied to a carbonation/calcination loop for CO2 capture. In: 4th International conference on clean coal technologies, Dresden, Germany; 2009.

[32] Arias B, Grasa GS, Abanades JC. Effect of sorbent hydration on the average activity of CaO in a Ca-looping system. Chem Eng J 2010;163:324–30.

[33] Materic BV, Sheppard C, Smedley SI. Effect of repeated steam hydration reactivation on CaO-based sorbents for $CO_2$ capture. Environ Sci Technol 2010;44:9496–501.

[34] Phalak N, Deshpande N, Fan LS. Investigation of high-temperature steam hydration of naturally derived calcium oxide for improved carbon dioxide capture capacity over multiple cycles. Energy Fuels 2012;26:3903–9.

[35] Arias B, Grasa GS, Alonso M, Abanades JC. Post-combustion calcium looping process with a highly stable sorbent activity by recarbonation. Energy Environ Sci 2012;5:7353–9.

[36] Alonso M, Rodríguez N, Grasa G, Abanades JC. Modelling of a fluidized bed carbonator reactor to capture $CO_2$ from a combustion flue gas. Chem Eng Sci 2009;64:883–91.

[37] Rodríguez N, Alonso M, Abanades JC. Average activity of CaO particles in a calcium looping system. Chem Eng J 2010;156:388–94.

[38] Charitos A, Hawthorne C, Bidwe AR, Korovesis L, Schuster A, Scheffknecht G. Hydrodynamic analysis of a 10 $kW_{th}$ calcium looping dual fluidized bed for post-combustion $CO_2$ capture. Powder Technol 2010;200:117–27.

[39] Diego ME, Arias B, Abanades JC. Modeling the solids circulation rates and solids inventories of an interconnected circulating fluidized bed reactor system for $CO_2$ capture by calcium looping. Chem Eng J 2012;198–199:228–35.

[40] Coppola A, Montagnaro F, Salatino P, Scala F. Attrition of limestone during fluidized bed calcium looping cycles for $CO_2$ capture. Combust Sci Technol 2012;184:929–41.

[41] Grasa GS, Abanades JC. $CO_2$ capture capacity of CaO in long series of carbonation/calcination cycles. Ind Eng Chem Res 2006;45:8846–51.

[42] Blamey J, Anthony EJ, Wang J, Fennell PS. The calcium looping cycle for large-scale $CO_2$ capture. Prog Energy Combust Sci 2010;36:260–79.

[43] Yu F-C, Phalak N, Sun Z, Fan L-S. Activation strategies for calcium-based sorbents for CO2 capture: a perspective. Ind Eng Chem Res 2011;51:2133–42.

[44] Donat F, Florin NH, Anthony EJ, Fennell PS. Influence of high-temperature steam on the reactivity of CaO sorbent for $CO_2$ capture. Environ Sci Technol 2012;46:1262–9.

[45] Arias B, Grasa G, Abanades JC, Manovic V, Anthony EJ. The effect of steam on the fast carbonation reaction rates of CaO. Ind Eng Chem Res 2012;51:2478–82.

[46] Dean CC, Blamey J, Florin NH, Al-Jeboori MJ, Fennell PS. The calcium looping cycle for $CO_2$ capture from power generation, cement manufacture and hydrogen production. Chem Eng Res Des 2011;89:836–55.

[47] Romeo LM, Catalina D, Lisbona P, Lara Y, Martínez A. Reduction of greenhouse gas emissions by integration of cement plants, power plants, and $CO_2$ capture systems. Greenhouse Gas Sci Technol 2011;1:72–82.

## 4.3 Análisis de la recarbonatación como técnica de reactivación del sorbente

Como se ha indicado en la sección 1.3, la disminución de la capacidad de captura de $CO_2$ de las partículas de CaO a medida que experimentan sucesivos ciclos de carbonatación-calcinación es una de las principales limitaciones de los sistemas CaL. Aunque este inconveniente se puede contrarrestar mediante la adición de caliza fresca, es conveniente reducir este aporte para evitar un aumento de los requerimientos energéticos del calcinador y la generación de cantidades elevadas de purga, lo que haría casi obligatorio establecer una sinergia con la industria cementera, que no es fácil de alcanzar en muchas situaciones concretas. Es por ello que en los últimos tiempos se están proponiendo distintas opciones para la reactivación del sorbente destinadas a minimizar el consumo de caliza fresca (ver sección 1.3). Entre estas alternativas, el grupo de captura de $CO_2$ del INCAR-CSIC ha propuesto recientemente la técnica de recarbonatación (Abanades *et al.* 2012; Arias *et al.* 2012), que se encuentra en desarrollo bajo el proyecto europeo ReCaL (www.recal-project.eu).

La idea de reactivación por recarbonatación surge como resultado de las observaciones que muestran que la actividad residual de las partículas de CaO se estabiliza en valores más altos cuando la carbonatación se lleva a cabo durante tiempos largos y/o condiciones intensas de reacción (Barker 1973; Lysikov *et al.* 2007; Sun *et al.* 2008). Basándose en esta evidencia, Abanades *et al.* (2012) propusieron la inclusión de una etapa de recarbonatación del sorbente a la salida del carbonatador, de modo que, en condiciones de mayor temperatura y concentración de $CO_2$ los sólidos aumentan ligeramente su contenido en $CaCO_3$ por encima de su conversión media máxima. En un estado ideal de operación, este incremento permite compensar la pérdida de actividad que experimentará el sorbente durante el

siguiente ciclo de calcinación, de manera que su capacidad de captura de $CO_2$ se mantiene constante.

En esta sección se muestran los avances realizados durante esta Tesis Doctoral con el objetivo de llevar a la práctica esta técnica, que incluyen el diseño preliminar de reactores específicos para el proceso de recarbonatación en continuo, integrado dentro del esquema de circulación de sólidos estudiado en las secciones 4.1 y 4.2. Para alcanzar este objetivo, se ha profundizado en primer lugar en el estudio cuantitativo de las cinéticas de reacción que afectan al proceso (sección 4.3.1) para pasar después a la resolución de un modelo de reactor de recarbonatador (sección 4.3.2) que permite diseñar dicho reactor y elegir las ventanas de operación más adecuadas para el mismo. Los resultados de este trabajo han permitido rediseñar una de las *loop-seals* de la planta piloto de La Pereda para adaptarla como reactor de recarbonatación y ejecutar nuevas campañas experimentales para el proyecto europeo ReCaL. Sin embargo, estos trabajos realizados en planta piloto (en curso) quedan fuera del alcance de esta Tesis Doctoral.

### 4.3.1 Estudio de la cinética de la reacción de recarbonatación

El objetivo del trabajo incluido en la sección 4.3 es la modelización del reactor en el que se llevará a cabo la recarbonatación. En este sentido, uno de los aspectos que es necesario conocer es la cinética de la reacción que tiene lugar en su interior, lo que constituye el objeto de estudio de la *Publicación V*.

En este trabajo se ha realizado un estudio del comportamiento cinético de la reacción de carbonatación de CaO en condiciones de alta concentración de $CO_2$ y elevada temperatura, que son características de la etapa de recarbonatación. Para ello, se han realizado pruebas en una termobalanza ya descrita por Grasa *et al.* (2009) con muestras de caliza previamente cicladas, que se han sometido a secuencias de calcinación-carbonatación-

recarbonatación para determinar la velocidad de reacción y la conversión alcanzada durante la recarbonatación. De este modo, se han realizado diversos experimentos variando la temperatura de la etapa de recarbonatación entre 700 y 800ºC y la presión parcial de $CO_2$ entre 60 y 100 kPa, con el objetivo de determinar el efecto de estas variables sobre la cinética de la reacción de recarbonatación e identificar una ventana de condiciones de operación adecuadas para el proceso. También se ha analizado el efecto que tiene la presencia de vapor de agua en la atmósfera de reacción.

Con toda la información recogida durante los experimentos se han obtenido los parámetros cinéticos del modelo de reacción conocido como *Random Pore Model* o RPM (Bhatia y Perlmutter 1983; Grasa *et al.* 2009), que permite predecir la conversión de los sólidos con el tiempo. Asimismo, se ha propuesto una expresión cinética simplificada para la recarbonatación, y se ha determinado el valor de la constante aparente de reacción. Esta expresión es análoga a la empleada en los modelos del carbonatador propuestos por Alonso *et al.* (2009) y Charitos *et al.* (2011), y resulta más adecuada para su integración en los modelos de reactor por su sencillez.

Por último, se han realizado ensayos para cuantificar el incremento en la capacidad de captura de $CO_2$ del sorbente cuando se integra una etapa de recarbonatación en el proceso. Para ello se han realizado experimentos a dos temperaturas de recarbonatación (700 y 800ºC), sometiendo una muestra de caliza fresca a 75 ciclos de calcinación-carbonatación-recarbonatación en una atmósfera de $CO_2$ puro. Las curvas generadas que representan la actividad de las partículas de CaO en función del número de ciclos constatan un aumento en la conversión residual del sorbente debido a la presencia de la recarbonatación como técnica de reactivación.

Este trabajo ha dado lugar a la *Publicación V*, localizada en la sección 4.3.3, y en la que se muestran los resultados obtenidos y su discusión.

### 4.3.2 Desarrollo del modelo del reactor de recarbonatación

Una vez que se dispone de la información cinética fiable sobre la reacción de recarbonatación, el siguiente paso es la modelización y diseño del reactor de recarbonatación o recarbonatador. Es por ello que durante la realización de esta Tesis Doctoral se ha desarrollado un modelo del recarbonatador, incluido en la *Publicación VI*, cuyo objetivo es determinar la eficacia del reactor en términos de la conversión alcanzada por los sólidos en función de las condiciones de operación.

Como ya se ha mencionado anteriormente, el reactor de recarbonatación es un dispositivo en el que se pone en contacto una corriente de partículas parcialmente carbonatadas con un gas rico en $CO_2$ para así, incrementar su contenido en $CaCO_3$ por encima de lo que se conoce como conversión media máxima. Para la modelización de este reactor se ha considerado que se trata de un reactor de lecho fluidizado burbujeante, lo que garantiza tiempos de residencia de los sólidos elevados (del orden del minuto) y, al mismo tiempo, un buen contacto gas-sólido. Además, se ha utilizado el modelo propuesto por Kunii y Levenspiel (1990) para reactores de lecho fluidizado burbujeante que operan con partículas finas con el objetivo de definir dicho contacto gas-sólido en el interior del reactor.

Por otra parte, es previsible que una parte sustancial del gas desaparezca como consecuencia de su reacción con las partículas de CaO. Esta reducción de volumen se ha tenido en cuenta mediante la división del reactor en Z elementos longitudinales con respecto a la fase gas, de modo que los flujos de gas de salida de un elemento se corresponden con los de entrada del elemento siguiente. Cada uno de estos elementos se caracteriza porque la variación de volumen es prácticamente nula, por lo que se puede aplicar el modelo de Kunii y Levenspiel (1990), pensado para sistemas de volumen constante. Asimismo, se supone flujo pistón para el gas en el interior de cada elemento, mientras que los sólidos siguen un comportamiento de

mezcla perfecta en el interior del reactor. Por tanto, su conversión es la misma independientemente de su posición en el recarbonatador.

En el modelo del recarbonatador también se ha considerado que en los casos en los que la conversión de los sólidos de entrada al recarbonatador sea inferior a la media máxima de las partículas, su carbonatación hasta este valor es instantánea. Esto se debe a que la cinética de la reacción de carbonatación es mucho más alta que la de recarbonatación, tal y como se indica en la *Publicación V*. No obstante, una vez alcanzada la conversión media máxima, los sólidos reaccionan de acuerdo a la expresión cinética obtenida durante el análisis mostrado en dicha publicación. Además, se considera que la recarbonatación tiene lugar a velocidad constante durante un tiempo $t^*_R$ hasta que se alcanza un incremento de conversión máximo, y a partir de ese momento se asume que la velocidad de reacción es nula.

Por último, se define la variable $f_{a,R}$, que representa la fracción de partículas que han estado en el reactor por un tiempo inferior a $t^*_R$ y que, por tanto, continúan siendo activas para la recarbonatación. Por el contrario, se considera que aquellas partículas con un tiempo de residencia superior a $t^*_R$ han alcanzado su conversión máxima de recarbonatación y ya no participan en el proceso. Por lo tanto, la conversión media de las partículas en el recarbonatador es función del valor de $f_{a,R}$. Esta definición de $f_{a,R}$ es análoga a la empleada en los modelos del reactor de carbonatación (Alonso *et al.* 2009; Charitos *et al.* 2011), y su cálculo se realiza en base a la distribución de tiempos de residencia en un reactor de mezcla perfecta.

Teniendo en cuenta las suposiciones anteriores es posible formular el modelo del recarbonatador, cuya resolución conlleva un procedimiento iterativo basado en $f_{a,R}$ que se describe en la *Publicación VI*, ubicada en la sección 4.3.4. Esta publicación presenta además un diseño preliminar del recarbonatador empleando el modelo definido previamente. De este modo, se seleccionan las dimensiones y la velocidad de gas adecuada para alcanzar

una determinada eficacia de recarbonatación. Finalmente, se realiza un análisis de sensibilidad con el objetivo de determinar el grado de dependencia de los resultados obtenidos con los principales parámetros del modelo.

### 4.3.3 Publicación V

**Determination of CaO Carbonation Kinetics under Recarbonation Conditions**

Publicado en:

*Energy & Fuels*

*Volumen* 28

Páginas 4033-4042

Año 2014

energy&fuels

Article

pubs.acs.org/EF

# Determination of CaO Carbonation Kinetics under Recarbonation Conditions

G. Grasa,*[,†] I. Martínez,[†] M. E. Diego,[‡] and J. C. Abanades[‡]

[†]Instituto de Carboquímica, Consejo Superior de Investigaciones Científicas (CSIC), Miguel Luesma Castán 4, 50018 Zaragoza, Spain

[‡]Instituto Nacional del Carbón, Consejo Superior de Investigaciones Científicas (CSIC), Francisco Pintado Fé 26, 33011 Oviedo, Spain

**ABSTRACT:** This work investigates the kinetics of the reaction of $CO_2$ with CaO particles partially carbonated that are forced to increase their carbonate content at high temperatures in an atmosphere of rich $CO_2$. This additional recarbonation reaction on particles that have already completed their fast carbonation stage is the basis of a novel process that aims to increase the $CO_2$ carrying capacity of sorbents in calcium looping $CO_2$ capture systems. The CaO reaction rates and the maximum carbonation conversions after the recarbonation step were measured on a thermogravimetric analyzer, and the results indicate that they are highly dependent upon the temperature and $CO_2$ partial pressure, with steam also being a contributing factor. The reaction mechanism governing the reaction rates during the carbonation and recarbonation reactions is explained by the combined control of the chemical reaction and $CO_2$ diffusion through the $CaCO_3$ product layer. An extension of the random pore model adapted to multi-cycled CaO particles was successfully applied to calculate the CaO molar conversion as a function of the time and the recarbonation conditions, using kinetic parameters consistent with previously published results on carbonation kinetics under typical flue gas conditions.

## INTRODUCTION

$CO_2$ capture and storage (CCS) is a major mitigation option for addressing the problem of climate change, and there is a range of mature $CO_2$ capture technologies that could be rapidly deployed if the right incentives were in place.[1] The potential for reducing costs in optimized plants with already existing $CO_2$ capture technologies is important. However, a number of emerging $CO_2$ capture technologies may offer much deeper cost savings.[1]

Among these emerging technologies is the post-combustion calcium looping (CaL) process, which is based on the carbonation reaction of CaO and $CO_2$. It has experienced rapid growth in recent years from a mere concept (first proposed by Shimizu et al.[2]) to small-scale pilot demonstration of interconnected reactors[3−7] and, more recently, to larger scale pilots[8−10] of up to 1.7 $MW_{th}$.[11,12] In a typical CaL system, the CaO particles react with $CO_2$ contained in the flue gas in the carbonator unit, which operates at high temperatures (650−700 °C) to form $CaCO_3$. This carbonate is calcined by the oxy-combustion of coal at temperatures of around 880−910 °C in a second circulating fluidized bed, the calciner (see Figure 1). The high-temperature gas and solids streams allow for an efficient heat recovery that can be integrated with a steam cycle to generate additional power.[13−16] In this way, the energy penalty associated with the capture process is reduced to 6−7 net points assuming standard equipment in the air separation unit (ASU) required for oxy-combustion and in the $CO_2$ compression and purification unit (CPU). Any improvement in the ASU or CPU elements of the oxy-fuel combustion systems will also benefit the CaL system because the consumption of $O_2$ in the calciner still remains the main energy penalty in the process and a major cost component.

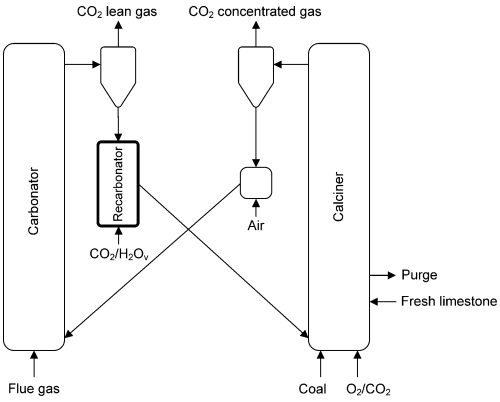


**Figure 1.** Block diagram of a CaL system, including a recarbonator reactor.

A well-known drawback of all CaL technologies is the decay in the $CO_2$ carrying capacity that the sorbent experiences with the number of calcination/carbonation cycles.[17−21] The low cost and availability of the raw limestone material used in CaL systems allow for a sufficiently large makeup flow of limestone to compensate for the decay in activity, making it possible to purge the system of ashes and $CaSO_4$. It is, however, important

**Received:** February 5, 2014
**Revised:** April 28, 2014
**Published:** April 28, 2014





dx.doi.org/10.1021/ef500331t | *Energy Fuels* 2014, 28, 4033−4042

for the development of large-scale CaL technology to be able to operate with a minimum sorbent requirement and maximum sorbent stability.[21−23] For this reason, intensive research is being carried out to find ways to reactivate CaO materials and to obtain more stable CaO-based sorbents, as explained in recent reviews by Anthony[24] and Blamey et al.[25]

Recently, our group proposed[26] a novel process to increase and stabilize the $CO_2$ carrying capacity of CaO particles in a CaL system. This is achieved by including a short recarbonation stage between the carbonator and calciner, in which highly carbonated particles from the carbonator are forced to increase their conversion to slightly above their "maximum carrying capacity" (usually signaled by the end of the fast carbonation period under normal carbonation conditions). The fundamentals of the process are based on the ability of CaO to react with $CO_2$ up to conversions over 80% after 10 cycles of 24 h in pure $CO_2$, as shown by Barker.[18] More recent experimental studies have revealed that extended carbonation times (up to 30 min) lead to sorbents exhibiting greater residual activity,[27,28] with respect to the activity of solid sorbents subjected to shorter reaction times.[29] Similar results were found with sorbents tested under higher $CO_2$ partial pressures.[30,31] Also, the use of pure $CO_2$ and long carbonation reaction times was investigated as a method to increase $CO_2$ carrying capacities, but contradictory results at thermogravimetric analysis (TGA) and fluidized-bed lab scale[32] were obtained.

The recarbonation process proposed in this study includes a new reaction step carried out in a separate reactor (the recarbonator in Figure 1), where the partially carbonated stream of solids exiting the carbonator unit is placed in contact with a highly concentrated $CO_2$ stream at high temperature (generated in the calciner unit). The purpose of this is to produce an additional conversion of the solids under the slow reaction regime to achieve an increase in the carbonate conversion that will compensate for the decay in the $CO_2$ capture capacity that the solids will undergo the next time that they pass through the calciner and carbonator.[26]

It is well-known that the ability of CaO to react with $CO_2$ in the slow reaction regime has little impact on the $CO_2$ carrying capacity of the sorbent under the standard carbonation conditions in a CaL system. This is because the average residence times of the solids in the carbonator reactor amount to only a few minutes[6,7] for typical solids inventories and circulation flows. Besides, the average $CO_2$ partial pressures around the particles in the reactor are well below 15 kPa when the $CO_2$ capture efficiency is high. However, the sorbent may be reacting sufficiently fast under the enhanced carbonation conditions of the recarbonator reactor in Figure 1. The recarbonation process in Figure 1 opens up a new scenario for the study of carbonation reaction kinetics on the basis of the ability of CaO particles that are already partially carbonated to continue reacting with $CO_2$ at the high temperatures and $CO_2$ partial pressures present in the recarbonator reactor. Evaluation of the reaction kinetics in the slow reaction regime at a higher temperature and $pCO_2$ will be critical for the design of the recarbonator reactor. A substantial background of literature exists on the relevant kinetics and mechanism of reaction between CaO and $CO_2$, as reviewed in the following paragraphs.

Early experimental studies of the carbonation kinetics of CaO revealed the existence of two stages in the carbonation reaction rates:[2,18,19,21,33,34] a fast chemically controlled initial reaction stage and a second slower reaction stage controlled mainly by the diffusion of $CO_2$ through the product layer. Various models based on sorbent structural properties have been used in the literature to describe in detail the kinetics of these two reaction regimes, as compiled in the review by Stanmore and Gillot,[35] and they can be classified into grain models or pore models. The grain models for CaO carbonation see the particle as a porous structure consisting of a grain matrix formed as a result of the previous calcination step.[36−38] The size of the CaO grains determines to a large extent the amount of active surface for reaction. Stendardo and Foscolo[37] assumed an average grain size, with a uniform dispersion of CaO grains that are gradually transformed into $CaCO_3$. Bouquet et al.[36] applied a micrograin−grain model that distinguishes three differentiated reaction stages during the filling of all of the voids present in the CaO micrograins. During this void-filling process, the shrinking core model applied to the micrograin showed that there is a short kinetically controlled regime, followed by a combined control by chemical reaction and diffusion through the carbonate layer. Finally, $CO_2$ diffuses at the grain level through the carbonate to reach the inner CaO cores. A second group of researchers applied pore models that take into account the evolution of the pore size distribution of the sorbent during the carbonation reaction.[33,39] The random pore model (RPM) developed by Bhatia and Perlmutter[33] considered the pore structure as a network of randomly interconnected pores and defined the key particle structural parameters on the basis of this geometry. They developed a general expression for the instantaneous gas−solids local reaction rate applicable to porous systems in the presence of a product layer diffusion resistance.

Sun et al.[39] developed a new gas−solid model for the carbonation of CaO based on discrete pore size distribution measurements. This model uses the initial pore size distribution of the lime resulting from calcination of the fresh limestone as input data. The only fitting parameter used was the effective diffusivity through the product layer (which was also dependent upon the evolution of the pore system).

As mentioned above, the carbonation reaction shows an abrupt change from the chemical to the diffusional controlled regime, which has been generally attributed to the formation of a $CaCO_3$ product layer on the free CaO reaction surface.[18,20,21,29,33,36,39−42] Alvarez and Abanades[40] have established that the product layer thickness representing the transition between the fast and slow reaction regimes for reaction conditions of practical interest for CaL systems is around 50 nm. Using a simple pore model to interpret the data obtained from Hg porosimetry measurements, they described the progression of the carbonation reaction on the CaO surface as the filling of the available rich porous structure of the calcined material. Once the small pores and part of the large voids are covered with a $CaCO_3$ layer of around 50 nm, $CO_2$ diffusion is restricted, and this causes a slower conversion of the solids. Bouquet et al.[36] proposed that the transition between diffusion resistance at the micrograin to grain level starts once the voids between micrograins are filled with a $CaCO_3$ layer of around 43 nm. The scale of diffusion at the grain level is responsible for the drastic decay in the reaction rate, and the diffusion coefficient through the product layer decreases upon the formation of carbonate. Mess et al.[34] described the growth of the product layer as a coalescence phenomenon, in which the grain growth is highly dependent upon the temperature. The effective diffusion coefficient is expressed as a combination of the grain boundary diffusion coefficient and the bulk diffusion

coefficient through the product layer and is dependent upon the conversion of solids, as the grain boundary length diminishes, while the product layer becomes more developed. The effective diffusion coefficient decreases with the conversion of solids. The increasing resistance of $CO_2$ diffusion with increasing $CaCO_3$ content has also been noted by Stendardo and Foscolo[37] to fit the experimental carbonation conversion curves of calcined dolomite in their spherical grain model. Sun et al.[39] related the diffusion coefficient to the evolution of the pore system.

In contrast with these variable effective diffusion coefficients, Bhatia and Perlmutter[33] assumed a homogeneous product layer with a single diffusion coefficient only dependent upon the temperature to describe the diffusion process.

Recent studies on the effect of the temperature on the carbonation reaction of CaO under the diffusion reaction regime have shown that the reaction kinetics are improved when the reaction temperature is increased in what appears to be another fast reaction regime.[43] These findings reinforce the relation of the diffusion coefficient with the temperature and show that the contribution of the $CO_2$ diffusion resistance through the product layer to the total reaction rate is highly determined by the reaction temperature. Also, according to the detailed observations and modeling work by Li et al.,[43] the morphology of the product layer is largely dependent upon the reaction temperature. When the reaction temperature is increased, the thickness of the islands that initially form the $CaCO_3$ layer increases, while their density over the CaO surface diminishes leaving, for a given level of conversion, a higher fraction of free CaO surface for a chemically controlled reaction. This is a critical piece of information for understanding and interpreting the experimental results presented in this work.

The objective of this paper is to extend the scope of the experimental results available to model the carbonation reaction in the different stages of the system of Figure 1 and, in particular, to determine the effect of the main operating variables (i.e., the reaction temperature, the $CO_2$ partial pressure, and the presence of steam) upon the conversion achieved by CaO particles under recarbonation conditions. The kinetic parameters that govern the reaction in the new reaction conditions will be determined using the RPM. A second objective of the paper is to reinforce the experimental evidence of the positive effects of the recarbonation step on the increase in the residual $CO_2$ carrying capacities of CaO particles.

## EXPERIMENTAL SECTION

A Spanish limestone, Compostilla, presenting 93.04 wt % CaO (and main impurities 2.5 wt % $Fe_2O_3$, 0.76 wt % MgO, 0.46 wt % $K_2O$, 0.33 wt % $SiO_2$, and 0.37 wt % $TiO_2$) was used in the experimental tests to determine the principal variables affecting the carbonation reaction under recarbonation conditions. Most experiments were carried out with samples with a narrow particle size interval (75−125 $\mu$m) that were texturally characterized using a Quantachrome PoreMaster Hg porosimeter to estimate the pore volume and the pore size distribution. $N_2$ adsorption (Micromeritics ASAP2020) at 77 K was used to calculate the surface area by applying the Brunauer−Emmett−Teller (BET) equation to the adsorption isotherm.

The experimental tests were carried out on a TGA apparatus that has been described in detail in previous papers.[41] Briefly, the reactor consists of a quartz tube with a platinum basket suspended from it, inside a two-zone furnace. The furnace can be moved up and down by means of a pneumatic piston. The position of the furnace with respect to the platinum basket allows for alternation between calcination and carbonation conditions. The temperature and sample weight were continuously recorded on a computer. The reacting gas mixture ($CO_2$ and $O_2$/air) was regulated by mass flow controllers and fed through the bottom of the quartz tube. Steam was generated by external electric heating of the water flow controlled by a liquid mass flow controller and then introduced into the reaction atmosphere for some specific tests.

The materials used to determine the reaction kinetics of the carbonation reaction under recarbonation conditions (elevated reaction temperature and $CO_2$ partial pressure) were partially deactivated CaO particles, with an average $CO_2$ carrying capacity between 0.15 and 0.30 CaO molar conversion, which is representative of the activity of the average material circulating in a large-scale CaL system. To prepare this material, batches of around 150 mg of limestone were placed inside a platinum pan in the TGA apparatus and subjected to relatively standard calcination/carbonation cycles (the calcination of the sample was carried out at 875 °C in air for 30 min, and the carbonation was carried out at 650 °C in 5 kPa $CO_2$ in air for 30 min to ensure full saturation of the sorbent up to its maximum carrying capacity, $X_N$). The solids prepared by this procedure had been subjected to the recarbonation tests described below.

A total of 3 mg of partially deactivated sorbent was placed in the TGA pan in each individual kinetic test, and the total gas flow was set to $4 \times 10^{-6}$ $m^3/s$ to eliminate external diffusion resistances to the reaction.[41] To avoid any effect associated with the preparation of the samples that might interfere with the interpretation of the experimental results, every recarbonation test involved several standard calcination/carbonation cycles at the beginning of each test. The routine of the standard cycles was calcination at 875 °C in air for 5 min, followed by carbonation at 650 °C in 5 kPa $CO_2$ in air for 5 min. After several cycles under these standard conditions, a recarbonation stage was added to the routine just after the end of the carbonation stage of the solids. The effect that the recarbonation temperature (between 700 and 800 °C) and the $pCO_2$ in the reaction atmosphere (between 60 and 100 kPa $CO_2$) had on the carbonation reaction kinetics under recarbonation conditions was experimentally evaluated. The presence of steam during recarbonation was tested by including 15 vol % of steam in the $CO_2$ atmosphere in some specific tests. Some standard carbonation/calcination tests were also carried out to test whether the sorbent carbonation kinetic parameters were in agreement with the values presented in the literature for the CaO carbonation reaction.

Furthermore, to determine the impact that the recarbonation stage has on sorbent residual activity, around 10 mg of limestone sample was subjected to 75 repeated calcination/carbonation cycles according to the following routine: calcination of the sample at 875 °C in air for 5 min, carbonation at 650 °C in 5 kPa $CO_2$ in air for 5 min, and recarbonation in pure $CO_2$ for 5 min. The tests were carried out at recarbonation temperatures of 700 and 800 °C. For comparison purposes, the same material was also tested under a "typical" calcination−carbonation experimental routine without any recarbonation step (calcination at 875 °C in air for 5 min and carbonation at 650 °C in 5 kPa $CO_2$ in air for 5 min).

## RESULTS AND DISCUSSION

Figure 2 provides an example of the experimental results that illustrate the positive effect of the recarbonation step on the $CO_2$ maximum carrying capacity $X_{N,R}$, achieved by the sorbent at the end of the fast reaction period of the carbonation reaction and after several calcination−carbonation−recarbonation cycles. Two types of curves appear in this plot of the carbonate CaO conversion versus time: a gray line corresponding to the reference carbonation test conducted without recarbonation (after 17 standard cycles of calcination−carbonation) and a black line corresponding to the carbonation and recarbonation test conducted after 15 standard cycles and 2 additional cycles of calcination−carbonation−recarbonation stages. According to the nomenclature in Figure 2, $N$



dx.doi.org/10.1021/ef500331t | Energy Fuels 2014, 28, 4033−4042

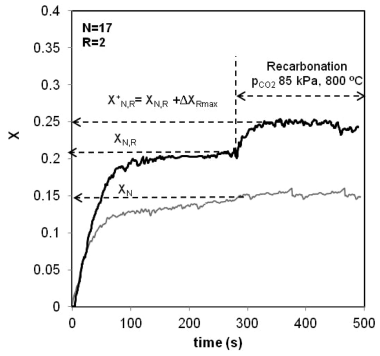


**Figure 2.** Example of the experimental carbonation and recarbonation CaO conversion curves after 17 calcination cycles ($N$ = 17 in both curves). The black curve is obtained after 15 standard cycles of calcination−carbonation and 2 cycles of calcination−carbonation−recarbonation ($R$ = 2). Calcination was at 875 °C in air. Carbonation was at 650 °C and 5 kPa $CO_2$ in air. Recarbonation was at 800 °C and 85 kPa $CO_2$ in air.

corresponds to the total number of calcinations experienced by the sample (17 in this case) and $R$ corresponds to the number of recarbonation stages (2 in the example of Figure 2).

This second curve has two clearly separate reaction stages under different reaction conditions. During the initial ∼280 s, the sorbent is reacting under typical carbonation conditions (650 °C and 5 kPa $CO_2$ in air, as in the case of the gray curve used as a reference) and the CaO conversion versus time curve shows a typical fast carbonation stage (which lasts for about 60−70 s in these conditions) controlled by the chemical reaction, followed by a slower reaction stage controlled by the combined resistance of the chemical reaction and $CO_2$ diffusion through the product layer,[33,41] although diffusion is the predominant resistance. The slow reaction period leads very rapidly to a characteristic stage of conversion, $X_N$ (without recarbonation) or $X_{N,R}$ (with recarbonation), as shown in Figure 2, which corresponds to the maximum $CO_2$ carrying capacity of the sorbent for each cycle number $N$ on both curves. After 280 s of carbonation, the reaction conditions remain unchanged in the reference experiment without recarbonation but they switched over to the conditions required by the recarbonator reactor in Figure 1 (in this particular test, 800 °C and 85 kPa $CO_2$) in the black curve.

As seen, thanks to the recarbonation stage, the $CO_2$ carrying capacity of the reactivated sorbent, $X_{N,R}$, has noticeably increased with respect to the reference value, $X_N$, for an identical number of calcination cycles. Furthermore, the slope of the initial fast reaction stage (chemically controlled) and the second slower reaction stage controlled by the diffusion are almost identical for the reactivated and non-reactivated curves under the carbonator operating conditions (first 280 s). This suggests that the kinetic constants and the diffusion parameters from the carbonation reaction rate expressions have not been affected very much by the inclusion of the recarbonation stage. Therefore, the cause of the rapid increase in carbonate conversion during recarbonation, $\Delta X_R$, must be the change in the reaction temperature and the $CO_2$ partial pressure.

As seen in Figure 2, once the experimental conditions have been switched over to the recarbonation conditions, the slope of the CaO conversion curves increases with respect to the slope of the diffusion regime at lower temperature until $X$ reaches a new plateau, $X^{+}_{N,R} = X_{N,R} + \Delta X_{R,max}$, in which the reaction rate slows down again. These experimental CaO conversion curves, which incorporate the gain in conversion during recarbonation, $\Delta X_{R,max}$, can be used to derive the kinetic parameters for the recarbonation reaction stage. As pointed out above, a series of experiments were carried out to evaluate the effect of the reaction temperature, the $CO_2$ partial pressure, and the presence of steam upon the recarbonation rates of CaO partially converted to $CaCO_3$ in the preceding reaction period at standard carbonation conditions.

Figure 3 shows experimental conversion curves in which the recarbonation temperature was 750 and 700 °C (under 85 kPa $CO_2$ in air). As seen, from a comparison of the experimental results of Figures 2 and 3, the $\Delta X_{R,max}$ achieved under recarbonation conditions is greatly affected by the temperature. In the series of Figure 2, carried out at 800 °C, the sorbent is able to achieve ≈0.04 additional conversion points in the space of 60 s, while the slope of the CaO conversion curve under recarbonation is less steep at lower temperatures and the value of $\Delta X_{R,max}$ is consequently smaller at the end of the recarbonation time fixed for this experiment. The presence of

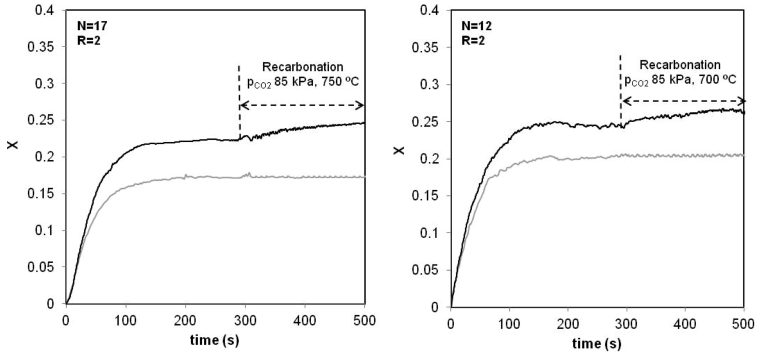


**Figure 3.** Experimental carbonation and recarbonation CaO conversion curves for two different recarbonation temperatures: (left) 750 °C and (right) 700 °C. Calcination and carbonation conditions are the same as in Figure 2

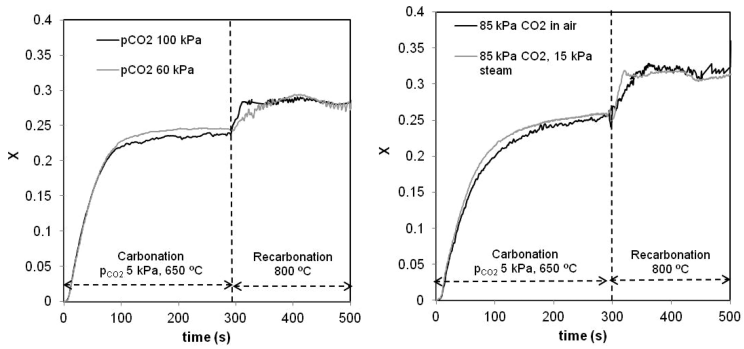


**Figure 4.** (Left) Effect of the $CO_2$ partial pressure on CaO conversion during recarbonation at 800 °C ($N$ = 12, and $R$ = 2). (Right) Effect of the presence of steam on CaO conversion during recarbonation at 800 °C and 85 kPa $CO_2$ ($N$ = 12, and $R$ = 2). Calcination and carbonation conditions are the same as in Figure 2

this plateau at which the carbonation reaction rate is extremely slow even under recarbonation conditions was also confirmed at these lower temperatures in other experiments with longer recarbonation times.

The presence of this second plateau in the conversion of CaO supports recent mechanistic studies by Li et al.,[43] who claim that the temperature affects the rate of growth of the carbonate product layer that forms over the entire surface of the CaO particles. The growth of the carbonate layer has been described as a coalescence phenomenon of $CaCO_3$ islands,[34,43] so that once the islands of $CaCO_3$ cover the whole of the CaO surface and reach a critical thickness, $CO_2$ diffusion through the $CaCO_3$ layer is severely hindered. The island growth rate has been directly related to the temperature,[34] as has the characteristic island dimension.[43]

To analyze the effect of the reaction atmosphere on the kinetics of the recarbonation reaction, several tests were carried out at 800 °C, in which the $pCO_2$ in the reaction atmosphere was varied from 60 to 100 kPa $CO_2$. As seen in the left panel of Figure 4, the reaction rate under recarbonation conditions increases with an increasing $CO_2$ concentration. However, the CaO conversion that marks the onset of the second plateau is independent of the $CO_2$ partial pressure, and from this point, the reaction rate is independent (and very slow) of the $CO_2$ partial pressure. This is in agreement with the expression formulated by Bhatia and Perlmutter for pure diffusion control.[33]

The effect that the presence of steam has on the recarbonation reaction was evaluated by carrying out a series of tests with 15 vol % steam in $CO_2$. The steam was added only during the recarbonation stage. The results presented in the right panel of Figure 4 correspond to two experiments carried out using a similar procedure with and without steam. After 10 standard calcination−carbonation cycles, several cycles, including a recarbonation stage, were carried out. The series presented corresponds to samples that experienced 12 calcinations ($N$ = 12) and 2 recarbonations ($R$ = 2) with the presence of steam (gray line) and without steam (black line). The experimental results show that the slope of the CaO conversion curve during recarbonation in the presence of steam is around 1.5 times larger than the slope of the conversion curve without steam. This qualitative trend was also observed in other similar experiments with steam and indicates that the reaction rate during recarbonation increases in the presence of steam, which is in agreement with experimental results compiled in the literature, from which it can be concluded that diffusion resistance is diminished in the presence of steam.[44,45]

To fit the experimental conversion data versus time, we have used the RPM[33] that has been adapted to model the carbonation reaction of sorbents that have experienced multiple calcination/carbonation cycles.[41] The main novelty of this adapted version of the RPM is the estimation of the sorbent structural parameters included in the model equations ($S$, $L$, $\varepsilon$, and $\Psi$) from the textural properties of the sorbent resulting from the calcination of the fresh limestone and the evolution of the CaO conversion with the number of cycles. To predict the evolution of the CaO conversion with time (experimental curves plotted in Figures 2−4), the general expression of the reaction rate can be integrated, taking into account the different controlling mechanisms: chemical reaction kinetic control and combined control by the reaction and diffusion through the product layer. There is also a third controlling mechanism, pure diffusion control, but in this case, the particles experience almost no increase in their carbonate content. From the previous experimental curves, it can be seen that the fast reaction stage of the carbonation reaction is controlled by the chemical reaction, and according to the model proposed by Grasa et al.,[41] the abrupt change to the slower reaction rate under carbonation conditions is determined by the formation of a product layer thickness of around 40 nm (the conversion associated with this layer thickness is referred to as $X_{K-D}$ in the study by Grasa et al.[41]). Equation 1 can be applied to predict the evolution of the CaO conversion with time under the chemically controlled regime, where $\Psi$ is the sorbent structural parameter and $\tau$ is the non-dimensional time.[41]

$$X = 1 - \exp\left(\frac{1 - \left(\frac{\tau}{2}\Psi + 1\right)^2}{\Psi}\right) \qquad \text{for } X \le X_{K-D} \tag{1}$$

Once the fast reaction stage has finished, from $X_{K-D}$ onward, the reaction can be modeled as combined control by the chemical reaction and diffusion but with the predominant control of diffusion phenomena through the product layer. These will be the phenomena that control the carbonation



dx.doi.org/10.1021/ef500331t | Energy Fuels 2014, 28, 4033−4042

reaction when the sorbent particles initiate a recarbonation reaction period, because they present a CaO conversion close to $X_{N,R}$ (see Figure 2). Equation 2 can be applied to predict the CaO carbonation conversion under this hypothesis of combined control until the sorbent reaches the conversion associated with the end of the fast recarbonation period, $X^{+}_{N,R}$ (see Figure 2).

$$X = X_{K-D} + \left(1 - \exp\left(\frac{1}{\Psi} - \frac{\left[\sqrt{1+\beta Z\tau} - \left(1 - \frac{\beta Z}{\Psi}\right)\right]^2 \Psi}{\beta^2 Z^2}\right)\right)$$

$$\text{for } X_{K-D} < X < X^{+}_{N,R} \quad (2)$$

Finally, a second dramatic decrease in the reaction rate appears on the experimental CaO conversion curves, once the sorbent reaches $X^{+}_{N,R}$. From this point onward, the conversion rate of CaO is very slow and the change in the mechanism that controls the carbonation reaction from combined control by the chemical reaction and diffusion to pure diffusional control might explain this decrease in the reaction rate. According to the experimental results, the evolution of the CaO conversion with time after $X^{+}_{N,R}$ is independent of the $CO_2$ partial pressure, which is consistent with a pure diffusion-controlled reaction regime.[33]

The previous experimental results and the mechanism proposed in the literature[36,40,41] indicate the importance of the experimental determination of the critical carbonate layer thickness on the free surfaces of CaO for establishing the transition between the different reaction regimes. For the new transition, when $X^{+}_{N,R}$ is reached and the reaction rate becomes negligible, the product layer thickness $h_D$ can be estimated as follows:

$$h_D = \frac{(X^{+}_{N,R} V^{M}_{CaCO_3} \rho_{CaO})}{S_{N,R} M_{CaO}} \quad (3)$$

where $S_{N,R}$ is the reaction surface at cycle $N$, calculated as the product of the reaction surface resulting from the calcination of the fresh limestone and the conversion at the end of the carbonation cycle after $N$ calcinations and $R$ recarbonations ($X_{N,R}$), $V^{M}_{CaCO_3}$ is the carbonate molar volume, $\rho_{CaO}$ is the CaO true density, and $M_{CaO}$ is the CaO molar weight. A consistent value of the $CaCO_3$ product layer thickness, $h_D$, of 70 nm has been estimated from the experimental data presented in Figures 2 and 4 for recarbonations carried out at 800 °C.

The sorbent kinetic parameters, i.e., the chemical reaction constant, $k_s$, and the effective product layer diffusion coefficient, $D$, were determined from the experimental CaO conversion curves with the aid of the RPM at different temperatures, as described in the study by Grasa et al.[41] Both parameters have been expressed in the form of Arrhenius expressions, and the values obtained for the pre-exponential factors ($k_{so}$ and $D_o$) and for the activation energies ($E_{aK}$ and $E_{aD}$) are presented in Table 1, together with the limestone textural and structural parameters that were measured experimentally.

**Table 1. Structural and Kinetic Parameters Resulting from the Calcination of the Fresh Limestone**

| structural parameters | | kinetic parameters | |
|---|---|---|---|
| $S$ ($m^2/m^3$) | $34.22 \times 10^6$ | $k_{so}$ ($m^4\ kmol^{-1}\ s^{-1}$) | $0.335 \times 10^{-5}$ |
| $L$ ($m/m^3$) | $2.94 \times 10^{14}$ | $E_{aK}$ (kJ/mol) | 21.3 |
| $\varepsilon$ | 0.37 | $D_o$ ($m^2/s$) | $3.37 \times 10^{-5}$ |
| $\Psi$ | 1.98 | $E_{aD}$ (kJ/mol) | 140 |

The activation energies obtained for both the chemical reaction kinetic constant and the diffusion coefficient through the product layer are in close agreement with the values reported in the literature for the carbonation reaction of cycled CaO particles from natural limestone. The chemical reaction shows a lower dependence upon the temperature, as indicated by the typically low values of $E_{aK}$.[33,41,42] In contrast, the diffusion coefficient shows a high dependence upon the temperature, as indicated by the high activation energies reported in the literature[33,34,41] and also found in this work. It should be noted that neither the pre-exponential factors nor the activation energies of the chemical reaction constant and the diffusion coefficient vary at any point along the conversion curves. Therefore, it must be the different reaction environments (in terms of the temperature and $CO_2$ partial pressure) that is responsible for the variation in the reaction rate and the final conversions achieved during the recarbonation period. The ability of the RPM to fit, with reasonable accuracy, such a wide variety of materials and operating conditions is a further validation of the general character of the model.

Figure 5 shows that the model proposed successfully fits the evolution of the CaO conversion with time under both carbonation and recarbonation conditions. As seen, the model predicts with sufficient accuracy the conversion curve of samples with a different $CO_2$ carrying capacity and also under different reaction conditions (in terms of the temperature and $CO_2$ partial pressure). However, to integrate the previous reaction rate expression in recarbonator reactor models using the system of Figure 1, a simplified kinetic expression is derived from the experimental conversion curves, taking into account the relative modest gains in conversion during recarbonation. By analogy with previous works on modeling the carbonator reactor,[41,46−49] the reaction rate during the recarbonation period is assumed to be constant from $X_{N,R}$ up to $X^{+}_{N,R}$. The CaO reaction surface available for the reaction in the recarbonator reactor ($S_{N,R,av}$) can then be expressed as

$$S_{N,R,av} = \frac{\Delta X_{R,max} \frac{\rho_{CaO}}{PM_{CaO}}}{(h_D - h_{max}) \frac{\rho_{CaCO_3}}{PM_{CaCO_3}}} \quad (4)$$

where $\Delta X_{R,max}$ is the maximum conversion achievable in the recarbonator reactor, $\rho_{CaO}$ and $\rho_{CaCO_3}$ are the densities of CaO and $CaCO_3$, respectively, $PM_{CaO}$ and $PM_{CaCO_3}$ are the molecular weights of CaO and $CaCO_3$, respectively, $h_{max}$ is the product layer thickness at the end of the fast reaction period in the carbonator (estimated as 40 nm according to the study by Grasa et al.[41]), and $h_D$ (70 nm according to the experimental results presented above) is the thickness of $CaCO_3$, which marks the end of the fast reaction stage in the recarbonator. In these conditions, the reaction rate can be expressed as

Energy & Fuels Article

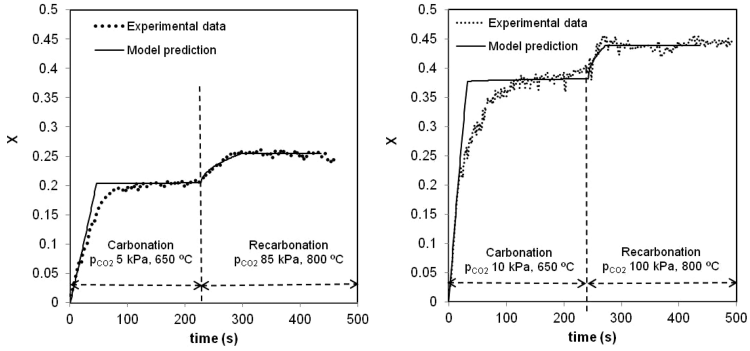


**Figure 5.** Comparison of the experimental data to the RPM predicted values using the parameters of Table 1. (Left) Carbonation was at 650 °C and 5 kPa $CO_2$ in air, and recarbonation was at 800 °C and 85 kPa $CO_2$ in air ($N$ = 17, and $R$ = 2). (Right) Carbonation was at 650 °C and 10 kPa $CO_2$ in air, and recarbonation was at 800 °C and 100 kPa $CO_2$ ($N$ = 7, and $R$ = 2).

**Table 2. Kinetic Parameters for the Recarbonation Reaction According to Equations 5 and 6 and Also the Values Obtained in the Presence of Steam**

| kinetic parameters according to eq 5 | | kinetic parameters according to eq 5 in the presence of steam | | kinetic parameters according to eq 6 | | kinetic parameters according to eq 6 in the presence of steam | |
|---|---|---|---|---|---|---|---|
| $k_{s0,R}$ ($m^4$ $kmol^{-1}$ $s^{-1}$) | $10.5 \times 10^3$ | $k_{s0,R}$ ($m^4$ $kmol^{-1}$ $s^{-1}$) | $14 \times 10^3$ | $k_{s0,R}$ ($s^{-1}$) | $28 \times 10^6$ | $k_{s0,R}$ ($s^{-1}$) | $40 \times 10^6$ |
| $E_{aR}$ (kJ/mol) | 230 | $E_{aR}$ (kJ/mol) | 230 | $E_{aR}$ (kJ/mol) | 200 | $E_{aR}$ (kJ/mol) | 200 |

$$\frac{dX}{dt} = k_{s,R} S_{N,R,av} (C_{CO_2} - C_{eq}) \qquad \text{for } X_{N,R} < X < X^{+}_{N,R} \tag{5}$$

This expression is a simplification of the grain model expression[46,50] successfully applied in previous works. The experimental values for $k_{s,R}$ obtained in the present work ranged from $3.5 \times 10^{-8}$ to $4.0 \times 10^{-9}$ $m^4$ $kmol^{-1}$ $s^{-1}$ for the series carried out at 800 and 700 °C, respectively, and at 85 kPa $CO_2$, from which the constant pre-exponential factor and the activation energy were derived (see Table 2). Also, by analogy with the approach adopted for the carbonator reactor models described in the literature,[7,46] the reaction rate expression can be represented as follows:

$$\frac{dX}{dt} = k_{s,R} X_{N,R} (\vartheta_{CO_2} - \vartheta_{eq}) \qquad \text{for } X_{N,R} < X < X^{+}_{N,R} \tag{6}$$

where $\vartheta_{CO_2}$ and $\vartheta_{eq}$ represent the $CO_2$ volume fraction in the gas phase and according to the equilibrium, respectively. According to this expression $k_{s,R}$ will be between 0.0044 $s^{-1}$ for the series carried out at 800 °C and 0.0005 $s^{-1}$ for the experiments conducted at 700 °C.

Table 2 also includes the kinetic parameters obtained from the experiments carried out in the presence of steam. As mentioned above, the presence of steam increases the conversion reaction rate, with the kinetic constant ranging according to eq 5 between $7.6 \times 10^{-8}$ $m^4$ $kmol^{-1}$ $s^{-1}$ at 800 °C and $5.6 \times 10^{-9}$ $m^4$ $kmol^{-1}$ $s^{-1}$ at 700 °C.

Finally, to gain a general overview of the impact of the recarbonation stage on the general $CO_2$ carrying capacity curves as a function of the number of carbonation−calcination cycles, several long duration series (75 cycles each) were conducted using three different recarbonation temperatures. Figure 6 shows the evolution of the $CO_2$ carrying capacity at the end of the fast carbonation period, $X_{N,R}$, against the number of calcination−carbonation cycles, $N$. For comparison, the figure includes the typical standard sorbent decay curve ($X_N$ versus $N$) obtained for the carbonation reaction at 650 °C and 5 kPa $CO_2$ for 5 min (series with bold symbols). The other two experimental series correspond to tests where the recarbonation step was carried out at 700 and 800 °C in pure $CO_2$ for 5 min. The experimental data were fitted to the typical expression from eq 7 of $X_N$ versus $N$,[29] and the derived parameters $k$ and $X_r$ that are compiled in Table 3 represent the deactivation constant and the residual capture capacity of the particles, respectively.

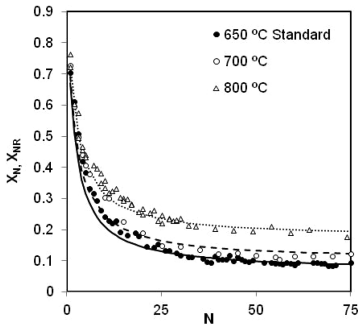


**Figure 6.** Evolution of $X_N$ (black dots) and $X_{N,R}$ (void symbols) versus the number of calcination cycles for two different temperatures of recarbonation. Carbonation was at 650 °C in all cases under 5 kPa $CO_2$; calcination was at 875 °C in air; and recarbonation was in pure $CO_2$ for 5 min after each carbonation.

$$X_N = \frac{1}{\left(\frac{1}{(1 - X_r)} + kN\right)} + X_r \tag{7}$$



dx.doi.org/10.1021/ef500331t | Energy Fuels 2014, 28, 4033−4042

Table 3. Sorbent Deactivation Parameters from the Expression $X_N$ versus $N$

| | $k$ | $X_r$ |
|---|---|---|
| 650 °C standard | 0.58 | 0.065 |
| recarbonated at 700 °C in pure $CO_2$ | 0.58 | 0.10 |
| recarbonated at 800 °C in pure $CO_2$ | 0.58 | 0.17 |

$X_r$ was selected as the only fitting parameter for the series at high temperatures and $CO_2$ partial pressures to help in the interpretation of results. The sorbent in the series at 650 °C displays values of $X_r$ that can be considered as the sorbent intrinsic deactivation parameters[31] and that are in close agreement with values reported in the literature for natural limestone and similar reaction conditions.[29] When a recarbonation stage is introduced into the experimental routine, the conversion under the diffusion-controlled regime makes a more important contribution to the total sorbent conversion. This is in agreement with the predictions of the model by Arias et al.[31] and with the experimental data widely reported in the literature.[18,21,27−29] This confirms that the addition of a recarbonation reaction stage after each calcination−carbonation cycle (see Figure 1) could help to counteract the deactivation of naturally derived CaO materials used in post-combustion $CO_2$ capture systems based on CaL.

## CONCLUSION

This work has experimentally confirmed that the introduction of a short (100−200 s) recarbonation stage on partially carbonated particles of CaO allows for the stabilization of sorbent carrying capacities at 0.15−0.20 molar conversion. High recarbonation temperatures (ideally between 750 and 800 °C), high partial pressures of $CO_2$ (over 60 kPa), and a certain presence of steam strongly favor the recarbonation reaction of CaO, reacting with $CO_2$ mainly in the slow diffusion reaction regime.

The RPM can be successfully adapted to multi-cycled particles to calculate the CaO molar conversion as a function of time and recarbonation conditions. The kinetic parameters needed to fit the recarbonation conversion curves are the same as those used to model the carbonation rates under normal carbonation conditions for the same sorbent ($k_{so}$, $0.335 \times 10^{-5}$ $m^4$ $kmol^{-1}$ $s^{-1}$; $E_{aK}$, 21.3 kJ/mol; $D_o$, $3.37 \times 10^{-5}$ $m^2/s$; and $E_{aD}$, 140 kJ/mol), which are also consistent with those published in previous works. This provides further validation of the RPM as being suitable for a much wider range of carbonation and recarbonation conditions. However, the modest recarbonation conversions achieved in each cycle also allow for the reaction to be modeled with simpler approaches with apparent reaction parameters that may be suitable for more general reactor models.

## AUTHOR INFORMATION

### Corresponding Author

*E-mail: gga@icb.csic.es.

### Notes

The authors declare no competing financial interest.

## ACKNOWLEDGMENTS

This work is supported by the European Programme of the Research Fund for Coal and Steel under RECaL Project RFCR-CT-2012-00008. Financial support for I. Martínez during her Ph.D. studies has been provided by the FPU Programme of the Spanish Ministry of Education (AP2009-3575). M. E. Diego acknowledges a fellowship grant under the CSIC JAE Programme, co-funded by the European Social Fund.

## NOMENCLATURE

$C_{CO_2,eq}$ = concentration of $CO_2$ ($kmol/m^3$) at equilibrium
$D$ = effective product layer diffusivity of $CO_2$ ($m^2/s$)
$D_o$ = pre-exponential factor of the effective diffusion coefficient ($m^2/s$)
$E_{aK}$, $E_{aD}$, and $E_{aR}$ = activation energy for the kinetic regime (K), activation energy for the combined diffusion and kinetic regime (D), and activation energy for the recarbonation reaction (R) in eqs 5 and 6 (kJ/mol)
$h_{K-D}$, $h_D$, and $h_{max}$ = critical product layer thickness (m) marking the transition between kinetic and diffusion reaction regimes (K−D), critical product layer thickness (m) marking the end of the diffusion regime (D), critical product layer thickness (m) marking the end of the fast reaction period in the carbonator (max)
$k$ = sorbent deactivation constant
$k_{s0,R}$ = pre-exponential factor for the recarbonation rate constant in eq 5 in $m^4$ $kmol^{-1}$ $s^{-1}$ or in $s^{-1}$ according to eq 6
$k_{s,R}$ = apparent kinetic constant of the recarbonation reaction in eq 5 in $m^4$ $kmol^{-1}$ $s^{-1}$ or in $s^{-1}$ according to eq 6
$k_{so}$ = pre-exponential factor for the reaction rate constant according to RPM ($m^4$ $kmol^{-1}$ $s^{-1}$)
$k_s$ = reaction rate constant for the surface reaction according to the RPM ($m^4$ $kmol^{-1}$ $s^{-1}$)
$L$ = total length of the pore system ($m/m^3$)
$M_{CaO}$ and $M_{CaCO_3}$ = molecular weight of CaO and molecular weight of $CaCO_3$ (kg/kmol)
$N$ = total number of calcination cycles
$R$ = number of calcination−carbonation−recarbonation cycles
$S$ = specific reaction surface ($m^2/m^3$)
$S_{N,R}$ = reaction surface for cycle $N$ after $R$ recarbonations ($m^2/m^3$)
$S_{N,R,av}$ = reaction surface available for recarbonation ($m^2/m^3$)
$t$ = time (s)
$V^M_{CaO}$ and $V^M_{CaCO_3}$ = molar volume of CaO and molar volume of $CaCO_3$ ($m^3$/kmol)
$X$ = CaO carbonate molar conversion
$X_N$ = $CO_2$ carrying capacity of CaO after $N$ calcination−carbonation cycles
$X_{N,R}$ = $CO_2$ carrying capacity of CaO after $N$ calcination−carbonation cycles that include $R$ cycles with a recarbonation stage after carbonation within the last cycle
$X^+_{N,R}$ = CaO carbonate molar conversion achieved at the end of the fast recarbonation period after $N$ calcination−carbonation and $R$ recarbonation cycles
$X_{K-D}$ = CaO carbonate molar conversion in the transition between kinetic and diffusion reaction regimes
$X_r$ = CaO carbonate molar conversion for very large cycle numbers $N$ or residual $CO_2$ carrying capacity of CaO
$Z$ = ratio of the volume of the product solid phase after reaction and before reaction

### Greek Letters

$\beta$ = parameter from the RPM that refers to the contribution of the chemical reaction and the $CO_2$ apparent diffusion coefficient through the product layer to the reaction rate
$\Delta X_R$ = increase in the CaO carbonate molar conversion attained because of recarbonation

$\Delta X_{R,max}$ = maximum increase in the CaO carbonate molar conversion attained during the fast recarbonation period
$\varepsilon$ = porosity
$\Psi$ = sorbent structural parameter from the RPM
$\rho_{CaO}$ and $\rho_{CaCO_3}$ = density of CaO and density of $CaCO_3$ ($kg/m^3$)
$\tau$ = parameter from the RPM referring to non-dimensional time
$\vartheta$ = volume fraction of $CO_2$

## REFERENCES


(1) Metz, B.; Davidson, O.; de Coninck, H.; Loos, M.; Meyer, L. *IPCC Special Report on Carbon Dioxide Capture and Storage. Prepared by Working Group III of the Intergovernmental Panel on Climate Change*; Cambridge University Press, New York, 2005; p 442.

(2) Shimizu, T.; Hirama, T.; Hosoda, H.; Kitano, K.; Inagaki, M.; Tejima, K. A twin fluid-bed reactor for removal of $CO_2$ from combustion processes. *Chem. Eng. Res. Des.* **1999**, *77* (1), 62−68.

(3) Abanades, J. C.; Anthony, E. J.; Lu, D. Y.; Salvador, C.; Alvarez, D. Capture of $CO_2$ from combustion gases in a fluidized bed of CaO. *AIChE J.* **2004**, *50* (7), 1614−1622.

(4) Alonso, M.; Rodríguez, N.; González, B.; Grasa, G.; Murillo, R.; Abanades, J. C. Carbon dioxide capture from combustion flue gases with a calcium oxide chemical loop. Experimental results and process development. *Int. J. Greenhouse Gas Control* **2010**, *4* (2), 167−173.

(5) Charitos, A.; Hawthorne, C.; Bidwe, A. R.; Sivalingam, S.; Schuster, A.; Spliethoff, H.; Scheffknecht, G. Parametric investigation of the calcium looping process for $CO_2$ capture in a 10 $kW_{th}$ dual fluidized bed. *Int. J. Greenhouse Gas Control* **2010**, *4* (5), 776−784.

(6) Rodríguez, N.; Alonso, M.; Abanades, J. C. Experimental investigation of a circulating fluidized-bed reactor to capture $CO_2$ with CaO. *AIChE J.* **2011**, *57* (5), 1356−1366.

(7) Charitos, A.; Rodríguez, N.; Hawthorne, C.; Alonso, M.; Zieba, M.; Arias, B.; Kopanakis, G.; Scheffknecht, G.; Abanades, J. C. Experimental validation of the calcium looping $CO_2$ capture process with two circulating fluidized bed carbonator reactors. *Ind. Eng. Chem. Res.* **2011**, *50* (16), 9685−9695.

(8) Galloy, A.; Bayrak, A.; Kremer, J.; Orth, M.; Plötz, S.; Wieczorek, M.; Zorbach, I.; Ströhle, J.; Epple, B. $CO_2$ capture in a 1 $MW_{th}$ fluidized bed reactor in batch mode operation. *Proceedings of the 5th International Conference on Clean Coal Technologies*; Zaragoza, Spain, May 9−12, 2011.

(9) Kremer, J.; Galloy, A.; Ströhle, J.; Epple, B. Continuous $CO_2$ capture in a 1 $MW_{th}$ carbonate looping pilot plant. *Chem. Eng. Technol.* **2013**, *36* (9), 1518−1524.

(10) Dieter, H.; Hawthorne, C.; Zieba, M.; Scheffknecht, G. Progress in calcium looping post combustion $CO_2$ capture: Successful pilot scale demonstration. *Energy Procedia* **2013**, *37*, 48−56.

(11) Sánchez-Biezma, A.; Ballesteros, J. C.; Diaz, L.; de Zárraga, E.; Álvarez, F. J.; López, J.; Arias, B.; Grasa, G.; Abanades, J. C. Postcombustion $CO_2$ capture with CaO. Status of the technology and next steps towards large scale demonstration. *Energy Procedia* **2011**, *4*, 852−859.

(12) Arias, B.; Diego, M. E.; Abanades, J. C.; Lorenzo, M.; Diaz, L.; Martínez, D.; Alvarez, J.; Sánchez-Biezma, A. Demonstration of steady state $CO_2$ capture in a 1.7 $MW_{th}$ calcium looping pilot. *Int. J. Greenhouse Gas Control* **2013**, *18*, 237−245.

(13) Martínez, I.; Murillo, R.; Grasa, G.; Carlos Abanades, J. Integration of a Ca looping system for $CO_2$ capture in existing power plants. *AIChE J.* **2011**, *57* (9), 2599−2607.

(14) Romano, M. Coal-fired power plant with calcium oxide carbonation for post-combustion $CO_2$ capture. *Energy Procedia* **2009**, *1*, 1099−1106.

(15) Romeo, L. M.; Abanades, J. C.; Escosa, J. M.; Paño, J.; Giménez, A.; Sánchez-Biezma, A.; Ballesteros, J. C. Oxyfuel carbonation/calcination cycle for low cost $CO_2$ capture in existing power plants. *Energy Convers. Manage.* **2008**, *49* (10), 2809−2814.

(16) Ströhle, J.; Lasheras, A.; Galloy, A.; Epple, B. Simulation of the carbonate looping process for post-combustion $CO_2$ capture from a coal-fired power plant. *Chem. Eng. Technol.* **2009**, *32* (3), 435−442.

(17) Curran, G. P.; Fink, C. E.; Gorin, E. Carbon dioxide-acceptor gasification process: Studies of acceptor properties. *Adv. Chem. Serv.* **1967**, *69*, 141−165.

(18) Barker, R. The reversibility of the reaction $CaCO_3 \rightleftarrows CaO + CO_2$. *J. Appl. Chem. Biotechnol.* **1973**, *23* (10), 733−742.

(19) Silaban, A.; Harrison, D. P. High-temperature capture of carbon dioxide: Characteristics of the reversible reaction between CaO(s) and $CO_2$(g). *Chem. Eng. Commun.* **1995**, *137*, 177−190.

(20) Abanades, J. C.; Alvarez, D. Conversion limits in the reaction of $CO_2$ with lime. *Energy Fuels* **2003**, *17* (2), 308−315.

(21) Abanades, J. C. The maximum capture efficiency of $CO_2$ using a carbonation/calcination cycle of $CaO/CaCO_3$. *Chem. Eng. J.* **2002**, *90* (3), 303−306.

(22) Abanades, J. C.; Rubin, E. S.; Anthony, E. J. Sorbent cost and performance in $CO_2$ capture systems. *Ind. Eng. Chem. Res.* **2004**, *43* (13), 3462−3466.

(23) Lisbona, P.; Martínez, A.; Lara, Y.; Romeo, L. M. Integration of carbonate $CO_2$ capture cycle and coal-fired power plants. A comparative study for different sorbents. *Energy Fuels* **2010**, *24* (1), 728−736.

(24) Anthony, E. J. Solid looping cycles: A new technology for coal conversion. *Ind. Eng. Chem. Res.* **2008**, *47* (6), 1747−1754.

(25) Blamey, J.; Anthony, E. J.; Wang, J.; Fennell, P. S. The calcium looping cycle for large-scale $CO_2$ capture. *Prog. Energy Combust. Sci.* **2010**, *36* (2), 260−279.

(26) Arias, B.; Grasa, G.; Alonso, M.; Abanades, J. C. Post-combustion calcium looping process with a highly stable sorbent activity by recarbonation. *Energy Environ. Sci.* **2012**, *5*, 7353−7359.

(27) Lysikov, I.; Salanov, N.; Okunev, G. Change of $CO_2$ carrying capacity of CaO in isothermal recarbonation−decomposition cycles. *Ind. Eng. Chem. Res.* **2007**, *46* (13), 4633−4638.

(28) Sun, P.; Lim, C. J.; Grace, J. R. Cyclic $CO_2$ capture by limestone-derived sorbent during prolonged calcination/carbonation cycling. *AIChE J.* **2008**, *54* (6), 1668−1677.

(29) Grasa, G. S.; Abanades, J. C. $CO_2$ capture capacity of CaO in long series of carbonation/calcination cycles. *Ind. Eng. Chem. Res.* **2006**, *45* (26), 8846−8851.

(30) Dennis, J. S.; Pacciani, R. The rate and extent of uptake of $CO_2$ by asynthetic, CaO-containing sorbent. *Chem. Eng. Sci.* **2009**, *64* (9), 2147−2157.

(31) Arias, B.; Abanades, J. C.; Grasa, G. S. An analysis of the effect of carbonation conditions on CaO deactivation curves. *Chem. Eng. J.* **2011**, *167* (1), 255−261.

(32) Salvador, C.; Lu, D.; Anthony, E. J.; Abanades, J. C. Enhancement of CaO for $CO_2$ capture in FBC environment. *Chem. Eng. J.* **2003**, *96*, 187−195.

(33) Bhatia, S. K.; Perlmutter, D. D. Effect of the product layer on the kinetics of the $CO_2$−lime reaction. *AIChE J.* **1983**, *29* (1), 79−86.

(34) Mess, D.; Sarofim, A. F.; Longwell, J. P. Product layer diffusion during the reaction of calcium oxide with carbon dioxide. *Energy Fuels* **1999**, *13* (5), 999−1005.

(35) Stanmore, B. R.; Gilot, P. Review—Calcination and carbonation of limestone during thermal cycling for $CO_2$ sequestration. *Fuel Process. Technol.* **2005**, *86*, 1707−1743.

(36) Bouquet, E.; Leyssens, G.; Schönnenbeck, C.; Gilot, P. The decrease of carbonation efficiency of CaO along calcination−carbonation cycles: Experiments and modelling. *Chem. Eng. Sci.* **2009**, *64* (9), 2136−2146.

(37) Stendardo, S.; Foscolo, P. U. Carbon dioxide capture with dolomite: A model for gas-solid reaction within the grains of a particulate sorbent. *Chem. Eng. Sci.* **2009**, *64* (10), 2343−2352.

(38) Liu, W.; Dennis, J. S.; Sultan, D. S.; Redfern, S. A. T.; Scott, S. A. An investigation of the kinetics of $CO_2$ uptake by a synthetic calcium based sorbent. *Chem. Eng. Sci.* **2012**, *69* (1), 644−658.

(39) Sun, P.; Grace, J. R.; Lim, C. J.; Anthony, E. J. A discrete-pore-size-distribution-based gas−solid model and its application to the reaction. *Chem. Eng. Sci.* **2008**, *63* (1), 57−70.
(40) Alvarez, D.; Abanades, J. C. Determination of the critical product layer thickness in the reaction of CaO with $CO_2$. *Ind. Eng. Chem. Res.* **2005**, *44* (15), 5608−5615.
(41) Grasa, G.; Murillo, R.; Alonso, M.; Abanades, J. C. Application of the random pore model to the carbonation cyclic reaction. *AIChE J.* **2009**, *55* (5), 1246−1255.
(42) Sun, P.; Grace, J. R.; Lim, C. J.; Anthony, E. J. Determination of intrinsic rate constants of the CaO−$CO_2$ reaction. *Chem. Eng. Sci.* **2008**, *63* (1), 47−56.
(43) Li, Z.; Fang, F.; Tang, X.; Cai, N. Effect of temperature on the carbonation reaction of CaO with $CO_2$. *Energy Fuels* **2012**, *26* (4), 2473−2482.
(44) Arias, B.; Grasa, G.; Abanades, J. C.; Manovic, V.; Anthony, E. J. The effect of steam on the fast carbonation reaction rates of CaO. *Ind. Eng. Chem. Res.* **2012**, *51* (5), 2478−2482.
(45) Manovic, V.; Anthony, E. J. Carbonation of CaO-based sorbents enhanced by steam addition. *Ind. Eng. Chem. Res.* **2010**, *49* (19), 9105−9110.
(46) Alonso, M.; Rodríguez, N.; Grasa, G.; Abanades, J. C. Modelling of a fluidized bed carbonator reactor to capture $CO_2$ from a combustion flue gas. *Chem. Eng. Sci.* **2009**, *64* (5), 883−891.
(47) Romano, M. C. Modeling the carbonator of a Ca-looping process for $CO_2$ capture from power plant flue gas. *Chem. Eng. Sci.* **2012**, *69* (1), 257−269.
(48) Lasheras, A.; Ströhle, J.; Galloy, A.; Epple, B. Carbonate looping process simulation using a 1D fluidized bed model for the carbonator. *Int. J. Greenhouse Gas Control* **2011**, *5* (4), 686−693.
(49) Ylätalo, J.; Ritvanen, J.; Arias, B.; Tynjälä, T.; Hyppänen, T. 1-Dimensional modelling and simulation of the calcium looping process. *Int. J. Greenhouse Gas Control* **2012**, *9*, 130−135.
(50) Grasa, G. S.; Abanades, J. C.; Alonso, M.; González, B. Reactivity of highly cycled particles of CaO in a carbonation/calcination loop. *Chem. Eng. J.* **2008**, *137* (3), 561−567.

### 4.3.4 Publicación VI

**Design of a Novel Fluidized Bed Reactor to Enhance Sorbent Performance in $CO_2$ Capture Systems Using CaO**

Publicado en:

*Industrial & Engineering Chemistry Research*

*Volumen* 53

Páginas 10059-10071

Año 2014

I&EC research
Industrial & Engineering Chemistry Research

Article

pubs.acs.org/IECR

# Design of a Novel Fluidized Bed Reactor To Enhance Sorbent Performance in $CO_2$ Capture Systems Using CaO

M. Elena Diego,*[†] Borja Arias,[†] Gemma Grasa,[‡] and J. Carlos Abanades[†]

[†]Instituto Nacional del Carbón (CSIC), Francisco Pintado Fe 26, 33011 Oviedo, Spain
[‡]Instituto de Carboquímica (CSIC), Miguel Luesma Castán 4, 50018 Zaragoza, Spain

**ABSTRACT:** This work deals with the modeling and design of a novel bubbling fluidized bed reactor that aims to improve the $CO_2$ carrying capacity of CaO particles in $CO_2$ capture systems by calcium looping (CaL). Inside the new reactor (the recarbonator) the particles that arrive from the carbonator of the CaL system react with a concentrated stream of $CO_2$, thereby increasing their carbonate content up to a certain value, which can be predicted by means of the model proposed. The recarbonator model presented in this work is based on the Kunii and Levenspiel model for bubbling bed reactors of fine particles. The reduction in the gas volume due to the reaction of $CO_2$ with CaO is taken into account by dividing the recarbonator into a number of reactor elements where the bubble properties are recalculated, whereas the solids are perfectly mixed throughout the bed. The model has been used to test the conceptual design of a CaL system that incorporates an additional recarbonator reactor to more than double the residual $CO_2$ carrying capacity of the sorbent (from 0.07 to 0.16). In a reference design case of a 1000 $MW_{th}$ coal-fired power plant it was found that the recarbonator cross section needs to be between 80 and 100 $m^2$ (about 40−50% the area of the carbonator reactor), the solid inventories around 1200−1500 $kg/m^2$, and the inlet $CO_2$ gas velocities between 0.6 and 0.9 m/s. This set of operating and design windows predicts an increase in the carbonate content of the particles in the recarbonator of around 0.02, which has been shown to be sufficient to sustain the increased average $CO_2$ carrying capacity of the sorbent.

## INTRODUCTION

$CO_2$ capture and storage (CCS) is one of the major options for contributing to the mitigation of climate change,[1] and several processes have been proposed in the past few years aimed at a less costly and more energy-efficient capture of $CO_2$. To this end, postcombustion calcium looping (CaL) stands out as a promising technology for $CO_2$ capture and is attracting increasing interest (see, for example, recent reviews[2,3]).

The CaL process relies on the use of lime as a $CO_2$ sorbent, which undergoes consecutive carbonation/calcination cycles. The pioneers of this process for combustion systems were Shimizu et al.,[4] who proposed a system of two fluidized beds (carbonator and calciner) and a method to regenerate the $CaCO_3$ in the calciner based on burning a fuel with pure $O_2$. The main process route today comprises two interconnected circulating fluidized bed (CFB) reactors, namely, the carbonator and the calciner (see Figure 1). The carbonator operates at temperatures of around 650 °C and contains active CaO particles, which react with the $CO_2$ of the flue gas entering this reactor. As a result, a $CO_2$-depleted gas leaves the carbonator and a partially carbonated stream of solids is transported to the calciner for regeneration. The calciner requires temperatures in the range of 880−950 °C to calcine not only the $CaCO_3$ from the carbonator but also the fresh limestone fed to the system to compensate for the decay of the $CO_2$ capture capacity of the lime with the number of carbonation/calcination cycles.[5,6] As mentioned above, the calcination reaction is endothermic, and heat is provided by burning coal in oxyfuel conditions inside the reactor. The calcined CaO solid stream is then transported back to the carbonator to initiate a new $CO_2$ capture cycle.

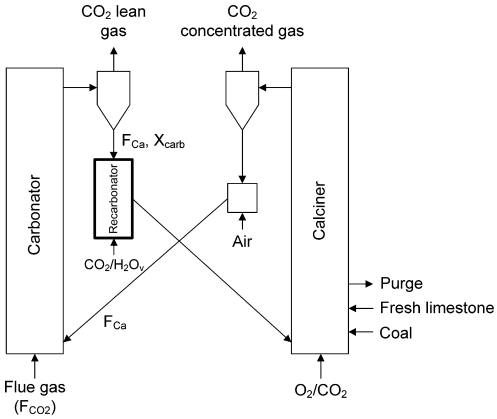


**Figure 1.** General scheme of a postcombustion calcium looping system that incorporates a bubbling fluidized bed recarbonator reactor to increase the $CO_2$ carrying capacity of the sorbent (CaO).

Provided that an adequate integration of all the heat sources is carried out, the CaL process is competitive and has a low overall energy penalty.[4,7−15] It has been possible to demonstrate the

**Received:** February 13, 2014
**Revised:** April 29, 2014
**Accepted:** May 22, 2014
**Published:** May 22, 2014





dx.doi.org/10.1021/ie500630p | *Ind. Eng. Chem. Res.* 2014, 53, 10059−10071

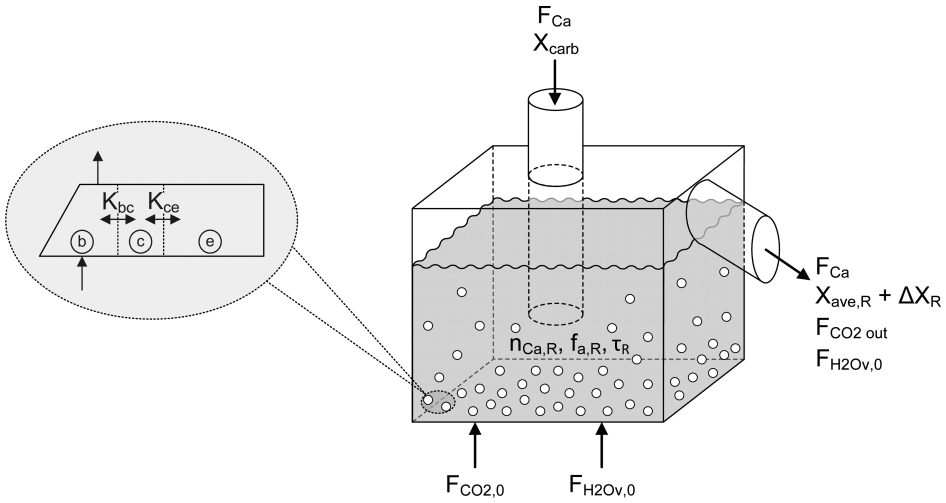


**Figure 2.** Scheme of the bubbling bed recarbonator with the main variables for reactor design. The bubble (b), cloud (c), and emulsion (e) regions are depicted on the left.

practical viability of the process at increasing scale in only a few years due to the close similarity of the reactors to those used in well-established circulating fluidized bed combustion technology. Several laboratory-scale experimental facilities contributed to validate the CaL concept,[16−20] and this has led to a rapid development of the process. Postcombustion CaL technology has reached the 1.7 $MW_{th}$ scale with a pilot plant in continuous operation in La Pereda, Spain.[21] Other pilots have also reported successful results in Germany (in Sttutgart (200 $kW_{th}$)[22] and Darmstadt (1 $MW_{th}$)[23]) or are being commissioned (a 1.9 $MW_{th}$ pilot in Taiwan[24]).

A critical aspect of the CaL system is, as mentioned above, the progressive deactivation experienced by the lime when it is subjected to consecutive cycles of carbonation and calcination.[5,6] Maintaining high $CO_2$ capture efficiencies while operating with low $CO_2$ sorbent carrying capacities requires an increase in the solid circulation rates between the reactors. This imposes high energy penalties on the process due to the rise in the heat requirements of the calciner.[25,26] Therefore, in the CaL process a continuous makeup flow of fresh limestone has to be fed in to stabilize the activity of the CaO particles at a sufficiently high value. Meanwhile, a continuous purge of solids leaves the system. The presence of a continuous makeup flow also imposes an energy penalty on the process, but this can be reduced if a synergy arrangement can be established with a cement manufacturer. Nonetheless, it is clear that it would be highly beneficial if the amount of fresh limestone required in the CaL process could be reduced. For this purpose, a number of modified sorbents and reactivation techniques are being studied.[3,27]

One of the first strategies proposed to increase the $CO_2$ carrying capacity of lime was the hydration of CaO particles,[28−31] which has been proven to be beneficial for the $CO_2$ capture capacity of the sorbent. Its main drawbacks are an increase in the tendency toward attrition due to the reduced mechanical stability of the hydrated lime and the energy penalty associated with the generation of large amounts of steam and low temperatures used in the hydration process (compared to those of the CaL system).[32] Sorbent doping is also a technique that is being studied as an alternative to increase the $CO_2$ carrying capacity of the CaO particles, but the results obtained so far are not conclusive.[27] The use of synthetic sorbents has also been proposed and recently reviewed by Kierzkowska et al.[27] The main concerns regarding these Ca-based sorbents are the limited availability of experimental results under operating conditions suitable for the CaL scheme and the economic impact that these sorbents may have on the process.[3,27,33] Finally, several authors have reported self-reactivation effects[34−39] during laboratory tests at large carbonation time scales or intense carbonation conditions. However, these effects are not expected to occur in postcombustion CaL applications because the intrinsic operating conditions do not allow such long solids residence times in the reactor or such carbonation conditions.[40]

This work focuses on a novel recarbonation process[41,42] that is also aimed at improving the $CO_2$ carrying capacity of the sorbent like the methods referred to in the previous paragraph. In this case, the reactivation concept is based on experimental evidence that extended carbonation times result in higher residual activities of lime.[34,43,44] In 1973, multicycle carbonation/calcination tests carried out by Barker[43] for carbonation times of 24 h in pure $CO_2$ revealed no significant decay in $CO_2$ carrying capacity (approximately 0.82 after 10 cycles). Further trials by Gottipati to reactivate spent sorbent for $SO_2$ capture using $CO_2$ failed to achieve the desired gains.[45] Nevertheless, more recent experiments focused on Ca looping systems under more moderate conditions than those of Barker[43](which are not suitable for large-scale continuous systems due to the long reaction times and carbonation conditions) have confirmed that prolonged carbonation times increase the residual activity of the CaO compared to experiments performed for short carbonation times.[34,44] High $CO_2$ partial pressures have also been shown to be beneficial for enhancing the reactivation of lime.[46]

In previous works[41,42] we proposed a variation of the CaL $CO_2$ capture system that incorporates a new recarbonator reactor

located between the carbonator and the calciner (see Figure 1). The recarbonator reactor, which is expected to operate at temperatures of between 750 and 850 °C, is fed with partially carbonated solids from the carbonator and a highly $CO_2$ concentrated gas stream. As a result, the particles are forced to increase their carbonate content beyond their maximum carrying capacity in the carbonator ($X_{ave,R}$) to a new higher value. In a stationary state, the resulting increase in the carbonate content in the recarbonator ($\Delta X_R$) with respect to $X_{ave,R}$ is enough to compensate for the subsequent decrease in the $CO_2$ carrying capacity the particles experience in the next calcination cycle. In these conditions, $X_{ave,R}$ retains the same value as at the exit of the carbonator. However, it is feasible in these conditions to stabilize the average maximum carrying capacity of the particles ($X_{ave,R}$) at values considerably higher than those reached in a classic CaL scheme without recarbonation ($X_{ave}$). In fact, it has been estimated from experimental measurements using thermogravimetric equipment that a $\Delta X_R$ as low as 0.02 may provide a residual activity of lime ($X_r$) equal to 0.16,[41,47] whereas the original $X_r$ without recarbonation is only between 0.07 and 0.10.

The purpose of this paper is to establish a first reactor design for the recarbonator reactor taking into account the typical operating conditions that can be expected in large-scale CaL systems and the information available on recarbonation kinetics and bubbling bed reactor gas−solid contact quality. Short solids residence times are likely to be needed in the recarbonator reactor to preserve reasonable dimensions, because a large solid circulation rate between the carbonator and the calciner reactors can always be expected if a high $CO_2$ capture efficiency is to be maintained. Therefore, a reactor model incorporating recent knowledge on the kinetics of the recarbonation reaction[40,41,47] together with well-established gas−solid contact reactor submodels[48] is needed to evaluate the extent of the impact of the recarbonator reactor in the scheme of Figure 1. This will contribute to the design of future pilots that will experimentally validate the improved $CO_2$ capture performance of the system studied in this work.

## RECARBONATOR REACTOR MODELING

A bubbling fluidized bed reactor configuration was chosen for the recarbonator, as schematically outlined in Figures 1 and 2. The recarbonator reactor is regarded as an enlarged fluidized bed loop-seal that receives solids from the carbonator cyclone (see Figure 2). This loop-seal is fluidized by the $CO_2$ that reacts in the recarbonator and/or steam to facilitate fluidization, as will be discussed below. The use of $CO_2$ needs to be minimized because it comes from recycled flue gas released from the calciner, so it is already clear that a substantial fraction of the flow of reacting gas ($CO_2$) will disappear from the gas phase into the solid phase. At the same time, it is important to guarantee that the recarbonator reactor is continuously fluidized. This is achieved by ensuring that there is at all times an excess of gas to remain above the conditions of minimum fluidization. This fluidizing gas must also allow the necessary circulation of solids through the standpipes and loop-seals of the existing CaL system, which is known to be very sensitive to the fluidization conditions in the reactors and the loop-seals[49] and to external control of the solid circulation rates between the reactors.[21]

For the sake of simplicity, the recarbonator reactor of Figure 2 is assumed to have a constant cross-sectional area and all of the $CO_2$ is injected through the bottom of the reactor (no secondary gas injections are considered). However, designs with a variable area to accommodate changes in the fluidizing gas flow rate due to the reaction of the $CO_2$ might be considered as feasible in the future. For the same reasons, a further design decision affects the type of fluidizing gas selected for the recarbonator. If $CO_2$ is the only gas fed to the reactor, the rapid depletion of $CO_2$ and associated defluidization will take place in situations when there is an excess of active CaO arriving in the recarbonator reactor (this defluidization phenomenon has already been reported to occur[50] in the loop-seal of an oxy-fired facility fluidized with pure $CO_2$). To prevent these situations from occurring and to facilitate a minimum flow of fluidizing gas, a certain flow of steam is fed to the recarbonator. The steam may also help to enhance the recarbonation reaction, as the positive effect of steam on the diffusionally controlled stage of the carbonation of CaO has been reported by several authors.[51,52] However, even when steam is used as an auxiliary fluidizing gas, a major fraction of the $CO_2$ fed through the bottom of the reactor ($F_{CO2,0}$) will disappear from the gas. This is schematically represented in Figure 2 and must be taken into account when modeling the gas−solid contact in the bubbling fluidized bed reactor.

To assess the effectiveness of the gas−solid contact in the recarbonator reactor, the model proposed by Kunii and Levenspiel (KL)[48] for bubbling beds of fine particles has been used in this work. The KL model postulates the existence of a bubble (b), cloud (c), and emulsion (e) phase (see Figure 2) and assumes spherical bubbles of a constant size, which rise faster than the gas that passes through the emulsion. Therefore, almost all of the gas moving through the bed of solids is located in the bubble phase, whereas the upflow of gas through the cloud and emulsion regions is small. The cloud and the emulsion are the dense regions and are considered to be at close to minimum fluidizing conditions. Besides, there are mass transfer phenomena between the bubble and the cloud and between the cloud and the emulsion, which can be quantified by means of the gas interchange rate coefficients defined by Kunii and Levenspiel ($K_{bc}$ and $K_{ce}$ respectively). The existence of these three separate regions introduces diffusion resistances to the progression of the recarbonation reaction.

In the model described in this work the recarbonation reaction has been limited to the cloud and the emulsion regions, where most of the solids are located. Therefore, the contribution of the bubble phase has been neglected. The mass balances of the three regions included within the bubbling bed reactor have been performed, using the notation in Figure 2. In the modeling of the gas phase, the reduction in the $CO_2$ flow rate along the height of the reactor is taken into account by dividing the reactor into a series of reactor elements in the axial direction, considering a plug flow pattern in the bubble phase. In each of these elements the change in the gas volume is moderate, and all bubble properties can be estimated as a constant value. With this procedure, the calculated outputs of each element (bubble density, bed porosity, gas and bubble velocities, molar flow, and molar fraction of $CO_2$) are the input parameters for the subsequent element. On the other hand, when modeling the solid phase, the assumption in the KL model of an instant and perfect mixing of solids is retained for the recarbonator reactor. Therefore, in any of the volume elements considered axially for the gas phase, the properties of the solids are identical and equal to the properties of the solids at the exit of the reactor.

If the axial bed height is divided into $Z$ volume elements, the formulation of the KL model requires the establishment of mass balances for the bubble, cloud, and emulsion regions depicted in Figure 2 for any element $i$ (between 1 and $Z$). This gives eqs 1, 2, and 3, respectively:

$$-u_{b,i}\frac{dC_{b,i}}{dz} = K_{bc}(C_{b,i} - C_{c,i}) \quad (1)$$

$$K_{bc}(C_{b,i} - C_{c,i}) = a_{1,i}\alpha_{c,i}(C_{c,i} - C_{eq}) + K_{ce}(C_{c,i} - C_{e,i}) \quad (2)$$

$$K_{ce}(C_{c,i} - C_{e,i}) = a_{1,i}\alpha_{e,i}(C_{e,i} - C_{eq}) \quad (3)$$

In these equations $u_{b,i}$ is the bubble rise velocity in the element $i$; $C_{b,i}$, $C_{c,i}$, and $C_{e,i}$ stand for the $CO_2$ molar concentrations in the bubble, cloud, and emulsion regions, respectively, of element $i$ in the recarbonator; and $C_{eq}$ is the $CO_2$ molar concentration at equilibrium conditions. $a_{1,i}$ is derived from the kinetics of the recarbonation reaction, which will be discussed below.

In addition, $\alpha_{c,i}$ and $\alpha_{e,i}$ represent the fractions of solids that are present in the cloud and the emulsion regions, respectively, for each element $i$. They can be calculated from the parameters $\gamma_c$ and $\gamma_{e,i}$ defined by Kunii and Levenspiel[48] as the volume of solids dispersed in the cloud and the emulsion regions, respectively, per volume of bubble:

$$\alpha_{c,i} = \frac{\gamma_c}{\gamma_c + \gamma_{e,i}} \quad (4)$$

$$\alpha_{e,i} = \frac{\gamma_{e,i}}{\gamma_c + \gamma_{e,i}} \quad (5)$$

The bubble fraction of the bed in element $i$, $\delta_i$, is required to obtain the $\gamma_{e,i}$ value.[48] The $\delta_i$ is calculated from the ratio between the superficial gas velocity and the velocity of the rising bubbles in the element when the minimum fluidization velocity is negligible with respect to the superficial gas velocity.[48] The velocity of the bubbles in a bubbling fluidized bed is a function of the superficial gas velocity, the minimum fluidization velocity, and the rise velocity of an isolated bubble and is here calculated for each element by means of the expressions proposed by Davidson and Harrison.[48,53] For this purpose, and for the sake of simplicity, the bubble diameter is assumed to be constant throughout the recarbonator, so that it is only the bubble fraction that diminishes along the reactor as $CO_2$ disappears from the gas phase to form $CaCO_3$.

It should also be noted that the porosity of the bed in every specific element $i$ can be calculated when $\delta_i$ is known. This porosity results from the sum of the bubble fraction and the porosity of the dense regions, which are assumed to be at close to minimum fluidizing conditions.[48] Finally, the gas interchange coefficients $K_{bc}$ and $K_{be}$ are calculated by means of the expressions given by Kunii and Levenspiel.[48] These coefficients depend on the velocity and porosity at minimum fluidizing conditions, the bubble diameter, and the molecular diffusion coefficient of the gas.

To extend the differential balances of eqs 1−3 to an overall reactor element, it is assumed that the gas in the bubble phase can be described by means of a plug flow model (PFR). By combining the previous expressions and the PFR equations of a system with a constant volume, the $CO_2$ concentration in the bubble phase can be obtained for each element $i$ as a function of the height along the element ($z_i$):

$$C_{b,i} = \frac{1}{1 - a_{2,i}}[((1 - a_{2,i})C_{b\,in,i} - a_{3,i})\, e^{-K_{bc}(1-a_{2,i})z_i/u_{b,i}} + a_{3,i}] \quad (6)$$

In the above equation $a_{2,i}$ and $a_{3,i}$ are constants in each volume element $i$. They result from the combination of several variables when the integral that leads to eq 6 is written and are given by eqs 7 and 8, respectively:

$$a_{2,i} = \frac{K_{bc}}{K_{bc} + a_{1,i}\alpha_{c,i} + \frac{K_{ce}a_{1,i}\alpha_{e,i}}{K_{ce} + a_{1,i}\alpha_{e,i}}} \quad (7)$$

$$a_{3,i} = \frac{a_{1,i}\alpha_{c,i}C_{eq} + \frac{K_{ce}a_{1,i}\alpha_{e,i}C_{eq}}{K_{ce} + a_{1,i}\alpha_{e,i}}}{K_{bc} + a_{1,i}\alpha_{c,i} + \frac{K_{ce}a_{1,i}\alpha_{e,i}}{K_{ce} + a_{1,i}\alpha_{e,i}}} \quad (8)$$

Additionally, the $CO_2$ concentration in the cloud and the emulsion regions of any reactor element $i$ can be obtained at any height by the expressions shown below, which are derived from combining eqs 2 and 3:

$$C_{c,i} = a_{2,i}C_{b,i} + a_{3,i} \quad (9)$$

$$C_{e,i} = \frac{K_{ce}}{K_{ce} + a_{1,i}\alpha_{e,i}}C_{c,i} + \frac{a_{1,i}\alpha_{e,i}C_{eq}}{K_{ce} + a_{1,i}\alpha_{e,i}} \quad (10)$$

Once the $CO_2$ concentration in the bubble phase at the exit of element $i$ is known, its gas conversion ($X_{CO2,i}$) can be calculated by means of eq 11 because the volume of gas remains virtually constant inside the reactor element:

$$X_{CO2,i} = \frac{C_{b\,in,i} - C_{b\,out,i}}{C_{b\,in,i}} \quad (11)$$

The value of $X_{CO2,i}$ obtained allows the moles of $CO_2$ that have reacted inside element $i$ to be calculated and, hence, the number of moles of $CO_2$ that leave element $i$ and enter element $i + 1$. This value is also used to estimate the new operating parameters that will be used for element $i + 1$, that is, the inlet concentration of $CO_2$, the bubble and gas velocities, the bubble density, and the bed porosity in this reactor element. Finally, the gas conversion attained inside the overall reactor due to recarbonation and calculated by means of the gas balance ($X_{CO2,GB}$) is

$$X_{CO2,GB} = \frac{F_{CO2\,in,1} - F_{CO2\,out,Z}}{F_{CO2\,in,1}} \quad (12)$$

where $F_{CO2\,out,Z}$ is the molar flow of $CO_2$ that leaves the recarbonator and $F_{CO2\,in,1}$ represents the $CO_2$ that enters the first reactor element.

In the previous eqs 2, 3, 7, 8, and 10 the term $a_{1,i}$ contains information relating to the kinetics of recarbonation at particle level. The investigation of the kinetics of the carbonation reaction has been the subject of many studies.[4,43,54−57] Nevertheless, very little quantitative information has been reported in relation to recarbonation conditions (very high partial pressures of $CO_2$ and temperatures over 750 °C) as these are unusual in carbonator reactors (partial pressures of $CO_2$ well below 0.1 atm and temperatures of around 650 °C). However, recent thermogravimetric studies by our group published elsewhere[47] have demonstrated that the kinetic parameters (pre-exponential factor and activation energy) derived for the carbonation conditions are still valid for the recarbonation conditions. A typical example of such an experiment, which represents a conversion versus time curve of a calcined sample subjected to carbonation and recarbonation, is presented in Figure 3.

Because the particles arriving at the carbonator are perfectly mixed and contain a wide distribution of particles with a different

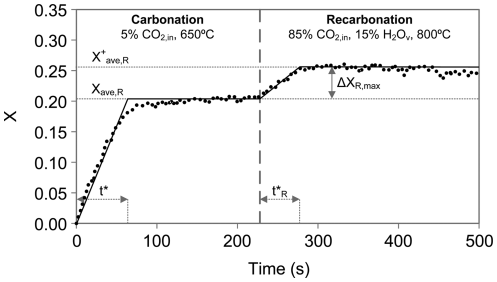


**Figure 3.** Example of a typical conversion versus time curve during carbonation and recarbonation stages.

cycle number, we have used the subscript "ave" to refer to the average particle properties, although in this particular example of Figure 3, these average properties correspond to 2 cycles of carbonation−recarbonation−calcination of a previously deactivated sorbent (after 15 standard carbonation−calcination cycles).[47] Furthermore, to distinguish from previous definitions of the $CO_2$ carrying capacity of the sorbent, we have referred to the average $CO_2$ carrying capacity of the particles arriving from the calciner to the carbonator in the system of Figure 1 as $X_{ave,R}$. Figure 3 indicates that in the carbonator reactor these particles are subjected to a carbonation step, during which they undergo a maximum carbonate conversion equal to $X_{ave,R}$ if they have a residence time in the carbonator longer than the characteristic time $t^*$. These particles carbonated to their maximum $CO_2$ carrying capacity are unable to react with $CO_2$ under carbonation conditions (see the negligible progress in conversion between 80 and 220 s in Figure 3). However, when they are subjected to the conditions in the recarbonator reactor (at 800 °C and 85%v $CO_2$ in steam in the example of Figure 3) a new reaction stage is initiated. As a result, the particles increase their carbonate content from $X_{ave,R}$ to a higher value, which can be represented as $X^+_{ave,R} = X_{ave,R} + \Delta X_{R,max}$, if the recarbonation is allowed to progress until $t^*_R$.

In a recent paper focused on the kinetics of these reactions, we observed[47] that the recarbonation process goes through a fast period where the reaction rate is constant from the onset of the recarbonation period at $X_{ave,R}$ until the solids reach a conversion of $X^+_{ave,R}$. Hereafter the reaction rate is zero. In these conditions and by analogy with the approach adopted for the carbonator reactor models described elsewhere,[20,58] the reaction rate in the recarbonator reactor is modeled using eqs 13a and 13b

$$\frac{dX}{dt} = k_{s,R} X_{ave,R} (\overline{\nu - \nu_{eq}}) \quad \text{for} \quad X_{ave,R} < X < X^+_{ave,R} \tag{13a}$$

$$\frac{dX}{dt} = 0 \quad \text{for} \quad X = X^+_{ave,R} \tag{13b}$$

where $k_{s,R}$ is the recarbonation reaction rate constant, $\nu$ is the volume fraction of $CO_2$ in the gas phase, and $\nu_{eq}$ is the volume fraction of $CO_2$ at equilibrium conditions.

The time required for the solids to attain maximum conversion after recarbonation ($X^+_{ave,R}$) in the reactor, $t^*_R$, can also be obtained from the maximum increase in the carbonate content of the particles within the recarbonator divided by the recarbonation reaction rate:

$$t^*_R = \frac{\Delta X_{R,max}}{dX/dt} \tag{14}$$

Furthermore, when using eq 13a to write the reaction term of the mass balances represented by eqs 2 and 3, the kinetic term $a_{1,i}$ can be derived as follows:

$$a_{1,i} = \frac{k_{s,R} X_{ave,R} \rho_s (1 - \varepsilon_i) f_{a,R} f_{Ca,R\,w}}{\delta_f \rho_{m,g} M_s} \tag{15}$$

where $\rho_s$ is the solids density, $\varepsilon_i$ is the bed porosity in the reactor element $i$, $f_{a,R}$ is the fraction of solids that are active for the recarbonation reaction, $f_{Ca,R\,w}$ is the mass fraction of calcium that is involved in the recarbonation process (the inerts are subtracted), $\rho_{m,g}$ is the molar density of the gas, and $M_s$ is the molecular weight of the calcium solids.

It must be pointed out here that Figure 3 and the choice of the kinetic constant $k_{s,R}$ for the recarbonation period are consistent with the experimental information available from TG tests reported elsewhere.[41,47] From the recent experiments carried out by Grasa et al.[47] the apparent kinetic constant for the recarbonation ($k_{s,R}$) is 0.004 $s^{-1}$ (vs $k_S$ = 0.33 $s^{-1}$ obtained for the carbonation reaction at 650 °C[20]), and this is the value used in this work for the simulation studies. It should be noted that this is a conservative $k_{s,R}$, because the presence of steam in the reaction atmosphere is known to lead to higher values of the kinetic constant as a result of the enhancement in the recarbonation reaction. As Figure 3 indicates, despite the kinetic constant during recarbonation being 2 orders of magnitude slower than the constant during fast carbonation, a substantial rate of recarbonation reaction can be achieved thanks to the increased $CO_2$ concentration in the recarbonator reactor. This is essentially the fundamental idea behind the proposed reactivation process, as particles are forced to regain a higher carbonation conversion (a synonym for $CO_2$ carrying capacity) as they go through the recarbonator reactor so that the subsequent loss in activity during the next calcination cycle allows higher levels of $CO_2$ carrying capacities to be sustained.[41,47]

Finally, in the KL model equations for the recarbonator reactor it is implicitly assumed (through the term $f_{a,R}$ in eq 15) that an average fraction of active solids exists in the solid phase within the bed, which is the only fraction of solids that reacts with the gas phase. Indeed, the fraction of particles that have been in the recarbonator for a period longer than $t^*_R$ have increased their carbonate content by $\Delta X_{R,max}$ and they are no longer able to react with $CO_2$ (see eq 13b). Only the fraction of particles that have remained in the reactor for a period shorter than $t^*_R$ is able to recarbonate, and it represents the active fraction of particles:

$$f_{a,R} = 1 - e^{-t^*_R/\tau_R} \tag{16}$$

This is an analogous procedure to that of the carbonator reactor described elsewhere.[58] It takes into account the ideal residence time distribution of the particles entering a well-mixed fluidized bed,[59] which has been proven to be successful for modeling laboratory-scale[19,20] and large-scale pilot data[21] of fluidized bed carbonator reactors. The mean residence time of the solids inside the recarbonator, $\tau_R$, can be obtained as the ratio between the number of Ca moles inside the recarbonator ($n_{Ca,R}$) and the flow of Ca moles ($F_{Ca}$):



dx.doi.org/10.1021/ie500630p | Ind. Eng. Chem. Res. 2014, 53, 10059−10071

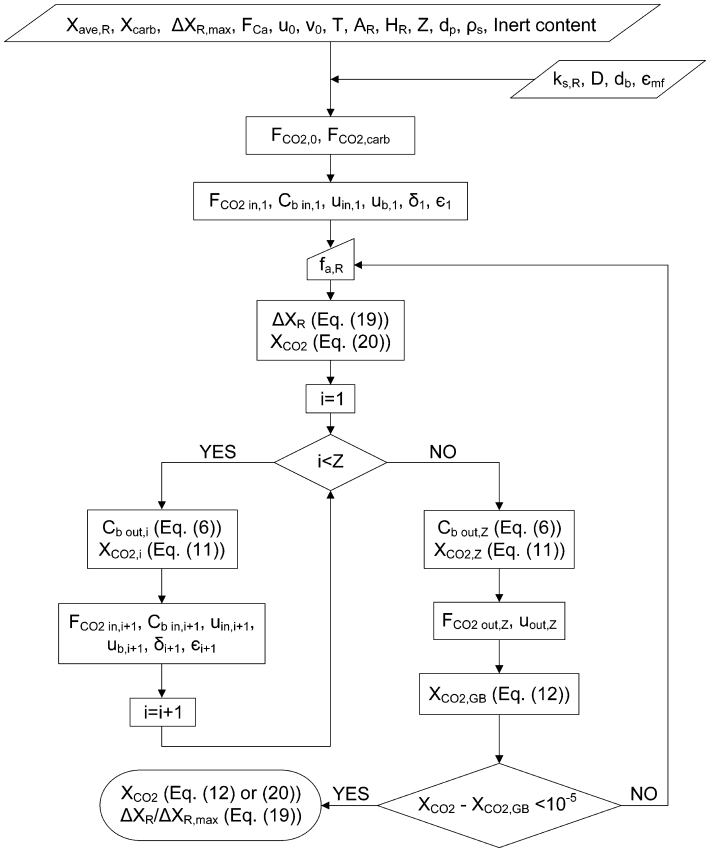


**Figure 4.** Scheme of the calculation procedure for the proposed model.

$$\tau_R = \frac{n_{Ca,R}}{F_{Ca}} \tag{17}$$

The calculation of the increase in calcium carbonate moles circulating between the carbonator and the calciner due to recarbonation ($F_{Ca}\Delta X_R$) requires the definition of the $\Delta X_R$ term, which is the average of the conversion achieved by the particles with a residence time below the threshold for achieving the maximum conversion and those that have reached the maximum conversion $X^+_{ave,R}$ (or the extra carbonation conversion $\Delta X_{R,max}$):

$$\Delta X_R = f_{a,R}\Delta X_{R,t<t^*_R} + (1 - f_{a,R})\Delta X_{R,t>t^*_R} \tag{18}$$

The two addends of the previous equation can be obtained by following the same procedure as that described by Alonso et al.[58] for a carbonator reactor, taking into account the residence time distribution of the particles inside perfectly mixed reactors. Rearrangement of these expressions leads to the carbonate conversion of the particles inside the recarbonator:

$$\Delta X_R = \Delta X_{R,max}\frac{\tau_R}{t^*_R}(1 - e^{-t^*_R/\tau_R}) = -\frac{\Delta X_{R,max} f_{a,R}}{\ln(1 - f_{a,R})} \tag{19}$$

The $CO_2$ mass balance then gives the following conversion in the gas phase:

$$X_{CO2} = \frac{F_{Ca}}{F_{CO2\ in,1}}\Delta X_R \tag{20}$$

On the other hand, the calculation of $t^*_R$ for each element (eq 14), requires the definition of the average $CO_2$ volume fraction in the reacting phases (cloud and emulsion) to obtain the value of $dX/dt$ (eq 13a). Because this is also changing in the $Z$ axial reactor elements adopted for the resolution of the model, it has to be estimated by taking into account these plug flow reactors for the gas while maintaining a perfect and instant mixing of solids throughout the bed. Thus

$$k\tau_i = \frac{\rho_{m,g}\nu_{b\ in,i}X_{CO2,i}}{(\overline{\nu_c} - \overline{\nu_{eq}})_i\alpha_{c,i} + (\overline{\nu_e} - \overline{\nu_{eq}})_i\alpha_{e,i}} \tag{21}$$

$$k\tau_i = \frac{\rho_{m,g}}{a_{4,i}}\ln\left(\frac{a_{4,i}C_{b\ in,i} + a_{5,i}}{a_{4,i}C_{b\ out,i} + a_{5,i}}\right) \tag{22}$$

where $\nu_{b\ in,i}$ is the $CO_2$ volume fraction in the bubble phase at the inlet of element $i$, $\nu_c$ and $\nu_e$ are the $CO_2$ volume fractions in the



dx.doi.org/10.1021/ie500630p | Ind. Eng. Chem. Res. 2014, 53, 10059−10071

cloud and the emulsion, respectively, and $a_{4,i}$ and $a_{5,i}$ are constants and can be calculated by means of expressions 23 and 24:

$$a_{4,i} = \alpha_{c,i}a_{2,i} + \frac{\alpha_{e,i}K_{ce}a_{2,i}}{K_{ce} + a_{1,i}\alpha_{e,i}} \quad (23)$$

$$a_{5,i} = \alpha_{c,i}a_{3,i} + \frac{\alpha_{e,i}K_{ce}a_{3,i} + a_{1,i}\alpha_{e,i}^2 C_{eq}}{K_{ce} + a_{1,i}\alpha_{e,i}} - C_{eq}(\alpha_{c,i} + \alpha_{e,i}) \quad (24)$$

Finally, the combination of eqs 21 and 22 gives the average of the difference between the $CO_2$ concentration in both the cloud and the emulsion regions and that at equilibrium conditions in a specific reactor element:

$$(\overline{\nu_c - \nu_{eq}})_i\alpha_{c,i} + (\overline{\nu_e - \nu_{eq}})_i\alpha_{e,i} = \frac{a_{4,i}\nu_{b\,in,i}X_{CO2,i}}{\ln\left(\frac{a_{4,i}C_{b\,in,i} + a_{5,i}}{a_{4,i}C_{b\,out,i} + a_{5,i}}\right)} \quad (25)$$

The solution of the model applied above allows the calculation of the gain in the carbonate conversion of the particles inside the recarbonator reactor, the efficiency of the reactor (taken to be the ratio between $\Delta X_R/\Delta X_{R,max}$), and the conversion of the gas ($X_{CO2}$). It should be noted that the carbonation conversion of the solids arriving at the reactor ($X_{carb}$) is not equal to $X_{ave,R}$ but slightly lower under the typical operating conditions of the carbonator. This means that particles arriving at the recarbonator first have to be carbonated up to $X_{ave,R}$ before the recarbonation process can take place. This carbonation process is assumed here to be virtually instantaneous, as the kinetic constant of the carbonation is much higher than that of the recarbonation reaction and the recarbonator is also operating at a high temperature and with a high concentration of $CO_2$.

As discussed by Arias et al.[41] the fraction of unconverted active CaO ($X_{ave,R} - X_{carb}$) arriving in the recarbonator has to be kept to a minimum because the carbonation of this CaO translates into a higher demand for $CO_2$ in the recarbonator (and a higher associated cost). However, this fraction of active CaO is beneficial in that it increases the temperature of the solids in the recarbonator reactor thanks to the exothermic carbonation reactions taking place in the atmosphere of concentrated $CO_2$. In this work we consider that the $CO_2$ available for the actual recarbonation of the particles is the $CO_2$ entering the reactor minus the $CO_2$ used for this instantaneous carbonation. Therefore, this is the gas flow that will be considered to be involved in the recarbonation process and that will be used to calculate the properties of the bed, such as the bubbles velocity and the bubble density in the reactor. This approach is supported by assuming that the particles inside the recarbonator are well mixed and the solids which are constantly arriving at the recarbonator at $X_{carb}$ are rapidly distributed throughout the reactor and react instantaneously to reach $X_{ave,R}$.

The recarbonator model is solved by following an iterative procedure (see Figure 4) that was programmed using Matlab. Once all of the inlet parameters of the model are fixed, the procedure begins with the calculation of the $CO_2$ used to carbonate the particles from $X_{carb}$ up to $X_{ave,R}$ ($F_{CO2,carb}$). Then, the $CO_2$ consumed in this process is subtracted from the total $CO_2$ fed to the reactor ($F_{CO2,0}$) and the inlet flows and parameters of the first reactor element are calculated, as outlined in Figure 4. Assuming a first tentative value of $f_{a,R}$, the conversion of the gas can be calculated by using the expressions obtained through the solids balance (eq 20) and the gas balance (eq 12).

To obtain the gas conversion from the gas balance, it is necessary to solve all of the $Z$ reactor elements of the recarbonator (100 volume elements have been used in the simulations), where the outlet parameters of an element $i$ are the inlet variables for the next element $i + 1$ while identical solid properties are maintained in all of the elements. Finally, the gas conversions given by eqs 20 and 12 are compared. If the difference between them is found to be less than the defined tolerance value, the iterative process based on $f_{a,R}$ ends, leading to the value of the conversion of the gas and the efficiency of the recarbonator. Nevertheless, if the difference is higher than the tolerance value, the process is repeated again using a new value of $f_{a,R}$ until a solution is found.

In this way, the model is able to calculate for a given set of reaction conditions (inlet gas concentration and reactor temperature), inlet mass and gas flows, and reference reactor volume, the average recarbonation conversion achieved by the solids at the exit of the reactor, and in turn the efficiency of the recarbonation reaction, the gas conversion, and the gas flow rates and compositions at the exit of the reactor. Consequently, the model can be used as a simulation tool to analyze the key design parameters of the reactor to achieve the targeted level of recarbonation efficiency.

## SIMULATION OF THE RECARBONATOR REACTOR

In the following paragraphs we report a design exercise to illustrate how to determine the volume of the recarbonator reactor, using the solution procedure described above for the reference set of operating conditions and model parameters compiled in Table 1. One of the problems in selecting the reference conditions for the reactor is that, as indicated in Figure 1, the recarbonator reactor is a part of a three-reactor CaL system, so that the input flows for the recarbonator reactor are the output flows of the carbonator reactor and the output flows in the recarbonator reactor also have an impact on the performance of the calciner and carbonator reactors. Therefore, for the sake of clarity in the present simulation exercise, we have chosen a set of boundary conditions and input flows for the recarbonator reactor that are considered constant and independent of the carbonator and calciner performances. The calciner is assumed to operate with 100% calcination efficiency with respect to the $CaCO_3$ flow entering the calciner, and the carbonator is assumed to operate

**Table 1. Input Parameters for the Recarbonator Model**

| ref operating variable | value |
|---|---|
| $X_{ave,R}$ | 0.20 |
| $X_{carb}$ | 0.17 |
| $\Delta X_{R,max}$ | 0.03 |
| $F_{Ca}$ (mol/s) | 10 000 |
| $F_{CO2,0}$ (mol/s) | 700 |
| $T$ (°C) | 800 |
| $\nu_0$ | 0.85 |
| $d_p$ ($\mu$m) | 100 |
| $\rho_s$(kg/m$^3$) | 2000 |
| inerts (%w) | 30 |
| **model parameter** | **value** |
| $k_{s,R}$ (s$^{-1}$) | 0.004 |
| $D$ (m$^2$/s) | $1.98 \times 10^{-4}$ |
| $d_b$ (m) | 0.05 |
| $\varepsilon_{mf}$ | 0.43 |
| $K_{bc}$ (s$^{-1}$) | 6.47 |
| $K_{ce}$ (s$^{-1}$) | 3.94 |



dx.doi.org/10.1021/ie500630p | Ind. Eng. Chem. Res. 2014, 53, 10059−10071

with 85% carbonation efficiency with respect to the flow of active CaO entering the carbonator. It is beyond the scope of this work to analyze in detail how these efficiencies can be obtained in practice. However, these can be considered reasonable assumptions in light of the experimental results obtained from pilots of different scale[16−23] and carbonator model predictions[12,20,21,58,60] for reactors operating with sufficient solid residence times and active flows of solids.

Also indicated in Table 1 is the fact that we are assuming an average carrying capacity of the solids entering the carbonator and recarbonator reactors of $X_{ave,R} = 0.20$. This level of activity is made possible in the system of Figure 1 by the combined effect of a certain limestone makeup flow to the calciner and the positive effect of the recarbonation conversion $\Delta X_R$ that will be achieved in the recarbonator reactor. In principle, we fix this value of $X_{ave,R} = 0.20$ in Table 1 as an input parameter, although it is at the same time a design target for the recarbonator reactor to reach this average $CO_2$ carrying capacity by minimizing the makeup flow of limestone to the calciner. This means that if the recarbonator reactor is ineffective, a large makeup flow of limestone will be required to reach the $CO_2$ carrying capacity of 0.20 adopted as a reference. In contrast, if the recarbonator reactor achieves a $\Delta X_R$ of around 0.02, it has been experimentally demonstrated[41,42,47] that a residual conversion of lime of 0.16−0.17 can be achieved. In that case a very small makeup flow of limestone will be required to achieve the targeted $X_{ave,R} = 0.20$. The addition of a small makeup flow of limestone will always be necessary to purge ashes and $CaSO_4$ and to maintain a reasonable buildup of inert materials in the system.[26] Earlier works describing the CaL system mass balances[57,60−63] provide detailed methods for quantifying the makeup flow requirements of limestone to sustain a certain level of average $CO_2$ carrying capacity as a function of the limestone deactivation parameters and the ash and sulfur present in the fuel burned in the calciner.

The input of solids into the reactor ($F_{Ca}$ in Figure 2) is assumed to be 10000 mol/s as a reference, and this solids stream is assumed to contain a typical 30% of inert material (ash and $CaSO_4$ as discussed by Diego et al.[26]). The carbonate conversion of this calcium flow to the recarbonator is $X_{carb} = 0.17$ (because of the 85% carbonation efficiency assumed in the carbonator). The resulting $CO_2$ capture rate in the carbonator of 1700 mol/s would correspond to the $CO_2$ captured from a power plant of about 1000 $MW_{th}$, equipped with a carbonator reactor of about 200 $m^2$ of cross-sectional area operating at around 5 m/s. These are all typical targets for large-scale carbonator reactors,[12,16−23,58,60] comparable in size to the commercial circulating fluidized bed combustors with a similar thermal input. The purpose of these assumptions about the carbonator dimensions is to be able to compare the dimensions of the new recarbonator reactor against large-scale reactors in "standard" calcium looping $CO_2$ capture systems. Additionally, the $\Delta X_{R,max}$ of the lime particles is taken to be 0.03, which is a conservative value according to the experimental data reported elsewhere.[41,47] The values assumed for $X_{ave,R}$ and $\Delta X_{R,max}$ lead to a maximum sorbent conversion at recarbonator outlet $X^+_{ave,R} = 0.23$.

Finally, the gas input to the recarbonator reactor is assumed to have 85%v of $CO_2$ and 15%v of steam, whereas the reaction temperature is taken to be 800 °C, because these operating conditions have been proven to be adequate for fast recarbonation kinetics.[47] The $CO_2$ molar flow rate to the recarbonator is set in the reference case at 700 mol/s, which leaves an excess molar flow of $CO_2$ for the recarbonation once the particles have been carbonated up to $X_{ave,R}$ (this process consumes 300 mol $CO_2$/s). For the KL model parameters, the particles are assumed to have an average size of 100 $\mu$m and a density of 2000 kg/$m^3$, which are typical values in CaL systems, and the bubble diameter is assumed to be 0.05 m. The recarbonation rate constant is taken as 0.004 $s^{-1}$ on the basis of the discussion in the previous section and the experimental data obtained by Grasa et al.[47]

Figure 5 presents a first set of model predictions for the reference case of Table 1, in which the efficiency of the recarbonator reactor (ratio $\Delta X_R/\Delta X_{R,max}$) is calculated as a function of the reactor volume. Four different curves have been generated for different expanded reactor heights (0.5, 1, 2, and 3 m). This means that, for a given reactor volume, four different cross sections of the reactor and gas velocities are plotted in the figure, because the total molar flow of gas has been fixed in the reference Table 1. Furthermore, in each of the curves of Figure 5, the changes in reactor volume translate into proportional changes in the cross-sectional area and superficial gas velocity. The specific conditions in each case (superficial gas velocity, gas conversion) result in a different bed porosity, which allows calculating the inventory of solids within the recarbonator for a given reactor geometry.

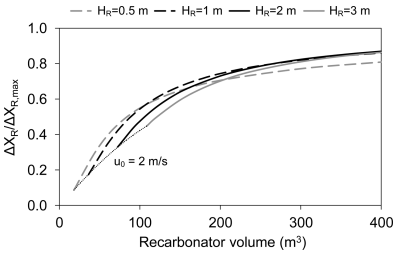


**Figure 5.** Efficiency of the recarbonator reactor ($\Delta X_R/\Delta X_{R,max}$) as a function of reactor volume, using different expanded reactor heights. Operating conditions were as in Table 1.

The figure shows the expected trend of an initial sharp increase in reactor efficiency as the volume of the reactor (and associated solids residence time, $\tau_R$) increases. For larger recarbonator volumes the increase in reactor efficiency is more moderate because the total consumption of $CO_2$ moles is high, so that the $CO_2$ molar concentration is closer to equilibrium and the solids conversion approaches its maximum ($\Delta X_{R,max} = 0.03$ as indicated in Table 1). When the four curves of Figure 5 are compared, it can be seen that shallower reactors are more efficient than deep beds for smaller reactor volumes, whereas the opposite happens at higher reactor volumes.

This trend can be explained on the basis of the two effects described next. When the superficial gas velocity is lower (this is the case of shallower reactors, because the inlet molar flow of gas is constant), the expansion of the bed is lower, so that for a given reactor volume, the mean residence time of the particles inside the recarbonator and, thus, the reactor efficiency are higher. This effect dominates on the left-hand side of Figure 5. Nevertheless, this expected trend is not repeated for large reactor volumes, as another effect controls the right-hand side of the figure. For a given height of the expanded bed, if the inlet molar flow of gas is constant, an increase in the recarbonator volume translates into a decrease in the superficial gas velocity. As a consequence, the solids tend to concentrate in the emulsion region rather than in

the cloud region (see the expressions for $\gamma_e$ and $\gamma_c$ in the KL model[48]). It is known that the diffusion of $CO_2$ to the emulsion phase suffers more hindrance, and this region tends to get closer to the $CO_2$ concentration of the equilibrium, as a result of which the recarbonation reaction rate is slowed down. This effect is more pronounced at lower gas velocities, that is, for higher reactor volumes and shallower recarbonator reactors, and it explains the change in the tendency observed in Figure 5. A limit has been marked in Figure 5, which is represented by the dotted line on the left-hand side of the figure corresponding to a maximum fluidizing velocity of 2 m/s. The lower velocity limit is imposed by the minimum fluidization velocity, $u_{mf}$. However, this is not shown in Figure 5 because none of the cases represented in this figure lead to velocities below $u_{mf}$.

These results seem to indicate that a target of very high recarbonator efficiencies (ratios $\Delta X_R/\Delta X_{R,max} > 0.9$) may not be realistic because they would entail very large reactor volumes and/or very large cross sections. For comparison purposes the cross section of the carbonator and calciner in Figure 1 for this reference case will be of the order of 200 $m^2$ (which is in turn comparable to the cross section of a circulating fluidized bed combustor in a power plant of 1000 $MW_{th}$, used as a reference for the data in Table 1). The $\Delta X_R$ targeted in the recarbonator is 0.02 ($\Delta X_R/\Delta X_{R,max}$ = 0.66), as was explained above. Therefore, reactor volumes of around 150−200 $m^3$ would be required depending on the expanded bed height. It is necessary to reach a compromise between sufficiently high reactor efficiencies during recarbonation and reasonable recarbonator dimensions. For this purpose, a recarbonator with a cross section of between 80 and 100 $m^2$ (approximately 40 or 50%, respectively, of that of the carbonator) and 2 m of expanded bed height has been selected as a reasonable trade-off.

The effect of the superficial gas velocity at the entrance to the recarbonator reactor for a given set of reactor dimensions (100 $m^2$ of cross section and 2 m of expanded bed height as chosen above) is represented in Figure 6, for two operating temperatures

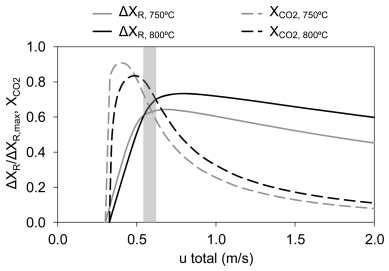


**Figure 6.** Efficiency of the recarbonator reactor ($\Delta X_R/\Delta X_{R,max}$) and gas conversion ($X_{CO2}$) as a function of the total inlet gas velocity at two operating temperatures (750 and 800 °C) for a recarbonator of 100 $m^2$ and 2 m of expanded bed height. Solid flows and gas characteristics were as in Table 1.

(750 and 800 °C). In this case, the flow of solids entering the reactor is retained as in Table 1, but the gas flow rate is allowed to change, as indicated by the gas velocity at the entrance to the reactor. At very low gas velocities, the efficiency of the reactor deteriorates very rapidly in this example because the limiting factor hindering the reaction is the lack of $CO_2$ to sustain the fast carbonation stage (between $X_{carb}$ and $X_{ave,R}$) and the recarbonation. In actual fact, the efficiency is zero if the inlet $CO_2$ molar flow is allowed to be exactly that required for instantaneous carbonation up to $X_{ave,R}$ plus the $CO_2$ associated with the equilibrium (gas velocity of around 0.3 m/s in Figure 6). The efficiency of the reactor reaches a maximum at around $u_0$ = 0.8 m/s (800 °C) and $u_0$ = 0.7 m/s (750 °C) (equivalent to $F_{CO2,0}$ = 770 mol/s and $F_{CO2,0}$ = 700 mol/s, respectively) and then drops slightly as the excess $CO_2$ fed to the recarbonator expands the bubbling bed (leading to a reduction in the residence time of the solids as discussed above) without increasing the solids conversions. The excess $CO_2$ at the inlet also causes a drop in $CO_2$ conversion, $X_{CO2}$, calculated with eq 12 or 20 and also represented in Figure 6.

The efficiency in the conversion of $CO_2$ in the recarbonator reactor, $X_{CO2}$, needs to be maximized because this is a recycle flow that is obtained from the gas stream that leaves the calciner of Figure 1. However, the gas flow of $CO_2$ entering the recarbonator must be kept sufficiently high to maintain the high partial pressure of $CO_2$ required for fast recarbonation and the intense fluidizing conditions so that it can serve as a loop-seal between the carbonator and calciner reactors. The shaded area in Figure 6 represents a reasonable compromise between a recarbonator efficiency of 0.60−0.70 ($\Delta X_R$ of around 0.02) and a $X_{CO2}$ value of no less than 0.70 for an operating temperature in the recarbonator of 800 °C. The results show that an inlet gas velocity of around 0.6 m/s is enough to attain the targeted $\Delta X_R$ of 0.02 while maintaining at the same time a sufficiently high gas conversion (73%). This results in a mean residence time of the particles inside the recarbonator reactor of 167 s and a $CO_2$ molar flow of 251 mol/s available for recarbonation (after the particles have attained $X_{ave,R}$ and after the subtraction of the $CO_2$ moles associated with the equilibrium). At the temperature of operation chosen as a reference in Table 1 (800 °C), a minimum of 315 mol $CO_2$/s needs to be fed into the reactor to compensate for the total molar flow of $CO_2$ consumed in the reaction up to $X_{ave,R}$ plus the flow of $CO_2$ related to the equilibrium ($\nu_{CO2,eq}$ = 0.217)). If the recarbonator cross section were 80 or 90 $m^2$, an inlet gas velocity of 0.9 and 0.7 m/s would be required, respectively, instead of 0.6 m/s, and the gas conversions would be lower (50 and 66%, respectively). On the other hand, the less favorable kinetics at 750 °C[47] leads to lower reactor efficiencies in this particular example and for this particular set of kinetic parameters ($k_{s,R}$ is taken to be 0.002 $s^{-1}$ at 750 °C).

It should be highlighted that the total values of $CO_2$ consumption are only a small fraction (<10%) of the $CO_2$ generated in the calciner, which typically has a thermal input comparable to the power plant feeding flue gases to the carbonator of Figure 1[4,7−9,11,13,25] and therefore generates flows of $CO_2$ that are 1 order of magnitude higher. As for the steam requirements, they do not entail any additional penalty to the process because the recarbonator is directly fed using the gas stream that exits the calciner (prior to the condensation and purification step), which provides sufficient steam for recarbonation.

The previous design examples confirm that there are sufficiently wide design and operating windows to build and operate a recarbonator reactor aimed at the desired targets of sorbent recarbonation. There are, however, still a number of uncertainties to be addressed, but these will be overcome as more data are obtained from the pilot testing campaigns in the 1.7 $MW_{th}$ pilot of La Pereda.[21] One such uncertainty is the extent of the impact of the recarbonator reactor temperature on the recarbonation conversions. The temperature chosen in this work

as a reference (800 °C) is necessary to provide sufficiently fast recarbonation rates and reasonable recarbonator dimensions as pointed out above. However, this temperature is difficult to reach in practice when the inlet temperature of the solids from the carbonator is 650 °C and only around 5 net points of exothermic carbonation conversion (from $X_{carb} = 0.17$ to $X_{ave,R} + \Delta X_R = 0.22$) are available for reaction during recarbonation. An adiabatic heat balance to the reactor reveals that a temperature increase of only about 60−70 °C can be expected in the recarbonator in these conditions. If recarbonation were ineffective at a temperature between 700 and 750 °C because of the unfavorable kinetics,[47] an additional means of increasing the temperature in the recarbonator reactor would be needed, such as an increase in the temperature of the carbonator (up to 700 °C the carbonator efficiency is still >80% for typical coal flue gases), a parallel oxyfuel combustion of a small flow of fuel and $O_2$ fed to the recarbonator, or the preheating of the carbonated solids leaving the carbonator using a high-temperature flue gas.[64] The energy penalty associated with these processes in the overall system would be minimum, as all the heat provided in the recarbonator to increase the temperature of the solids would lead to a proportional decrease in the heat requirements in the calciner. In fact, the recarbonation process should not entail a noticeable increase in the energy requirements of the calciner in the CaL system. This is because the additional heat demand in the calciner associated with the calcination of a solids stream with a higher carbonate content would be compensated for by the higher temperature of the solids arriving at the calciner of Figure 1 from the recarbonator.

A sensitivity analysis has been carried out to investigate the impact of the main model parameters on the calculated efficiency, $\Delta X_R/\Delta X_{R,max}$. Figure 7 depicts the influence that $d_b$, $K_{bc}$, $K_{ce}$, $\gamma_c$, and $k_{s,R}$ have on the efficiency of the recarbonator when these parameters are altered between 50 and 150% with respect to the central values shown in Table 1. The solid flow and the gas properties correspond to those of Table 1, whereas the geometry of the recarbonator has been fixed at 100 $m^2$ and 2 m of expanded bed height and the inlet gas velocity at 0.6 m/s.

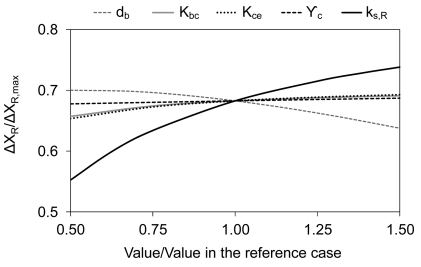


**Figure 7.** Sensitivity analysis of the effect of $d_b$, $K_{bc}$, $K_{ce}$, $\gamma_c$, and $k_{s,R}$ on recarbonation efficiency. Solid and gas properties were as in Table 1. The inlet gas velocity is 0.6 m/s.

As can be seen in Figure 7, the bubble size has only a slight influence on the recarbonator efficiency. It is known that when the bubble size decreases, $CO_2$ transfer from the bubble to the cloud and subsequently to the emulsion is favored. However, the bed porosity also increases, and this translates into a reduction of the mean residence time of the particles inside the recarbonator. Nonetheless, these two effects compensate each other in the recarbonator reactor under these operating conditions, resulting in a virtually unchanged recarbonator efficiency (see Figure 7). It is important to note that the opposite happens when the bubble diameter increases. If the recarbonator efficiency were affected by an increase in the bubble size along the reactor, internals or some other device could be installed to reduce the size of the bubbles and boost the mass transfer of $CO_2$ to the emulsion phase. The effect of the interchange rate coefficients $K_{bc}$ and $K_{ce}$ has also been studied. It should be noted that these parameters are influenced by the bubble diameter, so that they have implicitly changed with $d_b$, but in that case the mean residence time has also altered due to changes in the bed porosity. When only $K_{bc}$ and $K_{ce}$ vary ($\tau_R$ remains virtually constant), it can be observed that the recarbonator efficiency is hardly affected. The same happens when $\gamma_c$ takes values ranging from 50 to 150% of that of the reference case: there is only a negligible effect on the efficiency of the recarbonator. The influence of $\gamma_e$ has not been considered in this study because it depends on the bed porosity, which changes in each case. Besides, it is directly related to $\gamma_c$, so that a change in $\gamma_c$ also produces a change in $\gamma_e$.

Finally, the kinetic constant is the parameter that most influences the recarbonator performance, although its effect is also limited. As expected, higher values of $k_{s,R}$ result in higher recarbonation efficiencies. However, as the final solids conversion is also affected by the equilibrium, the available molar flow of $CO_2$ for recarbonation, and the mean solids residence time inside the recarbonator, the efficiency increase is limited. Nevertheless, the $\Delta X_R/\Delta X_{R,max}$ ratio diminishes more sharply for the lowest values of $k_{s,R}$, as can be seen from Figure 7.

The results presented in Figures 5−7 indicate that there are reasonable design and operating windows for the recarbonator reactor to achieve the desired targets of increased carbonation conversion. More importantly, this increase in conversion could allow the process to proceed with a significantly lower makeup flow for a specific target of average $CO_2$ carrying capacity and $CO_2$ capture efficiency and lead to a reduction in the operational costs associated with CaL technology. Work is in progress to retrofit the La Pereda 1.7 $MW_{th}$ pilot[21] with a recarbonator reactor to experimentally test this process variant of the postcombustion calcium looping system and exploit its advantages. The reactor model described in this paper will serve as a tool for interpreting and scaling up results obtained from the pilot.

## CONCLUSIONS

A mathematical model of a fluidized bed recarbonator reactor, the aim of which is to increase the average $CO_2$ carrying capacity of the sorbent in a calcium looping $CO_2$ capture system, can be solved by integrating into the KL model the kinetic information available for the carbonation and the recarbonation reactions. The simulations of a large-scale system have identified reasonable operating windows where adequate recarbonation conversions (of the order of a 0.02 net increase in CaO conversion to $CaCO_3$) can be achieved and, hence, average $CO_2$ carrying capacities close to 0.20 can be sustained. The solution of the recarbonator model indicates that average residence times from 100 to 170 s are sufficient for this purpose. An expanded bed height of 2 m, a cross-sectional area of between 80 and 100 $m^2$, and an inlet gas velocity ranging from 0.6 and 0.9 m/s are required. These dimensions and conditions could be achieved with the loop-seals used to connect the carbonator and calciner reactors in the calcium looping system.

A sensitivity analysis reveals that changes of ±50% with respect to the reference case in intrinsic model parameters such as the

interchange rate coefficients ($K_{bc}$ and $K_{ce}$) and the volume of solids in the cloud region divided by the volume of bubbles ($\gamma_c$) would hardly affect the final recarbonation conversion. It was also found that the bubble diameter has only a slight effect on the recarbonator efficiency within a range of moderate values, whereas the kinetic constant ($k_{s,R}$) stands out as the most influential parameter of the model, although the effect of this parameter is also restricted given the limited variation observed in recarbonation kinetic experiments. In fact, it is calculated that the recarbonator efficiency diminishes by 19% and increases by 8% when compared to that of the reference case for $k_{s,R}$ values of 0.002 and 0.006 $s^{-1}$ respectively, which correspond to variations of 50 and 150% with respect to the reference $k_{s,R}$.

The model presented in this study is useful for the prediction and interpretation of the performance of a recarbonator, and it can be used as a tool for the design of recarbonator reactors in future calcium looping systems for $CO_2$ capture.

## AUTHOR INFORMATION


### Corresponding Author

*(M.E.D.) E-mail: marlen@incar.csic.es. Tel:+34 985 11 90 90. Fax: +34 985 29 76 62.


### Notes

The authors declare no competing financial interest.

## ACKNOWLEDGMENTS

The financial support provided by the European Community's Research Fund for Coal and Steel under the ReCaL project (RFCR-CT-2012-00008) is acknowledged. M.E.D. acknowledges the award of a fellowship grant under the CSIC JAE Program, cofunded by the European Social Fund.

## NOMENCLATURE

$A_R$ = cross-sectional area of the recarbonator ($m^2$)
$a_{1,i}$ = parameter of the recarbonator element $i$ ($s^{-1}$)
$a_{2,i}$ = parameter of the recarbonator element $i$
$a_{3,i}$ = parameter of the recarbonator element $i$ ($mol/m^3$)
$a_{4,i}$ = parameter of the recarbonator element $i$
$a_{5,i}$ = parameter of the recarbonator element $i$ ($mol/m^3$)
$C_{b,i}$ = $CO_2$ molar concentration in the bubble phase of the recarbonator element $i$ ($mol/m^3$)
$C_{b\ in,i}$ = $CO_2$ molar concentration in the bubble phase at the inlet of the recarbonator element $i$ ($mol/m^3$)
$C_{b\ out,i}$ = $CO_2$ molar concentration in the bubble phase at the outlet of the recarbonator element $i$ ($mol/m^3$)
$C_{c,i}$ = $CO_2$ molar concentration in the cloud phase of the recarbonator element $i$ ($mol/m^3$)
$C_{e,i}$ = $CO_2$ molar concentration in the emulsion phase of the recarbonator element $i$ ($mol/m^3$)
$C_{eq}$ = $CO_2$ molar concentration at equilibrium conditions ($mol/m^3$)
$D$ = molecular diffusion coefficient of the gas ($m^2/s$)
$d_b$ = bubble diameter (m)
$d_p$ = mean particle diameter (m)
$F_{Ca}$ = molar flow of Ca moles between reactors (mol/s)
$F_{CO2,0}$ = total molar flow of $CO_2$ fed to the recarbonator reactor (mol/s)
$F_{CO2,carb}$ = molar flow of $CO_2$ consumed for the carbonation reaction up to $X_{ave,R}$ inside the recarbonator (mol/s)
$F_{CO2\ in,i}$ = molar flow of $CO_2$ that enters the recarbonator element $i$ (mol/s)
$F_{CO2\ out,i}$ = molar flow of $CO_2$ that leaves the recarbonator element $i$ (mol/s)
$f_{a,R}$ = active fraction of particles inside the recarbonator
$f_{Ca\ R,w}$ = mass fraction of calcium involved in the recarbonation reaction
$H_R$ = height of the recarbonator reactor (m)
$K_{bc}$ = gas interchange coefficient between the bubble and the cloud regions ($s^{-1}$)
$K_{ce}$ = gas interchange coefficient between the cloud and the emulsion regions ($s^{-1}$)
$k_{s,R}$ = apparent kinetic constant for the recarbonation reaction ($s^{-1}$)
$M_s$ = molecular weight of the Ca solids (kg/mol)
$n_{Ca,R}$ = number of calcium moles inside the recarbonator (mol)
$T$ = temperature (°C)
$t^*$ = characteristic time of the carbonation reaction after which the reaction rate is zero (s)
$t^*_R$ = characteristic time of the recarbonation reaction after which the reaction rate is zero (s)
$u_{b,i}$ = bubble velocity in the recarbonator element $i$ (m/s)
$u_{in,i}$ = gas velocity at the inlet of the recarbonator element $i$ (m/s)
$u_{out,i}$ = gas velocity at the outlet of the recarbonator element $i$ (m/s)
$u_0$ = total inlet gas velocity to the recarbonator (m/s)
$X$ = CaO carbonate molar conversion
$X_{ave}$ = average CaO carbonate molar conversion achieved at the end of the fast carbonation period
$X_{ave,R}$ = average CaO carbonate molar conversion achieved at the end of the fast carbonation period in the presence of a recarbonator reactor
$X_{ave,R}^+$ = average CaO carbonate molar conversion achieved at the end of the fast recarbonation period
$X_{carb}$ = CaO carbonate molar conversion at the exit of the carbonator
$X_{CO2}$ = $CO_2$ gas conversion
$X_{CO2,i}$ = $CO_2$ gas conversion inside the recarbonator element $i$
$X_{CO2,GB}$ = $CO_2$ gas conversion calculated by means of the gas balance
$X_r$ = residual conversion of the particles
$Z$ = number of elements into which the recarbonator reactor is divided for the calculations
$z_i$ = height at the recarbonator element $i$ (m)

### Greek symbols

$\alpha_{c,i}$ = fraction of solids present in the cloud region of the recarbonator element $i$
$\alpha_{e,i}$ = fraction of solids present in the emulsion region of the recarbonator element $i$
$\Delta X_R$ = increase in the CaO carbonate molar conversion due to recarbonation
$\Delta X_{R,max}$ = maximum increase in the CaO carbonate molar conversion of the particles due to recarbonation if allowed to progress to the end of the fast recarbonation period
$\delta_i$ = bubble density in the recarbonator element $i$
$\varepsilon_i$ = bed porosity of the recarbonator element $i$
$\gamma_c$ = volume of solids dispersed in the cloud region per volume of bubbles
$\gamma_{e,i}$ = volume of solids dispersed in the emulsion region per volume of bubbles inside the recarbonator element $i$
$\rho_{m,g}$ = molar density of the gas ($mol/m^3$)
$\rho_s$ = solids density ($kg/m^3$)
$\tau_R$ = mean residence time inside the recarbonator (s)

$\nu$ = volume fraction of $CO_2$ in the gas phase
$\nu_c$ = volume fraction of $CO_2$ in the cloud region
$\nu_e$ = volume fraction of $CO_2$ in the emulsion region
$\nu_{eq}$ = volume fraction of $CO_2$ at equilibrium conditions
$\nu_{in,i}$ = volume fraction of $CO_2$ at the inlet of the recarbonator element $i$
$\nu_0$ = volume fraction of $CO_2$ at the inlet of the recarbonator

## REFERENCES


(1) Metz, B.; Davidson, O.; Coninck, H.; Loos, M.; Meyer, L. *Special Report on Carbon Dioxide Capture and Storage*; Intergovernmental Panel on Climate Change; Cambrige University Press: New York, 2005.

(2) Anthony, E. J. Solid Looping Cycles: A New Technology for Coal Conversion. *Ind. Eng. Chem. Res.* **2008**, *47*, 1747.

(3) Blamey, J.; Anthony, E. J.; Wang, J.; Fennell, P. S. The Calcium Looping Cycle for Large-Scale $CO_2$ Capture. *Prog. Energy Combust. Sci.* **2010**, *36*, 260.

(4) Shimizu, T.; Hirama, T.; Hosoda, H.; Kitano, K.; Inagaki, M.; Tejima, K. A Twin Fluid-Bed Reactor for Removal of $CO_2$ from Combustion Processes. *Chem. Eng. Res. Des.* **1999**, *77*, 62.

(5) Abanades, J. C.; Alvarez, D. Conversion Limits in the Reaction of $CO_2$ with Lime. *Energy Fuels* **2003**, *17*, 308.

(6) Grasa, G. S.; Abanades, J. C. $CO_2$ Capture Capacity of CaO in Long Series of Carbonation/Calcination Cycles. *Ind. Eng. Chem. Res.* **2006**, *45*, 8846.

(7) Abanades, J. C.; Anthony, E. J.; Wang, J.; Oakey, J. E. Fluidized Bed Combustion Systems Integrating $CO_2$ Capture with CaO. *Environ. Sci. Technol.* **2005**, *39*, 2861.

(8) Romeo, L. M.; Abanades, J. C.; Escosa, J. M.; Paño, J.; Giménez, A.; Sánchez-Biezma, A.; Ballesteros, J. C. Oxyfuel Carbonation/Calcination Cycle for Low Cost $CO_2$ Capture in Existing Power Plants. *Energy Convers. Manage.* **2008**, *49*, 2809.

(9) Romano, M. Coal-Fired Power Plant with Calcium Oxide Carbonation for Postcombustion $CO_2$ Capture. *Energy Proc.* **2009**, *1*, 1099.

(10) Hawthorne, C.; Trossmann, M.; Galindo Cifre, P.; Schuster, A.; Scheffknecht, G. Simulation of the Carbonate Looping Power Cycle. *Energy Proc.* **2009**, *1*, 1387.

(11) Yongping, Y.; Rongrong, Z.; Liqiang, D.; Kavosh, M.; Patchigolla, K.; Oakey, J. Integration and Evaluation of a Power Plant with a CaO-Based $CO_2$ Capture System. *Int. J. Greenhouse Gas Control* **2010**, *4*, 603.

(12) Lasheras, A.; Ströhle, J.; Galloy, A.; Epple, B. Carbonate Looping Process Simulation Using a 1D Fluidized Bed Model for the Carbonator. *Int. J. Greenhouse Gas Control* **2011**, *5*, 686.

(13) Martínez, I.; Murillo, R.; Grasa, G.; Abanades, J. C. Integration of a Ca Looping System for $CO_2$ Capture in Existing Power Plants. *AIChE J.* **2011**, *57*, 2599.

(14) Lisbona, P.; Martínez, A.; Lara, Y.; Romeo, L. M. Integration of Carbonate $CO_2$ Capture Cycle and Coal-Fired Power Plants. A Comparative Study for Different Sorbents. *Energy Fuels* **2010**, *24*, 728.

(15) Zhao, M.; Minett, A. I.; Harris, A. T. A Review of Techno-economic Models for the Retrofitting of Conventional Pulverised-Coal Power Plants for Post-Combustion Capture (PCC) of $CO_2$. *Energy Environ. Sci.* **2013**, *6*, 25.

(16) Abanades, J. C.; Alonso, M.; Rodríguez, N.; González, B.; Grasa, G.; Murillo, R. Capturing $CO_2$ from Combustion Flue Gases with a Carbonation Calcination Loop. Experimental Results and Process Development. *Energy Proc.* **2009**, *1*, 1147.

(17) Lu, D. Y.; Hughes, R. W.; Anthony, E. J. Ca-Based Sorbent Looping Combustion for $CO_2$ Capture in Pilot-Scale Dual Fluidized Beds. *Fuel Process. Technol.* **2008**, *89*, 1386.

(18) Charitos, A.; Hawthorne, C.; Bidwe, A. R.; Sivalingam, S.; Schuster, A.; Spliethoff, H.; Scheffknecht, G. Parametric Investigation of the Calcium Looping Process for $CO_2$ Capture in a 10 $kW_{th}$ Dual Fluidized Bed. *Int. J. Greenhouse Gas Control* **2010**, *4*, 776.

(19) Rodríguez, N.; Alonso, M.; Abanades, J. C. Experimental Investigation of a Circulating Fluidized-Bed Reactor to Capture $CO_2$ with CaO. *AIChE J.* **2011**, *57*, 1356.

(20) Charitos, A.; Rodríguez, N.; Hawthorne, C.; Alonso, M.; Zieba, M.; Arias, B.; Kopanakis, G.; Scheffknecht, G.; Abanades, J. C. Experimental Validation of the Calcium Looping $CO_2$ Capture Process with Two Circulating Fluidized Bed Carbonator Reactors. *Ind. Eng. Chem. Res.* **2011**, *50*, 9685.

(21) Arias, B.; Diego, M. E.; Abanades, J. C.; Lorenzo, M.; Diaz, L.; Martínez, D.; Alvarez, J.; Sánchez-Biezma, A. Demonstration of Steady State $CO_2$ Capture in a 1.7 $MW_{th}$ Calcium Looping Pilot. *Int. J. Greenhouse Gas Control* **2013**, *18*, 237.

(22) Dieter, H.; Hawthorne, H.; Bidwe, A. R.; Zieba, M.; Scheffknecht, G. The 200 $kW_{th}$ Dual Fluidized Bed Calcium Looping Pilot Plant for Efficient $CO_2$ Capture: Plant Operating Experiences and Results. *21st International Conference on Fluidized Bed Combustion*, Naples (Italy), June 3−6, 2012; p 397.

(23) Kremer, J.; Galloy, A.; Ströhle, J.; Epple, B. Continuous $CO_2$ Capture in a 1-$MW_{th}$ Carbonate Looping Pilot Plant. *Chem. Eng. Technol.* **2013**, *36*, 1518.

(24) Chang, M. H.; Huang, C. M.; Liu, W. H.; Chen, W. C.; Cheng, J. Y.; Chen, W.; Wen, T. W.; Ouyang, S.; Shen, C. H.; Hsu, H. W. Design and Experimental Investigation of Calcium Looping Process for 3-$kW_{th}$ and 1.9-$MW_{th}$ Facilities. *Chem. Eng. Technol.* **2013**, *36*, 1525.

(25) Rodriguez, N.; Alonso, M.; Grasa, G.; Abanades, J. C. Heat Requirements in a Calciner of $CaCO_3$ Integrated in a $CO_2$ Capture System Using CaO. *Chem. Eng. J.* **2008**, *138*, 148.

(26) Diego, M. E.; Arias, B.; Alonso, M.; Abanades, J. C. The Impact of Calcium Sulfate and Inert Solids Accumulation in Post-Combustion Calcium Looping Systems. *Fuel* **2013**, *109*, 184.

(27) Kierzkowska, A. M.; Pacciani, R.; Müller, C. R. CaO-Based $CO_2$ Sorbents: From Fundamentals to the Development of New, Highly Effective Materials. *ChemSusChem* **2013**, *6*, 1130.

(28) Hughes, R. W.; Lu, D.; Anthony, E. J.; Wu, Y. Improved Long-Term Conversion of Limestone-Derived Sorbents for in Situ Capture of $CO_2$ in a Fluidized Bed Combustor. *Ind. Eng. Chem. Res.* **2004**, *43*, 5529.

(29) Manovic, V.; Anthony, E. J. Steam Reactivation of Spent CaO-Based Sorbent for Multiple $CO_2$ Capture Cycles. *Environ. Sci. Technol.* **2007**, *41*, 1420.

(30) Zeman, F. Effect of Steam Hydration on Performance of Lime Sorbent for $CO_2$ Capture. *Int. J. Greenhouse Gas Control* **2008**, *2*, 203.

(31) Phalak, N.; Wang, W.; Fan, L. S. $Ca(OH)_2$-Based Calcium Looping Process Development at The Ohio State University. *Chem. Eng. Technol.* **2013**, *36*, 1451.

(32) Arias, B.; Grasa, G. S.; Abanades, J. C. Effect of Sorbent Hydration on the Average Activity of CaO in a Ca-Looping System. *Chem. Eng. J.* **2010**, *163*, 324.

(33) Yu, F.-C.; Phalak, N.; Sun, Z.; Fan, L.-S. Activation Strategies for Calcium-Based Sorbents for $CO_2$ Capture: A Perspective. *Ind. Eng. Chem. Res.* **2011**, *51*, 2133.

(34) Lysikov, A. I.; Salanov, A. N.; Okunev, A. G. Change of $CO_2$ Carrying Capacity of CaO in Isothermal Recarbonation−Decomposition Cycles. *Ind. Eng. Chem. Res.* **2007**, *46*, 4633.

(35) Manovic, V.; Anthony, E. J. Thermal Activation of CaO-Based Sorbent and Self-Reactivation during $CO_2$ Capture Looping Cycles. *Environ. Sci. Technol.* **2008**, *42*, 4170.

(36) Manovic, V.; Anthony, E. J.; Grasa, G.; Abanades, J. C. $CO_2$ Looping Cycle Performance of a High-Purity Limestone after Thermal Activation/Doping. *Energy Fuels* **2008**, *22*, 3258.

(37) Manovic, V.; Anthony, E. J.; Loncarevic, D. $CO_2$ looping cycles with CaO-based sorbent pretreated in at high temperature. *Chem. Eng. Sci.* **2009**, *64*, 3236.

(38) Chen, Z.; Song, H. S.; Portillo, M.; Lim, C. J.; Grace, J. R.; Anthony, E. J. Long-Term Calcination/Carbonation Cycling and Thermal Pretreatment for $CO_2$ Capture by Limestone and Dolomite. *Energy Fuels* **2009**, *23*, 1437.

(39) Ozcan, D. C.; Shanks, B. H.; Wheelock, T. D. Improving the Stability of a CaO-Based Sorbent for $CO_2$ by Thermal Pretreatment. *Ind. Eng. Chem. Res.* **2011**, *50*, 6933.

(40) Arias, B.; Abanades, J. C.; Anthony, E. J. Model for Self-Reactivation of Highly Sintered CaO Particles during $CO_2$ Capture Looping Cycles. *Energy Fuels* **2011**, *25*, 1926.

(41) Arias, B.; Grasa, G. S.; Alonso, M.; Abanades, J. C. Post-combustion Calcium Looping Process with a Highly Stable Sorbent Activity by Recarbonation. *Energy Environ. Sci.* **2012**, *5*, 7353.
(42) Abanades, J. C.; Arias, B.; Grasa, G. Device and Method for the Capture of $CO_2$ by CaO Carbonation and for Mantaining Sorbent Activity. PCT/ES2012/070426, 2012.
(43) Barker, R. The Reversibility of the Reaction $CaCO_3 \rightleftarrows CaO + CO_2$. *J. Appl. Chem. Biotechnol.* **1973**, *23*, 733.
(44) Sun, P.; Lim, C. J.; Grace, J. R. Cyclic $CO_2$ Capture by Limestone-Derived Sorbent during Prolonged Calcination/Carbonation Cycling. *AIChE J.* **2008**, *54*, 1668.
(45) Anthony, E. J.; Bulewicz, E. M.; Jia, L. Reactivation of Limestone Sorbents in FBC for $SO_2$ Capture. *Prog. Energy Combust. Sci.* **2007**, *33*, 171.
(46) Anthony, E. J.; Lu, D.; Salvador, C. Reactivation of Lime-Based Sorbents by $CO_2$ Shocking. U.S. 7,879,139 B2, 2011.
(47) Grasa, G.; Martínez, I.; Diego, M. E.; Abanades, J. C. Determination of Carbonation Kinetics of CaO under Recarbonation Conditions. *Energy Fuels* **2014**10.1021/ef500331t.
(48) Kunii, D.; Levenspiel, O. Fluidized Reactor Models. 1. For Bubbling Beds of Fine, Intermediate, and Large Particles. 2. For the Lean Phase: Freeboard and Fast Fluidization. *Ind. Eng. Chem. Res.* **1990**, *29*, 1226.
(49) Diego, M. E.; Arias, B.; Abanades, J. C. Modeling the Solids Circulation Rates and Solids Inventories of an Interconnected Circulating Fluidized Bed Reactor System for $CO_2$ Capture by Calcium Looping. *Chem. Eng. J.* **2012**, *198*−*199*, 228.
(50) Liljedahl, G. N.; Turek, D. G.; ya Nsakala, N.; Mohn, N. C.; Fout, T. E. Alstom's Oxygen-Fired CFB Technology Development Status for $CO_2$ Mitigation. In *31st International Technical Conference on Coal Utilization & Fuel Systems*, Clearwater, FL, USA, 2006.
(51) Manovic, V.; Anthony, E. J. Carbonation of CaO-Based Sorbents Enhanced by Steam Addition. *Ind. Eng. Chem. Res.* **2010**, *49*, 9105.
(52) Donat, F.; Florin, N. H.; Anthony, E. J.; Fennell, P. S. Influence of High-Temperature Steam on the Reactivity of CaO Sorbent for $CO_2$ Capture. *Environ. Sci. Technol.* **2011**, *46*, 1262.
(53) Davidson, J. F.; Harrison, D. *Fluidized Particles*; Cambridge University Press: New York, 1963.
(54) Bhatia, S. K.; Perlmutter, D. D. Effect of the Product Layer on the Kinetics of the $CO_2$-Lime Reaction. *AIChE J.* **1983**, *29*, 79.
(55) Silaban, A. High Temperature Capture of Carbon Dioxide: Characteristics of the Reversible Reaction between CaO(s) and CO2(g). *Chem. Eng. Commun.* **1995**, *137*, 177.
(56) Mess, D.; Sarofim, A. F.; Longwell, J. P. Product Layer Diffusion during the Reaction of Calcium Oxide with Carbon Dioxide. *Energy Fuels* **1999**, *13*, 999.
(57) Abanades, J. C. The Maximum Capture Efficiency of $CO_2$ Using a Carbonation/Calcination Cycle of $CaO/CaCO_3$. *Chem. Eng. J.* **2002**, *90*, 303.
(58) Alonso, M.; Rodríguez, N.; Grasa, G.; Abanades, J. C. Modelling of a Fluidized Bed Carbonator Reactor to Capture $CO_2$ from a Combustion Flue Gas. *Chem. Eng. Sci.* **2009**, *64*, 883.
(59) Levenspiel, O. *Chemical Reaction Engineering*; Wiley: New York, 1999.
(60) Romano, M. C. Modeling the Carbonator of a Ca-Looping Process for $CO_2$ Capture from Power Plant Flue Gas. *Chem. Eng. Sci.* **2012**, *69*, 257.
(61) Li, Z.-s.; Cai, N.-s.; Croiset, E. Process Analysis of $CO_2$ Capture from Flue Gas Using Carbonation/Calcination Cycles. *AIChE J.* **2008**, *54*, 1912.
(62) Hawthorne, C.; Charitos, A.; Perez-Pulido, C. A.; Bing, Z.; Scheffknecht, G. Design of a Dual Fluidised Bed System for the Post-Combustion Removal of $CO_2$ Using CaO. Part I: CFB Carbonator Reactor Model. *9th International Conference on Circulating Fluidized Beds*, Hamburg, Germany, 2008.
(63) Romeo, L. M.; Lara, Y.; Lisbona, P.; Escosa, J. M. Optimizing Make-up Flow in a $CO_2$ Capture System Using CaO. *Chem. Eng. J.* **2009**, *147*, 252.
(64) Abanades, J. C.; Arias, B.; Diego, M. E.; Martínez, I. System for $CO_2$ Capture from a Combustion Flue Gas Using a $CaO/CaCO_3$ Chemical Loop. EP13382206.

# 5. Conclusiones

El trabajo realizado durante esta Tesis Doctoral permite concluir que los procesos de captura de $CO_2$ con CaO post-combustión e *in situ* que hacen uso de reactores de lecho fluidizado circulante son viables en condiciones de operación cercanas a las esperadas en sistemas a escala industrial. Se ha demostrado que las tendencias observadas con anterioridad en instalaciones de menor tamaño se reproducen a escala de planta piloto de 0.3-1.7 $MW_t$. La validación experimental a estas escalas de las tecnologías de carbonatación-calcinación para sistemas de captura de $CO_2$ en gases de combustión de carbón (post-combustión) o de captura durante la combustión de biomasa en lecho fluidizado (*in situ*) constituye una etapa crítica para el escalado de estas tecnologías. Asimismo, estos estudios han permitido avanzar en la modelización del sistema para la interpretación de la información experimental y para la identificación de condiciones de operación adecuadas y de configuraciones mejoradas del sistema de captura de $CO_2$.

Las conclusiones específicas que se desprenden de los trabajos realizados en ambas rutas de proceso (captura de $CO_2$ post-combustión e *in situ*) se indican a continuación.

*Demostración experimental de la captura de $CO_2$ post-combustión*

- Los experimentos realizados en la planta piloto de 1.7 $MW_t$ han demostrado la viabilidad de la tecnología de CaL post-combustión a escala pre-industrial. Los resultados obtenidos confirman que es posible alcanzar eficacias de captura de $CO_2$ en el carbonatador superiores al 90% en condiciones reales de operación en cuanto a tratamiento de gases reales, velocidades de gas, circulación de sólidos entre reactores, alimentación continua de caliza y carbón,

extracción de cenizas en continuo y calcinación en atmósfera de oxi-combustión.

- Se confirma que el inventario de CaO activo en el carbonatador es una variable crítica para la obtención de elevadas eficacias de captura de $CO_2$. Si el inventario de partículas en el carbonatador es alto (500-1000 kg/m$^2$s), es posible operar con este reactor como un absorbedor efectivo de $CO_2$ incluso con partículas desactivadas (conversiones medias máximas, $X_{ave}$, cercanas a la actividad residual) y flujos de circulación de sólidos moderados (2-5 kg/m$^2$s). Por el contrario, altos valores de $X_{ave}$ permiten operar en condiciones de menores inventarios de sólidos en el carbonatador (100-200 kg/m$^2$).
- Las partículas que participan en el proceso absorben el azufre que entra al sistema junto con el gas de combustión y el carbón alimentado al calcinador, dando lugar a eficacias de desulfuración superiores al 95%, incluso en el caso de partículas altamente desactivadas para la captura de $CO_2$. Esta característica permite considerar las purgas del proceso como material adecuado para la desulfuración en calderas de lecho fluidizado circulante.
- La utilización total del sorbente, medida como la suma de $X_{ave}$ y la conversión molar a $CaSO_4$, es superior a la esperada por la curva de desactivación del sorbente, lo que permitirá reducir el flujo de caliza fresca alimentada al sistema en instalaciones futuras a gran escala.
- El balance de carbono se ha cerrado con éxito en condiciones de estado estacionario en el carbonatador. Los valores de la constante de reacción aparente calculada y de las actividades de los sólidos medidas son similares a los encontrados en plantas de menor tamaño, lo que confirma la reproducibilidad de los resultados y sugiere cierta facilidad en el escalado de este tipo de instalaciones

empleando el conocimiento ya adquirido acerca de calderas de lecho fluidizado circulante comerciales.

*Demostración experimental de la captura de $CO_2$ in situ*

- La combustión de biomasa y captura simultánea de $CO_2$ se ha demostrado en una planta piloto de 300 $kW_t$. Se han alcanzado eficacias de captura del 70-95% en escenarios de operación cercanos a los esperados a nivel industrial en términos de velocidades de gas, circulación de sólidos y alimentación continua de biomasa y caliza fresca al sistema.
- Se confirma que es necesario mantener la temperatura del combustor-carbonatador en un estrecho intervalo de operación alrededor de 700ºC con el objetivo de alcanzar elevados valores de eficacia de captura de $CO_2$ a la vez que se maximiza la combustión de biomasa y se minimizan las emisiones de CO.
- La comparación de los resultados procedentes de diversas campañas experimentales realizadas en la planta piloto de 300 $kW_t$ ratifica que la eficacia de captura de $CO_2$ es altamente sensible al valor del inventario de sólidos en el combustor-carbonatador y a la actividad de las partículas de CaO a igualdad del resto de condiciones de operación.
- Es posible lograr eficacias de captura de $CO_2$ cercanas al 80% en el combustor-carbonatador con circulaciones de sólidos entre reactores de 2-5 $kg/m^2s$, inventarios de sólidos en el reactor de 200-400 $kg/m^2$ y una actividad de las partículas de CaO modesta (alrededor de 0.15-0.20).

- Los resultados experimentales obtenidos en la planta piloto de 300 $kW_t$ con combustión de pellets de biomasa y captura de $CO_2$ *in situ* se pueden interpretar por medio de un modelo de reactor de combustión y carbonatación simultánea. La constante aparente de reacción calculada de este modo toma un valor de 0.095 $s^{-1}$.
- Los datos extraídos indican que para alcanzar eficacias de captura de $CO_2$ del 90% con respecto al equilibrio es necesario que el tiempo espacial activo en el combustor-carbonatador tome un valor de 0.1 h.

*Análisis hidrodinámico de sistemas CaL de reactores de lecho fluidizado circulante interconectados*

- La similitud existente entre los sistemas CaL y las calderas de lecho fluidizado circulante comerciales (CFBCs) en cuanto a las propiedades de los sólidos y las condiciones de operación permiten aplicar los modelos y correlaciones desarrollados para CFBCs a las configuraciones CaL.
- La circulación de sólidos entre el carbonatador y el calcinador que se obtiene como resultado de las condiciones hidrodinámicas en los reactores no coincide necesariamente con la requerida para alcanzar una determinada eficacia de captura de $CO_2$ (relación molar Ca/C). Si el flujo de sólidos es menor que el requerido, entonces no es posible conseguir la eficacia de captura de $CO_2$ deseada y se requiere un cambio en las condiciones de operación. Por el contrario, si es mucho mayor, el exceso de flujo de sólidos debe ser recirculado hacia este mismo reactor. Esta estrategia favorece además el buen funcionamiento de los reactores, ya que incrementa los tiempos de residencia de las partículas en los mismos y limita la demanda energética del calcinador.

*Estudio de la acumulación de $CaSO_4$ y cenizas en sistemas CaL que emplean carbón*

- La alimentación continua de gases de combustión que contienen $SO_2$ y de carbón con un cierto contenido en azufre y cenizas a las instalaciones CaL post-combustión dan lugar a la acumulación de $CaSO_4$ y cenizas en el sistema. El flujo de caliza que se introduce continuamente y su purga asociada deben garantizar que existe una fracción de CaO activo en el sistema adecuada para la captura de $CO_2$.
- Los balances de materia y energía aplicados al sistema de reactores interconectados indican que un incremento en el contenido en azufre del carbón alimentado al calcinador desde el 0.5 hasta el 1% provoca un efecto similar al generado por aumentar la fracción de cenizas en este mismo carbón desde el 5 al 20%.
- La resolución de los balances de materia en los sistemas CaL confirman que varios de los procesos de reactivación propuestos para incrementar la $X_{ave}$ del sorbente reducen drásticamente el flujo de caliza fresca que es necesario alimentar al sistema. Sin embargo, estos beneficios sólo se pueden aprovechar en su totalidad si se alimenta gas de combustión limpio al carbonatador (sin $SO_2$) y combustibles libres de azufre y cenizas al calcinador. En caso contrario, los efectos positivos mencionados se ven reducidos por la necesidad de purgar $CaSO_4$ y cenizas del sistema. Los sorbentes sintéticos de alta calidad se pueden por tanto descartar como posibles candidatos para las aplicaciones de CaL en sistemas que emplean carbón, ya que es muy probable que la necesidad de alimentación de caliza fresca para purgar el $CaSO_4$ y las cenizas presentes haga que sean económicamente inviables.

*Estudio de la reactivación del sorbente por recarbonatación*

- Experimentos llevados a cabo en termobalanza bajo condiciones típicas de carbonatación y calcinación han mostrado que es posible estabilizar la actividad de las partículas en valores cercanos a 0.20 si, tras la carbonatación y antes de iniciar la etapa de calcinación, se somete a los sólidos a una etapa de recarbonatación en condiciones intensas de carbonatación.
- Los experimentos termogravimétricos realizados han mostrado que las condiciones óptimas para que la recarbonatación tenga lugar a altas velocidades de reacción son temperaturas alrededor de 800ºC, concentraciones de $CO_2$ superiores al 80%v y contenidos moderados de vapor de agua (10-20%v).
- La etapa rápida del proceso de recarbonatación es corta y da lugar a un incremento en el contenido en $CaCO_3$ de los sólidos de entre 0.02 y 0.05 puntos con respecto a la conversión máxima que se alcanza durante la fase de carbonatación en cada ciclo. Tras esta etapa, comienza un proceso muy lento de carbonatación dominado por la presencia de resistencias difusionales. La presencia de vapor de agua en la atmósfera de reacción favorece la cinética de la recarbonatación, aunque la conversión a $CaCO_3$ alcanzada por las partículas al final de la etapa de recarbonatación es independiente de la presencia de vapor durante la reacción.
- Dado que las conversiones de recarbonatación son limitadas, si se realiza un balance adiabático a un reactor de lecho fluidizado ideal para la recarbonatación se obtiene que el aumento esperado de temperatura en el recarbonatador es del orden de 60-70ºC, lo que resulta insuficiente para alcanzar las temperaturas óptimas de recarbonatación. Por tanto, se requiere un aporte adicional de calor, que se puede suministrar mediante el precalentamiento de las

corrientes gaseosas de entrada al reactor, el incremento de la temperatura de operación del carbonatador, el calentamiento de los sólidos que salen del carbonatador empleando una corriente gaseosa a alta temperatura y/o a través de la combustión de una pequeña cantidad de combustible con oxígeno puro en el recarbonatador.

- Se ha desarrollado un modelo de reactor capaz de predecir el comportamiento del recarbonatador en base al modelo de Kunii y Levenspiel para el contacto gas-sólido en reactores fluidizados de lecho burbujeante e incorporando la información cinética obtenida previamente en los experimentos termogravimétricos. El modelo del recarbonatador tiene en cuenta la reducción en el volumen de gas inherente al proceso de recarbonatación y permite calcular la conversión de los sólidos y del gas (eficacia del reactor) en función de las condiciones de operación.
- Estudios realizados bajo suposiciones conservadoras indican que no es posible lograr eficacias del reactor muy elevadas con tamaños moderados del reactor de recarbonatación, aunque éstas tampoco son necesarias para conseguir un incremento limitado de la actividad de las partículas.
- El modelo se ha empleado para obtener un diseño preliminar de un reactor de recarbonatación. Los resultados indican que es posible doblar prácticamente la actividad residual de los sólidos mediante recarbonatación con tiempos de residencia de las partículas de entre 100 y 170s en el reactor, a pesar de que los incrementos en el contenido en $CaCO_3$ alcanzados en cada ciclo durante la recarbonatación son moderados. Este resultado es muy alentador para el desarrollo futuro de este sistema de reactivación del sorbente para los sistemas CaL, que es además de bajo coste, eficiente energéticamente y está altamente integrado en el proceso.

# 6. Conclusions

The main conclusions derived from this Doctoral Thesis are based on experimental confirmation of Calcium Looping post-combustion and *in situ* $CO_2$ capture technologies that employ circulating fluidized bed reactors on a large pilot scale operating in conditions close to those that might be expected in future large-scale systems. It is demonstrated that the trends previously observed in smaller facilities are also reproducible at the scale of 0.3-1.7 $MW_{th}$ pilot plants. The experimental validation of carbonation-calcination technologies for $CO_2$ capture from flue gases derived from coal combustion (post-combustion) or during biomass combustion in fluidized beds (*in situ*) is a critical step for the scaling up of these technologies. Moreover, the studies carried out as part of this Thesis have made progress in the modeling approaches required for interpreting the experimental data and for identifying reasonable operating windows and improved configurations of the $CO_2$ capture system.

The specific conclusions obtained for both process routes (post-combustion and *in situ* $CO_2$ capture) are explained below.

*Experimental demonstration of post-combustion $CO_2$ capture*

- The experiments conducted in the 1.7 $MW_{th}$ La Pereda pilot plant have demonstrated that post-combustion CaL technology is viable at pre-industrial scale. The results confirm that $CO_2$ capture efficiencies higher than 90% can be attained under realistic operating conditions in terms of treatment of real flue gases, gas velocities, solid circulation rates between reactors, continuous coal and limestone feeding, continuous ash removal and calcination under oxy-fired conditions.
- The results confirm that the active CaO inventory inside the carbonator reactor is a key variable for achieving high $CO_2$ capture

efficiencies. In fact, if there is a high solid inventory inside the carbonator (500-1000 kg/m$^2$s) this reactor can perform as an effective $CO_2$ even with highly deactivated particles ($CO_2$ carrying capacity, $X_{ave}$, close to the residual activity of 0.06-0.10 in Ca molar conversion) and moderate solid circulation rates (2-5 kg/m$^2$s). However, high values of $X_{ave}$ make it possible to operate with low carbonator solid inventories (100-200 kg/m$^2$).

- The particles involved in the process absorb the sulfur that enters the system with the flue gas and the coal fed to the calciner, resulting in a desulfurization efficiency higher than 95%, even in the case of highly deactivated particles for $CO_2$ capture. This allows purges from CaL systems to be used as suitable material for desulfurization in circulating fluidized bed boilers.
- The total utilization of the sorbent, calculated as the sum of $X_{ave}$ and the molar fraction of $CaSO_4$, is higher than might be expected from the sorbent deactivation curves. This will make it possible to reduce the make-up flow of fresh limestone in future large scale systems.
- The carbon balance was satisfactorily closed during steady state operation of the carbonator. The calculated apparent kinetic constant and the measured values of particle activity are similar to those found in smaller pilot plants, which confirms the reproducibility of these results and suggests that CaL facilities could be easily scaled up using state-of-the-art knowledge of similar circulating fluidized bed combustor systems that are already commercially available.

*Experimental demonstration of in situ $CO_2$ capture*

- Simultaneous biomass combustion and $CO_2$ capture has been demonstrated in a 300 $kW_{th}$ pilot plant. $CO_2$ capture efficiencies of between 70 and 95% were achieved in scenarios close to those that might be expected at industrial scale in terms of gas velocities, solid circulation rates and continuous biomass and limestone feeding.
- In order to attain high $CO_2$ capture efficiencies, maximize combustion efficiency and minimize emissions of CO, it is necessary to maintain the combustor-carbonator within a narrow operating window at around 700ºC.
- A comparison of the experimental results of different testing campaigns in the 300$kW_{th}$ pilot plant evidences that $CO_2$ capture efficiency is heavily dependent upon the solid inventory inside the combustor-carbonator and on the activity of CaO particles when all the other operating conditions are similar.
- $CO_2$ capture efficiencies close to 80% can be achieved inside the combustor-carbonator when the solid circulation rate is between 2-5 $kg/m^2s$, the solid inventory inside the reactor is 200-400 $kg/m^2$ and the activity of the CaO particles is modest (around 0.15-0.20).
- The experimental results obtained from the tests conducted in a 300 $kW_{th}$ pilot that burns biomass pellets and uses CaO to capture $CO_2$ *in situ* can be interpreted by means of a reactor model that takes into account simultaneous combustion and carbonation reactions. The apparent carbonation kinetic constant calculated using the model takes a value of 0.095 $s^{-1}$.
- The data obtained during the tests indicate that active space times of 0.1 h are required in the combustor-carbonator in order to attain a normalized $CO_2$ capture efficiency of around 90%.

*Hydrodynamic analysis of interconnected circulating fluidized bed CaL reactor systems*

- The similarity between CaL systems and commercial circulating fluidized bed combustors (CFBCs) in terms of particle properties and operating conditions allows models and correlations developed for CFBCs to be applied to CaL configurations.
- The circulation of solids between the carbonator and calciner reactors in a Calcium Loping system resulting from the hydrodynamic conditions in the risers does not necessarily coincide with the circulation of solids required to attain a certain $CO_2$ capture efficiency (Ca/C molar ratio). If the flow of solids is lower than that required, then it is not possible to achieve the desired level of $CO_2$ capture efficiency and a change in the operating conditions is necessary. If the solid flow is much higher, the excess flow of solids needs to be recirculated back to the same reactor. This strategy will also enhance the performance of the reactors, as it will lead to longer particle residence times in the risers and limit the energy demand in the calciner.

*Study of the accumulation of $CaSO_4$ and ashes in coal-based CaL systems*

- The continuous feeding of flue gases containing $SO_2$ and of coal containing sulfur and ashes to post-combustion CaL systems results in the accumulation of $CaSO_4$ and ashes in the system. The make-up flow of limestone and associated purge of solids must ensure that there is a sufficient fraction of active CaO in the system for $CO_2$ capture.
- Applying mass and energy balances to the interconnected reactor system reveals that an increase in the sulfur content of the coal fed to the calciner from 0.5 to 1% has a similar effect to that caused by an increment in the ash fraction of the coal from 5 to 20%.

- The mass balances solved for the Calcium loop confirm that several of the proposed reactivation processes intended to increase the $X_{ave}$ drastically reduce the make-up flow requirements. However, these benefits will only be fully effective if clean flue gas is fed to the carbonator and fuels free of sulfur and ash are burnt in the calciner. Otherwise, these positive gains will be undermined by the need to purge both $CaSO_4$ and ashes. High quality synthetic sorbents can be ruled out as candidates for CaL in coal-based applications because the minimum make-up flow requirements to purge $CaSO_4$ and ashes will most likely make them economically prohibitive.

*Study of sorbent reactivation by means of recarbonation*

- During cyclic thermogravimetric tests conducted under typical carbonation and calcination conditions it was observed that it is possible to stabilize the activity of the particles at values close to 0.20 by subjecting the solids to a recarbonation stage under intense carbonation conditions after carbonation and prior to the calcination stage of the cycle.
- Thermogravimetric tests have shown that the optimum conditions for the recarbonation reaction to proceed at a high reaction rate are temperatures of around 800ºC, a $CO_2$ concentration of over 80%v and a modest steam content (10-20%v).
- The fast recarbonation stage is short and leads to an increase in carbonate conversion of between 0.02-0.05 points with respect to the maximum carbonation conversion achieved during the standard carbonation stage in each cycle. After this stage, an extremely slow diffusionally-controlled carbonation process ensues. The presence of steam in the reaction atmosphere favours the kinetics of

recarbonation, although the conversion of $CaCO_3$ at the end of the recarbonation stage is independent of the presence of steam.

- Due to the limited recarbonation conversions, an adiabatic heat balance for an ideal fluidized bed reactor to achieve the recarbonation reaction indicates that the expected increase in temperature inside the recarbonator is of the order of 60-70ºC, which is insufficient to achieve optimum recarbonation temperatures. An additional heat input is therefore required, which can be supplied by preheating the gas flows entering the reactor, by increasing the carbonator operating temperature (which is the temperature at which the solids arrive at the recarbonator), by heating the solids that exit the carbonator using a high temperature flue gas and/or by burning a small amount of fuel with pure oxygen inside the recarbonator.
- A reactor model capable of predicting the performance of the recarbonator based on the Kunii and Levenspiel model for gas-solid contact in bubbling bed reactors and incorporating the kinetic information previously obtained in the thermogravimetric tests has been developed. The recarbonator model takes into account the reduction in gas volume inherent in the recarbonation process, and it allows the solid and gas conversions (reactor efficiency) to be calculated as a function of the operating conditions.
- The model has been used to obtain a preliminary design of a recarbonator reactor. The results indicate that mean residence times of the particles inside the recarbonator of between 100 and 170s are sufficient to almost double the residual activity of the particles by means of recarbonation, despite the moderate increase in the carbonate conversion as a result of recarbonation in each cycle. This is an encouraging result for the development of this low-cost,

highly-integrated and energy efficient sorbent reactivation process for calcium looping systems.

# Referencias


Abanades, J. C., Álvarez, D. (2003). Conversion Limits in the Reaction of $CO_2$ with Lime, *Energy & Fuels*, 17, 308-315.

Abanades, J. C., Anthony, E. J., Lu, D. Y., Salvador, C., Álvarez, D. (2004). Capture of $CO_2$ from combustion gases in a fluidized bed of CaO, *AIChE Journal*, 50, 1614-1622.

Abanades, J. C., Anthony, E. J., Wang, J., Oakey, J. E. (2005). Fluidized Bed Combustion Systems Integrating $CO_2$ Capture with CaO, *Environmental Science & Technology*, 39, 2861-2866.

Abanades, J. C., Alonso, M., Rodríguez, N., González, B., Grasa, G., Murillo, R. (2009). Capturing $CO_2$ from combustion flue gases with a carbonation calcination loop. Experimental results and process development, *Energy Procedia*, 1, 1147-1154.

Abanades, J. C., Murillo, R., Fernandez, J. R., Grasa, G., Martínez, I. (2010). New $CO_2$ Capture Process for Hydrogen Production Combining Ca and Cu Chemical Loops, *Environmental Science & Technology*, 44, 6901-6904.

Abanades, J. C., Alonso, M., Rodríguez, N. (2011a). Biomass Combustion with in Situ $CO_2$ Capture with CaO. I. Process Description and Economics, *Industrial & Engineering Chemistry Research*, 50, 6972-6981.

Abanades, J. C., Alonso, M., Rodríguez, N. (2011b). Experimental validation of in situ $CO_2$ capture with CaO during the low temperature combustion of biomass in a fluidized bed reactor, *International Journal of Greenhouse Gas Control*, 5, 512-520.

Abanades, J. C., Arias, B., Grasa, G. (2012). Device and method for the capture of $CO_2$ by CaO carbonation and for maintaining sorbent activity. PCT/ES2012/070426.

Abanades, J. C. (2013). Calcium looping for $CO_2$ capture in combustion systems. Fluidized bed technologies for near-zero emission combustion and gasification, Scala, F. (Ed.). Woodhead Publishing Limited: Oxford, Cambridge, Philadelphia, New Delhi.

Abanades, J. C., Arias, B., Diego, M. E., Martínez, I. (2013) System for $CO_2$ capture from a combustion flue gas using a $CaO/CaCO_3$ chemical loop. EP13382206.

Alonso, M., Rodríguez, N., Grasa, G., Abanades, J. C. (2009). Modelling of a fluidized bed carbonator reactor to capture $CO_2$ from a combustion flue gas, *Chemical Engineering Science*, 64, 883-891.

Alonso, M., Rodríguez, N., González, B., Grasa, G., Murillo, R., Abanades, J. C. (2010). Carbon dioxide capture from combustion flue gases with a calcium oxide chemical loop. Experimental results and process development, *International Journal of Greenhouse Gas Control*, 4, 167-173.

Alonso, M., Rodríguez, N., González, B., Arias, B., Abanades, J. C. (2011). Biomass Combustion with in Situ $CO_2$ Capture by CaO. II. Experimental Results, *Industrial & Engineering Chemistry Research*, 50, 6982-6989.

Arias, B., Grasa, G. S., Alonso, M., Abanades, J. C. (2012). Post-combustion calcium looping process with a highly stable sorbent activity by recarbonation, *Energy & Environmental Science*, 5, 7353-7359.

Barker, R. (1973). The reversibility of the reaction $CaCO_3 \rightleftarrows CaO+CO_2$, *Journal of Applied Chemistry and Biotechnology*, 23, 733-742.

Bhatia, S. K., Perlmutter, D. D. (1983). Effect of the product layer on the kinetics of the $CO_2$-lime reaction, *AIChE Journal*, 29, 79-86.

Blamey, J., Anthony, E. J., Wang, J., Fennell, P. S. (2010). The calcium looping cycle for large-scale $CO_2$ capture, *Progress in Energy and Combustion Science*, 36, 260-279.

Boot-Handford, M. E., Abanades, J. C., Anthony, E. J., Blunt, M. J., Brandani, S., Mac Dowell, N., Fernandez, J. R., Ferrari, M.-C., Gross, R., Hallett, J. P., Haszeldine, R. S., Heptonstall, P., Lyngfelt, A., Makuch, Z., Mangano, E., Porter, R. T. J., Pourkashanian, M., Rochelle, G. T., Shah, N., Yao, J. G., Fennell, P. S. (2014). Carbon capture and storage update, *Energy & Environmental Science*, 7, 130-189.

Borgwardt, R. H. (1985). Calcination kinetics and surface area of dispersed limestone particles, *AIChE Journal*, 31, 103-111.

Carbon Tracker (2013). Unburnable Carbon 2013: Wasted Capital and Stranded Assets.

Chang, M. H., Huang, C. M., Liu, W. H., Chen, W. C., Cheng, J. Y., Chen, W., Wen, T. W., Ouyang, S., Shen, C. H., Hsu, H. W. (2013). Design and Experimental Investigation of Calcium Looping Process for 3-$kW_{th}$ and 1.9-$MW_{th}$ Facilities, *Chemical Engineering & Technology*, 36, 1525-1532.

Charitos, A., Hawthorne, C., Bidwe, A. R., Sivalingam, S., Schuster, A., Spliethoff, H., Scheffknecht, G. (2010). Parametric investigation of the calcium looping process for $CO_2$ capture in a 10 $kW_{th}$ dual fluidized bed, *International Journal of Greenhouse Gas Control*, 4, 776-784.

Charitos, A., Rodríguez, N., Hawthorne, C., Alonso, M., Zieba, M., Arias, B., Kopanakis, G., Scheffknecht, G., Abanades, J. C. (2011). Experimental Validation of the Calcium Looping $CO_2$ Capture Process with Two Circulating Fluidized Bed Carbonator Reactors, *Industrial & Engineering Chemistry Research*, 50, 9685-9695.

Coppola, A., Montagnaro, F., Salatino, P., Scala, F. (2012). Attrition of Limestone during Fluidized Bed Calcium Looping Cycles for $CO_2$ Capture, *Combustion Science and Technology*, 184, 929-941.

Curran , P. G., Fink Carl, E., Gorin, E. (1967). $CO_2$ Acceptor Gasification Process. Studies of acceptor properties. Fuel Gasification, American Chemical Society: Vol. 69, 141-165.

Darde, A., Prabhakar, R., Tranier, J.-P., Perrin, N. (2009). Air separation and flue gas compression and purification units for oxy-coal combustion systems, *Energy Procedia*, 1, 527-534.

Dean, C. C., Blamey, J., Florin, N. H., Al-Jeboori, M. J., Fennell, P. S. (2011a). The calcium looping cycle for $CO_2$ capture from power generation, cement manufacture and hydrogen production, *Chemical Engineering Research and Design*, 89, 836-855.

Dean, C. C., Dugwell, D., Fennell, P. S. (2011b). Investigation into potential synergy between power generation, cement manufacture and $CO_2$ abatement using the calcium looping cycle, *Energy & Environmental Science*, 4, 2050-2053.

Dieter, H., Hawthorne, H., Bidwe, A. R., Zieba, M., Scheffknecht, G. (2012). The 200 $kW_{th}$ Dual Fluidized Bed Calcium Looping Pilot Plant for Efficient $CO_2$ Capture: Plant Operating Experiences and Results, 21st International Conference on Fluidized Bed Combustion, Naples (Italy), 397-404.

Dieter, H., Bidwe, A. R., Varela-Duelli, G., Charitos, A., Hawthorne, C., Scheffknecht, G. (2014). Development of the calcium looping $CO_2$ capture technology from lab to pilot scale at IFK, University of Stuttgart, *Fuel*, 127, 23-37.

Fink, C., Curran, G., Sudbury, J. (1974), $CO_2$ Acceptor Process Pilot Plant - 1974 Rapid City, South Dakota, Proceedings of the Sixth Synthetic Pipeline Gas Symposium, Chicago.

Fuertes, A. B., Álvarez, D., Rubiera, F., Pis, J. J., Marbán, G., Palacios, J. M. (1991). Surface-area and pore-size changes during sintering of calcium-oxide particles, *Chemical Engineering Communications*, 109, 73-88.

Galloy, A., Ströhle, J., Epple, B. (2011). Design and operation of a 1 $MW_{th}$ carbonate and chemical looping CCS test rig, *VGB PowerTech*, 91, 64-68.

Global CCS Institute (2013). The Global Status of CCS 2013, Melbourne, Australia.

González, B., Grasa, G. S., Alonso, M., Abanades, J. C. (2008). Modeling of the Deactivation of CaO in a Carbonate Loop at High Temperatures of Calcination, *Industrial & Engineering Chemistry Research*, 47, 9256-9262.

Grasa, G. S., Abanades, J. C. (2006). $CO_2$ Capture Capacity of CaO in Long Series of Carbonation/Calcination Cycles, *Industrial & Engineering Chemistry Research*, 45, 8846-8851.

Grasa, G. S., Abanades, J. C. (2007). Narrow fluidised beds arranged to exchange heat between a combustion chamber and a sorbent regenerator, *Chemical Engineering Science*, 62, 619-626.

Grasa, G. S., Alonso, M., Abanades, J. C. (2008). Sulfation of CaO Particles in a Carbonation/Calcination Loop to Capture $CO_2$, *Industrial & Engineering Chemistry Research*, 47, 1630-1635.

Grasa, G., Murillo, R., Alonso, M., Abanades, J. C. (2009). Application of the random pore model to the carbonation cyclic reaction, *AIChE Journal*, 55, 1246-1255.

Hawthorne, C., Charitos, A., Perez-Pulido, C. A., Bing, Z., Scheffknecht, G. (2008). Design of a dual fluidised bed system for the post-combustion removal of $CO_2$ using CaO. Part I: CFB carbonator reactor model, 9th International Conference on Circulating Fluidized Beds, Hamburg, Germany.

Hawthorne, C., Trossmann, M., Galindo Cifre, P., Schuster, A., Scheffknecht, G. (2009). Simulation of the carbonate looping power cycle, *Energy Procedia*, 1, 1387-1394.

Hawthorne, C., Dieter, H., Bidwe, A., Schuster, A., Scheffknecht, G., Unterberger, S., Käß, M. (2011). $CO_2$ capture with CaO in a 200 $kW_{th}$ dual fluidized bed pilot plant, *Energy Procedia*, 4, 441-448.

IEA (2012a). Energy Technology Perspectives 2012, OECD/IEA, Paris.

IEA (2012b). Capture, Transport and Storage of $CO_2$.

IEA (2013a). Redrawing the Energy-Climate map. World Energy Outlook Special Report.

IEA (2013b). World Energy Outlook 2013.

IEA (2013c). Technology Roadmap. Carbon capture and Storage.

IPCC (2005). Special report on carbon dioxide capture and storage. Cambridge University Press: Cambridge, United Kingdom and New York, NY, USA.

IPCC (2013). Climate Change 2013: The Physical Science Basis. Cambrige University Press: Cambridge, United Kingdom and New York, NY, USA.

IPCC (2014). Climate Change 2014, Mitigation of Climate Change. Cambridge University Press: Cambridge, United Kingdom and New York, NY, USA.

Johnsson, F., Leckner, B. (1995). Vertical distribution of solids in a CFB-Furnace, 13th International Conference on Fluidized Bed Combustion, Orlando, Florida, USA, 671-679.

Junk, M., Reitz, M., Ströhle, J., Epple, B. (2013). Thermodynamic Evaluation and Cold Flow Model Testing of an Indirectly Heated Carbonate Looping Process, *Chemical Engineering & Technology*, 36, 1479-1487.

Kierzkowska, A. M., Pacciani, R., Müller, C. R. (2013). CaO-Based $CO_2$ Sorbents: From Fundamentals to the Development of New, Highly Effective Materials, *ChemSusChem*, 6, 1130-1148.

Kremer, J., Galloy, A., Ströhle, J., Epple, B. (2013). Continuous $CO_2$ Capture in a 1-$MW_{th}$ Carbonate Looping Pilot Plant, *Chemical Engineering & Technology*, 36, 1518-1524.

Kunii, D., Levenspiel, O. (1990). Fluidized reactor models. 1. For bubbling beds of fine, intermediate, and large particles. 2. For the lean phase: freeboard and fast fluidization, *Industrial & Engineering Chemistry Research*, 29, 1226-1234.

Lasheras, A., Ströhle, J., Galloy, A., Epple, B. (2011). Carbonate looping process simulation using a 1D fluidized bed model for the carbonator, *International Journal of Greenhouse Gas Control*, 5, 686-693.

Li, Y., Buchi, S., Grace, J. R., Lim, C. J. (2005). $SO_2$ Removal and $CO_2$ Capture by Limestone Resulting from Calcination/Sulfation/Carbonation Cycles, *Energy & Fuels*, 19, 1927-1934.

Lisbona, P., Martínez, A., Lara, Y., Romeo, L. M. (2010). Integration of Carbonate $CO_2$ Capture Cycle and Coal-Fired Power Plants. A Comparative Study for Different Sorbents, *Energy & Fuels*, 24, 728-736.

Lu, D. Y., Hughes, R. W., Anthony, E. J. (2008). Ca-based sorbent looping combustion for $CO_2$ capture in pilot-scale dual fluidized beds, *Fuel Processing Technology*, 89, 1386-1395.

Lysikov, A. I., Salanov, A. N., Okunev, A. G. (2007). Change of $CO_2$ Carrying Capacity of CaO in Isothermal Recarbonation−Decomposition Cycles, *Industrial & Engineering Chemistry Research*, 46, 4633-4638.

Manovic, V., Anthony, E. J., Loncarevic, D. (2009). $SO_2$ Retention by CaO-Based Sorbent Spent in $CO_2$ Looping Cycles, *Industrial & Engineering Chemistry Research*, 48, 6627-6632.

Martínez, I., Murillo, R., Grasa, G., Abanades, J. C. (2011a). Integration of a Ca looping system for $CO_2$ capture in existing power plants, *AIChE Journal*, 57, 2599-2607.

Martínez, I., Murillo, R., Grasa, G., Rodríguez, N., Abanades, J. C. (2011b). Conceptual design of a three fluidised beds combustion system capturing $CO_2$ with CaO, *International Journal of Greenhouse Gas Control*, 5, 498-504.

Martínez, I., Grasa, G., Murillo, R., Arias, B., Abanades, J. C. (2013). Modelling the continuous calcination of $CaCO_3$ in a Ca-looping system, *Chemical Engineering Journal*, 215–216, 174-181.

Nussbaumer, T. (2003). Combustion and Co-combustion of Biomass: Fundamentals, Technologies, and Primary Measures for Emission Reduction, *Energy & Fuels*, 17, 1510-1521.

Ozcan, D. C., Alonso, M., Ahn, H., Abanades, J. C., Brandani, S. (2014). Process and Cost Analysis of a Biomass Power Plant with in Situ Calcium Looping $CO_2$ Capture Process, *Industrial & Engineering Chemistry Research*, 53, 10721-10733.

Plötz, S., Bayrak, A., Galloy, A., Kremer, J., Orth, M., Wieczorek, M., Ströhle, J., Epple, B. (2012). First Carbonate Looping Experiments with a 1 $MW_{th}$ Test Facility Consisting of Two Interconnected CFBs, 21$^{st}$ International Conference on Fluidized Bed Combustion, Naples (Italy), 421-428.

PTRC (2013). http://ptrc.ca/projects/weyburn-midale (visitado en Julio 2014).

Rodríguez, N., Alonso, M., Grasa, G., Abanades, J. C. (2008). Heat requirements in a calciner of $CaCO_3$ integrated in a $CO_2$ capture system using CaO, *Chemical Engineering Journal*, 138, 148-154.

Rodríguez, N., Alonso, M., Abanades, J. C. (2010). Average activity of CaO particles in a calcium looping system, *Chemical Engineering Journal*, 156, 388-394.

Rodríguez, N., Alonso, M., Abanades, J. C. (2011). Experimental investigation of a circulating fluidized-bed reactor to capture $CO_2$ with CaO, *AIChE Journal*, 57, 1356-1366.

Romano, M. (2009). Coal-fired power plant with calcium oxide carbonation for postcombustion $CO_2$ capture, *Energy Procedia*, 1, 1099-1106.

Romano, M. C. (2012). Modeling the carbonator of a Ca-looping process for $CO_2$ capture from power plant flue gas, *Chemical Engineering Science*, 69, 257-269.

Romeo, L. M., Abanades, J. C., Escosa, J. M., Paño, J., Giménez, A., Sánchez-Biezma, A., Ballesteros, J. C. (2008). Oxyfuel carbonation/calcination cycle for low cost $CO_2$ capture in existing power plants, *Energy Conversion and Management*, 49, 2809-2814.

Romeo, L. M., Lara, Y., Lisbona, P., Escosa, J. M. (2009). Optimizing make-up flow in a $CO_2$ capture system using CaO, *Chemical Engineering Journal*, 147, 252-258.

Romeo, L. M., Catalina, D., Lisbona, P., Lara, Y., Martínez, A. (2011). Reduction of greenhouse gas emissions by integration of cement plants, power plants, and $CO_2$ capture systems, *Greenhouse Gases: Science and Technology*, 1, 72-82.

Sánchez-Biezma, A., Diaz, L., López, J., Arias, B., Paniagua, J., de Zárraga, E., Álvarez, J., Abanades, J. C. (2012). La Pereda $CO_2$: A 1.7 MW Pilot to test Post-combustion $CO_2$ Capture with CaO, 21st International Conference on Fluidized Bed Combustion, Naples (Italy), 365-372.

Sánchez-Biezma, A., Paniagua, J., Diaz, L., Lorenzo, M., Álvarez, J., Martínez, D., Arias, B., Diego, M. E., Abanades, J. C. (2013). Testing postcombustion $CO_2$ capture with CaO in a 1.7 $MW_{th}$ pilot facility, *Energy Procedia*, 37, 1-8.

Scripps Institution of Oceanography at UC San Diego (2014). https://scripps.ucsd.edu/programs/keelingcurve/ (visitado en Julio 2014).

Shell (2014). http://www.shell.com.mx/innovation/meeting-demand/getting-more/eor.html (visitado en Julio 2014).

Shimizu, T., Hirama, T., Hosoda, H., Kitano, K., Inagaki, M., Tejima, K. (1999). A Twin Fluid-Bed Reactor for Removal of $CO_2$ from Combustion Processes, *Chemical Engineering Research and Design*, 77, 62-68.

Silaban, A., Harrison, D. P. (1995). High temperature capture of carbon dioxide: characteristics of the reversible reaction between $CaO_{(s)}$ and $CO_{2(g)}$, *Chemical Engineering Communications*, 137, 177-190.

Statoil (2013a). http://www.statoil.com/en/technologyinnovation/newenergy/co2capturestorage/pages/sleipnervest.aspx (visitado en Julio 2014).

Statoil (2013b). http://www.statoil.com/en/technologyinnovation/newenergy/co2capturestorage/pages/insalah.aspx (visitado en Julio 2014).

Statoil (2013c). http://www.statoil.com/en/technologyinnovation/newenergy/Co2CaptureStorage/Pages/Snohvit.aspx (visitado en Julio 2014).

Strelow, M., Schlitzberger, C., Röder, F., Magda, S., Leithner, R. (2012). $CO_2$ Separation by Carbonate Looping Including Additional Power Generation with a $CO_2$-$H_2O$ Steam Turbine, *Chemical Engineering & Technology*, 35, 431-439.

Ströhle, J., Junk, M., Kremer, J., Galloy, A., Epple, B. (2014). Carbonate looping experiments in a 1 $MW_{th}$ pilot plant and model validation, *Fuel*, 127, 13-22.

Sun, P., Grace, J. R., Lim, C. J., Anthony, E. J. (2006). Removal of $CO_2$ by Calcium-Based Sorbents in the Presence of $SO_2$, *Energy & Fuels*, 21, 163-170.

Sun, P., Lim, C. J. y Grace, J. R. (2008). Cyclic $CO_2$ capture by limestone-derived sorbent during prolonged calcination/carbonation cycling, *AIChE Journal*, 54, 1668-1677.

Telesca, A., Calabrese, D., Marroccoli, M., Tomasulo, M., Valenti, G. L., Duelli, G., Montagnaro, F. (2014). Spent limestone sorbent from calcium looping cycle as a raw material for the cement industry, *Fuel*, 118, 202-205.

Wang, J., Anthony, E. J., Abanades, J. C. (2004). Clean and efficient use of petroleum coke for combustion and power generation, *Fuel*, 83, 1341-1348.

Ylätalo, J., Ritvanen, J., Arias, B., Tynjälä, T., Hyppänen, T. (2012). 1-Dimensional modelling and simulation of the calcium looping process, *International Journal of Greenhouse Gas Control*, 9, 130-135.

Ylätalo, J., Parkkinen, J., Ritvanen, J., Tynjälä, T., Hyppänen, T. (2013). Modeling of the oxy-combustion calciner in the post-combustion calcium looping process, *Fuel*, 113, 770-779.

Ylätalo, J., Ritvanen, J., Tynjälä, T., Hyppänen, T. (2014). Model based scale-up study of the calcium looping process, *Fuel*, 115, 329-337.

Yongping, Y., Rongrong, Z., Liqiang, D., Kavosh, M., Patchigolla, K., Oakey, J. (2010). Integration and evaluation of a power plant with a CaO-based CO2 capture system, *International Journal of Greenhouse Gas Control*, 4, 603-612.

Yu, F.-C., Phalak, N., Sun, Z., Fan, L.-S. (2011). Activation Strategies for Calcium-Based Sorbents for $CO_2$ Capture: A Perspective, *Industrial & Engineering Chemistry Research*, 51, 2133-2142.

ZEP (2013a). The Costs of $CO_2$ Capture. Post-demonstration CCS in the EU.

ZEP (2013b). The Costs of $CO_2$ Transport. Post-demonstration CCS in the EU.

Zhao, M., Minett, A. I., Harris, A. T. (2013). A review of techno-economic models for the retrofitting of conventional pulverised-coal power plants for post-combustion capture (PCC) of $CO_2$, *Energy & Environmental Science*, 6, 25-40.

CSIC

Consejo Superior de Investigaciones Científicas